Physico-mechanical Characterisation of a Novel and Commercial CAD/CAM Composite Blocks

A thesis submitted to the University of Manchester for the degree of

Doctor of Philosophy

in the Faculty of Biology, Medicine and Health Sciences

2019

NADA ALI B ALHARBI

Division of Dentistry

Table of Contents

Word counts: 45,294

Table of Figures

List of Tables

List of Abbreviations

°C	Centigrade
µg/ml	Microgram per millilitre
µg/mm^3	Microgram per cubic millimetre
µl	Microliter
µm	Micrometre
ANOVA	Analysis of Variance
ASTM	American Society for Testing and Materials
ISO	International Organization for Standardization
BisEMA	Bisphenol A ethoxylate dimethacrylate
BisGMA	Bisphenol A glycidyl dimethacrylate
UDMA	Urethane dimethacrylate
TEGDMA	Triethylene glycol di-methacrylate
BP	Benzyl peroxide
HEMA	2-Hydroxyethyl methacrylate
C=C	Carbon double bond
CQ	Camphor Quinone
d	Day
DC	Degree of conversion
LED	Light-emitting diodes
m	Month
Mg (%)	Percentage mass change
ml	Millilitre
g	gram
RO	Reverse Osmosis
MMA	Methyl methacrylate
mW	Milliwatts
nm	Nano metre
p	Estimated probability of rejecting the null hypothesis
pH	Potential hydrogen

psi	Pounds per square inch
PTFE	Polytetrafluoroethylene
s	Second
SD	Standard deviation
IQR	Interquartile range
SL	Solubility
SP	Sorption
UV	Ultraviolet
VH/VHN	Vickers hardness number
Vol%	Percentage content by volume
wt%	Percentage content by volume
α	Significance level
h	hour
CAD/CAM	Computer Aided Design/Computer Aided Manufacturing
PICN	Polymer Infiltrated Ceramic Network
PICN-GC	Polymer Infiltrated Glass Ceramic Network
PICN-PC	Polymer infiltrated Polycrystalline Ceramic Network
PMMA	Polymethyl Methacrylate

Abstract

Ceramics and resin composites have been used in dentistry as restorative materials for over fifty years ago, and meanwhile their properties have been substantially improved. Recently a new class of restorative materials known as 'polymer infiltrated ceramic network-PICN' materials has been introduced as CAD/CAM materials, and to optimise the performance of ceramic and composite materials by combining them into a single material. The aim of the present research was to assess PICN in comparison to conventional materials with respect to their composition, structure, physical and mechanical properties. A new polycrystalline based PICN material was fabricated and assessed in this study.

Alumina discs were fabricated and sintered at different temperatures followed by silanaisation and UDMA-TEGDMA resin polymer infiltration. The density, optical properties and biaxial flexural strength were assessed and the microstructure was examined using a scanning electron microscope. It was found that polymer infiltration significantly improved the density% of ceramic samples. An increase in sintering temperature results in a significant improvement in the optical properties but not the biaxial flexural strength.

The effect of sintering temperature, the quality and the quantity of ceramic compositions on the mechanical coherence of PICN materials and other restorative materials were assessed and compared at different microstructural dimensions: macro, micro and nano. Materials showed variable results and micro hardness and nano hardness of the studied materials increased systematically with an increase in filler loading. Mechanical properties of PICN ceramic were significantly influenced by the sintering temperatures of their ceramic matrices. The elastic modulus values showed bimodal distribution and associated with the various phases present which were able to be distinguished at nano level.

Sorption and solubility were assessed after 7 months of water storage. Water sorption of CAD/CAM composite blocks are material-dependent and are affected by the filler weight percentage. Commercial and model PICN ceramics showed hydrolytic stability between resin composite and conventional ceramic, reflecting its microstructural components. Sintering temperature appears to have a significant effect on the hydrolytic stability of PICN ceramics.

Declaration

No portion of the work referred to in the thesis has been submitted in support of an application for another degree or qualification of this or any other university or other institute of learning.

Nada Ali B Alharbi

2019

Copyright Statement

I. The author of this thesis (including any appendices and/or schedules to this thesis) owns certain copyright or related rights in it (the "Copyright") and s/he has given The University of Manchester certain rights to use such Copyright, including for administrative purposes.

II. Copies of this thesis, either in full or in extracts and whether in hard or electronic copy, may be made only in accordance with the Copyright, Designs and Patents Act 1988 (as amended) and regulations issued under it or, where appropriate, in accordance with licensing agreements which the University has from time to time. This page must form part of any such copies made.

III. The ownership of certain Copyright, patents, designs, trademarks and other intellectual property (the "Intellectual Property") and any reproductions of copyright works in the thesis, for example graphs and tables ("Reproductions"), which may be described in this thesis, may not be owned by the author and may be owned by third parties. Such Intellectual Property and Reproductions cannot and must not be made available for use without the prior written permission of the owner(s) of the relevant Intellectual Property and/or Reproductions.

IV. Further information on the conditions under which disclosure, publication and commercialisation of this thesis, the Copyright and any Intellectual Property and/or Reproductions described in it may take place is available in the University IP Policy (see http://documents.manchester.ac.uk/DocuInfo.aspx?DocID=2442 0), in any relevant Thesis restriction declarations deposited in the University Library, The University Library's regulations (see http://www.library.manchester.ac.uk/about/regulations/) and in The University's policy on Presentation of Theses.

The Author

I graduated from King Abdulaziz University in Jeddah in 2008, gaining a BDS degree with second honours with a GPA of 4.2. I then worked as a teaching assistant in the Faculty of Dentistry of Taibah University during 2009-2011 in the Department of Fixed Prosthodontics. In 2012 I was awarded a scholarship by the university to continue my postgraduate studies and I became a member of the full-time three-year MSc (Clin) Fixed and Removable Prosthodontics programme at the University of Manchester, graduating with merit in 2015. In September 2015, I began a full-time four-year clinical PhD course leading to Doctor of Clinical Dental Science in Fixed and Removable Prosthodontics.

I was appointed as the Division of Dentistry PGR representative from 2016 to 2018. In addition, I acted as a clinical tutor for undergraduate dental students at the University of Manchester in 2017. In 2016 and 2017, I was awarded two prizes for the best poster and oral presentations by the division of Dentistry at the University of Manchester. I am also a reviewer for the journal of Dental Materials and the journal of Aesthetic and Restorative Dentistry.

In 2018, I was honoured to be elected as a participant in a collaborative research between the University of Manchester and Boston University. Later that year, I went to Boston University (BU) Henry M. Goldman School of Dental Medicine for a 30-day collaborative visit. I was involved in fabrication, mechanical and microstructural characterisations of a newly invented material by Dr Russell Giordano whom I worked there under his direct supervision.

I have attended the following meetings during my PhD study:

- Clinical Fractography in Dental Materials Wokshop (Germany,2016)
- The British Society of Prosthodontics (BSSPD) Annual Conference- Poster Presentation (Manchester,2016)
- The British Society of Prosthodontics (BSSPD) Annual Conference- Poster Presentation (London,2017)
- 4th Euro BioMAT - European Symposium and Exhibition on Biomaterials and Related Areas – Oral Presentation (Germany, 2017)

- 24th European Dental Materials Conference – Poster Presentation (London, 2017)
- Faculty of BMH Show case- Poster Presentation (Manchester, 2017)
- IADR/PER General Session (London,2018)

I have also presented aspects of my research at the following meetings:

- The British Society of Prosthodontics (BSSPD) Annual Conference- Poster Presentation (Manchester,2016)
- The British Society of Prosthodontics (BSSPD) Annual Conference- Poster Presentation (London,2017)
- 4th Euro BioMAT - European Symposium and Exhibition on Biomaterials and Related Areas – Oral Presentation (Germany, 2017)
- 24th European Dental Materials Conference – Poster Presentation (London, 2017)
- Faculty of BMH Show case- Poster Presentation (Manchester, 2017)

Acknowledgment

First and foremost praise to ALLAH, the almighty and the greatest for guiding me throughout my life and for giving me the strength and determination during my study and for being with me when no one else is around.

Now, I would like to express my sincere gratitude to my supervisors Professor Nick Silikas and Professor Julian Satterthwaite and Dr Helen Chen. They have guided and supported me throughout this project. I appreciate the time and energy that they have given to make this work the best that it can be.

I also would like to acknowledge my clinical supervisors Dr Reza Roudsari, Dr Joanne Cunliffe, Professor Nick Grey, and Mr Warren Martin and all the clinical staff and nurses at the Prosthodontics Department at the University of Manchester for their support.

I also wish to extend my thanks to Mrs Shena Reynolds, Mrs Leigh Evans, and Mr Brian Daber for their time and encouragement during my study.

I also would like to gratefully acknowledge BU Henry M. Goldman School of Dental Medicine staff and students for their great support and exceptional hospitality. A special gratitude to my mentor at BU, Dr Russell Giordano for his endless support and guidance.

Sincere gratitude is due to Dr Nigel Hodson at the Bioimaging Facility (BioAFM Unit), Faculty of Biology, Medicine and Health and Mr Will Williams at the Department of Materials for their massive technical support and guidance during my nano-mechanical analysis. Also, I would like to thank Dr Yuwei Fan at to BU Henry M. Goldman School of Dental Medicine for his help and technical support during my visit to BU.

I am grateful to my friends and colleagues Dr Mahir Mira, Abdulrahman Alshabib, Khalid Althagafi, Hamad Algamaiah, Mariam Almansour and Dr Ruwaida Alshali for their massive support and guidance during my study. Special thanks to Mrs Randa Alharbi and Mr Mohammad Alshahrani for the graphic supports.

I am also grateful to Taibah University and the Saudi Cultural Bureau for sponsoring me during my studies and for allowing me the opportunity to continue them at the postgraduate level.

Last but not least, to all those I came to know in Manchester, for providing an unforgettable experience for me during my seven-year stay.

Dedication

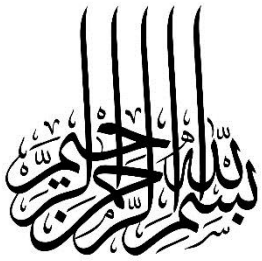

IN THE NAME OF ALLAH
THE ALL KNOWING, THE MOST WISE

To my Mom *Ghalyah Hadid*,

who told me once:

"*when you start something, make sure that you are willing to finish it right*"

To my Dad *Ali Alharbi*,

who raised me to be independent, dedicated and not to be settle for anything less than what I really want.

To my siblings,

Mamdouh, Hammad, Hind, Kholoud, Ghadah, Reem and *Ahmed*

for their tremendous encouragement and guidance throughout my experience. And, I extend my gratitude to all my lovely nephews and nieces.

Chapter 1

General Introduction and Literature Review

1.1 Introduction to Dental Restorations

The loss of tooth structure may occur due to pathological and non-pathological reasons. Dental caries or teeth decay is one of the most prevalent causes of tooth structure loss among people worldwide (1). It is considered an infectious disease and individuals are susceptible to this disease throughout their life time. It can cause a localised destruction of the hard tooth tissue due to the acidic by-product which results from bacterial fermentation of a carbohydrate-rich diet (2).

Dental caries has a multifactorial aetiology that starts with a microbial shift within a complex biofilm. It is now universally accepted that four main factors are necessary to produce a demineralisation or cavitation. These factors are:

- Tooth surface
- Bacteria in dental biofilm
- Dietary carbohydrates
- Time

The diseases process initiates inside the bacterial biofilm that is located on the surface of the tooth. The early sign of caries presents as a surface demineralisation of the enamel. Over time the disease can either progress into cavitation of the tooth or may repair and remineralise (3).

Dental caries can be easily preventable provided that one of the above factors is eliminated at an early stage. However, the disease progresses slowly in a large number of the population leading to unfavourable consequences. These are pain, poor functions and aesthetic, and infection which may sometimes even be life -threatening.

The early management of caries was to excise the caries-prone fissures around the diseased tissue as an ‘extension for prevention’. The management concept has changed over time and relies on more preventable and preservative approaches such as fluoride applications, removal of biofilm and pits and fissure sealants. However, the caries progression rate varies among individuals and the need for excising diseased tissue and restoring the resultant cavity, and the need to intervene where there is cavitation of the surface is still needed in a large number of people.

Restoring or replacing the lost tooth structure has been practiced since ancient times. A variety of materials including stone chips, ivory, human teeth, cork, gums and metal foils were used until the eighteen century. Queen Elizabeth I used cloth fragments to fill in her dental cavities. Fauchard who is referred sometimes as the father of modern dentistry used tin foil to fill cavities in teeth (4).

As the overriding goal in dentistry is to improve the quality of life for dental patients, a wide variety of dental biomaterials have been used to accomplish that goal. Restorative materials for the replacement of the missing or damaged portion of tooth structure have been rapidly progressed over the past decades. However, despite improvements, none of these materials are considered as permanent. Dentists and biomaterial scientists are still working on improving the quality of dental restorations in order to develop an ideal restorative material. The properties of an ideal material include:

- Biocompatible
- Permanently bond to the tooth and/or bone
- Exhibit similar physical and mechanical properties to the tooth enamel, dentin and other dental structures.
- Match the natural colour and appearance of tooth structure.
- Being regenerative or initiating tooth repair
- Radiopaque

Restoring teeth to mimic the aesthetic appearance of natural teeth is one of the main goals of contemporary restorative dentistry. In 1989 an international congress held in California, titled “The criteria for placement and replacement of dental restorations”, established the principle that the non-aesthetic appearance of a restoration was a valid reason for replacing it (5). Today, the most commonly used aesthetic materials are resin-based composites and ceramic (and hybrids of these two).

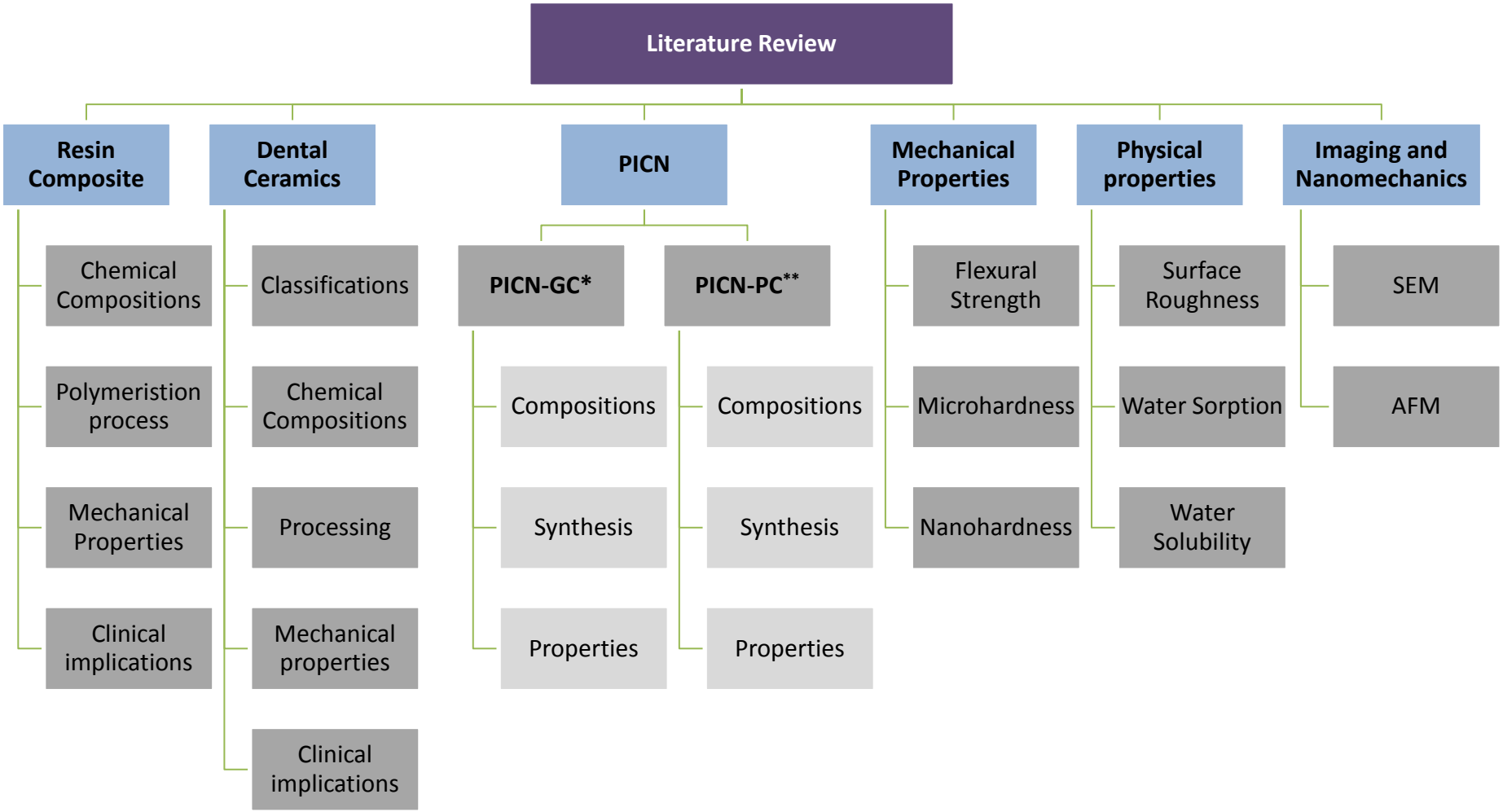

Figure 1.1 General outline of the literature review of the present study.

**Polymer infiltrated glass ceramic network*

***Polymer infiltrated polycrystalline ceramic network*

1.2 Introduction to Resin composites

A composite material is a material that is made from two or more different substances with different physical or chemical properties, which when combined together produce a material that has properties better than the individual components. Composite can be available naturally or synthetically. Natural composites may be represented as dentine or bones, while synthetic composite materials include concrete reinforced with steel or polymer reinforced with additive or fillers (6). Dental resin composite is a type of synthetic composite that is used in dentistry as a restorative material to replace lost or damaged tooth structure. Dental composite is basically composed of three main components, 1) resin based matrix comprising: i) monomer system ii) initiator system to initiate the free radical polymerisation and iii) stabiliser to maximise the shelf life of the uncured resin composite and the chemical stability for the cured resin composite.; 2) inorganic fillers and 3) coupling agent to act as a bridge connecting the inorganic fillers with the resin matrix (7).

1.2.1 Resin Matrix

1.2.1.1 PMMA and Epoxy Resins

The first resin used in dentistry as a filling material was polymethyl methacrylate (PMMA) which was in the 1930s(8). However, this material was associated with many drawbacks including high coefficient of thermal expansion, high polymerisation shrinkage, marginal discoloration and serious pulp damage. Because of these limitations, PMMA resins were replaced by epoxy resins which set at room temperature and showed relatively less polymerisation shrinkage. However, the use of epoxy resins as restorative materials stopped because of their slow setting reaction (7, 9). Figure 1.2 shows the basic chemical structure of a) MMA and b) Epoxy resins.

a)

b)

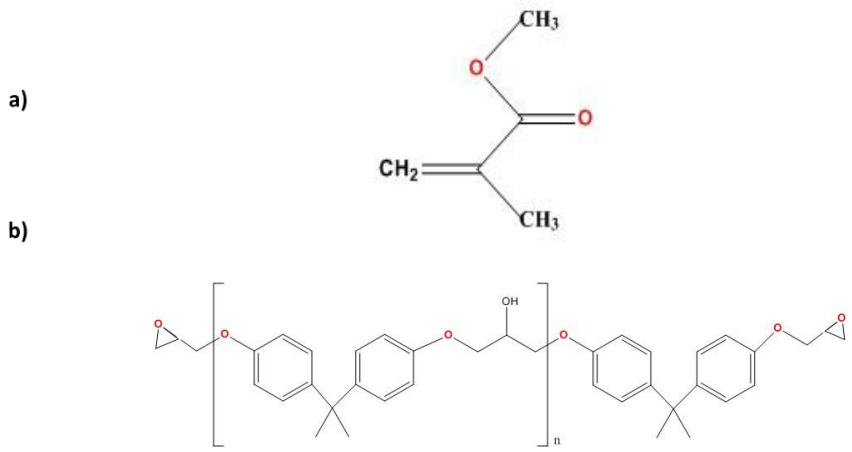

Figure 1.2 Chemical structures of a) MMA b) Epoxy resin.

1.2.1.2 Bis-GMA Resins

Bis-GMA is a by-product reaction of an epoxy resin (ethylene glycol of bis-phenol A) and methyl methacrylate (2,2-bis[4-(2-hydroxy-3-methacryloyloxypropoxy)phenyl]propane) which was developed by Bowen (1962)(10), hence why it is sometimes called Bowen's Resin. Bis-GMA can be described as an aromatic ester of dimethacrylate oligomers that has two terminal hydroxyl (–OH) groups to enable them to form hydrogen bonds between monomers which explains its high viscosity (Figure 1.3) (11). This monomer is still being used in modern dentistry because of its superior properties compared to PMMA. Bis-GMA has a large molecular size and chemical structure leading to a lower concentration of reactive groups and hence relatively less polymerisation shrinkage, rapid setting reaction, stiffer and stronger material (12).

One of the major drawbacks to the use of a monomer with a large molecular size is that it is very viscous and not easy to manipulate. In order to improve the handling property in clinical practice, this monomer is often diluted with low molecular mass dimethacrylate monomers such as triethylene glycol dimethacrylate [TEGDMA]. Alternative options include replacing one of the –OH groups with an ethoxy group (-CH_2-CH_2-O-) to produce an ' ethoxylated Bis-GMA' (13).

1.2.1.3 UDMA *Resins*

UDMA, 1,6-bis (methacrylyloxy-2-ethoxycarbonylamino)-2,4,4 trimethylhexane, (Figure 1.3) was first developed by Foster and Walker in 1974 (14)as an alternative monomer to bis-GMA. It is produced as a reaction by-product of 2,4,4-trimethylhexamethylene diisocyanate and 2-hydroxyethyl methacrylate (HEMA) and it is now included in many modern composites either as a sole monomer or in combination with other different monomers. In comparison to bis-GMA, UDMA has relatively lower molecular mass with less viscosity due to absence of the hydroxyl group, which leads to superior mechanical properties and higher degree of conversion and thus less polymerisation shrinkage (15).

1.2.1.4 TEGDMA Resins

TEGDMA, [triethyleneglycol-dimethacrylate] (Figure 1.3) is an ester of ethyleneglycol and the α, β-unsaturated methacrylic acid. This monomer is included in many modern composites due to its excellent viscosity and copolymerisation behaviour. Its low molecular weight (286 g mol^{-1}) and reduced viscosity (η= 0.05 Pa.s) produces a significant increase in its degree of conversion. However, the high degree of conversion leads to clinically unacceptable polymerisation shrinkage(16) and thus it is commonly either combined or totally replaced with a monomer that has low viscosity and relatively higher molecular weight such as ethoxylated bisphenol-A dimeth-acrylate (BisEMA: MW = 540 g mol^{-1}, η =3 Pa.s) (17).

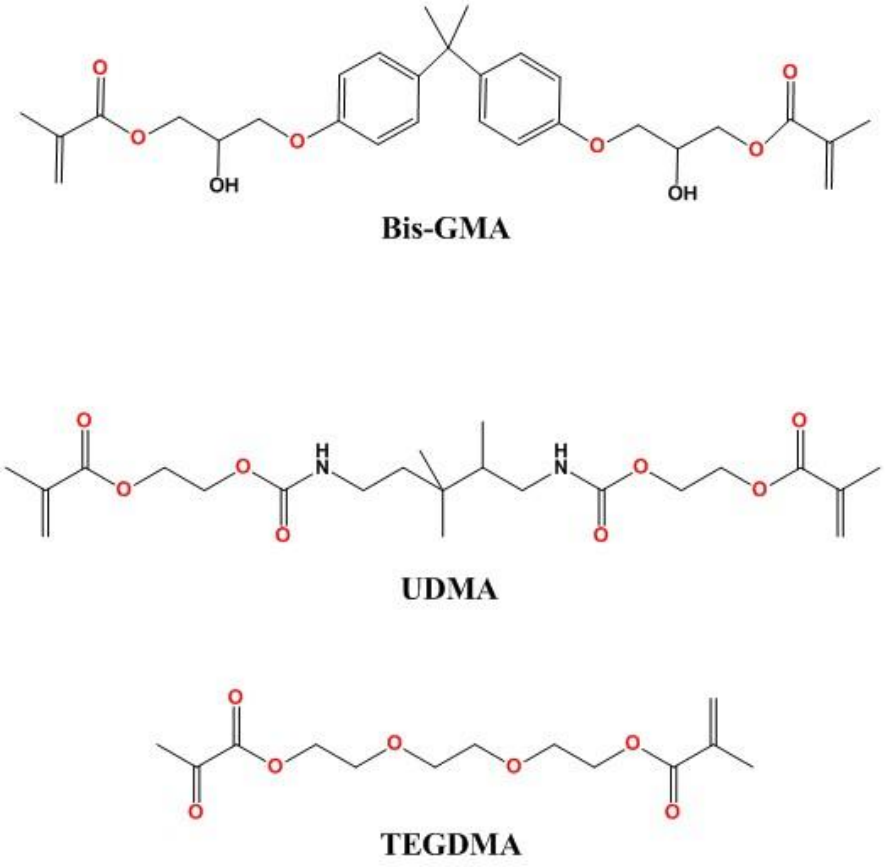

Figure 1.3 Chemical structures of Bis-GMA, UDMA and TEGDMA

1.2.2 Fillers

1.2.2.1 Development and Roles of Filler Particles:

Fillers are added as a reinforcement to improve the overall physical and mechanical properties of dental composite. When compared to an unfilled resin, filled composite is stronger, more stable during and after the polymerisation reaction and has better handling and optical properties (18).

Fillers with different chemical compositions are used in resin composite. The first fillers used to reinforce early resin composites were quartz. Major drawbacks of adding quartz were due to its radiolucency and also its abrasivity which could cause wear of opposing enamel. In modern resin composite however, common fillers used are radiopaque silicate particles based on oxides of barium, strontium, zinc, aluminum, or zirconium. These fillers are added because of their advantageous mechanical and optical properties and ease of use (19).

1.2.2.2 Types of Filler Particles

Resin composites are generally classified according to the size and the volume fractions of their filler particles. Based on the size of the particles, resin composites were originally categorised by Lutz and Philips (1983) into: conventional (8 - 12 μm), small particle (1 - 5 μm), microfilled (0.04 - 0.4 μm), and hybrid (1.0 μm) (20). The microfilled then being subcategorised according to the type of incorporated pre-polymerised filler into: spherical, agglomerated and splintered (21). However, Willems *et al*. (1992) suggested that the term 'hybrid' should no longer be used as most of modern resin composite are now hybrid with two or more range of particles sizes to achieve superior mechanical properties, good handling and the ability to maintain a high surface polish (22). Alternatively, resins composite can be classified according the volume fraction of filler particles into: midway-filled (< 60 vol %) and compact-filled (> 60 vol %), with classifications of ultrafine (avg. particle size < 3 μm) and fine (avg. particle size > 3 μm) within each category.

Current hybrid resin composites are then further classified as "micro hybrid", and "nano hybrid". The particle size in micro hybrid composites, which initially were referred as "minifills", ranges from 40 nm to 1.0 μm. In nano hybrid, the small particles were further refined and reduced into nano sized fillers with 5 to 100 nm (21). In general, these composites are widely adopted as modern restorative materials due their superior mechanical properties and can be used for both anterior and posterior teeth (23).

Nano scale fillers can also be used on its own in "nanofill" composites. These fillers can be incorporated either as individual particles (20-75 nm) or in combinations (nano-clusters) of an overall size of 0.6-1.4 μm (24). Nano-filled resin composites show high translucency, and due to the small size of the particles have high polish and polish retention. Their mechanical and physical properties and their wear resistance are similar to those of hybrid composites. They can be used in load-bearing regions in addition to aesthetically critical area (25).

1.2.3 Coupling Agent

Stress distribution and homogeneity in dental composite are achieved if resin matrix and inorganic fillers are well adhered to each other. Because resin composites are made of two dissimilar materials (organic and inorganic) a third intermediate material is required to improve the bonding of the organic resin to mineral surfaces of fillers. This can be achieved by coating the surface of the filler particles with a silane coupling agent which may provide an overall improvement of the mechanical properties of the final resin composite material. Silane or organosilane is a hybrid inorganic-organic bifunctional molecule that can react with the filler with its methoxysilane group and resin monomers by its methacrylate functional group. The history of the use of silanes as coupling agent dates back to 1962, when Plueddemann (1991) assessed the role of silane as a coupling agent in glass-reinforced polyester and epoxy composite (26). The most commonly used silane in resin composite is 3-methacryloxypropyltrimethoxysilane (MPS). Other types of silane agents, such as 3-acryloxypropyltrimethoxysilane (APM), and 10-methacryloxydecyltrimethoxysilne (MDS) are also employed in dental applications. The selection of different types of silane in dental composite is largely dependent on the type of filler used (27).

1.2.4 Initiators and Accelerators

The polymerisation reaction of dental composite can be initiated either chemically (self-cure) or by visible light (photopolymerisation). In chemically activated composite, an organic peroxide initiator reacts with a tertiary amine accelerator to produce free radicals which in turn break off the double bond of the oligomer molecules to start the polymerisation reaction. On the other hand, the initiation mechanism in light cured composite starts when the initiator (most often D,L-camphorquinone - CQ), acts as a sensitizer and absorbs the visible light to form a photoexcitationcomplex (CQ*-amine exciplex) with a tertiary amine (a hydrogen-donating agent) and subsequently generates amine-derived free radicals. Some resin composites incorporate the two initiation processes together to form what is commonly known as a ‘dual cure’ system. In this system, the polymerisation is activated by the light and then progresses by self-curing (28).

1.2.5 Inhibitors

In order to prevent the premature polymerisation of dental composite, inhibitors are added to the resin matrix. These inhibitors are added with a controlled concentration to a level that does not interfere with initiator functions. Examples of commonly used inhibitors are butylated hydroxytoluene and monomethyl ether of hydroquinone (4).

1.2.6 Pigments

In order to modify the colour of resin composite to match the shades of natural teeth, inorganic oxides are often added in small amounts. Varieties of shades are available ranging from very light to yellow and grey and different colour scales are also supplied to assist in the selection of a suitable shade. Oxides of iron are the most commonly added pigments and UV absorbers may be added also to help in colour stabilisation which might otherwise change due to oxidation. Other additives may be added to minimise the yellow effect of CQ by their blue light reflection property (28).

1.2.7 Polymerisation Reactions

The polymerisation reaction of resin composite generally takes place in three stages: activation or initiation, propagation and termination (Figure 1.4). The increase in the amount of cross-linking of the polymerised resin can be explained by the presence of difunctional carbon double bonds.

Many other factors also affect the degree of polymerization of resin composites, including the shade, light curing duration, increment thickness, light unit system used, cavity diameter, cavity location, light curing tip distance from the resin surface, the type of substrate through which the light is cured (e.g., curing through ceramic, enamel, or dentin), filler type, and temperature (4, 29-33).

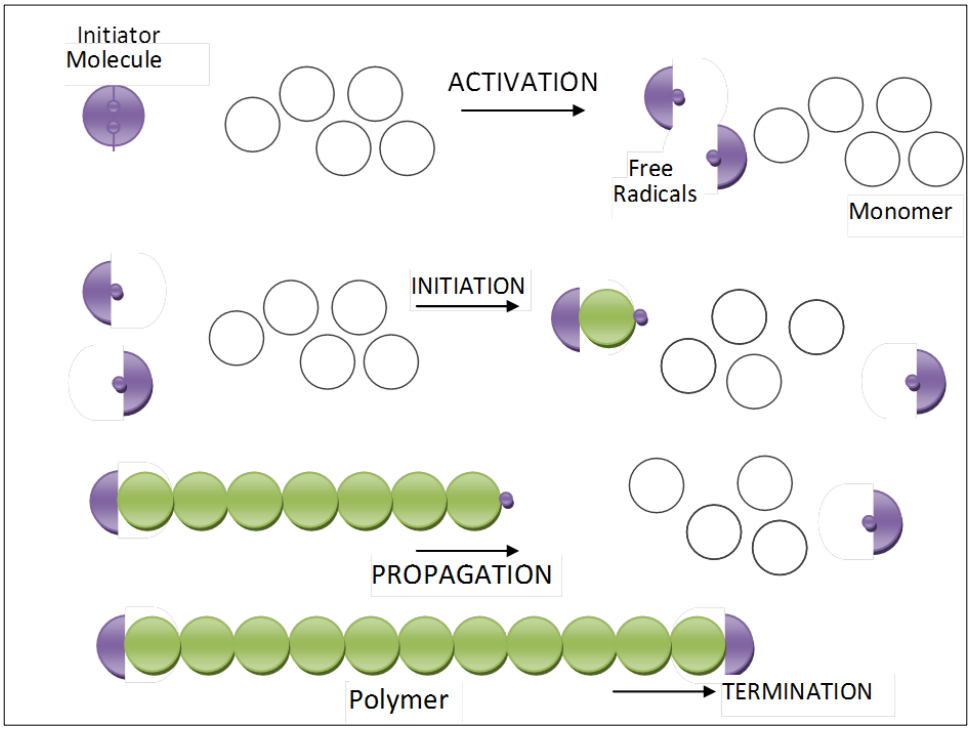

Figure 1.4 Polymerisation process in resin composite. Free radicals are generated by the activation process; initiate the cross-linking reaction or polymerisation. The chain length continues to propagate until no monomer is available or termination reaction occurs. Reaction terminates when the two ends of the chain couple together.

1.2.8 Physico-mechanical Properties of Dental Composite

1.2.8.1 Strength Properties of Resin Composite

In addition to good aesthetic properties, resin composites have shown relatively good physical and mechanical properties. Current resin composite materials may be used for posterior restoration as well as for anterior restoration. Posteriorly located defects (Class I or II) require restorative materials that have high mechanical properties in order to withstand occlusal loads which are relatively higher compared to anterior (34).

Although *in vitro* mechanical properties do not necessarily reflect the clinical performance, they help clinicians to compare and select between materials and brands. Testing of the mechanical properties also provides a way to evaluate the effect of changing material composition on these properties. In resin composite, changing filler composition, filler size, matrix viscosity and polymerisation system have a great influence on mechanical properties (35-37).

Compressive strength is the internal resistance of a material that is subjected to an axially applied force. Tensile strength is the capacity of the material to elongate or stretch upon applying such force. Flexural strength is one of the most essential properties that is usually tested to assess a restorative material. In general, strength can be calculated by dividing the applied force by the cross sectional area perpendicular to that force. To measure the elastic deformation, usually an elastic modulus test is employed. Modulus of elasticity describes the relative rigidity or stiffness of a material with a high number indicating a stiff material. Ideally, it is required to be similar to that of the tooth structure so both parts (the restorative material and the tooth) behave similarly under load. However, resin composite typically has a lower elastic modulus that of dentine and enamel which are ranged between 14 GPa (dentine) to 84 GPa (enamel) (38).

1.2.8.2 Hardness of Resin Composite

Hardness is usually defined as the resistance of a material to indentation. The indentation is developed on the surface of a material as a result of an applied sharp-pointed force. More detailed description about this property and measurement will be explained later in this chapter. Hardness of a resin composite, like any other mechanical property, is

influenced by the quantity and the quality of its chemical compositions and the polymerisation process. It has been studied extensively in the literature and found to be an effective way to determine the degree of polymerisation, with the degree of cure or depth of cure being significantly correlated with the surface hardness of composite (39-41). Surface hardness has been also used to indicate the wear property of the material or the ability of this material to produce wear effect on the opposing substrate (42).

1.2.8.3 Fracture Toughness of Resin Composite

Fracture toughness is the capacity of a material to withstand an applied stress before a certain amount of plastic deformation or fracture occurs. In particular, it describes the resistance of a material containing cracks or flaws to the catastrophic propagation of these cracks or flaws under applied stresses. The fracture toughness is inversely proportional to the square root of the flaw depth into the surface. Higher fracture toughness values indicate stronger materials that are highly resistant to fracture. The fracture toughness of resin composite has been assessed and reported previously: it is greatly influenced by inorganic content, particularly the filler content, size and shape (43, 44).

1.2.9 Clinical Implications of Dental Composite

Posterior resin composite has been used for more than 40 years. Early composite showed more clinical challenges and higher failure rates compared to amalgam (45, 46). Since then, many studies have been conducted to improve the materials in terms of their mechanical properties, clinical techniques and handling abilities. However, there are still some clinical challenges that may affect the performance and the longevity of resin composite as a restorative material. Current evidence indicates that these challenges are related to the material itself, the clinical application or dental practitioners.

1.2.9.1 Materials Related Challenges

Early studies on posterior composite materials observed extensive wear of composite which affected the durability of the material in the oral cavity (46). Wear is influenced by filler compositions, filler size and bonding between fillers and resin matrix (47). Excessive wear can result from loss of filler particles that are located on the surface of a composite

restoration. Loss of filler particles is related to either its large size, or weak bond between filler and resin matrix (48). Water sorption can also accelerate the wear rate by hydrolytic breakdown of filler surface layers (49). Current composite materials are composed of much smaller filler particles allowing more filler loading and show improvement in terms of wear resistance. However, wear is still a problem especially in molar areas where broad occlusal/functional surfaces and high masticatory forces are considered to be relatively more challenging than anterior teeth or contact-free areas (50).

Other complications like surface roughness (51), colour instability (52), bulk fracture (53) and polymerisation shrinkage (54) have been reported. Despite improvements in composition and hence mechanical properties, these problems are still not completely resolved. These indicate that further research is required and welcomed to improve the durability of resin composite, especially those made for posterior areas.

1.2.9.2 Dentist Related Challenges

It is generally accepted that dental composite is technique sensitive; experience and clinical skills may play a significant role in the outcome of composite restorations, for example significant difference in wear rates has been found between different operators (50). Operative challenges include the ability to place a void-free restoration, optimum moisture control, optimum finishing and providing a smooth surface finish.

1.2.9.3 Patient Related Challenges

The patient receiving the restoration is also a factor in performance of composite restorations. Differences in wear rates have been noticed between different study populations (45, 55). The differences are most likely correlated to differences in individual masticatory forces, parafunctional habits, salivary quality and quantity, and oral hygiene maintenance (56, 57). Dietary factors such as hardness and abrasiveness of foods can also affect the durability of restorations and might lead to an early failure (58).

1.3 Introduction to Ceramic Restorations

The desire for an aesthetic restoration that mimics the shade and translucency of natural teeth has led to the development of ceramic materials, and these are now regarded as a fundamental component of dentistry. The development of ceramics in dentistry actually dates back to 1889, when Charles H. Land introduced the porcelain jacket crown (59).

The basic chemical composition of ceramics involves a mixture of metallic and non-metallic elements which form ionic and/or covalent inter-atomic bonds. The inherent nature of these bonds defines the hard, stiff and brittle properties of ceramic materials (60).

Structurally, dental ceramics are comprised mainly of silica, a common component of sand or quartz. Silica is polymorphic, which means that it has the ability to exist in a number of crystalline or amorphous forms. In the crystalline phase the atoms display a regular periodic arrangement and are densely packed together in a tetrahedral shape. However, when molten silica is rapidly cooled, a process known as 'vitrification', the atoms tend to lose their long-range order and the silica solidifies into an amorphous glass phase. Against this background, dental ceramics tend to behave differently under different local conditions (60, 61).

1.3.1 Classifications of Dental Ceramics

1.3.1.1 Classification Based on the Chemical Compositions

Three types of all-ceramic material are currently available, predominantly glassy materials, partially-crystalline materials, and polycrystalline materials. The glass content provides aesthetic translucency, whereas the crystalline content contributes to strength and superior mechanical properties. The structure of the predominantly glassy materials is amorphous and is composed mainly of silica; their ceramic nature mimics the optical properties of enamel and dentine, but it has poor mechanical properties, and for this reason its use is mainly limited to veneers, or overlay veneers on metal or ceramic cores (62).

In order to improve mechanical properties, manufacturers developed partially crystalline ceramic by adding some ceramic particles such as aluminium oxide (Al_2O_3) and leucite. However, the crystalline content not only affects the mechanical properties of the ceramic but also its optical properties, such as translucency and opalescence (63). For example, in the case of a very translucent tooth a predominantly glassy ceramic is a better choice due to its more acceptable optical properties. On the other hand, in the case of a moderately discoloured tooth a ceramic with high crystal content is a more suitable option, since it can mask the underlying discoloration.

Unlike the types described above, polycrystalline ceramics have no glass content, the crystals being condensed and arranged in regular crystalline arrays which enable an 'anti-crack propagation' feature to be created. Such an arrangement provides greatly improved mechanical properties, such as strength and fracture toughness, as will be explained later.

1.3.1.2 Classifications Based on the Fabrication Techniques

Dental ceramics can be also classified according to manufacturing method. The most commonly used methods are: powder composition (layering technique), slip casting, hot pressing and computer aided design-computer aided manufacture (CAD-CAM) (64).

- ***Powder Layered Ceramics***

Powder layering is a traditional technique and is commonly used for porcelain in porcelain-fused-to-metal (PFM) and all-ceramic crowns. It involves the addition of moist powder to a die in order to build up the crown. The porcelain is then condensed by removal of excess fluid followed by vacuum firing. The major disadvantage of this technique is the porosity developed during the condensation step and the dispersed arrangement of the crystals in the glassy material. As a result, this technique produces porcelain of relatively low strength and poor mechanical properties (64).

- ***Slip Casted Ceramics***

Slip casting involves the formation of a framework over which the porcelain can be applied. The 'slip' is a viscous mixture of powder and water which is applied as a thin layer over the mould before sintering with molten glass. The advantage of this technique compared with layering is that the crystals are highly concentrated and form a network

that provides a ceramic with good mechanical properties. However, the technique is not popular due to its technical difficulty, which requires multiple steps to achieve accurate fit (64).

- ***Hot Pressed Ceramics***

Hot-pressed ceramics involve investment and wax burn-out. Initially a wax-up of a prosthesis is created and invested. The mould is then heated and the wax completely removed. Following this, a highly viscous crystalline ceramic in a glassy mixture is slowly pressed into the mould. Unlike earlier techniques, the ceramic produced using this technique has lower porosity (64).

1.3.2 CAD/CAM Ceramics

Background

The introduction of computer-aided design-computer-aided manufacturing (CAD-CAM) in dentistry dates back to the 1970's, with major developments in the 1980's (65). Since then, a variety of CAD-CAM systems are available in dental markets and employed in fabrications of many modern dental restorations: examples of these systems include Sopha®, Cerec® and Procera® systems.

The rational for the use of CAD/CAM in dentistry is to construct dental restorations with high precision in a simple way and with little or no human intervention. The basic CAD/CAM production involves three steps (Figure 1.5): scanning, CAD modeling, and CAM production. The prepared teeth are digitally scanned, either intraorally or from a master cast. Using a computer the data are then processed and the restoration designed. The data from the computer are programmed into a milling machine and a prefabricated ingot is milled to reproduce the shape of the designed prosthesis. The ingot can either take the form of a partial or fully sintered ceramic, the former being softer and much easier to mill, but it requires an additional final sintering stage to develop full density and strength.

CAD/CAM Ceramic Materials

I. CAD/CAM-Compatible Feldspathic Ceramics

The first CAD/CAM compatible ceramic was made in 1985 in the form of inlay using a ceramic block comprising fine grain feldspathic ceramic (VitaTM Mark I, Vita Zahnfabrik, Bad Sackingen, Germany) (66). A prospective study evaluated the clinical performance of these inlays and onlays for about 10 years and found a success rate of 90.4% was achieved (67). However, over 36% breakage rate in 2 years was also reported (68).

VitaTM Mark II (Vita Zahnfabrik, Bad Sackingen, Germany) was developed specifically for CEREC (CerecTM 1 – Siemens GmbH,Bensheim, Germany) and showed better mechanical properties with flexural strength of 100-160 MPa (69, 70). Clinical studies showed 94.7% survival rate at 5 years period which decreased to 85.7% after 10 years (71, 72). However, this material is not recommended to be used in heavy load-bearing areas (i.e. posterior regions) due to its limited strength properties (73).

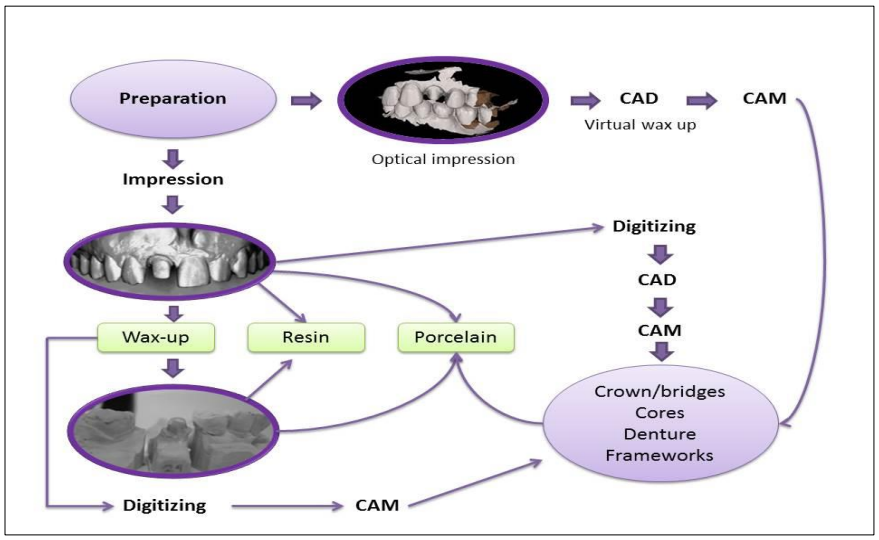

Figure 1.5 Clinical and laboratory steps to obtain CAD-CAM restorations.

CAD-CAM feldspathic ceramic blocks are generally made similarly to the conventional feldspathic porcelain but produced differently via a process called 'extrusion moulding'. In this process, the ceramic mixture is pressed and extruded through a nozzle to provide its normal form. Then, the produced blocks are dried for several days before the sintering process (74).

II. CAD/CAM and Mica-Based Ceramics

Mica ceramic is a type of glass ceramic was first made in early 1970's by George H. Beall (75). It is made of a group of sheet silicate (phyllosilicate) minerals with varying concentrations of Si, K, Na, Ca, F, O, Fe and Al (76). Mica-based ceramics are available in the market and the most commercially popular product has been Dicor™ (Dentsply, York, USA) which is produced for conventional and CAD/CAM fabrication. Machinable mica has greater than 25% more crystalline phase than the one used for laboratory productions; hence this may explain the higher flexural strength of the former (229MPa) compared to the latter (77). Clinically, CAD/CAM mica ceramics show similar survival rate to feldspathic based ceramics. However, mica ceramics have been shown to have a higher breakage rate than feldspathic in a 2 year period (77, 78). Dicor has been well studied in the literature, but due to its high breakage rates, this material is no longer available in the market.

III. CAD/CAM with Leucite-Reinforced Ceramics

ProCAD™ (Ivoclar-Vivadent, Schaan, Liechtenstein) was the first leucite-reinforced CAD/CAM ceramic used in restorative dentistry and its first appearance in the dental market was in 1998. It is a heat pressed ceramic containing a high amount of leucite crystals (35 vol%). ProCAD™ was followed by Empress™ CAD (Ivoclar-Vivadent) in 2006 which has a higher concentration of leucite crystals (45 vol%) with a finer particle size of about 1–5 μm that helps resist machining damage. The mean flexural strength was found to be around 160 MPa and it is recommended for single crown restorations. Another example of this category is Paradigm™ C (3M ESPE, Seefeld, Germany)(61).

IV. CAD/CAM Milling Lithium Disilicate Reinforced Ceramics

CAD/CAM milling lithium disilicate reinforced ceramic was developed in order to extend the use of all-ceramic restorative materials into more complex treatments such as fixed partial dentures. It is a glass ceramic based on a SiO_2–Li_2O system with a crystalline phase containing a lithium disilicate ($Li_2Si_2O_5$) that constitute about 70% of the volume. A lithium disilicate CAD/CAM ceramic IPSTM e.max CAD (Ivoclar-Vivadent) was first introduced in 2006 as a chair-side monolithic restorative material. The blocks are manufactured in a process based on the so-called pressure-casting procedure used in the

glass industry and are supplied also in a pre-crystallization form, sometimes called 'blue-state'. The blue ceramic contains metasilicate and lithium disilicate nuclei and exhibits a flexural strength of 130 ±30 MPa. In this state the block can be milled easily, after which the restoration is re-crystallized in a chair-side ceramic oven at 850 °C in vacuum for 20–25 min. During this heat treatment, the metasilicates are dissolved, lithium disilicate crystallizes and the ceramic is glazed at the same time. The block also changes from blue to the chosen shade and translucency. The ceramic contains 70 vol% of crystals of approximately 1.5 µm in size and the strength increases dramatically to 360 MPa (79). Few clinical studies are available to provide a sufficient evidence-based recommendation regarding the use of lithium disilcate ceramics in restorative dentistry. However, current clinical studies have shown that the short term survival rate (2-5 years) is 97% - 100% and the long term survival (up to 10 years) ranges from 71.4% to 87.9 (80-83).

V. CAD/CAM and Glass Infiltrated Alumina and Zirconia Ceramics

Slip-cast glass-infiltrated ceramics that have at least two interpenetrating phases intertwined throughout the material are also available. They have been available for CAD/CAM production since 1993; ceramic blocks can be fabricated by dry pressing the ceramic powder into a mould and compacted until an open pore microstructure is reached. In comparison to the conventional slip casting technique, the number of pores is lower yet more homogenous. The material is then sintered and infiltrated by a molten glass which is drawn into the macro pores via capillary action (61).

Glass infiltrated ceramics are available in the market and commonly known as 'InCeram' which is referred to Vita™ InCeram with its classic group of ceramics (InCeramTM Alumina, Spinell and Zirconia, Vita Zahnfabrik, Bad Sackin-gen, Germany). *In vitro* studies have reported the flexural strength for InCeramTM Alumina, Spinell and Zirconia to be 450–600 MPa, 350 MPa, and 700 MPa, respectively (70).

CAD/CAM InCeram™ Spinell has the most translucency compared to other groups and is generally recommended for aesthetic areas (anterior restorations). CAD/CAM InCeram™ Alumina is relatively less aesthetic and usually recommended for single crowns (79). CAD/CAM InCeram™ Zirconia has the highest fracture toughness in this group. However, due to the opacity of zirconia, it has the least aesthetic property and it is recommended to be used for posterior crowns as substructures (84).

1.3.3 Clinical Implications of Dental Ceramics

Although ceramics have relatively superior mechanical properties to resin composite, clinical evidence tends to show catastrophic mechanical failure of ceramic restorations (85). Table 1.1 shows the survival rates as reported by prospective studies.

Fracture of veneering porcelain or ceramic copings in all ceramic restorations is the most commonly reported failure that requires total replacement of a restoration. Other reported causes of failure include: marginal inadaptability, secondary caries, framework fracture, loss of abutment vitality and loss of retention (86, 87).

Table 1.1 Studies details and their reported survival range in years.

Study	Material	Type of Restoration	Type of Study	Place	Sample size	Survival (Years)
(88)	Lava	FPD	Prospective	University	20	1-5
(89)	DC-Zirkon	FPD	Prospective	University	23	2
(90)	Procera (alumina)	Crowns	Prospective	Private practice	205	0.5-5
(91)	IPS e.max	Crowns Inlays	Prospective	University	36 45	2.5-4.6 1.7-5
(92)	IPS Empress 2	FPD	Prospective	University	30	1-2
(93)	In-Ceram Spinell	Crowns	Prospective	University	19	1.2-4
(94)	In-Ceram Alumina	Crowns	Prospective	Not reported	95	2-4

All ceramic systems traditionally comprise coping ceramics and overlying porcelain veneers. Such 'bi-layer' designs lead to several challenges/drawbacks, including multi-step fabrications, different mechanical properties between the two layers and the veneer-coping bond strength (95). The success of all ceramic restorations is largely dependent on the thickness of the underlying coping and the bond between the coping and the overlying veneers. Since the coping is significantly tougher than the overlying ceramic, this bond plays a critical role for their success (96). Optimising the thickness of these two layers is essential to maintain the balance between the generated stresses during mastication. Although it is recommended to increase the thickness of the porcelain

veneer to increase the fracture resistance(97, 98), such increase would not be possible without either over-contouring the restoration; hence interfere with its cleansability, or over-reduction of the underlying tooth preparation (99).

Monolithic ceramics have been developed to overcome some of the drawbacks of all ceramic restorations. However, their microstructures and compositions that provide superior mechanical properties do not tend to provide comparable aesthetics, and vice versa. A more recent approach is to manipulate zirconia by adding translucent additives, to produce an acceptable translucency. However, the chemical inertness of the zirconia and its superior physical properties, make providing a strong and durable cement-zirconia bond quite of a challenge (100).

1.4 Polymer Infiltrated Glass Ceramics Network (PICN)

Polymers with various matrix compositions and different percentages of ceramic and resin fillers are currently available as monolithic blocks for use with CAD/CAM systems. The rational of developing these materials is to provide a material that has better mechanical properties, lower discoloration rates, and higher wear resistance than conventional polymerized polymers. Better manufacturing processes, which consist of high pressures and temperatures, lead to better and more constant restoration qualities. Current CAD/CAM polymer-infiltrated ceramics can be divided into two types: polymer infiltrated glass ceramic and polymer infiltrated polycrystalline.

1.4.1 Polymer Infiltrated Glass Ceramic (Vita Enamic)

An alternative polymer based CAD/CAM material was invented by Dr Russell Giordano in order to improve mechanical and aesthetic properties (101). This material is based on a polymer infiltrated ceramic network (PICN) in which the properties of the resin composite and ceramic are combined. The aim of its development was to form a restorative material with properties similar to enamel and dentine that could be easily repaired. PICN has different nomenclature in published literature, including: hybrid ceramics, resin-ceramic blocks, and ceramic composites. To avoid conflicts with resin composite and for a proper material description, the term PICN has been used throughout the current study.

1.4.1.1 Composition

The mechanical and physical properties of a dental material are largely influenced by its composition and microstructure. In dental ceramic, the microstructure (which is largely ruled by the sintering process) affects a variety of aspects including the coefficient of thermal expansion, chemical solubility and optical properties (102).

Compositional analysis of PICN shows a dominant ceramic-network (86 wt%) (Table 1.2) with a fine-structure feldspar ceramic network interconnected with a polymer-based network (14 wt%). A large amount of carbon is found in the polymer phase. Some micro-cracks are observed between the phases of the materials (103-105).

Table 1.2 Composition of the ceramic part in PICN as provided by the manufacturer.

Chemical compositions	Abbreviation	wt%
Silicon dioxide	SiO_2	58 – 63%
Aluminum oxide	Al_2O_3	20 – 23%
Sodium oxide	Na_2O	9 – 11%
Potassium oxide	K_2O	4 – 6%
Boron trioxide	B_2O_3	0.5 – 2%
Zirconia	ZrO_2	< 1%
Calcium oxide	CaO	< 1%

1.4.1.2 Synthesis and fabrication of PICN

In order to determine the mechanical properties and clinical performance of a material, it is important to understand its microstructural characterization. Scanning electron microscopy (SEM) is commonly used to provide topographic and microstructural information such as particle size and shape. Energy dispersive spectroscopy (EDS) and finite element analysis (FEA) are additional tools that provide more chemical detail (EDS) on the material phases and behaviours (FEA).

The synthesis of PICN requires multiple steps. First, ceramic powder is compressed into blocks and then sintered into a porous network after adjusting the particle size and the firing temperature. Then the pre-sintered ceramic blocks are conditioned with a coupling agent to allow for a chemical adhesion between ceramic and resins. The blocks are then infiltrated with resin polymer network by capillary action followed by subsequent heat induced polymerization (106).

The dominant component in polymer infiltrated porcelain is the feldspar ceramic network (86 wt%) interpenetrated with a copolymer-based network (UDMA and TEGDMA) (103). However, there is little information on the microstructural composition of this material.

1.4.1.3 Mechanical Properties

PICN shares the advantages of resin composites, such as less wear to the opposing natural teeth, the possibility to be repaired and the ability to form chemical bonds with adhesive resin cements (107). *In vitro* studies have shown that PICN has similar flexural strength to dentine but a lower compressive strength (108).

Studies assessing and comparing the mechanical properties of PICN and other restorative materials are debatable (Table 1.3), mostly when flexural strength is evaluated. According to Albero *et al* (2015), PICN showed a flexural value (180.9 MPa) that lay between feldspathic porcelain (Mark II:137.8 MPa) and lithium disilicate (IPS e.max:271.6 MPa) (109). The value was similar to that of nano-ceramic resin composite (Lava Ultimate; 164.3 MPa). Other studies (110, 111) on the other hand have shown greater flexural strength values for nano-ceramic resin in comparison to PICN. Coldea *et al* (2013) also compared PICN with different classes of ceramics. The highest values of 3-point flexural strength were for yttria-stabilized tetragonal zirconia polycrystal (Y-TZP) (1358 MPa), followed by glass-infiltrated alumina-based ceramic (402MPa), lithium disilicate glass–ceramic (344 MPa), PICN (158 MPa) and feldspathic porcelains (Mark II: 137 MPa and VM9: 121 MPa) (106).

Three-point flexural strength followed by Weibull analysis was also conducted by Homaei *et al* (2016). The flexural strength values were 886.9 MPa for Y-TZP, 356.7 MPa for lithium disilicate glass–ceramic and 135.8 MPa for PICN (112). These results were similar to Coldea *et al*., where the greatest values were found for the groups Y-TZP and lithium disilicate glass–ceramic (106, 109, 111). However, for the Weibull modulus PICN showed the greatest value (19.7), suggesting high structural reliability.

Other mechanical properties have been also investigated including fracture toughness, edge strength, wear resistance, and surface damage tolerance (110, 113). Fracture toughness is defined as the critical stress intensity level at which a given flaw starts to grow, and “indicates the ability of a material to resist rapid crack propagation and its consequent catastrophic failure” (83). In other words, fracture toughness provides important information about the brittleness nature of the material used. According to ISO specifications for dental ceramics, “Fracture toughness is an important property since it is

inherent to the material and can be used to predict other properties, such as strength which is sensitive to flaw size and flaw population" (84). The fracture toughness of PICN has been evaluated by Della Bon *et al* (2014) using the single edge V-notch beam (SEVNB) method (ISO6872). The mean value obtained for PICN in that study was 1.51 MPa√m. Compared to other ceramic materials, the fracture toughness value of PICN was greater than feldspathic porcelains (Mark II and VM9) (1 MPa√m), but lower than polycrystalline ceramics such as glass infiltrated alumina based ceramic, litium disilicate, and Y-TZP (3.73, 2.37 and 4.94 MPa √m, respectively) (103).

Vickers hardness has also been evaluated and compared to other ceramics via micro indentation in several studies (106, 109, 112). PICN demonstrates lower hardness values compared to glass ceramics and Y-TZP but greater than nano-ceramic resin composites. These studies indicate that the hardness of values of PICN are similar to dental tissues.

Coldea *et al*. evaluated damage tolerance of PICN1 and a new experimental PICN2 (with a polymer reinforcement phase) using Vickers indentation. PICN materials and other different types of CAD/CAM blocks were tested and seven Vickers indentation loads (1.96, 4.9, 9.81, 19.61, 29.42, 49.03, and 98.07 N) were applied for each bending bar. Three-point Flexural strength values were obtained for each material before and after the indentations. As the indentation load increased, the flexural strength of the materials decreased. At an applied load of 98.07 N, Y-TZP was the material with the highest value of strength degradation (81%), followed by VM9 porcelain(77%), lithium disilicate glass–ceramic (72%), Mark II porcelain (64%),PICN1 (62%), glass-infiltrated alumina-based ceramic (56%) and PICN2 (51%). PICN2 showed the lowest strength degradation. PICN 2 and glass-infiltrated alumina-based ceramic showed flexural strength stability until a Vickers indentation load of 4.9 N. The initial strength of all other materials decreased significantly at the minimum indentation load of 1.96 N. PICN2 showed higher damage tolerance to indentation than lithium disilicate glass ceramic. Thus, introduced flaws by grinding adjustment or chewing are expected to have less effect on the strength of PICN clinically (113).

Table 1.3 Properties of PICN material and their corresponding values and/or range of values, according to the literature.

Mechanical property	Value	Reference
Flexural strength (3-point bending)	213.1 (±59.9) MPa	(107)
Flexural strength (3-point bending)	124 Mpa	(110)
Compressive strength of implant-supported crowns	2386–1935 N	(114)
Compressive strength of zirconia implant-supported crowns	0.22–0.26 kN	(112)
Weibull modulus	4.99	(105)
Weibull modulus	19.7	(112)
Elastic modulus	27.26 GPa	(110)
Elastic modulus	37.95 (±0.34) GPa	(103)
Vickers hardness	1,70 GPa	(109)
Vickers hardness	261.7 Hv	(112)
Fracture toughness	1. 4 MPa $m^{1/2}$	(112)
Fracture toughness	1.09 (±0.05) MPa $m^{1/2}$	(115)
Density	2.0960.01 g/cm^3	(103)
Fatigue resistance of crowns: load 198 N/1.2 millions of cycles 1.6 Hz	No crowns failed	(105)

1.4.1.4 Optical Properties

While dental ceramics and glass ceramics in particular have superior aesthetics and colour stability, CAD/CAM resin composites have better machinability and direct reparability. However, compared to conventional resin composites, contemporary CAD/CAM composites are believed to be generally superior in terms of mechanical properties, owing to the standardised and controlled industrial production wherein the polymerisation process is optimised due to high temperature and pressure.

Studies investigating the optical behaviour of PICN, on the other hand, are relatively limited and debatable. Quek *et al* (2018) investigated the colour (ΔE) and translucency

changes (ΔTP) of PICN and compared it to different CAD/CAM composites after exposure to various staining solutions by using both a spectrophotometer and a shade-matching device. PICN was found to have the least colour stability after being exposed to tea solution. Another study found greater shade differences in both nano-ceramic resin (LU) and PICN than lithium disilicate ceramic (IPS e.max) (116). However, other studies have found that the colour stability of PICN specimens was better than LU specimens after immersion in coffee and red wine, and also found that the residual discoloration values of PICN were smaller than that of LU after a bleaching procedure of these stained specimens (117, 118). In general, it seems that PICN shade stability is similar or relatively better than resin composite but less than dental ceramics.

1.4.1.5 Surface roughness

The quality of surface topography has a great influence on the longevity of any dental material. Surface roughness can affect the success of a restoration on biological and aesthetic levels. A restoration with a rough surface might have poorer aesthetics and can be more prone to plaque accumulation. *In vivo* studies on the threshold surface roughness for bacterial plaque retention have shown that a mean roughness above 0.2 µm is related to a substantial increase in bacterial retention. Not only that but it is also important for a patient comfort to have a restoration with a smooth surface, with a roughness up to 0.3 µm being easily detected by the tip of a patient's tongue .

The surface roughness of different CAD/CAM materials has been evaluated and compared (119). Between ceramics, PICN and resin composites, the rougher material was resin composite, followed by PICN and feldspathic porcelain. In the current literature, surface roughness of PICN materials are evaluated following certain procedures such as cyclic mechanical loading (e.g tooth brushing), different polishing techniques or surface treatments.

Surface roughness of PICN and pressed glass ceramic following 60,000 cycles of tooth brushing under 20 N was previously evaluated (120). PICN showed lower surface roughness change compared to glass ceramic. Other study, showed similar roughness behaviour to natural enamel (121). Under SEM, micro-cracks and pitting defects were detected at the wear facet suggesting fatigue wear which may be attributed to the fact

that PICN is an interpenetrating phase composite with combination of ceramic and polymer(120). Such combination may make the PICN more damage tolerant with some degree of elastic deformations (113).

The type of finishing method has a significant role on the surface roughness of PICN. Different finishing procedures produce different values of surface roughness. The manufacturer of PICN (Vita) suggests 3 different finishing and polishing procedures (Technical Kit, Clinical Kit and VITA Enamic Glaze), which have been evaluated and compared: the greatest surface roughness values are found for Glaze Groups. Clinical Kit and Technical Kit groups did not show a significant difference regarding surface roughness. Thus, it is suggested that the use of the Technical and Clinical Kits can give better performance of the PICN material (122).

The effect of different surface treatments on the surface roughness of PICN materials was also previously investigated. Hydrofluoric acid 10% (HA) and tribochemical silica-coating (TCS) surface treatments produced higher surface roughness than 37% phosphoric acid. Prominent undercuts and honeycomb-shaped surface irregularities were noticed in HA specimens while in TCS specimens, sharply demarcated acute angled surface features caused by spallation of small areas of the glass matrix were detected (123).

1.5 Glass and Polymer-infiltrated Polycrystalline

1.5.1 Introduction

The final properties of ceramic materials are influenced by the amount of crystalline phase, the size and type of crystals, and their dispersion within the glass matrix. In general, increasing the amount of the crystalline phase will lead to better mechanical reinforcement of ceramic materials (124).

Polycrystalline ceramics sometimes referred as 'load-bearing bioinert oxide ceramics', are types of ceramic that demonstrate useful mechanical properties combined with excellent chemical stability and tissue compatibility. Aluminium oxide (alumina, Al_2O_3) or zirconium oxide (ZrO_2) are both common types of polycrystalline ceramics used in dentistry. Being oxides, does not mean that they are subjected to oxidative reactions. In fact, this implies a complete inhibition of the release of cytotoxic ions due to corrosive attacks in the body, thereby providing high biological safety (125). This is why sometimes these are referred as 'bio-ceramics' in the literature.

Despite the current appeal of zirconia, alumina is a technologically important material widely used in numerous applications. It was first introduced in the 1970s (126) and was the first polycrystalline ceramic to be used in dentistry.

1.5.2 Chemical Compositions and Structural Characterization of Alumina

Unlike zirconia, alumina (Al_2O_3) can exist in many multi-stable phases that would irreversibly transform into alpha-alumina when heated up to 1050–1200°C, depending on the crystal properties of the metastable precursors. In nature, alumina exists in its anisotropic crystalline phase of α-Al_2O_3, as corundum or emery if it contains impurities. It also occurs as gemstones (Figure 1.6) with a colour depending on the doping elements (e.g. ruby red due to the presence of chromium, or sapphire blue in different shades due to the presence of Ti^{3+} or Fe^{3+} ions in the lattice) (125).

The crystal structure of alpha-alumina is known to have a close-packed hexagonal arrangement of oxygen ions. In its lattice, each aluminum cation (Al^{3+}) is surrounded by oxygen anions O_2- that form two regular triangles on both sides, twisted by 180° and lying on parallel planes. From the thermodynamic point of view, alpha-alumina is the most

stable aluminum oxide compared to its transient, metastable counterparts. The strong ionic and covalent chemical bonds between Al^{3+} and O^{2-} contribute to the characteristic material properties, such as high melting point; low electric and thermal conductivity; high elastic modulus (stiffness) and hardness; and excellent resistance to the attack of strong inorganic acids, such as orthophosphoric or hydrofluoric acid (125).

Some of the physical properties of alumina can be drawbacks when used in dentistry. The high melting point especially makes it impossible to shape alumina ceramics by casting; high hardness (20–30 GPa) makes machining difficult and costly; and high stiffness (10 times larger modulus than that of dentine) contributes to high elastic mismatch between the natural tooth structure and the prosthetic work (125).

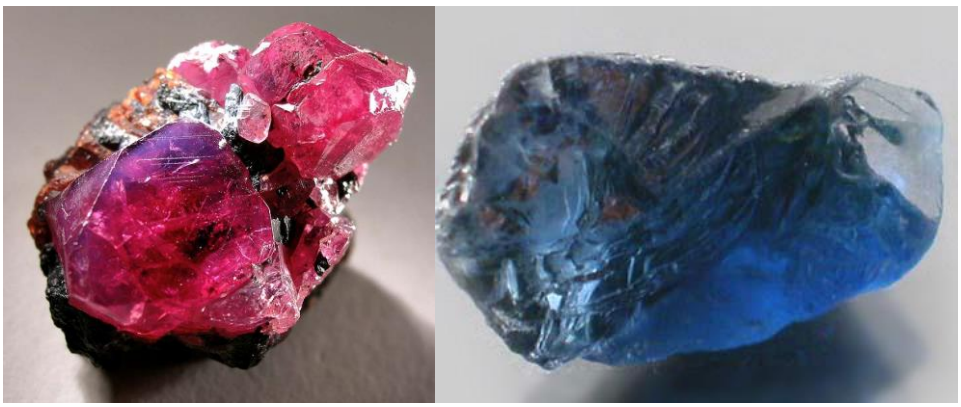

Figure 1.6 Two forms of alumina precursors (Corundum), ruby (left) and sapphire blue (right) depending on the doping elements present.

1.5.3 Physico-Mechanical Properties of Alumina

As a consequence of clinical demands, medical grade alumina has undergone substantial improvements, especially with regards to mechanical properties and reliability. Mechanical improvement involves an increase in the flexural strength (from less than 400 MPa to more than 600 MPa in some medical-grade alumina used in orthopedics). This is because of the many improvements introduced in materials processing (e.g. the selection of raw materials used as precursors, powder processing, sintering, quality control, etc.) (127).

The introduction of high-purity powders and the limit set for the content of calcia, alkali metal oxides, and silica impurities by ISO 6474 in 1980, largely reduced the problem of strength degradation in alumina. CaO, NaO, and SiO_2 play an important role in the mechanical stability of alumina. CaO interaction with the aqueous environment, together with calcium migration and segregation, is responsible for strength degradation (128, 129). While SiO_2 indirectly increases the risk of fatigue fracture by hindering densification and promoting grain growth during sintering (130). Moreover, silica and alkalis (e.g. NaO) can segregate at grain boundaries, and their dissolution in physiologic liquids may lead to accelerated fatigue fracture (131). For the same reason, MgO added to alumina as a sintered additive to enhance densification while preventing discontinuous grain growth, has to be tuned to avoid deleterious excessive formation of Al_3MgO_4 spinel.

Alumina can be used as pure polycrystalline material or can be prepared and applied in a variety of forms and microstructure, such as fillers to reinforce porcelain and composite resin, or as matrix for interpenetrating-phase composites. Alumina composites can be made with metals, glass, polymers and other ceramics such as zirconia (126).

Mclean and Hughes in 1965 published the first study describing the concept of reinforcing a porcelain veneer with an alumina substructure. The aluminous core was a mixture of 50 wt% Al_2O_3 and silica that was fired and covered with a porcelain veneer to achieve optimum aesthetics. However, the flexural strength of this core material was low (approximately 131 MPa) which limited its application for anterior teeth (132).

Another application of alumina in dentistry is the Procera-allCeram system which was developed by Andersson and Oden in 1993. These restorations were composed of a

densely sintered, high purity aluminum oxide (Al_2O_3) (more than 99.9%) veneered with a compatible low-fusing dental porcelain. They were sintered up to 1600 °C after milling to achieve full density; however, it was associated with 15 - 20% shrinkage. The material had high opacity and flexural strength was reported to be approximately 600 MPa which made it suitable for single crowns and short span posterior fixed partial dentures (133).

In-Ceram is another alumina dental application which was first introduced in 1989 by the French dental material scientist Michael Sadoun (134) . This system was based on glass (68 vol%) infiltration of a partially sintered porous aluminum oxide matrix (27 vol%). This material showed reliable clinical outcomes for applications as single posterior crowns and short span bridges in the anterior region of the mouth (105, 135). In terms of flexural strength, it is found to be relatively stronger than pressed ceramics with a value of 548 MPa and a survival rate similar to PFM crowns placed in anterior teeth and premolars (135-137). At least eight clinical trials lasting between 5 and 7 years reported a success rate of 91.5 - 100 % for In-Ceram alumina; however, it has never been highly marketed (138). This glass infiltrated ceramic composite showed lower hardness, lower elastic modulus and higher fracture toughness than pure polycrystalline alumina (139).

1.5.4 Optical Properties

When considering aesthetics, all-ceramic restorations have the advantages of increased translucency as well as superior aesthetics. Heffernan *et al* evaluated the relative translucency of several ceramic materials and found that the addition of $MgAl_2O_4$ to the In-Ceram system (In-Ceram Spinell -VITA Zahnfabrik) resulted in a material with the highest amount of relative translucency (84). This was followed by IPS Empress (Ivoclar Vivadent), Procera (Nobel Biocare AB), and IPS Empress 2 (Ivoclar Vivadent) which had higher levels of translucency than In-Ceram Alumina (VITA Zahnfabrik), followed by In-Ceram Zirconia (VITA Zahnfabrik), which was comparable to a metal alloy. Therefore, In-Ceram Spinell, IPS Empress, and IPS Empress 2 were recommended for moderate to high translucency situations. Procera was recommended for average translucency situations, while In-Ceram Alumina and In-Ceram Zirconia were only recommended when matching to opaque natural teeth or in posterior and non-aesthetic zones.

In an attempt to improve the translucency, Yoshimura *et al*. described an approach to increase the translucency of In-Ceram alumina by 20.1 %. The approach was based on designing the glass composition for targeted glass viscosity and refractive index using a computer software and then infiltrating into porous alumina preform at 1200 ˚C (140).

1.5.5 Synthesis and Fabrication of Polymer Infiltrated Alumina

Most recent studies have compared the commercially available polymer infiltrated porcelain or glass infiltrated alumina with other CAD/CAM restorative materials. However, experimental attempts to utilize alumina as a matrix for polymer infiltration has received very limited focus. A few medical reports on the mechanical and osteo-conductivity of Bis-GMA composites have shown superior mechanical properties (126).

In dentistry, only a few studies have been conducted to develop polymer infiltrated alumina ceramics and study their properties. Chaiyabutr *et al* examined the effects of alumina particle size and sintered density on biaxial flexural strength and fracture toughness of glass and UDMA and TEGDMA polymer infiltrated matrices. They used three different alumina powders with different particle sizes (0.3-1.2 μm) (141). The findings of their study showed that reducing the particle size improved the sintered density and the

mechanical properties. They also found that increasing the sintering temperature lead to superior mechanical properties with less percent of porosities.

Craig and Francis (1998) described a method of developing a chemical bond between alumina particles using ortho-phosphoric acid that was later infused with epoxy resin polymer creating an interpenetrating phase composite (IPC) microstructure (142). This chemical bonding route developed at a temperature of 900 °C lower than that commonly used for partially sintered alumina. Aluminum chloride was also added to enhance the interaction between alumina and phosphoric acid and lead to the formation of stronger bonds at lower sintering temperatures. The open porosity in the ceramic composite decreased as the amount of phosphoric acid used in the process increased.

Kim *et al* (2012) also developed polymer-infiltrated alumina using photo-polymerised polyurethane acrylate (PUA) as an infiltrated polymer (143). The fabrication process was started with preparing the green body of ceramic matrix by a uniaxial pressing process using Al_2O_3 powder, which was then partially sintered at 1000°C for 1 h. At room temperature, a mixed polymer was infiltrated into the Al_2O_3 matrix in a vacuum chamber to allow homogeneous infiltration into all pores of ceramic matrix. The polymerisation of the polymer-infiltrated matrix was then carried out by UV light (1.5 mW/cm^2, 365 nm) for 3 min. The findings of that study confirmed that the composition ratio of resin had a significant positive effect on fracture strength and elastic modulus that were higher for polymer infiltrated alumina samples with higher resin/ceramic composition ratio.

The effects of the application of pressure and heating rate (fast and slow) during polymerization on the mechanical properties of UDMA-TEGDMA resin infiltrated alumina has been previously studied (139). A fabricated alumina matrix was infiltrated with resin and subjected to thermal polymerization with and without pressure and at heating rate of 0.1°C /min (slow) or 2 °C /min (fast). The heating rate was found to only have a significant effect on flexural strength when pressure was not used during polymerization. The slower heating rate resulted in better flexural strength. On the other hand, the pressure applied during polymerization led to higher strength of these PICNs compared to those which were polymerised without pressure.

1.6 Physico-mechanical Properties of Polymer-infiltrated Ceramics

1.6.1 Flexural Strength

Flexural strength can be defined as the maximum surface stress in a bent bar or a disc at the moment of failure (144). For a bar specimen, the failure stress value is referred to as three or four-point flexural strength while for the disc sample it is biaxial flexural strength (Figure 1.7). Three-point flexural strength can be calculated using the following equation:

$$\sigma = \frac{3PL}{2wt^2}$$

While the four-point flexural strength can be obtained via:

$$\sigma = \frac{3PL}{4wt^2}$$

Where:

$\boldsymbol{\sigma}$ = flexural strength

P= total applied load

L= distance between lower supports

w= width of specimen

t= thickness or height of specimen

One limitation of the three-point flexural test is that if the bar specimen does not fracture at the midpoint directly under the applied load, a correction must be made to calculate the fracture stress at the actual fracture location. Another limitation is undesirable edge failure, which may lead to an error in strength measurements(145).

The four-point flexural strength is preferred over the three-point test because the stress within the central loading span of the specimen is constant. Therefore, no correction is required if the fracture does not occur precisely at the midpoint. Hammant (1971) (146) stated that the four-point flexure test generates a uniform stress field along the surface and reduces the stress concentration near the loading midpoint. However, this test has not been used as frequently used as the three-point flexure test. This may be due to its

experimental difficulties and complex test fixture(147). In addition, the requirement of large specimen geometry is not representative of a restoration placed clinically.

The biaxial flexural test is preferred by some scientists to avoid the problem of edge fracture(145). This test is commonly used for the evaluation of flexural strength in dental ceramics (148, 149). It is based on a piston-on-three-balls design wherein the load is applied by means of a piston with a slightly curved contact surface and the disc specimen is supported by three steel balls. The main advantage of this test is that the maximum tensile stress occurs within the central loading area and the problem of edge fracture from the three-point test is eliminated. Also, the required diameter of the specimen in this test (12-15mm) represents the average width of molar teeth which makes the test more clinically relevant when compared to three or four- point flexural strength tests (4).

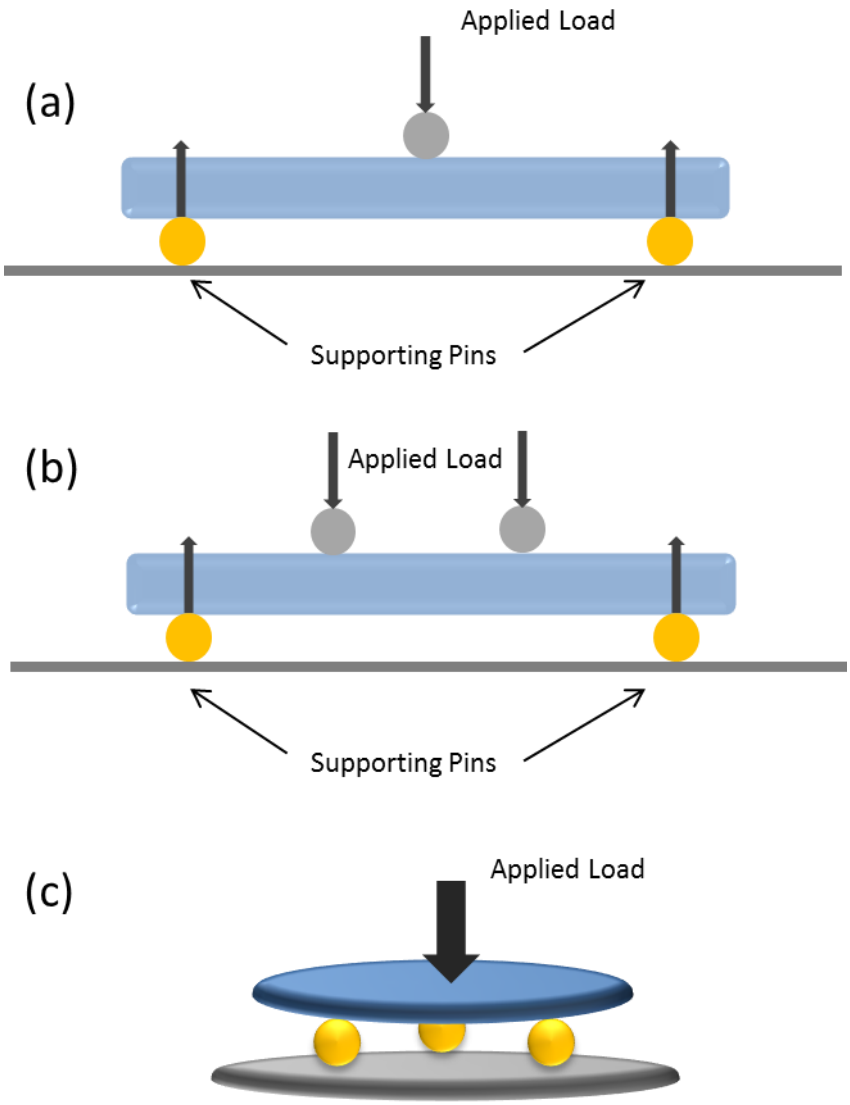

Figure 1.7 Different flexural strength test sets a) 3-point flexural strength b) 4-point flexural strength test c) biaxial flexural strength test.

1.6.2 Hardness

Hardness is defined as the resistance of a material to plastic deformation, usually indentation. However, it can be obtained through scratch, cutting, abrasion or bending tests. Hardness by indentation can be measured at different scales; macro, micro and more recently nano-scale. Measuring the hardness at macro scale is quick, simple and can give general mechanical information about the bulk material. However, when it comes to surface features relating to important properties of dental materials such as wear processes, such a scale is too large. Smaller scales such as micro and nano are usually employed when examining the mechanical properties of dental materials. There are several types of surface hardness tests and these are commonly classified into two types: macro-indentation tests (load > 1 kg) and micro-indentation tests (load < 1 kg). Micro-indentation is used in determining the hardness of dental restorative materials and is available using different shapes and loads depending on the material being tested. Examples of these are: Barcol, Brinell, Rockwell, Shore, Vickers and Knop. Vickers and Knoop indentations are the most commonly used in restorative dentistry. Hardness can be measured by dividing the applied force by the indentation area after force removal (37, 150).

1.6.2.1 Micro hardness

Micro indentation tests are commonly used in comparative studies of dental materials. Vickers diamond pyramid or Knoop elongated diamond pyramid are the types of intenders that are mostly used in the mechanical evaluation of dental restorative materials. In these tests, the indentation area is measured under a microscope to calculate the hardness at a prescribed load.

1.6.2.2 Nano indentation:

Recently new sensors and actuators allow indentation testing to be performed at submicron scales. This technique is called nano indentation and has been popular in investigating the mechanical properties of many materials such as, polymers, metals, glasses and ceramics. By use of such technique, progress has been achieved in mechanical

testing particularly in terms of control, sensitivity and data collection. The most common properties tested via nano indentation are hardness and modulus of elasticity.

During a typical nano indentation examination, a diamond indenter of a known geometry and dimension is pushed toward the surface of a tested material with a prescribed loading and unloading profile, and the penetration depth as well as the applied load are recorded. The data is then presented in the form of a load (P)-displacement (h) curve (sometimes called a *P-h curve*) (Figure 1.8). To calculate hardness, the load is divided by the contact area, which is determined by the geometry of the indenter. The elastic modulus (S) is measured from the slope of the upper portion of the unloading curve(151).

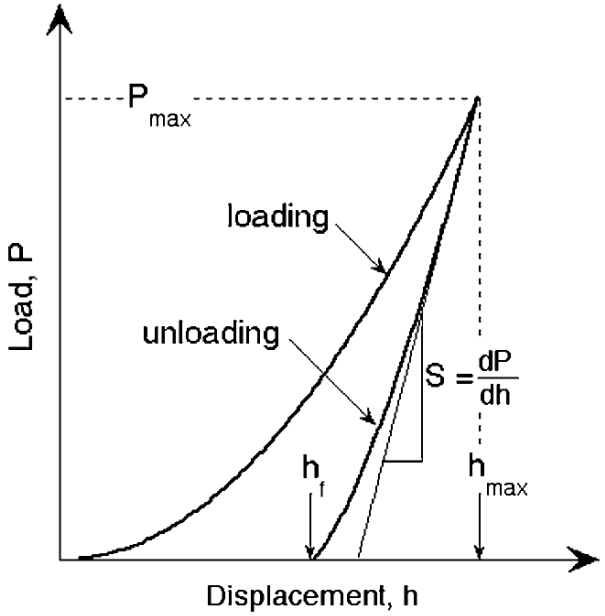

Figure 1.8 Schematic illustration of nanoindentation load-displacement curve with measured parameters. *Reproduced with permission from Journal of Materials Research* (152).

Another viscoelastic property called *creep* can be calculated from the load-displacement curve as shown in Figure 1.9. Creep shows the tendency of a solid material to move slowly or deform permanently when subjected to mechanical stresses. In nano indentation the tested specimen is gradually loaded until the pre-prescribed load is reached and held for a pre-set holding time (in seconds) to creep. The load is then gradually removed until the minimum load at which the indenter is held for another holding time to allow recovery (151).

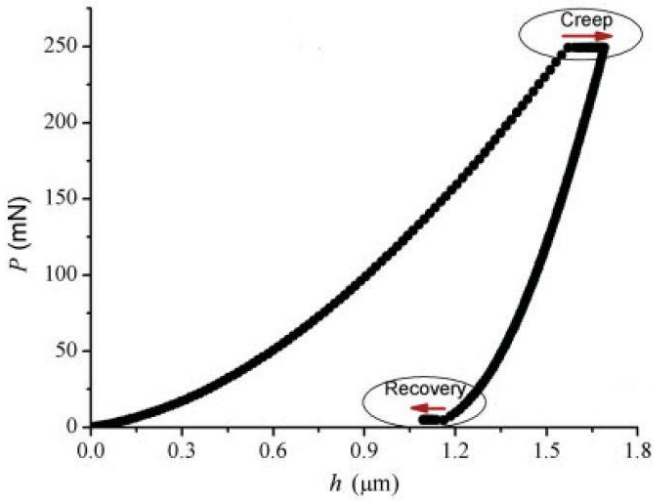

Figure 1.9 Typical load-displacement curve of nano indentation loading/unloading method showing the measurements of creep and recovery during the maximum load and the minimum load, respectively. *Reproduced with permission from Materials* (153).

1.6.3 Surface Roughness and Gloss

Surface roughness is defined as relatively finely spaced surface irregularities whose height, width and direction establish the predominant surface pattern. In dental materials, the surface properties are critical for their success, since they mediate the interaction of restorative materials with the oral environment. The shape, sharpness, size, the depth of the surface flaws and internal defects determines the mechanical and optical properties of any restorative material.

Surface roughness is a widely studied mechanical property. It has significant biological, mechanical and optical effects. Biological effects include plaque accumulation, gingival irritation, abrasion and increased wear of antagonists (154). Moreover, smooth surface reduce secondary caries(155), assists oral hygiene (156) and adds to the patient's comfort(157).

Surface roughness also affects the colour stability of a restoration; exterior discolouration increases as the surface roughness increases. Mechanical properties such as biaxial flexural strength, Vickers hardness, and elastic modulus have been found to be negatively associated with the average surface roughness profile.

Surface gloss is another factor playing an important role on aesthetic of composite resins. Gloss is a desirable characteristic for restorative materials as it mimics the appearance of

the enamel. More over glossy and smooth surfaces decrease the coefficient of friction and subsequently this may reduce the wear rate.

Various method and instruments can be used to measure the surface roughness of a restoration. These include qualitative such as visual inspections and surface finish comparison plates; or quantitative such as instruments with contact and non-contact measuring gauges. Contact methods involve running a measurement stylus across the surface; these instruments are called profilometers. Non-contact methods include: interferometry, laser triangulation, confocal chromatic aberration and atomic force microscopy.

1.6.3.1 Surface roughness parameters

Various measurements of surface roughness can be obtained. A roughness value can either be calculated on a 2D or 3D profiles. The 2D profile roughness parameter (Ra, Rq,...) are more common than area roughness parameters (Sa, Sq,..etc). The arithmetic average height measurement (Ra) is frequently used as a universal roughness parameter for general quality control (Gadelmawla *et al*, 2002). Other less commonly reported parameters include maximum valley depth (Rv), maximum peak height (Rp), and root mean square (Rq) (Figure 1.10).

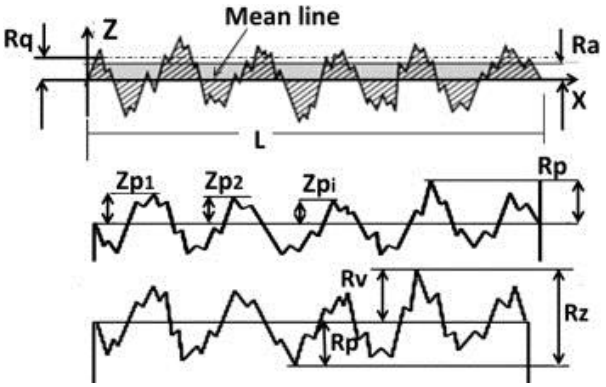

Figure 1.10 Details of the 2D surface roughness parameters. *Reproduced with permission from Wear* (158)**.**

1.6.4 Water Sorption and Solubility

Sorption by definition is a physical and chemical process in which one substance becomes attached to another. In terms of water sorption, it represents the amount of water adsorbed on to a surface or absorbed within the body of a material. In dental composite, the water sorption occurs by direct absorption into the polymeric resin matrix (Figure 1.11), whereas in glass fillers, water is only adsorbed on their surfaces.

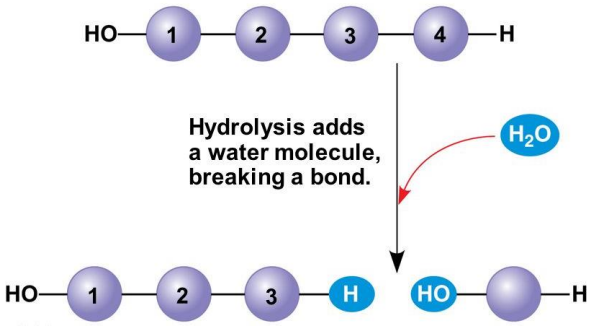

Figure 1.11 Hydrolysis- breaking down of polymer.

Ideally, a polymer-network should be insoluble with relatively high chemical and thermal stability. However, this is not the case for most monomers used in restorative dentistry. They can absorb water and chemicals from the environment, and release components into the surrounding environment. As water interacts with the polymer chains, it may produce some of the following effects in this order: (i) reorientation and chain displacement, i.e., reversible loosening or effective plasticization of the structure; (ii) solvation or reversible rupture of weak interchain bonds; (iii) irreversible disruption of the polymer matrix (microvoids) (159). Water molecules tend to penetrate the macromolecules of a material, force them apart which may then affect its dimensional stability and the durability.

Water sorption is a critical problem that affects the durability of most polymer-based restorative materials. A variety of undesirable outcomes can ensue including, hydrolysis-breaking down of bonds and interface leading to monomer elution (160-162), hygroscopic expansion (163, 164), deterioration of mechanical properties (165-167), stress and micro cracking (163, 164), and discolouration (168). In addition, water sorption may cause polymer plasticization reducing the hardness, wear resistance and its glass transition temperature whilst increasing the creep.

Therefore the water sorption and solubility of polymer-based restorative materials should be as low as possible (169). According to ISO 4049, a material is considered to be suitable as a restorative material when the water sorption is less than or equal to 40 μg/mm3 and the solubility is less than or equal to 7.5 μg/mm3 (170).

1.6.5 Imaging and Nano-mechanics

1.6.5.1 Scanning Electron Microscopy (SEM)

SEM, with its analytical features, has become a very powerful tool in studying the microstructures of ceramics in dentistry. Its analysis provides information about the shape and distribution of glassy and crystalline phases present (171). Studying the microstructure of ceramic materials plays a fundamental role in investigating what raw materials were used and how the ceramic was processed. Not only that, but also SEM analysis acts as a source of predicting or understanding some useful and important properties (172).

1.6.5.2 Components and Working Principle of SEM

Basically, there are key components (Figure 1.12) that are required for SEM machine and these include:

1. An electron source to generate high-energy electrons and it is called (electron gun).
2. A column with a series of condenser lenses.
3. Scanning coils deflection system
4. Detectors of backscattered and secondary electrons.
5. A chamber for the specimen.
6. Computer with an output monitor to display and analyse the scanned images.

A scanning electron microscope (SEM) uses a focused beam of high-energy electrons to generate a variety of signals at the surface of solid specimens. These signals are then detected via a secondary electron detector to provide information about the scanned specimen including external morphology (texture), chemical composition, and crystalline structure and orientation of materials making up the sample. A two-dimensional image is generated that represents spatial variations in these properties.

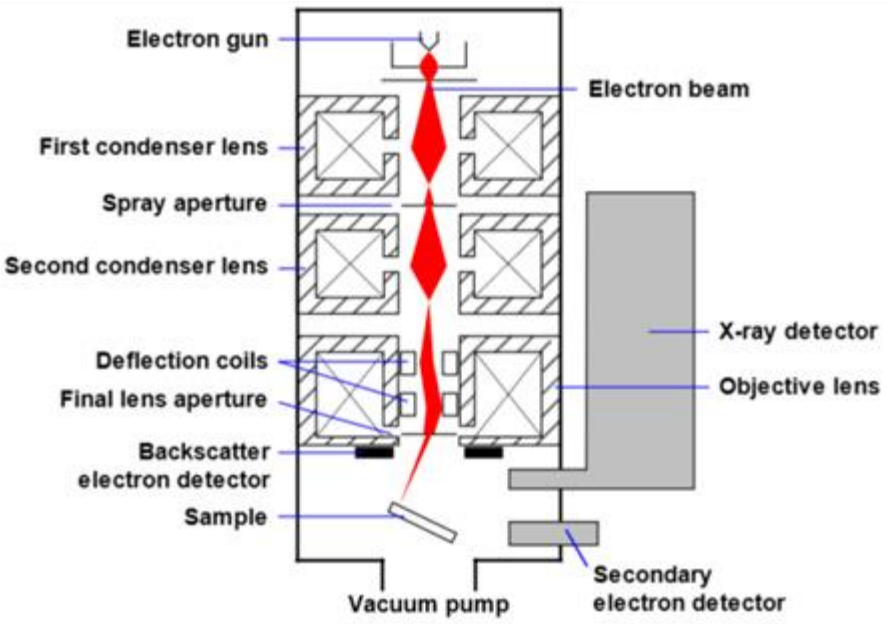

Figure 1.12 Basic work principle of SEM.

1.6.6 Atomic Force Microscopy (AFM) and Nano mechanics

- ***Background***

The progress of material science is underlain by a continual increase of our interactions with the surrounding physical environment. As knowledge has evolved, the critical length of cutting-edge of functional devices has shifted from the macro- to micro- scale and increasingly into nanoscale. With the scientific ability to control physical processes at nanometer scale, we have entered the era of nanomechanics. Following the micro to nano shift, material properties are often significantly altered in a scale at which critical differences are usually found.

Throughout history, many fields of science have throughout history rapidly made advantage of tools and techniques that allowed for the design of material properties at a finer scale. In dentistry, it is possible now to study, control and manipulate structures at nano scale. Atomic force microscopy (AFM) is a key method for studying the surface topography of any material in real time with no or minimal surface preparation. It allows high-level resolution imaging of a surface at a very high magnification; up to 10^8 and resolution of 0.1 nm in the x, y, and 0.01 nm axes in the z axis. It requires minimal

preparation of the sample and is still capable of evaluating the surface 3 dimensionally with a very small probe that follows the surface profile (173, 174).

AFM is a form scanning probe microscopy (SPM) that gathers information about a test specimen by probing its surface. Unlike SEM, AFM not only images the sample but also provides further quantitative information including dimensions, profile, roughness and periodicity. Moreover, because of the mechanism of imaging formation employed, there is no need for staining, dehydration, coating or working in a vacuum environment (174, 175). AFM can work in different environments (e.g. air, liquid or vacuum) regardless of conductive or optical properties of the sample. Table 1.4 presents main characteristics AFM compared to SEM and transmission electron microscopy (TEM).

Table 1.4 Comparison of Atomic Force Microscopy (AFM), Scanning electron microscopy (SEM) and Transmission electron microscopy (TEM) main characteristics. Adapted from Eaton and West (176).

	AFM	SEM	TEM
Sample type	Conductive/non-conductive	Conductive	Conductive
Sample preparation	Easy or none	Easy/difficult	Easy/difficult
Sample environment	Any	Vacuum/Gas	Vacuum
Horizontal resolution	0.1 nm	5 nm	0.1 nm
Vertical resolution	0.05 nm	NA	NA
Depth of field	Poor	Good	Poor
Imaging time	2 - 5 min	0.1 - 1 min	0.1 - 1 min
Maximum field of view	100 µm	1 mm	100 nm
Maximum sample size	Unlimited	30 mm	2 mm

- ***AFM Configuration***

An AFM uses a cantilever with a very sharp tip to scan a sample surface (Figure 1.13). As the tip approaches the surface, different modes of action occur upon initial selection. However, a common feature of all these modes is the method of image creation. The image is created as a result of measuring the forces occurring between the probe of the cantilever and the surface investigated. The probe is connected to the cantilever that is

bend under the influence of interatomic forces. Deflection of the cantilever is processed by the photodetector for a current signal, which allows obtaining a surface image of the sample. Due to the specificity of surface imaging, AFM is effective for virtually all groups of ceramic materials. This method is not limited by the mechanical, optical, or electrical properties of the materials (177-180).

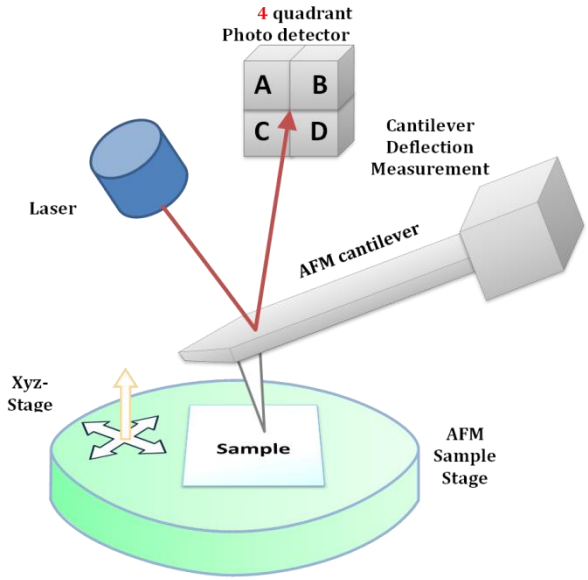

Figure 1.13 Basic work principle of AFM.

AFM Operational and Control Modes

There are several operational techniques in atomic force microscopy. They differ in the interacting force probe-sample aiming to characterise materials. Typically, the cantilever systems in AFM are operated in three different modes i) non-contact ii) contact and iii) tapping modes. For studying the nanomechanics, peak force mode or more recently peak force quantitative nanomechanics) are often employed where the AFM tip act as force-controlled nanoindentor(181). The following paragraphs explain each mode in brief.

Contact Mode

In this mode, also known as constant mode, the cantilever tip directly and continually touches the sample surface at a pre-set constant force (Figure 1.14-a). The cantilever deflection is kept constant while scanning the sample by the feedback loop. Image contrast depends on the applied force which depends on the cantilever spring constant. Softer cantilevers are often used for softer samples and vice versa. The drawback of this mode is that as the tip is in permanent contact with the surface while scanning; a

considerable shear force can be generated, causing sample damage, especially on very soft specimens, such as biomolecules or living cells(182).

Non-contact Mode

In this mode, the tip is in close proximity (without touching) with the sample and the attractive inter-atomic forces are detected and measured while scanning the surface (Figure 1.14-b). Images are taken by keeping a constant frequency shift during scanning, and this is performed by monitoring the pre-set amplitude of the cantilever oscillation at a fixed frequency and feeding the corresponding value to the feedback loop. The tip sample interactions are very small in non-contact mode, and good vertical resolutions can be achieved, whereas lateral resolution is lower than in other operating modes. Two major disadvantages of this mode are that it cannot be conducted in a liquid environment or even in air as there is a risk of the tip becoming trapped in the sample surface if a layer of liquid is still present. This is due to the low energy used to oscillate the cantilever in this mode(182).

Tapping Mode

This mode is considered as a key advance in AFM technology. In this mode, a high resolution imaging of samples that are difficult to examine using the contact AFM mode can be obtained. Problems such as friction and adhesion that are usually associated with conventional AFM imaging systems can be overcome. In this mode, the cantilever is oscillated at or near its natural resonant frequency using a piezoelectric actuator (Figure 1.14-c). The piezoelectric actuator applies a force on the cantilever base and causes the cantilever tip to vibrate at amplitudes which are typically in the range of 20–100 nm when the tip is not in contact with the surface. The vibrating tip is then moved close to the sample until it begins to lightly tap the surface. During scanning, the probe tip alternately touches the surface and lifts off at frequencies of about 50–500 Hertz. Owing to the energy losses caused by the intermittent contact of the tip with the surface, the amplitude of vibration changes according to the surface topography of the sample(182).

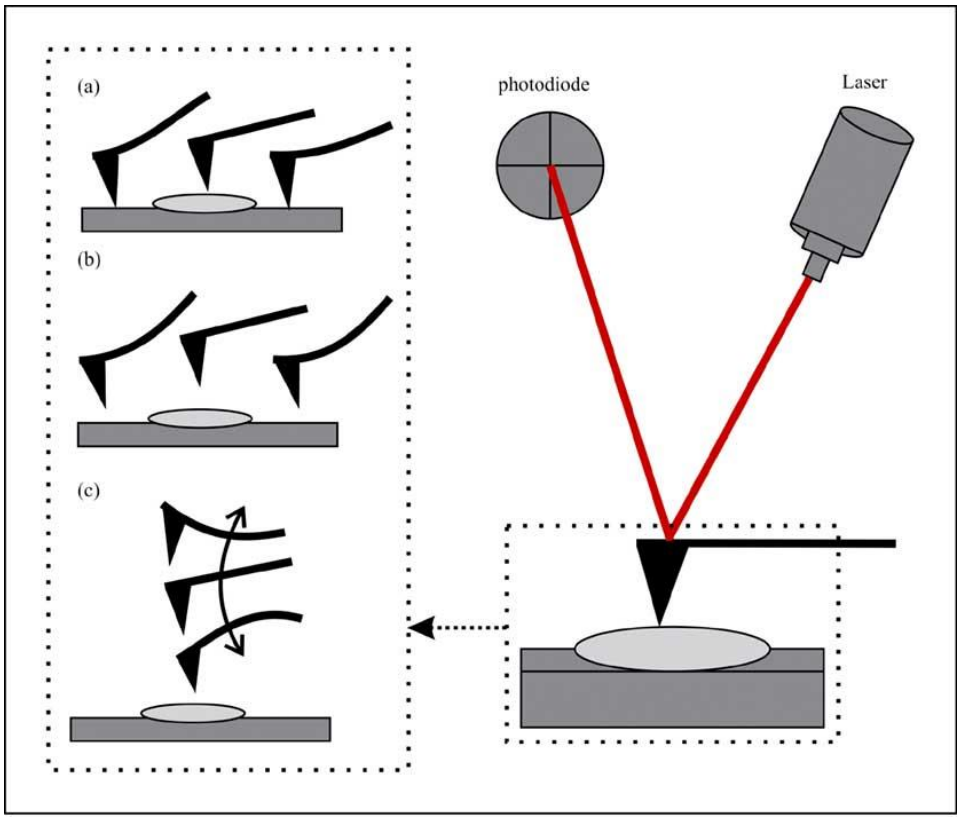

Figure 1.14 Working modes of AFM (a) contact mode (b) non-contact mode (c) tapping mode.

Peak Force Quantitative Nano-mechanical Mapping (PFQNM)

PFQNM is a new AFM mode launched by Bruker that uses tapping mode technology to record very fast force response curves at every pixel in the image, and uses the peak tip-sample interaction force as the feedback mechanism. PFQNM is able to acquire and analyse the individual force curves from each tap that occurs simultaneously while imaging the sample topography at high resolution. In addition, by maintaining control of direct force at a very low level (pN), this mode of scanning can limit indentation depths to deliver a non-destructive and high-resolution imaging technique to sensitive samples. Furthermore, material properties can be characterized over a very wide range to address samples in many different research areas. The advantage of this technique is that a high resolution mapping of nanomechanical properties can be achieved at a very high speed. In addition, it includes wide operating range for test samples, from extremely soft materials to very stiff metals (183).

1.7 Summary and Statement of The Problem

With the continuous introduction of new materials in dentistry, characterisation of material properties acts as a bridge between material sciences and clinical application and evaluation. The use of hybrid materials such as PICN to replace damaged or lost tooth structures is progressively increasing. The success of these materials in different applications is understood through clinical performance and experimental evaluation.

Fabrication of new interpenetrating phase polycrystalline ceramics with optimal mechanical properties and aesthetics is an area of ongoing research with published studies showing initial promising results regarding the mechanical properties, although no data is available in the published literature about their optical properties. Moreover, while the implication of nano-mechanics to the dental field for characterising the mechanical properties of tooth structures and dental materials has become popular, there is no information available in the literature about the nano-mechanics of polymer infiltrated polycrystalline ceramics. Therefore, more research is needed to be conducted in order to develop better restorative materials that fulfil the demand of fast growing CAD/CAM technology and the increasing interest in aesthetic solutions.

Chapter 2

General Aims and Objectives

The aim of this study was to characterize the physico-mechanical properties of fabricated PICN materials and to investigate their suitability as CAD/CAM based dental restorative material on the basis of comparative *in vitro* studies.

The specific objectives of this study were:

- To synthesize and fabricate interpenetrating-phase alumina composites at different temperatures with different densities.
- To investigate the effect of sintering temperature on the flexural strength and optical properties of PICN model materials.
- To investigate the elastic and viscoelastic properties of PICN and other CAD/CAM materials.
- To investigate the effect of microstructural compositions on the surface roughness and gloss of PICN and other CAD/CAM materials.
- To assess the water sorption and solubility of PICN and other CAD/CAM materials

A systematic approach of testing was followed to address the knowledge gap identified in this research. Five major *in vitro* experiments were performed according to the diagram shown in (Figure 2.1).

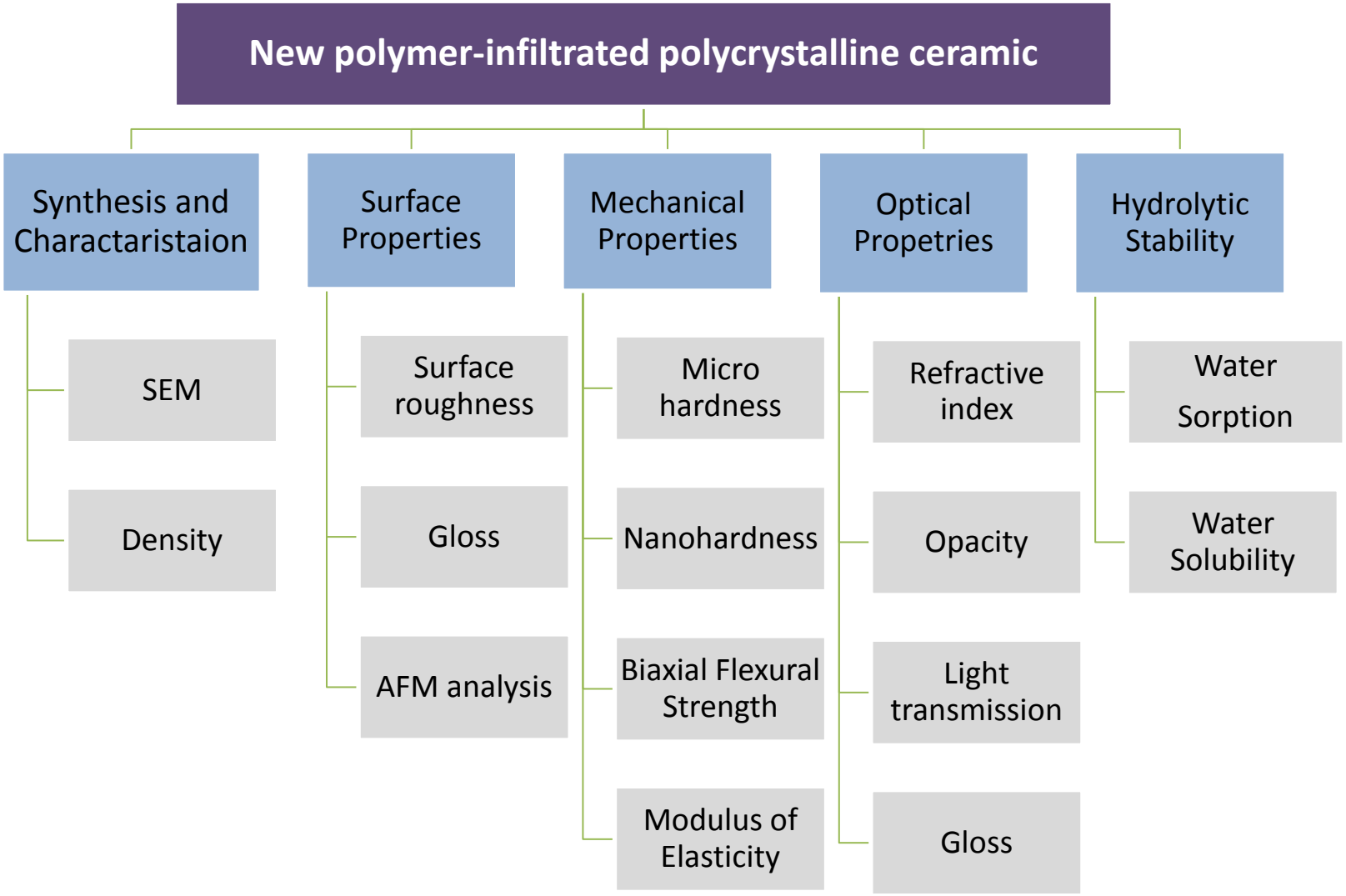

Figure 2.1 General outline of the present study.

Chapter 3

General Methodolgy

3.1 Introduction

Five *in vitro* studies were carried out in this research using a variety of standard techniques. The methodologies and techniques employed in each study are described in their respective chapters, however, a more detailed description of the procedures are included in this chapter.

3.2 Assessment of the effect of sintering temperature of PICN on physical and optical properties

3.2.1 Fabrication of PICN

3.2.1.1 Fabrication of Ceramic Matrix:

3.2.1.1.1 Slip Casting Technique

Fabrication of ceramic was made using the slip cast technique. The slip cast mix was prepared from 155 g of reverse osmosis (RO) water, 3.25 g of Darvan C-N (ammonium polymethacrylate) dispersing agent and 500 g of alumina powder (Aluminum oxide Al_2O_3,Al16SG, Almatis Inc., Leetsdale, PA)(Table 3.1) which was divided into 5 equal increments, added to liquid ingredients and then mixed at 2,000 RPM for 30 seconds using high speed GyroMixer to obtain a slurry mixture. The slurry mixture was then dispensed via a mechanical pipette (100-1000 μL, Pipetman, Gilson Inc., Middleton, WI) into cylindrical plastic moulds (with internal diameter of 15 mm and height of 20 mm) on a gypsum plate that was coated with a thin layer of alginate solution (Protanal 1816, FMC BioPolymer, Philadelphia, PA) (Figure 3.1). The alginate solution was made by mixing 1.5 g of alginate and 100 ml of water. The molds were then covered with a tissue paper and left on the bench at room temperature to be dried overnight.

On the next day, the specimens were gently removed from the moulds and bisque fired in a furnace (Ney Vulcan 3-1750, Dentsply NeyTech, Yucaipa, CA) at a heating rate of 5 °C/min and a holding time of 2 hours at 1050 °C to facilitate ease of handling afterwards (Figure 3.2).

A total of 80 samples were fabricated and divided randomly into four groups (Exp125-Exp130-Exp135-Exp155) according to their sintering temperatures. Specimens from each group (n=20) were sequentially smoothed with sandpapers up to 600 grit and checked under a light microscope to ensure no surface flaws or defects. Then all the specimens were labelled with an HB pencil.

Table 3.1 Chemical compositions and physical properties of the Alumina (Al16 SG) used in the current study as provided by the manufacturer.

	Al16 SG		
Compositions	Min	Max	Typical
Al_2O_3			99.8
Na_2O		0.1	.07
Fe_2O_3		0.03	.02
MgO		0.06	.05
SiO_2		0.05	0.03
CaO		0.05	0.02
B_2O_3		0.006	<0.005
Physical Properties			
Surface Area BET (m^2/g)	7	11.5	8.9
Wet -325 Mesh Sieve (%)	99.4		99.6
Cilas d90 (µm)		2.9	2.00
Cilas d50 (µm)	0.3	0.65	0.5
Ceramic Properties			
Green Density (g/cc)	2.15	2.25	2.17
Fired Density (g/cc)	3.88		3.89
Shrinkage (%)	17	18.5	17.7

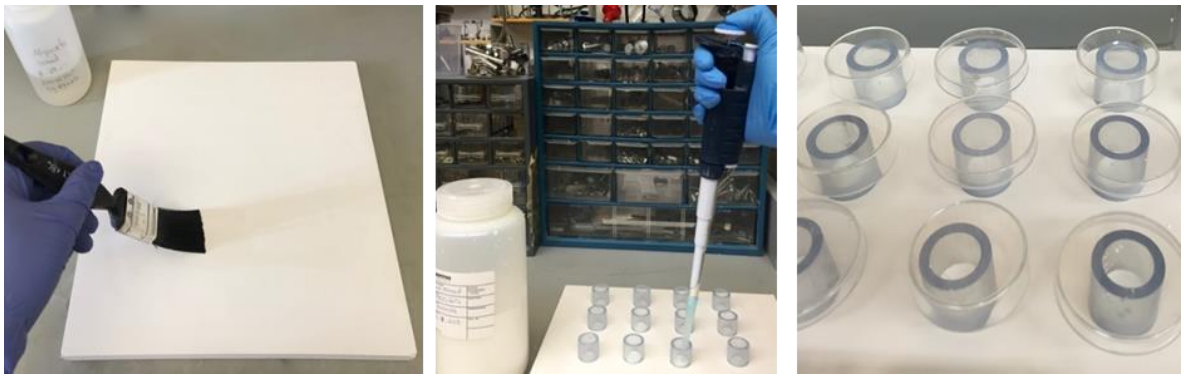

Figure 3.1 Slip casting alumina matrices. The gypsum board was coated with alginate (left). The slurry mixture was then dispensed into cylindrical moulds with pipette (middle). Specimens were covered to be dried overnight (right).

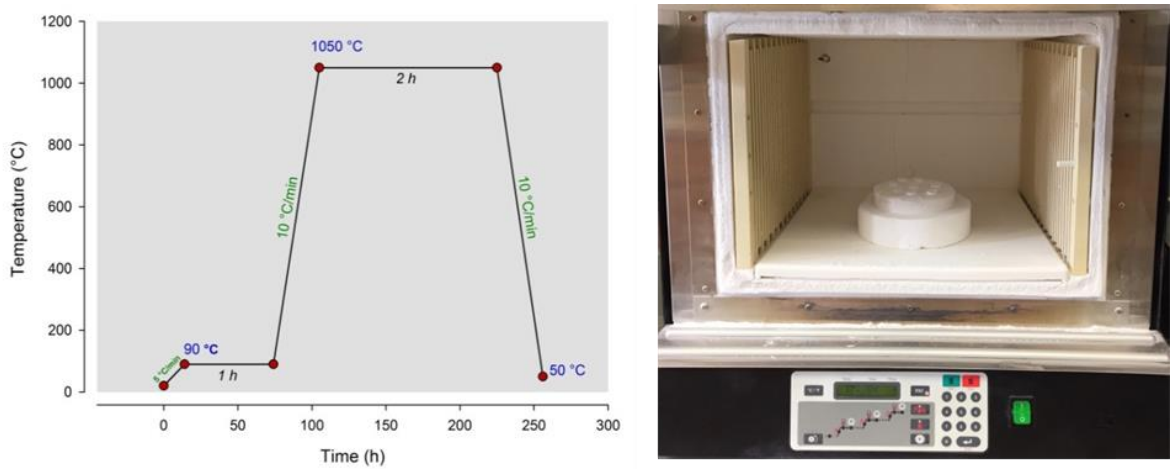

Figure 3.2 Temperature, time and heating rate settings for bisque firing (left). Ney Vulcan furnace was used for bisque firing of alumina matrix (right).

3.2.1.1.2 Partial Sintering of Matrix Specimens

All the alumina specimens were partially sintered in a high temperature furnace (Hot Spot 110, Zircar Zirconia Inc., Florida, NY) at the relevant temperatures for the allocated group (Figure 3.3). The temperature required to achieve a particular density of the matrix specimens for each group was determined previously via a temperature-density curve (Appendix III).

- First Group (Exp125) was sintered at 1250 °C.
- Second group (Exp130) was sintered at 1300 °C.
- Third Group (Exp135) was sintered at 1350 °C.
- Fourth Group (Exp155) was sintered at 1550 °C.

The sintering cycle was programmed to start with a heating rate of 10°C/min, then a holding time of 4 hours at the specified sintering temperature for each group and finally

cooling down with the same heating rate until 50 °C(Figure 3.4). The specimen was then removed from the furnace and let it to further cool down at room temperature. Each specimen was then sequentially finished and polished (up to 800 grit) to achieve the required thickness and to remove any surface irregularities.

Figure 3.3 Zircar Hot Spot furnace was used for sintering of alumina matrices**.**

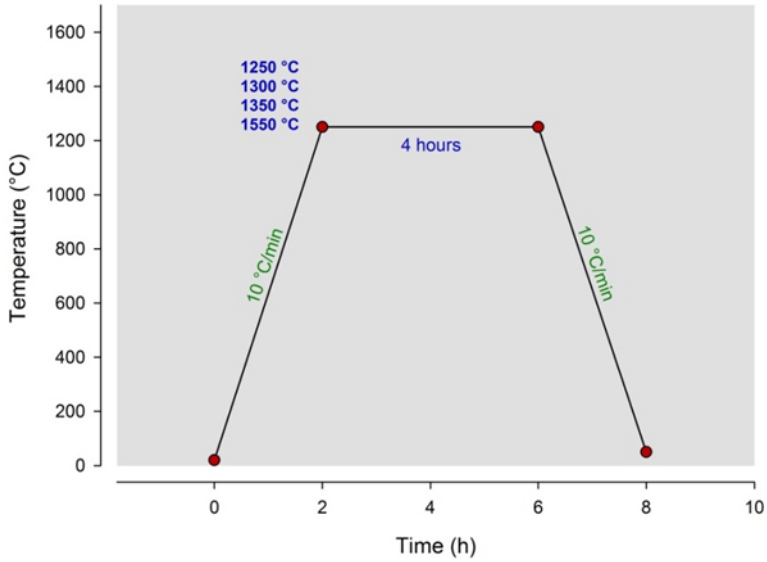

Figure 3.4 Sintering protocol of alumina matrix. Different sintering temperatures were chosen for each group.

3.2.1.2 Silanisation Procedure

To increase the wettability of the porous ceramic matrices and enhance the infiltration of resin monomers, all specimens were treated with saline solution. The solution was prepared by swirl mixing of 4 g of 3- methacryloxypropyltrimethoxysilane (MPS), 200 ml of Ethanol and 200 ml of RO water. The pH of the solution was adjusted by adding drops of glacial acetic acid until pH of 4 was reached and that was checked with pH paper indicator (Short range alkacid pH test paper, Fisher Scientific, Pittsburgh, PA) (Figure 3.5). The prepared silane was stored in a labelled bottle in the refrigerator and used for 6 months. The specimens were arranged vertically in a glass disc shaped dish and the silane solution was slowly added until halves of the specimens were submerged in the solution. The procedure was repeated for all the other groups. Then all the dishes were covered with glass jars to prevent evaporisation and left in a laboratory fume hood for 3 hours (Figure 3.6). After that, specimens were placed into oven (Vacuum oven1410, VWR, Radnor, PA) at 90 °C and 1 atm for 24 hours to dry.

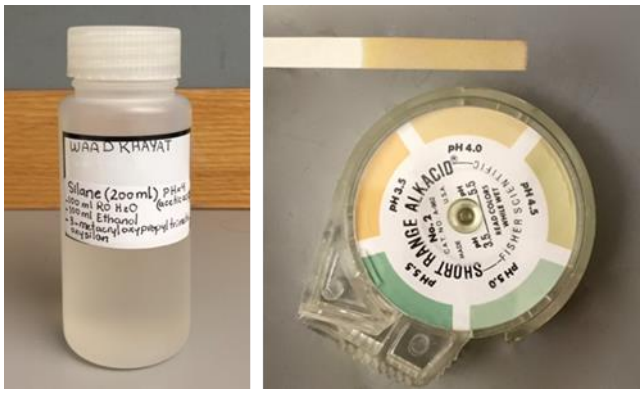

Figure 3.5 The pH of the silane solution (left) was checked with pH indicator paper (right).

Figure 3.6 Specimens were arranged into a plastic dish and were half-height soaked into silane for 3 hours in laboratory fume hood.

3.2.1.3 Resin monomers infiltration

380 g of TEGDMA was mixed with 3 g of (benzoyl peroxide) BP, the polymerization initiator for 2 minutes in GyroMixer. Then, 680 g of UDMA was added and mixed for a total of 6 min. The UDMA-TEGDMA resin was stored at 16 °C for 24 hours to allow the elimination of air bubbles rising to the surface after which it was stored in the refrigerator at 4 °C in a labelled bottle for 6 months, used several times and discarded when any changes or discoloration noticed.

The resin infiltration into the alumina matrix specimens was made using resin infusion apparatus; comprised of vacuum pump, resin chamber and specimen chamber (Figure 3.7). Resin mixture and specimens were carefully positioned into their designated chambers. These chambers were then evacuated and kept under vacuum pressure of $4x10^{-2}$ torr for 24 hours. Infusion was started by opening the valve that permitted the

flow of resin from the resin chamber to the specimen chamber through the connecting tube until the specimens were fully submerged. The specimens were kept submerged under vacuum in the specimen chamber for 2 hours and then stored soaked in the resin for 24 hours at 16 °C. After that, specimens were placed into plastic bags (25 mm with 0.1 mm thickness, Poly tubing, Uline, Pleasant Prairie, WI) and evacuated by a vacuum pump (Welch Vacuum pump, Thomas Industries Inc., Skokie, IL) that is connected to a tube with an attached head that fit tightly to the opening of the plastic bag, and then sealed using heat sealer (Impulse sealer, American International Electric Inc., City of Industry, CA). The bags were checked to ensure no leakage and no air bubbles were present inside the sealed bags (Figure 3.8).

Resin polymerisation was accomplished with heat and pressure in a water filled cylindrical isostatic pressure chamber (50x150 mm) (Figure 3.9). The chamber was connected to an external heater that was programmed to generate heat up to 100 °C (PiPress 50-150, Pober Industries, Waban MA 02468) (Figure 3.10) . Bagged specimens were carefully positioned in the chamber and filled with distilled water and closed properly with a straight piston and a plug with O-rings for sealing. The chamber was then subjected to a load of 500 kN by Enerpac hydraulic press using eclectic pump. A pump pressure was applied which produced a chamber pressure of 138 MPa. The specimens were kept under heat and pressure for 12 h before removing them from the chamber.

Figure 3.7 Resin fusion apparatus for resin infiltration with the two chambers; resin chamber (right) and specimen chamber (left).

Figure 3.8 Welch vacuum pump used to evacuate air from plastic bags (left). Evacuated plastic bags containing resin infiltrated specimens (right).

Figure 3.9 The sealed bags were carefully placed into heat connected chamber (left). The chamber was then placed into Enerpac hydraulic press to cure specimens with heat under pressure (right).

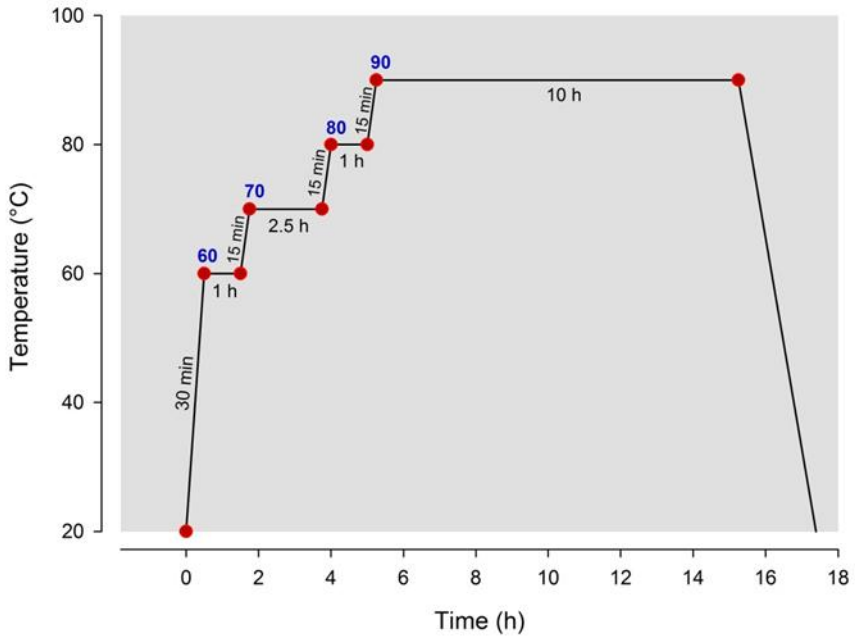

Figure 3.10 Heat polymerisation protocol for resin infiltrated alumina samples.

3.2.1.4 Finishing and Polishing

The specimens were removed from the bags and the excess polymer was trimmed and the surfaces were sequentially polished in an auto polishing machine (EcoMet 250 Grinder/Polisher with AutoMet power head, Buehler Ltd., Lake Bluff, IL). Diamond discs with grit sizes of 70, 45, 15 grit were used and then the specimens were further polished with 3, 1 and 0.25 µm polycrystalline diamond suspension to obtain glossy surfaces. The thickness of each specimen was re-measured with a digital calibre (Model # ID-F125E, Mitutoyo, America Corporation, IL).

3.2.2 Density Calculations

Specimen weight was measured using an analytical balance (Model# XS204, Mettler-Toledo LLC., Columbus, OH). Thickness and diameter were measured using a digital dial indicator (Model # ID-F125E, Mitutoyo, America Corporation, IL) (Figure 3.11). Three readings were taken for each parameter of each sample and the average of the three was calculated and recorded.

3.2.2.1 Density calculation of ceramic matrices specimens

The theoretical density percent (tP_0) for each specimen was calculated from the following equation:

$$tP_0 = P_0/tP \times 100 \quad \textbf{(1)}$$

where,

P_0 = density of porous ceramic matrix (g/cm^3) calculated from

$$tP_0 = m_0/\pi r^2 h \quad \textbf{(2)}$$

m_0 = mass of porous ceramic matrix (g)

r = radius of ceramic specimen (cm)

h = thickness of ceramic specimen (cm)

tP = theoretical density of ceramic (alumina = 3.98 g/cm^3)

3.2.2.2 Density Calculation of Resin Infiltrated Specimens

Weight, diameter and thickness of infiltrated specimens were measured and density after infiltration (P_I) was calculated using the same equation as above for density calculation. Infused density percent (Inf. P) was calculated using the following equations:

$$inf.P = (P_i/theoriticalP_i) \times 100 \quad \textbf{(3)}$$

$$theoriticalP_i = [(P_0/tP) \times tP] + [(1 - (P_0/tP)) \times P_r] \quad \textbf{(4)}$$

P_I = density after polymer infiltration

P_0 = porous ceramic density (from the above calculation)

tP = theoretical density of ceramic

P_r = theoretical density of polymer (1.1 g/cm^3)

Figure 3.11 Analytical balance (left) and digital dial indicator (right) were used to calculate specimens weights and dimensions.

3.2.3 SEM Analysis

Selected specimens from each group were prepared for scanning electron microscope imaging (Field Emission Variable Pressure Analytic Scanning Electron Microscope FESEM-VP- Hitachi SU6600, Hitachi High Tech, Oxford Instruments). Each specimen was ultrasonically cleaned with ethanol (Fisher Scientific, Pittsburgh, PA) for 10 min and then dried overnight at room temperature. Then they were sputter coated with gold/palladium for imaging. The microstructure of specimens was examined with a voltage of 15 kV at two different magnifications of 5000x and 10,000x.

3.2.4 Assessment of Optical Properties

Contrast ratio, translucent parameter and total light transmission were measured using a spectrophotometer (Color i7, X-Rite Inc., Grand Rapids, MI) for all specimens (Figure 3.12). The spectrophotometer was calibrated as recommended by the manufacturer and the setting of each mode was selected accordingly in the software (Color iQC). Each specimen was placed into the specimen holder, aligned with the sphere lens to allow the light transmission through the centre of the specimen in the transmittance compartment and the reading was taken and displayed on the screen (Figure 3.13). All the parameters were calculated automatically using the device software.

a. Opacity and Contrast Ratio:

The spectrophotometer was used to record the CIELAB coordinates (L*, a* and b*) of all the PIAN groups. Contrast ratio (CR) was calculated according to the following:

$$CR = \frac{Y_b}{Y_w} \quad \textbf{(5)}$$

Defined as the ratio of illuminance of the test material when it is placed on the black background (Y_b) to the illuminance of the same material when it is placed over a white background (Y_w).

b. Total Light Transmission:

Visible light transmission percentage was measured using the spectrophotometer for all the PICN model groups. This parameter is used to indicate the masking ability of the specimens over the background colour. The specimen is placed in front of the spherical entrance port of the equipment through which the light beam enters. The sphere collects all the light passing through the specimen. Measurements were made over the wavelength range 460 nm to 720 nm under the UV included condition.

c. Translucency Parameter

The values from L*, a* and b* coordinates recorded from the ceramic specimens placed on a black (B) and white (W) backgrounds were also used to estimate the translucency parameter (TP) according to the following:

$$TP = \sqrt{(L_b^* - L_w^*)^2((a_b^* - a_w^*)^2 + (b_b^* - b_w^*)^2} \quad \textbf{(6)}$$

Where (L*: value coordinate; a*: red–green coordinate and b*: yellow–blue coordinate).

d. Refractive Index

Refractive index was measured for all groups using refractive index meter II (Presidium instruments Ltd., Singapore) (Figure 3.14). Three readings from different locations were taken for each specimen and the average was calculated.

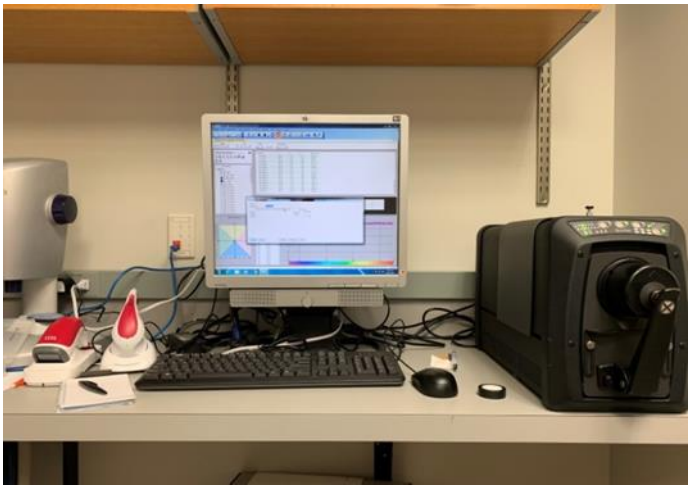

Figure 3.12 Color i7 spectrophotometer used to measure the optical properties of PICN.

Figure 3.13 A PICN specimen in place to measure CR and TP (left). For the LT measuremnt, the specimen was fixed with a holder and aligned against spherical lens.

Figure 3.14 Refractive index meter II used to measure refractive index of specimens.

3.3 Assessment of the effect of sintering temperature of PICN on flexural strength

All experimental groups were subjected to a biaxial flexure strength test. Maximum compressive load was measured in N using a universal testing machine (Model 5566A; Instron Corp, Canton, MA, USA) equipped with 1KN load cell and 0.8 mm load radius. Circular transparent adhesive stickers were fixed on the compression side of the specimens to avoid spreading of the fragments and provide better contact between the piston and the sample (Figure 3.15). Each specimen was positioned on a fixture with three steel rounded-end projections, equally apart from each other in a triangular position of an 11mm diameter circle. A round-tip piston (Ø =0.8 mm) was used to apply an increasing load (0.5 mm/ min) until catastrophic failure occurred. Settings were controlled and results were displayed using Bluehill 3 software. Flexural strength was calculated according to the following equations:

$$\sigma = -0.2387[\mathrm{P}(\mathrm{X}-\mathrm{Y})/b^2] \quad \textbf{(7)}$$

$$\mathrm{x} = [(1+\mathrm{v})\mathrm{In}(r_2/r_3)^2] + [(1-v)/2](r_2/r_3)^2 \quad \textbf{(8)}$$

$$\mathrm{y} = (1+\mathrm{v})[1+\mathrm{In}(r_1/r_3)^2] + [(1-v)/2](r_1/r_3)^2 \quad \textbf{(9)}$$

σ: biaxial flexural strength (MPa)

P: the total load causing fracture (N)

b: thickness at fracture origin (mm)

v: Poisson's ratio (0.23)

r_1: radius of the support circle (mm)

r_2: radius of the piston (mm)

r_3: radius of the specimen (mm)

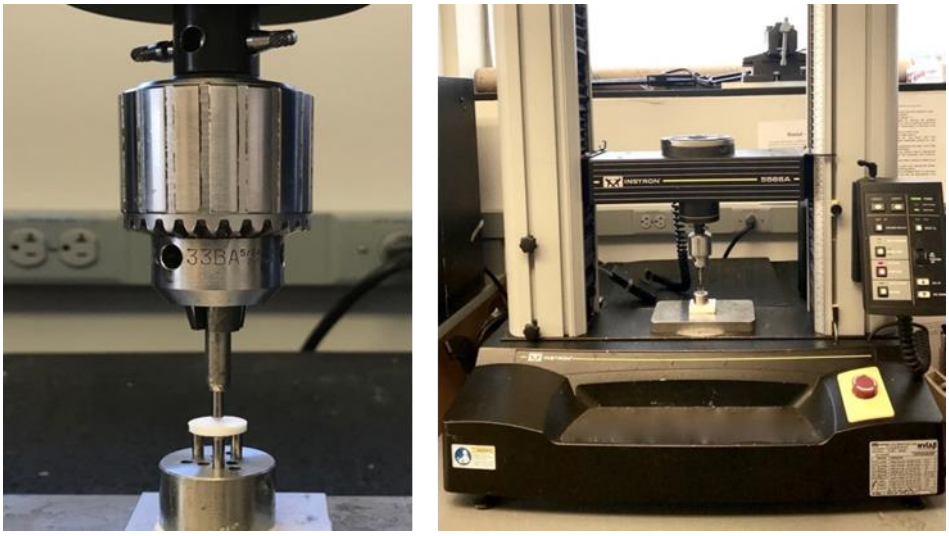

Figure 3.15 Fixture used for biaxial flexural strength test (left). Universal testing machine used to measure biaxial flexural strength (right).

3.4 Assessment of mechanical coherence of PICN and other CAD/CAM materials

A total of 12 restorative materials with different compositions were investigated in the study. Six were commercial CAD/CAM blocks; two were conventional composite and four were model CAD/CAM PICN ceramics.

3.4.1 Sample Preparation and Hardness Assessment:

A pilot study was conducted on specimens from each group to identify the sample size, applied load and the dwell time (s) for the nano and micro hardness experiments. Five samples from each group were found to be sufficient to indicate the statistical significant difference among the groups. Twenty-five bar shaped specimens (12x4x2 mm) were sectioned from CAD/CAM blocks to perform hardness assessments at nano and micro levels.

The specimens were sectioned using a precision cutting machine (Isomet 1000, Buehler, LakeBluff, USA) (Figure 3.16) and mounted in phenolic ring moulds (25x15 mm) (Buehler, Coventry, UK) and embedded in epoxy resin (Buehler, Coventry, UK) (Figure 3.17). The specimens were sequentially polished with silicon carbide grinding papers (P320, P600, P800, P1200, P2500 and P4000) and finished with 3 micron and 0.25 micron diamond paste using an OmegaPol metallurgical polisher machine (Spectrographic, United Kingdom). With light one-finger pressure applied on the specimen against the felt cloths

of the polishing machine, each polishing step was carried out for 5 min. Polished specimens were then checked using a light microscope at 10x,20x and 100x magnifications to ensure absence of scratches. An ultrasonic bath (Nusonic, Transsonic T310, Germany) was used to clean specimens in distilled water for 5 min. Each specimen was stored dry in a clean container at room temperature for 24 h before investigation.

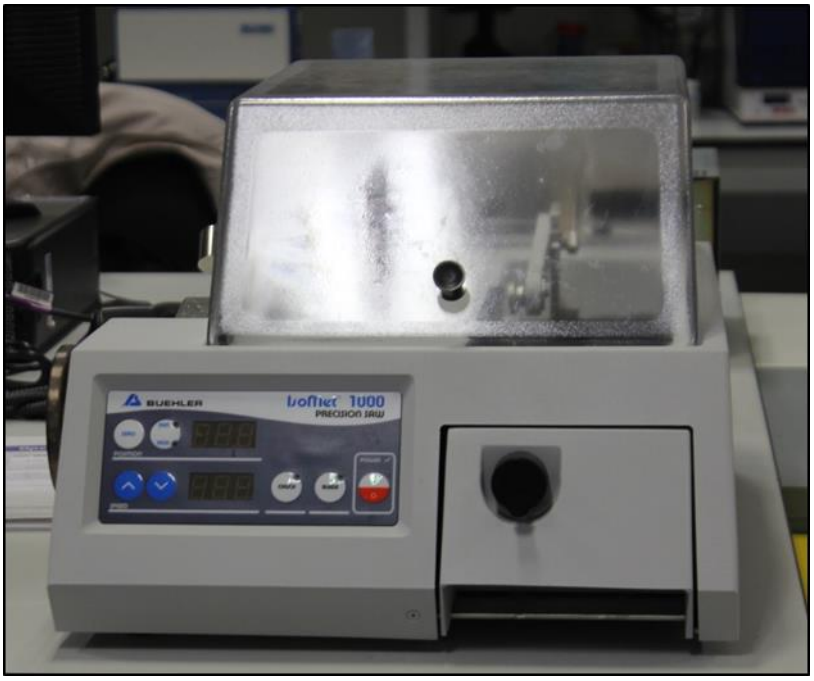

Figure 3.16 Isomet 1000 used in cutting the CAD/CAM ceramic blocks.

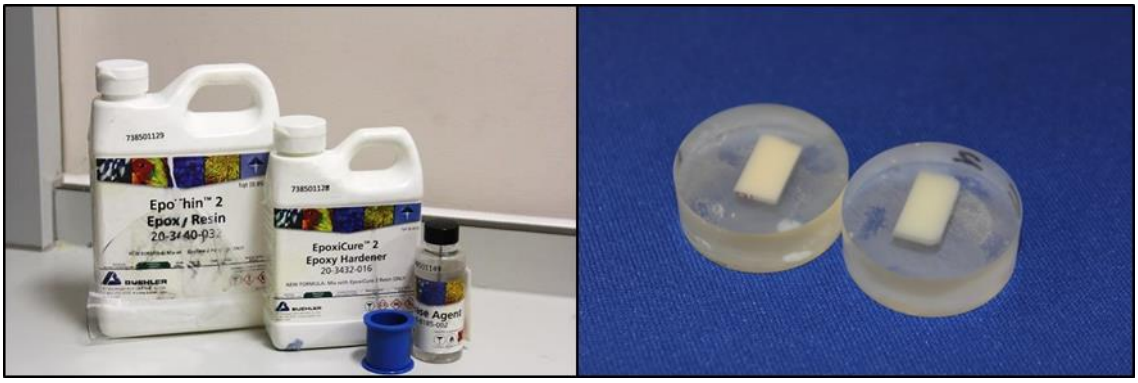

Figure 3.17 Ceramic samples prepared for nanoindentation testing. The specimens were embedded in self-cured epoxy resin in a cylindrical form.

3.4.2 Nanoindentation Assessment

Nanoindentaion measurements were performed at room temperature using a nanoindentor device (Nanovea M3, USA) (Figure 3.18). The device is fully automated with touch screen, automated controlled load and depth allowing work on different types of samples for quick nanoindentation results under ASTM standard including hardness, elastic Modulus and creep depth.

Nanovea M3 has two motorised axes, Y and Z, each with 40 mm travel and a resolution of 5 µm. The system utilizes a 250 µm range depth sensor with 0.003 nm resolution and 0.5 nm noise floor. The load sensor is available with a 400 mN range or 2000 mN range with resolution of 0.03 µN or 0.30 µN and the noise floor of 10 µN and 50 µN respectively.

The device is compatible with different types of indenters: Berkovich, Vickers, sphero-conical, fall and ball indenters. A Berkovich indenter with cone angle of 130.54° was used. The Poisson's ratio of the indenter is 0.07, and the elastic modulus was 1140 GPa; material type was set as ceramic where a Poisson's ratio of 0.3 was used for modulus calculation. Nanoindentation was performed at a 50 g load with 10 s pause/dwell (Figure 3.18). The sample was attached with cyanoacrylate glue to the provided metallic sample mounting block (38x15mm) which was magnetically attached to the sample holder of the nanoindenter device (Figure 3.19).

Figure 3.18 Nanovae indentation device with the selected test parameters used to examine the CAD/CAM ceramic specimens.

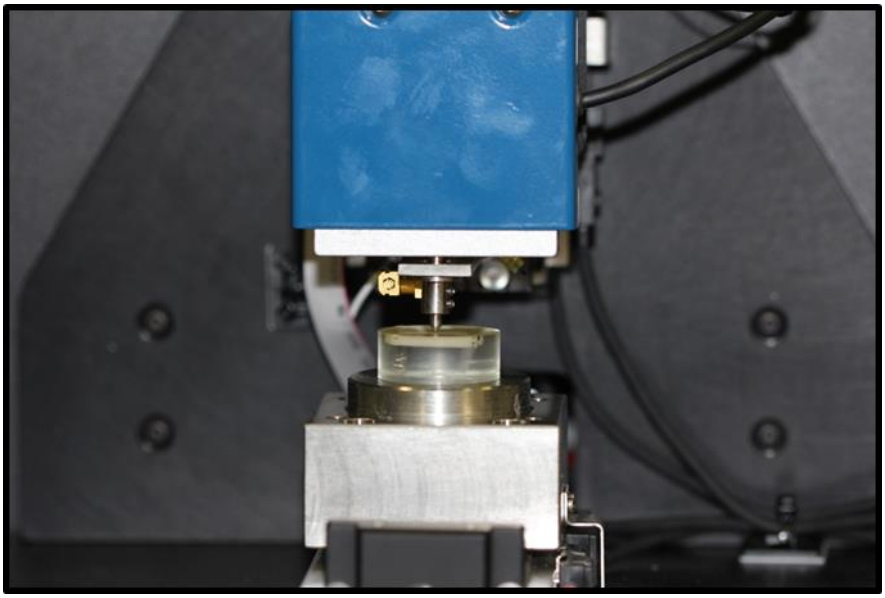

Figure 3.19 Mounted ceramic specimen under loading condition in the nanoindentation device.

Five continuous indents with a spacing of 250 µm were performed in a line. Five sets of 5 tests were perform on each CAD/CAM ceramic material. Nanohardness was calculated based on the following formula:

$$H = \frac{P}{A_p} \quad \textbf{(10)}$$

Where P is the applied load in mN and A_p is the projected area of the indentation. Elastic modulus was determined from the slope of the unloading curve of the load displacement data at the maximum load based on Oliver and Pharr method (152) as the following

$$E = \frac{1}{2} \times \frac{\sqrt{\pi}}{\sqrt{A}p} \times \frac{dh}{dp} \quad \textbf{(11)}$$

Where *dh* is the change in depth; *dp* is the difference in load.

3.4.3 Microhardness Assessment:

A specialised microhardness instrument (FM-700, Future Tech Corp., Japan) (Figure 3.20) with a Vickers diamond indenter was used. Five sequential measurements with a spacing equal to 4 times the diameter of the indentation were taken for each surface with a fixed 50 g load applied for 10s (dwell time). The hardness was automatically calculated by the machine, which can also be calculated via the following formula:

$$VHN = 0.1891 \times \frac{P}{d^2} \quad \textbf{(12)}$$

Where:

P is the applied load in Kgf.

d^2 is the Surface area of indentation in mm.

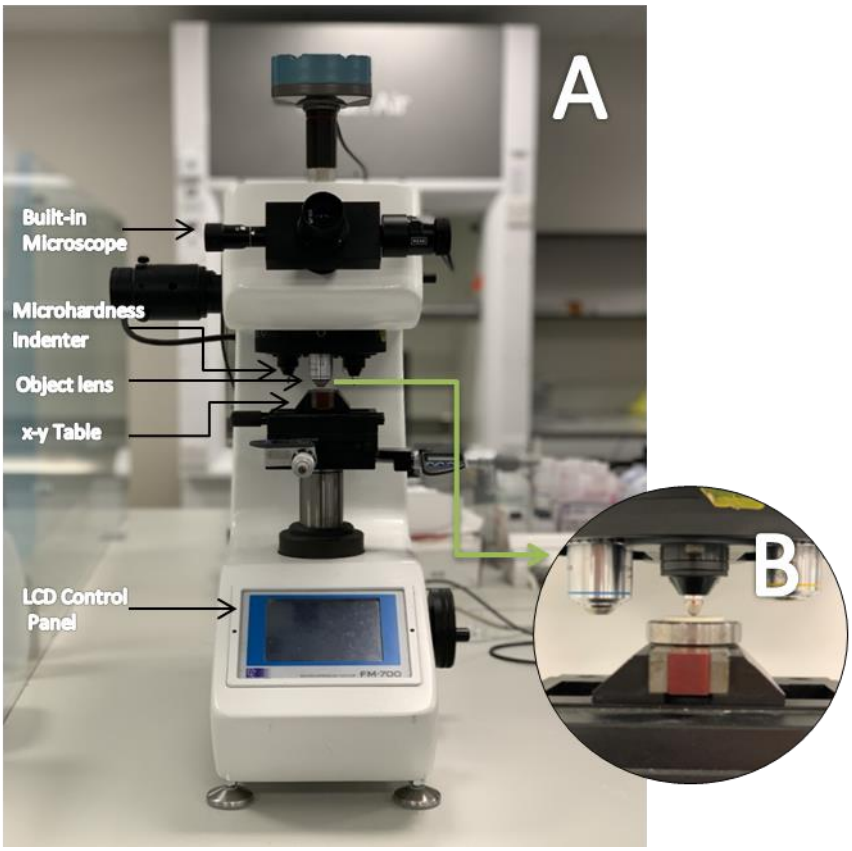

Figure 3.20 FM-700 micro hardness tester (A), with a representative specimen ready for testing (B).

3.4.4 Determination of Ceramic Content

Ceramic weight contents of the model PICN and other CAD/CAM blocks was determined by the standard ash method described in ISO 1172:1999 (184). The concept of this method is based on removing the organic matrix in a resin composite material by burning it out. All the specimens (n=3) were stored in a desiccator at 37 °C for 24h. A pre-heated silica crucible was used to contain the specimen throughout the experiment (Figure 3.22). The weight of each specimen was measured to an accuracy of 0.01 mg using a calibrated electronic analytical balance (Ohaus Analytical Plus, Ohaus Corporation, USA) (Figure 3.21). Specimens were heated in an electric furnace (Programat EP 5000, Ivoclar Vivadent, Liechtenstein, Austria) at 600°C (1200 °C for DK group) for 30 minutes to burn out the organic matrix and then placed back in the desiccator to cool down before re-weighing them. The latter weight consisted only of the inorganic component.

Ceramic weight fraction (wt%) was determined with the following formula:

$$Ceramic\ wt\% = \frac{(w_3 - w_1)}{(w_2 - w_1)} x100 \quad \textbf{(13)}$$

Where:

w_1 is the initial mass of the dry silica crucible.

w_2 is the initial mass of dry silica crucible plus dried sample.

w_3 is the final mass of the silica crucible and the residue of the burned sample.

Figure 3.21 Programat electric furnace was used to burn out the specimens (left) which were weighted before and after the burn out using calibrated analystical balacne (right).

Figure 3.22 A pre-heated silica crucible containing a PICN specimens before (left) and after burn out (right).

3.4.5 SEM Analysis:

Scanning electron microscopy (FEI Quanta 650 FEG, Oxford Instruments, UK) was used to characterise the cross-sectional microstructure of the five materials used in the present study. Specimens were ultrasonically cleaned and dried with hot air. After gold/palladium coating using a sputter coater (Quorum Q150T-S, Quorum Technologies Ltd, UK), specimens were viewed under a field emission mode with an accelerating voltage of 10KV and a working distance of 10 mm. Images at different magnifications were taken.

3.5 Assessment of surface properties and elastic modulus mapping

3.5.1 Atomic Force Microscope (AFM)

Atomic force microscopy was conducted using a Bruker Catalyst™ BioAFM (Bruker UK Ltd., Coventry, U.K (Figure 3.23) with a Nanoscope V controller, and operated under the Nanoscope controller software (v9.1). Images were captured in air at a humidity of <45% using pre-calibrated NM-RC-C diamond tipped probes (Bruker SAS, France) (Figure 3.23) using Peakforce Quantitative Nanomechanical (PFQNM) tapping mode. Data capture was performed at 5 locations on each sample with a 20x20 µm and a 3x3 µm images being collected at each site. Imaging was performed at approximately. 1Hz and at a resolution of 256 samples/line. Topography, and DMT modulus channel data were post-processed using Nanoscope Analysis (v1.50) (Figure 3.24); the calibration data supplied with the probes was inputted to the controller software at the capture stage. Average roughness (R_a), the root mean square roughness (Rq), and maximum roughness depth (R_{max}) values were extracted for all samples.

The elastic modulus of the sample was derived from AFM force curves and was based on the Derjaguin-Muller-Toporov (DMT) model (185), which was implemented into the Bruker NanoScope Analysis software. By definition, the DMT model fits the following equation.

$$F - F_{adh} = \frac{3}{4} E^* \sqrt{R(d - d_h)}^3 \quad \textbf{(14)}$$

Where

F is the applied force, F_{adh} the adhesion force between probe and the surface, *R* is the tip radius, $d - d_h$ the sample deformation, and E^* is the elastic modulus.

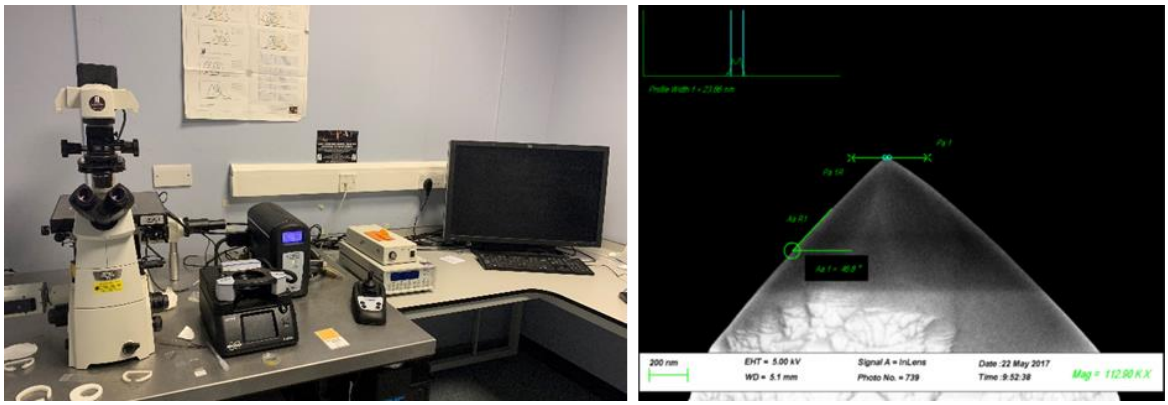

Figure 3.23 Bioscope Bruker Catalyst AFM was used to obtain elastic modulus and surface roughness data in the current study (left). SEM image with 112.9 KX magnification of one of the used diamond tips with calibrated nanoscale shapes and profiles (right).

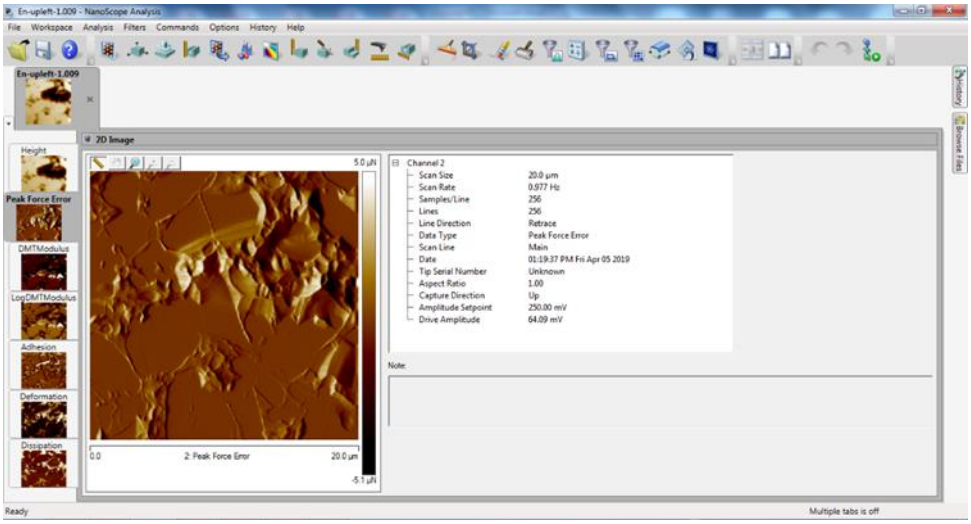

Figure 3.24 Screen-print of the front page of NanoScope analysis software used to analyse the scanned surface of a test specimen**.**

3.5.2 Gloss Measuremnt

The gloss of each specimen was measured using a glossometer instrument (Electomer 400, Novo-Curve, Electomer inc., Rochester Hills, Michigan) (Figure 3.25). The instrument was calibrated after every 3 readings according to the manufacturer instructions. To record the gloss value, each specimen was centrally positioned -at an operating angle of 60°- over the hidden aperture which is pinpointed by intersection of white lines marked on the top of the sample plate. Before pressing the read button, the specimen was with a black sheild to exclude external light during the measurement .

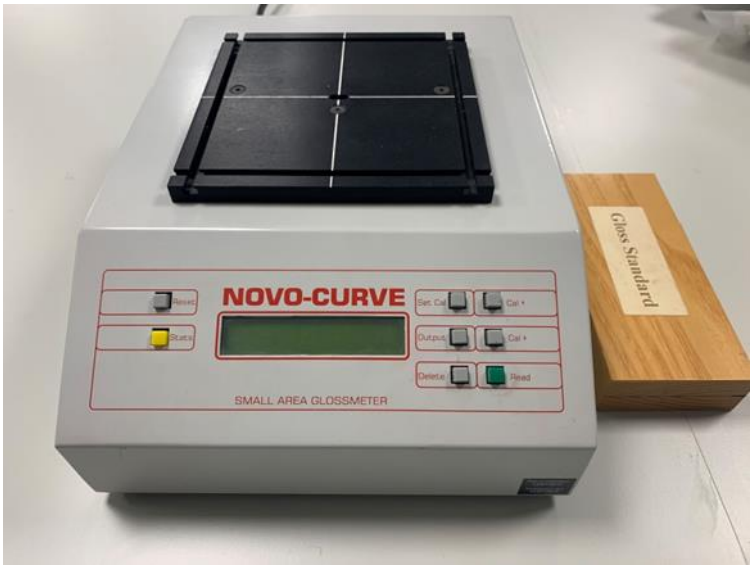

Figure 3.25 A calibrated Novo-Curve was used to measure the gloss of the test materials.

3.6 Sorption and Solubility

Five samples from each test material were soaked in an ultrasonic bath (Nusonic, Transsonic T310, and Germany) in distilled water for 5 min to remove debris and contamination. Samples were then transferred into separate labelled glass vials and stored in a lightproof desiccator with anhydrous self-indicating silica gel at 37 ± 1 °C (Figure 3.26). After 22h, all the samples were moved into another desiccator maintained at room temperature (23 ± 1) °C for 2 h and then weighed to an accuracy of 0.01 mg using a calibrated electronic analytical balance (Ohaus Analytical Plus, Ohaus Corporation, USA) (Figure 3.27). The measuring process was repeated on a daily basis until the mass change was not more than 0.1 mg at any 24 h time period according to ISO FDIS 4049:2009 specifications. The constant mass was then recorded as m1. Samples dimensions were then measured using an electronic digital calliper (Powerfix, OWIM GmbH & Co., KG, Germany) with an accuracy of 0.01 mm. Three measurements were recorded for each dimension and the average was then used to calculate the volume (V) of each sample in (mm3).

The samples were then stored in 10 ml of distilled water in an individual glass vial at 37 ± 1 °C. The samples were weighed at different time intervals (1, 7, 14, 30, 60, 90, 180 and 210 days). The mass recorded at each time was denoted as m2 (t). For every weighing cycle, samples were dried on a filter paper and air-blown before measurements and then returned into their vials after renewing the storage water to avoid variations in the pH with storage. At the end of the storage period, samples were reconditioned to a constant mass in a desiccator following the same conditioning protocol described above. The recorded mass was then denoted as m3.

The percentage mass change was calculated by the following equation:

$$Mg(\%) = \frac{m2\ (t) - \ m1}{m1} \times 100 \qquad \textbf{(15)}$$

This represents the apparent percentage amount of water absorbed by the tested material since sorption is opposed by solubility during storage which results in weight loss.

The percentage solubility which represents the total weight of components (including unreacted monomers, additives, or fillers) extracted by water was calculated by:

$$SL(\%) = \frac{m1-m3}{m1} \times 100 \quad \textbf{(16)}$$

To calculate the actual percentage amount of water absorbed by the tested material at the end of the storage period, the following formula was used:

$$SP\ (\%) = \frac{m2\ (7months)-m3}{m1} \times 100 \quad \textbf{(17)}$$

Water sorption (μg/mm^3) of each tested sample was calculated according to the following:

$$SP = \frac{m2-m3}{V} \quad \textbf{(18)}$$

Solubility measured in micrograms per cubic millimetre (μg/mm3) for each tested sample was calculated by:

$$SL = \frac{m1-m3}{V} \quad \textbf{(19)}$$

Figure 3.26 Desiccator showing the samples stored in separate glass vials with anhydrous self-indicating silica gel at the bottom prior to immersion in water and artificial saliva.

Figure 3.27 Electronic analytical balance used for weighing the test samples (Ohaus Analytical Plus, Ohaus Corporation, USA).

Chapter 4

The influence of Sintering Temperature on Optical Properties and Biaxial Flexural Strength of a Novel Polymer Infiltrated Polycrystalline Ceramics

4.1 Abstract

Objectives

To determine the effect of sintering temperature on the microstructure, refractive index, contrast ratio, translucency, light transmission and flexural strength of novel fabricated polymer infiltrated ceramics.

Materials and Methods

72 alumina specimens were fabricated by slip-casting into disc shapes (15 x 2 mm) and randomly divided into 4 groups according to the sintering temperature. The groups were labelled according to their sintering temperature (Exp125= 1250 °C ; Exp130=1300 °C; Exp135=1350 °C; Exp1550=1550 °C). After sintering, groups were silanated and dried overnight at 90°C. Then, UDMA-TEGDMA resin was prepared and infiltrated into the ceramic specimens under vacuum. Polymerisation was carried out at 90°C and under a pressure of 138 MPa. Specimens were polished to 1.5mm thickness and the density measured. Contrast ratio (CR), translucent parameter (TP) and light transmission (LT) were evaluated with a spectrophotometer (X-rite Ci7600); Refractive index was measured (Presidium Refractive Index Meter II); biaxial flexural strength was obtained (Instron 5566A) with a crosshead speed of 0.5mm/min; and the microstructure was examined using a scanning electron microscope (FESEM-VP-Hitachi SU6600). Statistical analyses were performed using the Kruskal-Wallis test and one-way ANOVA.

Results

Exp125 demonstrated the highest density improvement from (71.38%) to (99.22%) after polymer infiltration. Exp155 showed the lowest RI and CR values (1.79 and 97.14 %, respectively) but the highest TP and LT values (7.09 and 6.8%, respectively). No significant difference in flexural strength values was noticed between the groups. However, the flexural strength was positively correlated with the ceramic matrix density percentage.

Conclusions

Polymer infiltration significantly improves the density% of ceramic samples. An increase in sintering temperature results in a significant improvement in the optical properties but not in biaxial flexural strength.

Key words Hybrid-ceramic, Aluminium-Aluminium Oxide, Density, Flexural, Microstructure.

4.2 Introduction

Since the introduction of computer-assisted processing in various industries in the 1970's, the research and development of dental CAD/CAM technology have been actively pursued worldwide (186, 187). The last decade in particular has witnessed a dramatic increase in the use of CAD/CAM technology for the production of new indirect restorative materials. Such an increase has been triggered by advances in intra-oral imaging, in manufacturing technologies, and by environmental concerns related to the by-products of the classic manufacturing process of indirect dental restorations.

Two main types of materials are currently available for aesthetic CAD/CAM-processed indirect dental restorations: glass-ceramics/ceramics and resin composites. In general, ceramics are brittle in nature and this is considered as a significant drawback for such a material (188-190). The physical and mechanical properties of dental ceramics are governed by their chemical microstructure.

The microstructure of dental ceramic can be classified into three main categories based on the ratio of their glass and polycrystalline structures (62). These categories are predominantly glassy materials, partially filled glassy materials and polycrystalline materials. The glass content provides aesthetic translucency, whereas the crystalline content contributes to strength and superior mechanical properties (191). The structure of the predominantly glassy materials is amorphous and is composed mainly of alumina and silica. Their ceramic nature mimics the optical properties of enamel and dentine, but it has poor mechanical properties, and for this reason its use is mainly limited to veneers, or overlay veneers on metal or high-strength ceramic cores. Mechanical properties can be influenced by the incorporation of another phase in the form of reinforcing fibres, dispersed particles, or by fabricating interpenetrating-phase composites (141, 192). The classic approach is to imbed dispersed particles in the glassy matrix to increase the ratio of the crystalline phase. However, such an approach is challenging as mixing a dispersed phase into an amorphous matrix may promote voids and poor filler distribution within the glassy matrix, which eventually may negatively affect their clinical performance (193).

Interpenetrating-phase composites (IPCs) are a relatively new concept of ceramics reinforcing. Unlike the dispersed particles, IPCs are composed of a continuously connected ceramic phase interlocked with another continuously connected phase (142). Most resin composite materials are composed of dispersed fibres or filler particles within a binding matrix phase, whereas in an IPC, there is no isolated phase. Rather, each individual solid phase within the fully dense composite forms a completely interconnected network (194). This method has several advantages due to the fact that a higher volume of ceramic can be easily incorporated into the composite microstructure removing the limitation of the mixing dispersed particles in a continuous medium (194). One advantage is that the strength and fracture toughness are quite similar to a dense ceramic. The interlocking of these two phases is usually made by an infiltration technique. In such a technique, a ceramic with connected pores is prepared, sintered and then infiltrated with another phase, such as metal, polymer or glass (194, 195).

The fabrication process of dental interpenetrating-phase ceramics involves multiple steps. First, a porous ceramic matrix is produced by milling pre-sintered blocks, slip casting or compressing ceramic powder, which is commonly mixed with additives, such as dispersants, pH controllers or binders. This is followed by heat treatment of the ceramic framework to promote de-binding and consolidation of an interconnected network. Next, the ceramic framework is conditioned with a coupling agent to enhance the surface wettability and allow the capillary infiltration of the second phase, which can be melted lanthanum glass or polymer. The infiltration is then followed by solidification of the melted glass or thermal polymerisation of the resin polymers (135, 138, 141, 196).

Changing the processing techniques allows for various sizes and forms of porosities of ceramic frameworks by manipulating ceramic particle size and applying different sintering conditions (141, 197). Formation of a porous interconnected ceramic framework with good rigidity is a critical step in the fabrication of IPCs. The relative volume fractions of the two interconnected phases are primarily determined by the porosity of the ceramic phase. If closed pores are formed in the microstructure, they are not accessible for infiltration and may cause larger shrinkage, leading to compromised optical and mechanical properties. Ceramic strength normally increases because of the reduction of porosity through full densification during sintering process. However, for interpenetrating-phase composites, porosity is eliminated through the infiltration of a

second phase, leading to strengthening of the material and integration of the properties of the different phases. Interpenetrating-phase composites show better mechanical behaviours compared to the individual phases (198). It has been found that polymer infiltrated porcelain composites exhibit a flexural strength of 169 MPa, which is higher than that of porcelain (122 MPa) or polymer (135 MPa) (138, 199).

Vita Enamic is a polymer-infiltrated ceramic network material that was successfully developed and introduced to the dental market in 2012 (198). This material is composed of 75 vol% porous feldspathic porcelain infiltrated with 25 vol% resin polymers, namely UDMA and TEGDMA, based on a similar concept of manufacturing to glass infiltrated ceramic system (In-Ceram). Due to the fine structure of ceramic and the polymer network, this material demonstrates similar physical and mechanical performances to enamel and dentine (109, 200). There are currently few available clinical studies concerning the longevity of polymer-infiltrated ceramic restorations. However, laboratory studies have shown that Vita Enamic monolithic crowns have excellent resistance to wear and fatigue damage relative to traditional ceramic restorative materials (200, 201). Resin infiltrated ceramic shows more tolerance against crack propagation induced by dynamic fatigue. The existence of the polymer phase within the ceramic framework in Enamic material helps in spreading the plasticity upon loading, hence increasing the crack propagation resistance (202). PICN has a combination of low hardness and elastic modulus coupled with relatively high toughness which may enable rapid milling with minimal edge chipping(203). However, mechanical properties such as flexural strength and fracture toughness of Enamic have been shown to be significantly affected by thermocyclying which might affect its long term clinical success – it has been shown that the mean fracture-resistance value of thermocycled Enamic is below human occlusal forces (204). Critical defects that have been observed on fractured surfaces could explain the lower flexural strength value obtained with Enamic compared to polycrystalline ceramic (202).

Polymer-infiltrated ceramic shows promising results for use for single crowns (201); developing the material to be used for short/long span bridges through microstructure refinement has become a primary focus. Monolithic alumina that has smaller grain size and better mechanical behaviour and higher fracture toughness could be a good substitute for the feldspathic porcelain in Enamic.

Alumina (aluminum oxide, Al_2O_3) was the first polycrystalline ceramic to be used in dentistry (126). Dental applications of alumina-based ceramics include endodontic posts, orthodontic brackets, implants, and copings and frameworks for crowns and bridges (126). Alumina can be used as pure polycrystalline material or can be prepared and applied in a variety of forms and microstructures, such as fillers to reinforce porcelain and composite resin, or as matrix for interpenetrating-phase composites. Alumina composites can be formed with metals, glasses, polymers and other ceramics such as zirconia (205).

In-Ceram Alumina was introduced to the dental market in 1989, composed of 68 vol % alumina and 27 vol % glass (135). Its flexural strength of 548 MPa is superior to e-max pressed ceramics(formerly named Empress2) and its survival rate is similar to porcelain fused to metal crowns placed in anterior and premolar regions (136, 137). Multiple clinical trials (lasting between 5 and 7 years) reported a success rate of 91.5 - 100 % for In-Ceram alumina, though it has never been highly marketed (138). Its optical properties are limited, however. A high-translucency glass-infiltrated alumina ceramic has been fabricated with a higher translucency of 20.1 % compared with In-Ceram alumina (8.9 %) at the range of visible light (140).

Very limited focus has been placed on experimental attempts of utilizing polycrystalline ceramic for manufacturing dental polymer-ceramic composites and testing their properties. In the medical field, bone cements made with polymer-infiltrated alumina have superior mechanical properties and osteo-conductivity compared with conventional bone cements (126). The properties of polymer-ceramic composites are significantly influenced by ceramic microstructure, chemical composition of polymer, sintering cycle and polymerization process. The literature shows only a few dental studies that aimed to manufacture polymer infiltrated alumina composites and to investigate the influence of various manufacturing factors on their properties (141).

The aim of this study was to synthesize and fabricate interpenetrating-phase alumina composites at different temperatures with different densities.

4.3 Materials and Methods:

4.3.1 Fabrication of Ceramic Matrix:

Nano-sized alumina powder (Al_2O_3) (Almatis Inc., Leetsdale, PA,USA) was used by slip casting to prepare 72 specimens with a diameter of 15 mm and thickness of 2 mm. A slurry mix of alumina, water and ammonium polymethacrylate dispersing agent (Darvan C-N) was dispensed into cylindrical plastic moulds and left to dry overnight. Then specimens were randomly divided into four different polymer-infiltrated alumina networks (PIAN) groups (n=18) according to the sintering temperatures (Exp125 at 1250 °C; Exp130 at 1300 °C; Exp135 at 1350 °C and Exp155 at 1550 °C). The sintering temperature was first increased at a ramp rate of 5 °C/min and a holding time of 1 hour from room temperature to 1050 °C, then heated at a rate of 10 °C/min to the specified peak temperature, held for 4 hours, and then furnace-cooled.

4.3.2 Resin Polymer Infiltration

After sintering and before resin infiltration, all specimens were conditioned with a silane coupling agent, methacryloxypropyltrimethoxysilane (MPS) to improve adhesion between the ceramic and polymer. The porous alumina ceramic network structure was then infiltrated with a mixture of two monomers, triethylene glycol dimethacrylate (TEGDMA) and urethane dimethacrylate (UDMA), which were mixed in a 1:1.8 ratio in a vacuum chamber. Then, polymerization reactions were conducted at 100°C and 138 MPa for one hour to form a polymer network, leading to the formation of the PICN material.

4.3.3 Polishing and Density Calculations

Density of porous ceramic matrices

All the specimens were trimmed and sequentially polished with silicon carbide grinding papers (P320, P600, P800, P1200, P2500 and P4000) and finished with 3 micron and 0.25 micron diamond paste using an OmegaPol metallurgical polisher machine (Spectrographic, United Kingdom). The theoretical density percent (tP_0) for each specimen was calculated from the following equations:

$$tP_0 = P_0/tP \times 100 \quad \textbf{(20)}$$

$$tP_0 = m_0/\pi \mathrm{r}^2\, h \quad \textbf{(21)}$$

where:

P_0 = density of porous ceramic matrix (g/cm^3)

m_0 = mass of porous ceramic matrix (g)

r = radius of ceramic specimen (cm)

h = thickness of ceramic specimen (cm)

tP = theoretical density of ceramic (alumina = 3.98 g/cm^3)

Density calculation of resin infiltrated specimens

Weight, diameter and thickness of infiltrated specimens were measured and density after infiltration (P_I) was calculated using the same equation shown previously for density calculation. Infused density percent (Inf. P) was calculated using the following equations.

$$inf.P = (P_i/theoriticalP_i) \times 100 \quad \textbf{(22)}$$

$$theoriticalP_i = [(P_0/tP) \times tP] + [(1 - (P_0/tP)) \times P_r] \quad \textbf{(23)}$$

P_I = density after polymer infiltration

P_0 = porous ceramic density (from the above calculation)

tP = theoretical density of ceramic

P_r = theoretical density of polymer

4.3.4 Biaxial Flexural Strength

40 specimens (n=10) were subjected to a biaxial flexure strength test. Maximum compressive load was measured in N using a universal testing machine (Model 5566A; Instron Corp, Canton, MA, USA) equipped with a 1KN load cell and a 0.8 mm load radius. Circular transparent adhesive stickers were fixed on the compression side of the specimens to avoid spreading of the fragments and provide better contact between the piston and the sample. Each specimen was positioned on a fixture with three steel rounded-end projections, equally spaced from each other in a triangular position of an 11mm diameter circle. A round-tip piston (Ø =0.8 mm) was used to apply an increasing crosshead speed (0.5 mm/ min) until catastrophic failure occurred. Settings were controlled and results were displayed using Bluehill 3 software. Flexural strength was calculated according to the following equations (206):

$$\sigma = -0.2387[P\,(X - Y)/b^2] \quad \textbf{(24)}$$

$$X = [(1+ v)\,\ln\,(r_2 / r_3)^2] + [(1 - v) / 2]\,(r_2/r_3)^2 \quad \textbf{(25)}$$

$$Y = (1+ v)\,[1 + \ln\,(r_1 / r_3)^{2]} + (1 - v)\,(r_1 / r_3)^2 \quad \textbf{(26)}$$

σ: biaxial flexural strength (MPa)

P: the total load causing fracture (N)

b: thickness at fracture origin (mm)

v: Poisson's ratio (0.23)

4.3.5 Optical Properties Measurements

a. Total light transmission:

Visible light transmission for all the PIAN groups was measured using a spectrometer instrument (Color i7, X-Rite Inc., Grand Rapids, MI, USA). The instrument was calibrated as per manufacturer instructions and re-calibrated after measuring 3 samples. To take the measurement, each sample was first attached to the sample holder then base plate pins were aligned to the base plate mounting channel holes inside the transmission chamber. The holder position was carefully placed to be aligned with the sphere lens to allow the passage of light. Measurements were made over the wavelength range 460 nm to 720 nm under the UV included condition.

b. Contrast ratio:

The same spectrometer instrument was used to record the CIELAB coordinates (L*, a* and b*) of all the PIAN groups and automatically calculated the Contrast ratio (CR). CR was calculated according to the following (207):

$$CR = \frac{Y_b}{Y_w} \quad \textbf{(27)}$$

Defined as the ratio of illuminance of the test material when it is placed on the black background (Y_b) to the illuminance of the same material when it is placed over a white background (Y_w).

c. Translucency parameter

The values of a* and b* coordinates recorded from the ceramic specimens placed on black (B) and white (W) backgrounds were also used to estimate the translucency parameter (TP) according to the following (207):

$$TP = \sqrt{(L_b^* - L_w^*)^2((a_b^* - a_w^*)^2 + (b_b^* - b_w^*)^2} \quad \textbf{(28)}$$

d. Refractive index

Refractive index was measured for all groups using refractive index meter II (Presidium instruments Ltd., Singapore). Three readings from different locations were taken for each specimen and the mean was calculated.

$$n = \frac{c}{v} \quad \textbf{(29)}$$

c is the speed of light in vacuum = 299 792.46 km/s.

v is the speed of light in the medium.

4.3.6 SEM Analysis:

Specimens from each group were selected and prepared for scanning electron microscope imaging (Field Emission Variable Pressure Analytic Scanning Electron Microscope FESEM-VP- Hitachi SU6600, Hitachi High Tech, Oxford Instruments). Each specimen was sonicated with ethanol (Fisher Scientific, Pittsburgh, PA) for 10 min and dried overnight at room temperature. Then they were coated with gold/palladium for imaging. The microstructure of specimens was examined with a voltage of 15 kV at two different magnifications of 5000x and 10,000x.

4.3.7 Statistical Analysis:

The data were entered into a statistical software package (SPSS 23,Chicago,USA) and checked for normality using Shapiro-Wilk tests. The data relating to density and optical properties were analysed with Kruskal-Wallis tests and follow-up pairwise comparisons to assess the effect of sintering temperature. The flexural strength data were analysed using one-way analysis of variance (ANOVA) followed by Tukey *post-hoc* analysis for multiple comparisons. The effect of polymer infiltration on the density of ceramic matrices was analysed using a Wilcoxon Signed Rank test. Pearson Product Moment and Spearman Rank Order correlation analyses were used to assess the relationship between different variables. Significance levels for all tests was set at $\alpha = .05$.

4.4 Results:

The means, standard deviations, medians and interquartile range (IQR) values of densities and optical properties of the samples before and after infiltration are listed in Table 4.1 and Table 4.3, respectively. The means and the standard deviations of flexural strength values of the test groups are listed in Table 4.2. Alumina samples that were sintered at 1250 °C had the lowest density (2.78 g/cm^3) while those sintered at 1550 °C had the highest value (3.66 g/cm^3). However, after polymer infiltration, those sintered at 1550 °C had the lowest infused density percent (92.22%) compared to the 1250 °C sintering group which had the highest value (99.26%).

Statistical analysis revealed that there was significant differences in densities between all groups before infiltration (p<0.001). After infiltration, on the other hand, there was no statistically significant difference in density between Exp125, Exp130 and Exp135 (p>0.05). A statistically significant difference was found between Exp125 and Exp 155 after infiltration (p=0.01).

The Wilcoxon Signed Rank test revealed statistically significant differences in densities before and after infiltration for Exp125, Exp130 and Exp135 (p<0.001) (Figure 4.1). There was no significant difference in terms of density for Exp155 before and after polymer infiltration (p=0.91). Also, no statistical significant difference was found in flexural strength values between all the groups (p=0.16) (Figure 4.2).

For optical properties, Exp155 showed the lowest RI and CR values (1.79 and 97.14%, respectively) and the highest values of TP and LT (7.09 and 6.80%, respectively). No statistically significant differences were detected between Exp125, Exp130 and Exp 135 in terms of RI, CR and LT (p>0.05). However, Exp155 showed statistically significant difference values in all the optical properties (p<0.001).

Significant positive correlations were found between the sintering temperatures and TP, LT (Spearman Rank Order =0.89 and 0.67, respectively), flexural strength (Pearson Product Moment=0.34) and the densities of ceramic matrices (Spearman Rank Order =0.78) (p<0.05). Significant negative correlations were found between the sintering temperatures and RI and CR (Spearman Rank Order =-0.54 and -0.43, respectively (p<0.05)).

A significant negative correlation was also found between infused densities of polymer infiltrated ceramics and the sintering temperatures (Spearman Rank Order =-0.35, p=0.002).

SEM pictures of the microstructure of polymer infiltrated ceramics are shown in Figures 4.4-4.7. At a lower sintering temperature (1250-1300 °C), polymer infiltrated alumina showed a porous microstructure that consists of a network of smaller alumina grains, surrounded by the interpenetrating-polymer phase and some open pores (Figure 4.3 and Figure 4.4). The grains continued to grow in size and the microstructure become relatively denser as the temperature increased to 1350 °C (Figure 4.5). At higher temperature (1550°C) the crystal structure became more compact and much denser composed of faceted grains with larger size microstructure and distinct grain boundaries with sharp edges. Disappearing pores were noticed between the grains in Exp155 (Figure 4.6).

Table 4.1 Mean (M), standard deviation (SD), medians (MD) and interquartile range (IQR) values of density before (P_0) and after (Pi) polymer infiltration and infused density percent (*Inf.P%*) for polymer infiltrated alumina groups.

Group	P_0 (g/cm^3)		P_0 (%)		P_I (g/cm^3)		*Inf. P (%)*	
	M (SD)	MD (IQR)	M (SD)	MD (IQR)	M (SD)	MD (IQR)	M (SD)	MD (IQR)
Exp 125	2.79 (0.14)	**2.78** (0)[a]	71.72 (3.54)	**71.38** (7)[a]	3.10 (0.09)	**3.09** (0.19)[a]	97.06 (4.45)	**99.22** (4.83)[a]
Exp 130	3.02 (0.21)	**2.93** (0)[a,b]	77.58 (5.38)	**75.34** (10)[a,b]	3.26 (0.15)	**3.2** (0.28)[a,b]	95.95 (4.30)	**97.06** (4.26)[a,b]
Exp 135	3.18 (0.19)	**3.25** (0)[b,c]	82.69 (5.46)	**83.49** (7)[b,c]	3.40 (0.15)	**3.43** (0.2)[b,c]	93.39 (6.69)	**97.05** (13.15)[a,b]
Exp 155	3.56 (0.23)	**3.66** (0)[c]	91.50 (6.48)	**92.15** (13)[c]	3.65 (0.18)	**3.73** (0.35)[c]	91.67 (6.48)	**92.22** (12.43)[b]

Table 4.2 Mean, standard deviation of biaxial flexural strength for alumina groups.

Group	Sintering T (°C)	Flexural Strength (MPa)
Exp125	1250	**334.67** (59.91)[a]
Exp130	1300	**343.89** (55.45)[a]
Exp135	1350	**385.67** (65.31)[a]
Exp155	1550	**379.85** (60.29)[a]

Table 4.3 Mean, standard deviation, medians and interquartile range of different optical properties of alumina groups.

Group	RI		CR		TP		LT (%)	
	M (SD)	MD (IQR)	M (SD)	MD (IQR)	M (SD)	MD (IQR)	M (SD)	MD (IQR)
Exp125	1.97 (0.04)	**1.97** (0.06)[a]	98.99 (1.01)	**99.32** (0.89)[a]	00.43 (0.16)	**0.42** (0.26)[a]	1.88 (0.39)	**1.89** (0.46)[a]
Exp130	1.96 (0.06)	**1.96** (0.11)[a]	98.85 (1.02)	**99.36** (1.44)[a]	00.48 (0.20)	**0.47** (0.29)[a]	2.14 (0.61)	**2.33** (0.99)[a]
Exp135	1.99 (0.7)	**1.98** (0.21)[a]	99.04 (1.04)	**99.38** (0.84)[a]	03.99 (1.68)	**4.45** (2.53)[b]	2.46 (0.71)	**2.41** (0.48)[a]
Exp155	1.79 (0.05)	**1.79** (0.08)[b]	97.09 (0.96)	**97.14** (0.48)[b]	07.26 (0.81)	**7.09** (0.69)[c]	6.77 (0.422)	**6.80** (0.50)[b]

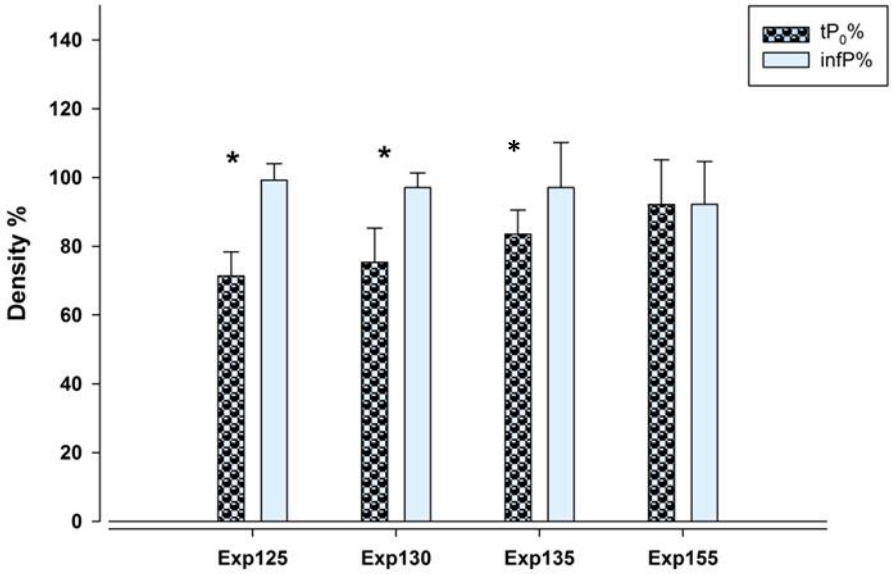

Figure 4.1 A bar chart illustrating the median density change of test materials before and after polymer infiltration. Error bars represent the interquartile range. Bars marked with a * indicate significantly different density values.

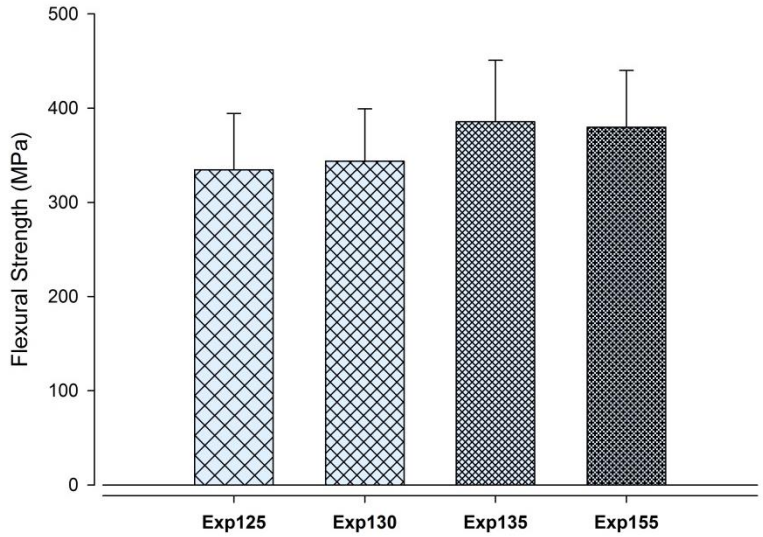

Figure 4.2 A bar chart representing the difference in the mean of flexural strength between the test groups. Error bars represents the standard deviations.

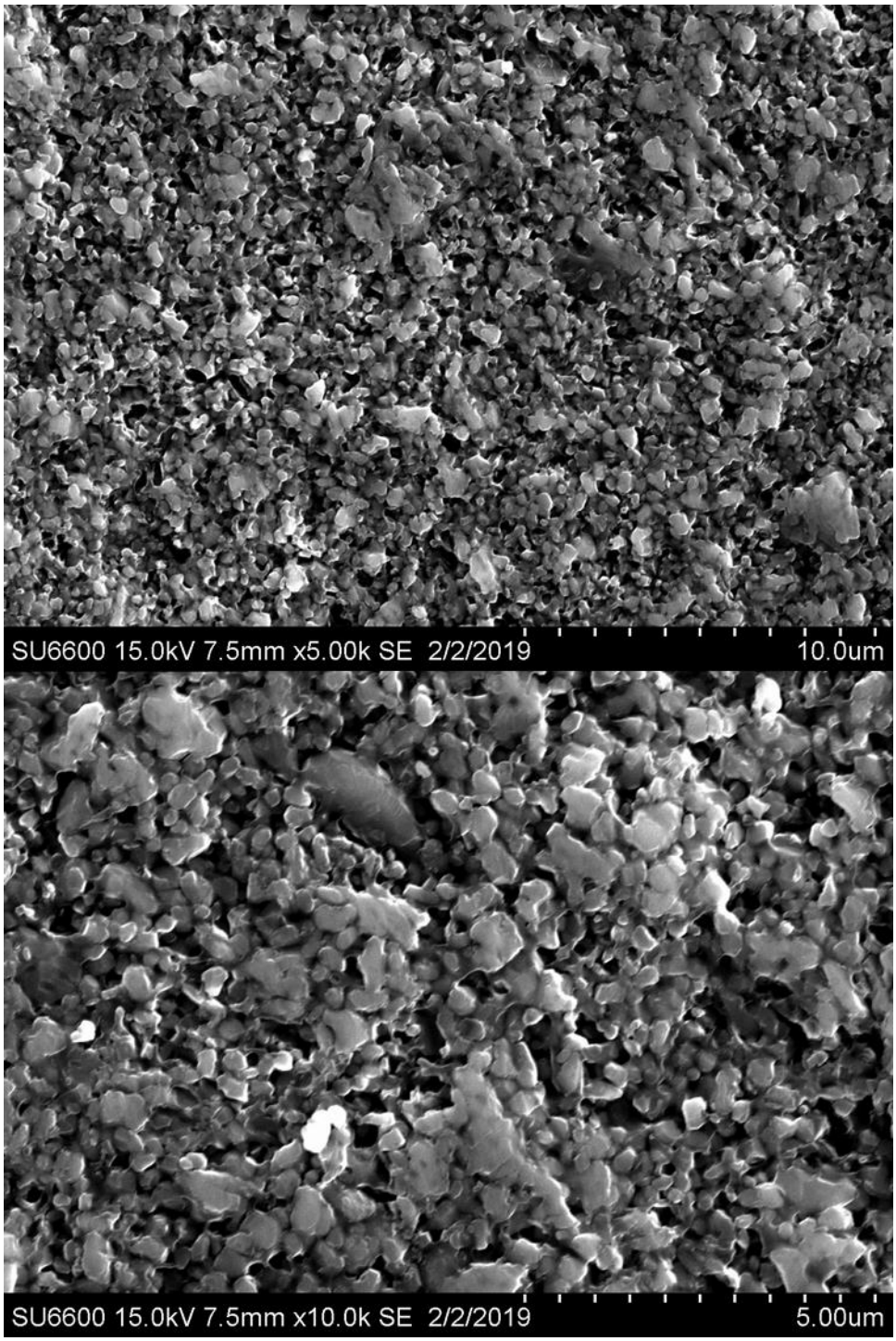

Figure 4.3 SEM pictures of polymer infiltrated alumina specimen (Exp 125) at magnification of 5000x and 10Kx.

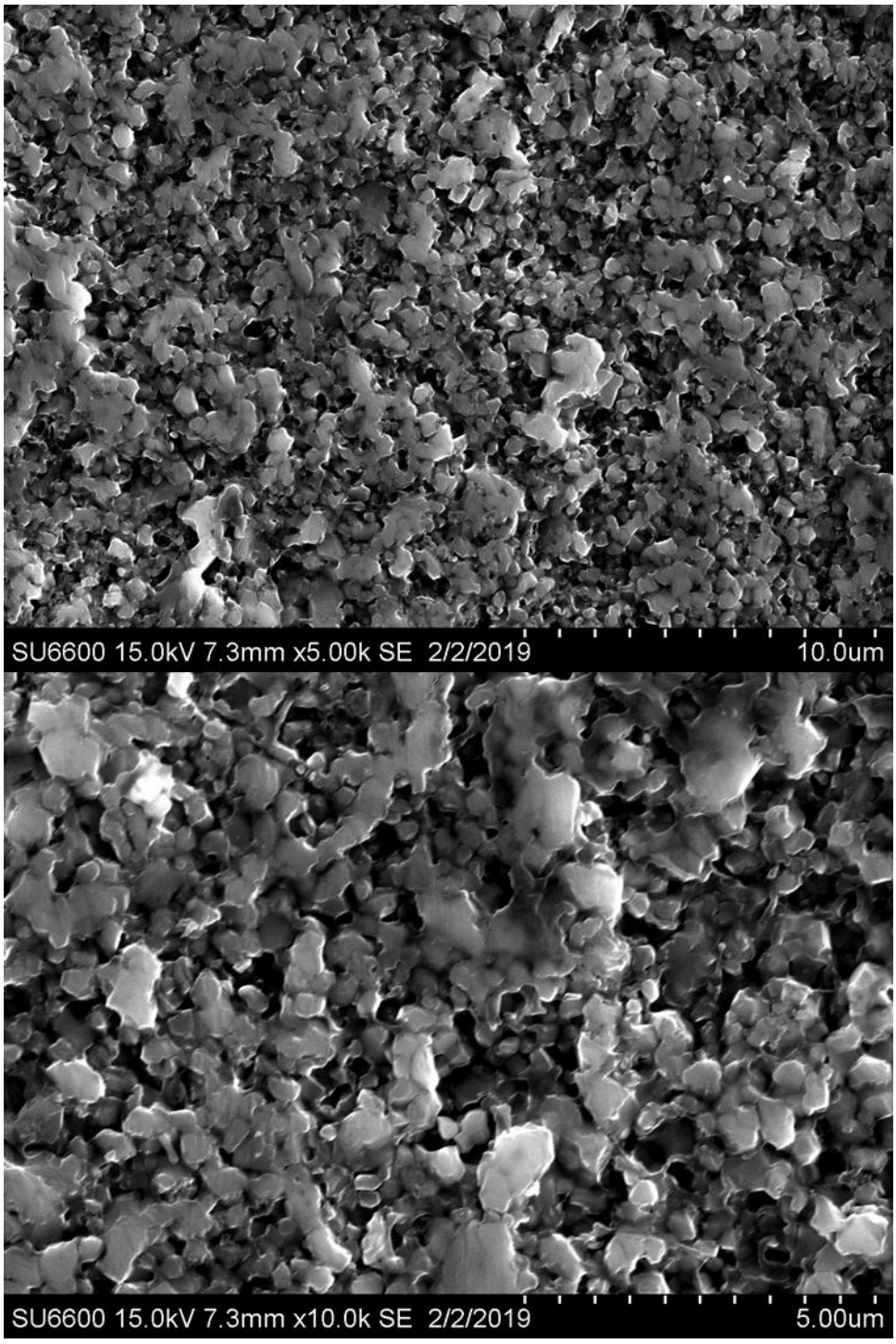

Figure 4.4 SEM pictures of polymer infiltrated alumina specimen (Exp 130) at magnification of 5000x and 10Kx.

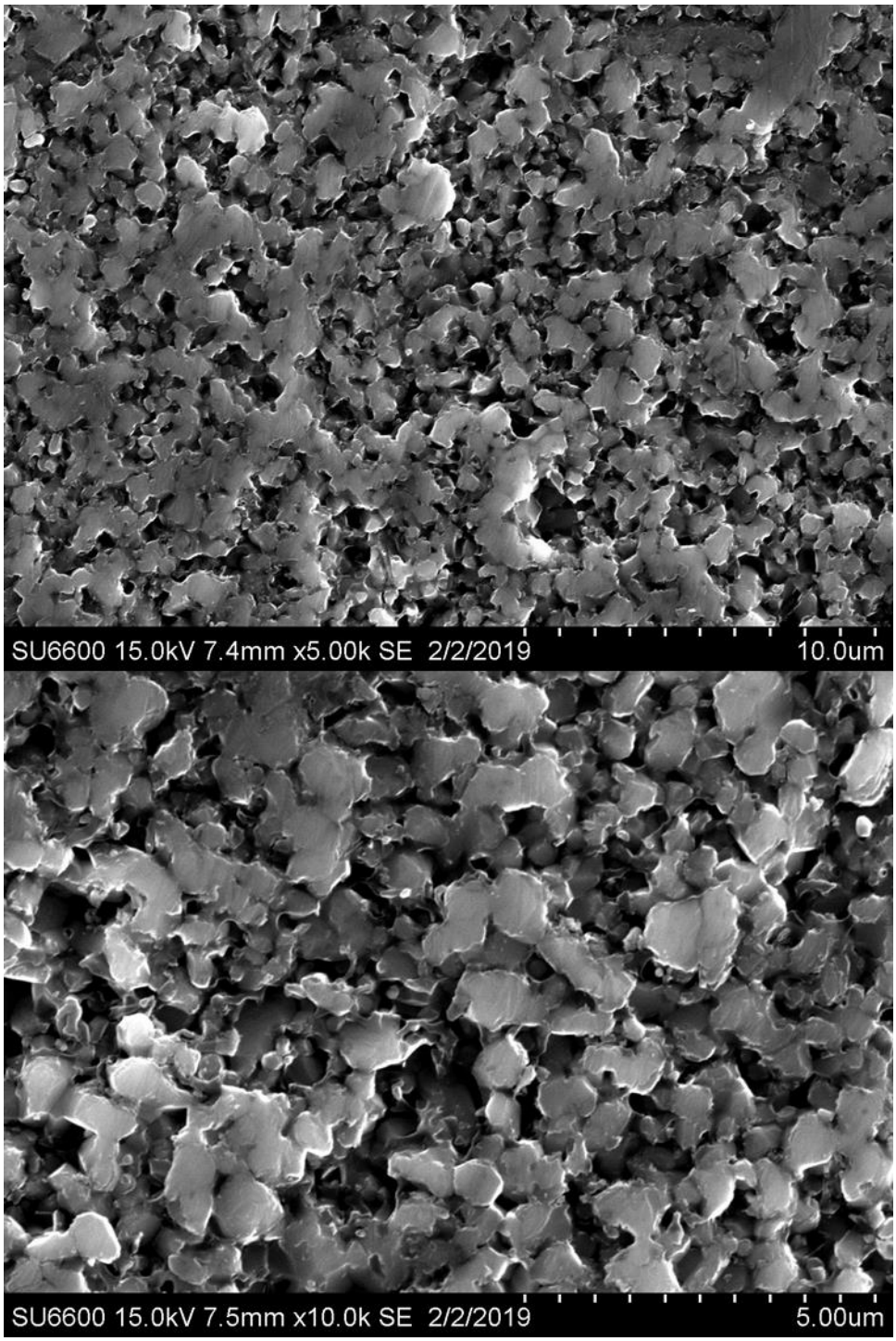

Figure 4.5 SEM pictures of polymer infiltrated alumina specimen (Exp 135) at magnification of 5000x and 10Kx.

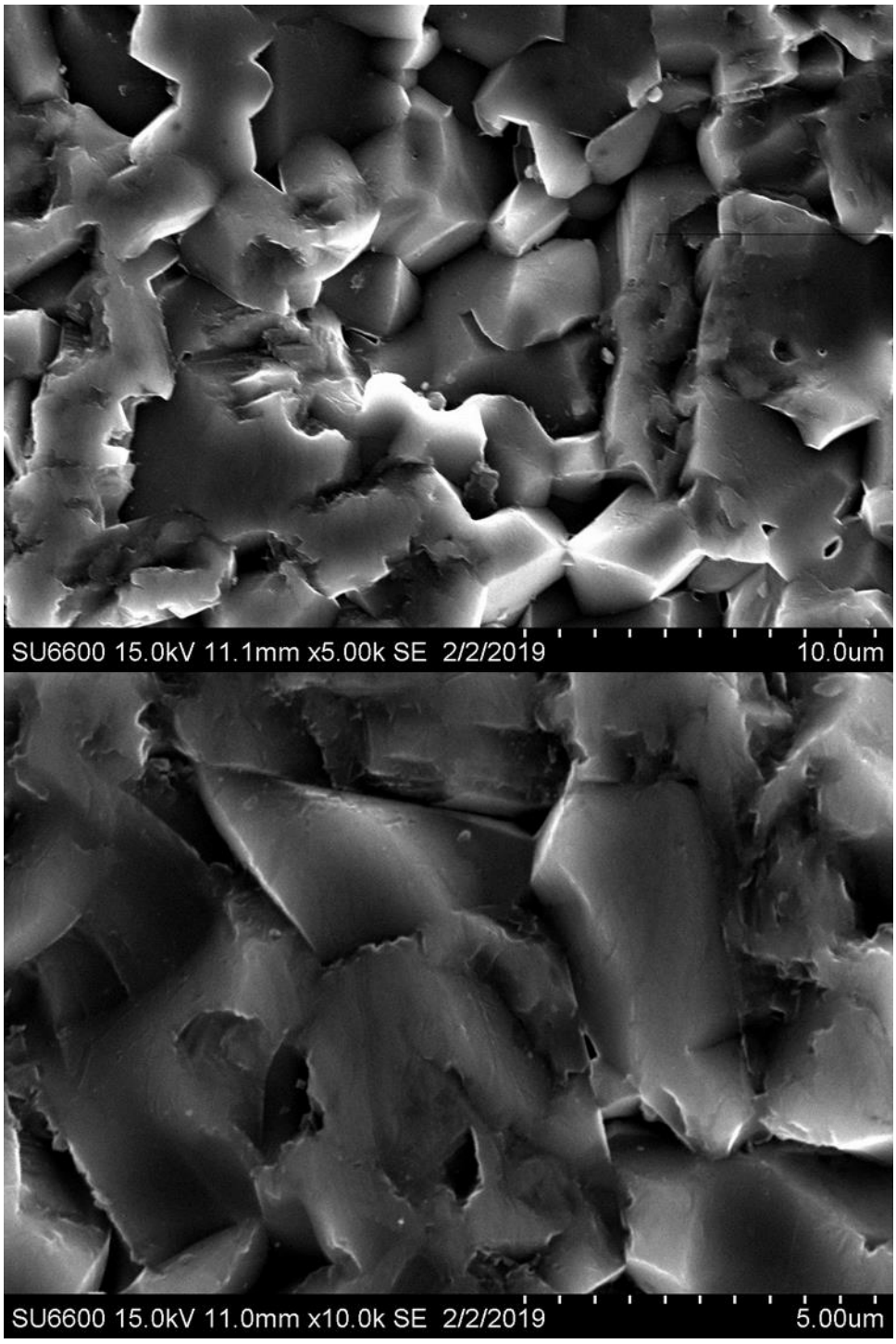

Figure 4.6 SEM pictures of polymer infiltrated alumina specimen (Exp 155) at magnification of 5000x and 10Kx.

4.5 Discussion

The aim of this study was to fabricate polymer-infiltrated ceramics with different sintering temperatures and to evaluate the effect of sintering temperature on the densities, optical and mechanical properties of the prepared samples. At a microstructure level, polymer-infiltrated ceramics consist of two phases, ceramic phase with grains and grains boundaries and polymer phase. The grains form as a result of ceramic consolidation (sintering) process at high sintering temperature. Consolidation of ceramic is a thermally activated process which begins when the ceramic particles adhere together and necks start to form. The complete consolidation occurs when grains boundaries and grains corners are established and pores are closed leading to an almost completely dense material (137).

The sintering process of ceramic is influenced by a variety of factors: the nature of the powder, impurities, intentional additions, pressing conditions, sintering temperature, time and atmosphere. The particle size also has a great influence on the sintering process of ceramic (141). The smaller the particle size, the better sinterability and the finer the grains will be. Larger particles result in an open porous structure which requires higher sintering, hence a higher chance of shrinkage (208). It has been reported that fine particles (less than 0.5 μm in diameter) contribute to the surface diffusion that results in necking between coarse particles (141, 209). In this study, the alumina powder used to fabricate the ceramic matrix had 0.4 μm particle size.

Grain size, form and orientation are affected by the colloidal forming techniques. A comparison between slip casting and uniaxial pressing of the ceramic powder revealed that the minimum density gradients in green bodies prepared by slip casting allows for obtaining more homogeneous materials in terms of translucency and microstructure (196). It was also found that slip casting works very well with small particles (micro or nano levels). The flexural strength and the fracture toughness of In-Ceram Alumina made with slip cast has been shown to be higher than that made via a dry press technique(210).

As mentioned above, sintering temperature and time also play a significant role in developing the ceramic microstructure. Complete densification of alumina particles requires sintering temperatures traditionally up to 1700–1800 °C involving grain boundary and volume diffusion. In the temperature range from 1050 to 1200 °C, with

help of the fine particles, the large particles are bonded to each other by surface diffusion and fusion of fine particles located in the contact area between large ones (211). It was also found that with increasing the sintering temperature from 1150 °C to 1550 °C, the alumina grain size increased from 0.29 μm to 9.8 μm, respectively (212). Higher sintering temperature has been shown to result in rapid grain growth and higher densification (143). These findings support the present study findings; as the sintering temperature increased, the density of ceramic matrix increased and pores decreased. Increasing the sintering temperature from 1250 ˚C to 1550 ˚C resulted in increasing the theoretical density % from 71.38% to 92.15%. Hence, the first null hypothesis was rejected. Obvious pores and loose microstructure with interconnected grains growth were observed at 1250 °C (Figure 4.4) indicating insufficient sintering and low density. This is supported by the 71.38% theoretical density. As the temperature increased, a relatively well-developed microstructure with fewer residual pores was observed (Figure 4.5-4.7). At 1550 °C, the crystal structure became more compact and much denser composed of faceted grains with larger size with the presence of sharp grain boundary edges. These findings could be explained by a previous study which demonstrated that the sintering process could eliminate the inter-particle pores of a granular material by atomic diffusion, which arise from capillary forces (213). As the temperature increased, the particles were sintered together and pores on the grain boundaries were reduced by solid-state diffusion. These changes of microstructure and density thereby lay the foundation to understand the effect of sintering temperature on mechanical properties which were investigated in the subsequent studies.

Grain size can also be controlled by the heat rate during sintering. A slow heating rate has been proven to be more effective in obtaining high density alumina with fine microstructure (212), with a heat rate of 8 °C /min resulting in a transparent alumina with a grain size of 0.27 μm, whereas a heating rate of 100 °C /min results in an opaque one with a larger grain size of 0.55 μm (212). In this study, a slow heating rate (10 °C /min) was selected to control the grain size growth. It is important to control the grain size of ceramic materials to ensure good optical and mechanical properties. In general, the grain size of polycrystalline ceramics should be smaller than the wavelength of the visible light to obtain high translucency and proper fracture strength (214).

Full densification of polycrystalline ceramic materials requires sintering at high temperature; this may be associated with sintering-induced shrinkage and abnormal grain growth. Therefore, polymer infiltrated ceramics could be a preferred way to produce dense materials by infiltrating polymer into a ceramic matrix that is sintered at a relatively low temperature to control grain growth and its influence on properties. As per the findings of this study, infiltration did improve the density of alumina samples; hence the second null hypothesis was rejected. However, the challenging part of manufacturing polymer-infiltrated ceramics is the unavoidable volume shrinkage during polymerisation. Polymerisation shrinkage of 8.8 % for UDMA and 14.4 % for TEGDMA has been measured elsewhere (215). As the polymerisation occurs within the capillaries of the porous ceramic, where the monomer availability is limited, it generates a defect or open pores in the microstructure. Such an effect will lead to interfacial de-bonding between the ceramic and the polymer phases. However, applying a high pressure during the polymerisation process has been proven to reduce the polymerisation speed as well as shrinkage (139). In this study, the polymerisation process was carried out under high pressure to reduce the shrinkage.

Factors like infused density% and sintering temperature have been shown to influence optical properties more than the biaxial flexural strength of polymer infiltrated ceramics. In this study, a significant difference was found between the test groups in terms of RI,CR,TP and LT. However, no significant difference was detected with regards to the flexural strength. Thus, the third null hypothesis was partially rejected.

Refractive index is defined as the ratio of light velocity in vacuum to that in a material (216). Common instruments to measure refractive index are Abbe refractometer, interferometry, and the Becke line test(217). In this study, a digital refractive index meter capable of measuring a wide range of refractive indexes (between 1 and 3) was used. The presence of multiphase, anisotropic ceramic microstructure and porosity can significantly influence the refractive index of polymer-infiltrated ceramics (217). The refractive index is much higher for ceramic than polymer, and this can affect the overall refractive index of the polymer-infiltrated ceramic and also result in opaque materials along the interfaces between ceramic and resin (218). This may explain the higher contrast ratio of the first three groups with more polymer infused density% as more light scattering occurs when passing through these phases with mismatched refractive indexes. It has been shown that

ceramic composites made of glass and ceramic with matching refractive indices showed less light scattering and more light transmission compared to commercial ceramic–glass composites (140). Previous studies have shown that the refractive index of dental composite is around 1.45 (11, 219-222). In this study, the refractive index was much higher, which could be explained by the anisotropic microstructure of alumina resulting in more light refraction through the arbitrary crystallographic orientation.

Translucency is considered a primary factor in achieving aesthetic dental materials. It gives a natural appearance and provides vitality to the dental restoration. It can be defined as the relative amount of light passage through an object (223). The more translucent the material is, the more light is transmitted with minimumal scattering. The translucency of a material can be measured by either relative translucency or absolute translucency. Relative translucency is measured by means of contrast ratio (CR=Yb/Yw) which is defined as the ratio of the illuminance (Y) of the test material when it is placed over a black background (Yb) to the illuminance of the same material when it is placed over a white background (Yw) [9]. This ratio increases with opaque materials and decreases towards zero with transparent materials [10]. Absolute translucency, on the other hand, can be measured as the percent of diffuse and direct transmitted light (total transmission T%) which necessitates the use of a dual beam integrating sphere radiometer or spectrophotometer able to capture all of the light transmitted through a specimen [11]. A true comparison between the absolute and the relative translucency has only been reported in one study (224), although various indices based on these concepts have been used without specifically referring to them. As there are currently no guidelines to describe which indices should be used to measure translucency in dentistry, many studies tend to use more than one index. In our study, contrast ratio, total light transmission and translucent parameter were used to measure translucency. As light scattering is more critical at shorter wavelengths and transmission can drop from 40% at 700 nm to less than 10% at 400 nm, in this study total light transmission was measured at the wavelength range of visible light. Other factors that contribute to reduced translucency include the thickness of the material and surface roughness. All specimens in this study were polished to give smooth surfaces and had a thickness of 1.5 mm (simulating the typical thickness of dental restorations) to control the effect of these factors on measurements of light transmission.

Sintering temperature seems to have a significant effect on the translucency of polymer-infiltrated alumina. The model group sintered at 1550 °C was the most translucent whereas those sintered at 1250 °C showed the least translucency. This confirms the findings of previous studies (225, 226): as the sintering temperature increases, the translucency increases by increasing grain size, sintered density, and reducing porosity, ultimately providing a more compact crystalline structure of ceramic. Larger grains increase the translucency of alumina by producing fewer grain boundaries but this, however, may reduce its mechanical properties.

Flexural strength is one of the most well established properties for evaluating the mechanical properties of ceramic materials in dentistry (227). Glass and ceramic fractography reveal that fracture in these materials is initiated by tensile stresses that can be often traced from surface flaws through the bulk of the material (228-230). A variety of methods may be used to determine the flexural strength which can be either uni-axial such as: 3-point-bending and 4-point-bending tests or bi-axial such as: piston-on-ring or piston-on-three-ball (231). The primary advantage of the biaxial method is that tensile stress at the central loading area and edges can be eliminated (232). Biaxial flexural strength tests using a piston on three balls were performed to evaluate the strength of tested materials in this study; strength values met those recommended by ISO 6872 protocol (> 100 MPa) (206).

Previous studies have shown that increasing the sintering temperature results in an increase of the flexural strength of porous ceramic matrices (233-235). In this study, there was a positive correlation between the sintering temperature and the density of porous ceramic. However, this was not the case after polymer infiltration. Increasing the sintering temperature did not significantly influence the strength of the polymer-infiltrated ceramics. This may have been due to the significance of the polymer infiltration step in strengthening porous ceramic materials. Resin infused ceramics have been shown to have greater biaxial flexural strength compared to porous and dense sintered ceramics (141); the flexural strength of partially sintered alumina (1250°C -1350°C) has been reported to be less than 200 MPa (236). In the current study, all the values obtained from different sintering temperature were above 300 MPa. The likely explanation for such an increase in the flexural strength is that residual stress from the polymerization shrinkage of heat-cured resin, probably constrained the system mechanically, creating tension

stresses (141). These tension stresses have to be overcome in the process of rupture and crack propagation and this enhanced the strength.

Compared with the currently available interpenetrating-phase ceramics in the dental market, the model polymer-infiltrated alumina showed a higher strength (334MPa-385 MPa) than Vita Enamic (191 MPa) (237) but less than glass-infiltrated alumina (In-Ceram alumina) (514 MPa)(238). Vita Enamic, on the other hand, has higher translucency (16.0) (237) compared with In-Ceram alumina (0.6) (239) and our model polymer-infiltrated alumina (ranged from 0.5 to 7). The translucency of a human tooth is reported to range from 15 to 19 with 1 mm thickness (207, 240).

The present study revealed novel and significant results relating to manufacturing and properties of polymer-infiltrated polycrystalline ceramics, reporting optical properties of these recently developed materials that have not been reported previously. In addition, this study focused on manufacturing the ceramic matrix by slip casting and partial sintering of a selected type of ceramic powder (alumina A16SG). Other brands with different particle sizes may require different processing and could result in other forms of microstructures that may significantly influence properties.

4.6 Conclusions

1. Sintering temperature has a significant influence on microstructure, porosity and density of the ceramic matrix. As sintering temperature increases, ceramic matrix density increases and porosity decreases.
2. The density of ceramic matrices increases significantly after polymer infiltration.
3. The increase in sintering temperature results in a significant improvement in the optical properties but not the biaxial flexural strength.
4. Ceramic matrix density has a significant influence on the flexural strength of polymer-infiltrated ceramics. Groups that initially had higher matrix density showed higher strength.

Chapter 5

Mechanical Coherence of a Novel Polymer Infiltrated Polycrystalline Ceramic and Other CAD/CAM Materials

5.1 Abstract

Objectives

The aim of this study was to investigate the mechanical properties of different sets of polymer infiltrated ceramics (PICN), compared to conventional ceramics and composites.

Materials and Methods

Twelve materials were tested: three CAD/CAM resin composites: Lava Ultimate (LU), Cerasmart (CS) and Grandio Bloc (GB); one commercial PICN material (Vita Enamic,VE), four model PICN ceramics sintered at different temperatures (Exp.125, Exp.130, Exp 135 and Exp 155); one ceramic filled Poly ether-ether ketone (Dentokeep, DP); one feldspathic ceramic block (Vitabloc Mark II, VM) and two conventional resin composite (Sinfony,Si and TPH Spectrum,Sp) were tested. 60 samples were prepared with the dimensions of 14×12×2 mm for CAD/CAM and DP materials, 15x2 mm for model PICN and conventional resin materials. Micro hardness of the specimens was assessed using an automatic micro hardness instrument (FM-700, Future-Tech Corp, Japan). A Vickers indenter was used and the micro hardness of specimens was measured under a load of 100 g for 10 s at room temperature. Nano hardness was also tested using an automatic Nano-indentor (Nanovea M3, USA) with a 50 g load with a 10 s pause/dwell. The hardness results obtained by micro indentation and nano indentation of all the test groups were compared using one-way ANOVA ($p \leq 0.05$). Tukey *post-hoc* test was used to determine the differences in micro and nano hardness between the groups. The surface morphology of the tested materials was studied by Scanning electron microscope (SEM).

Results

The nano hardness mean values of the studied materials ranged from 0.29 to 7.13 GPa. For micro hardness, the mean values ranged from 25.82 to 619.41 HV. Elastic modulus mean values ranged from 3.49 to 102.9 GPa. Statistically significant differences were found between the tested materials for all the studied mechanical properties. A positive correlation was found between nano hardness and micro hardness values in all the tested materials (Pearson correlation coefficient=0.94, $p<0.001$). Positive correlations between the amount of ceramics and hardness values in both micro-hardness and nano-hardness data were noticed (Pearson correlation coefficient= 0.81 and 0.78, p=0.001, respectively).

Conclusions

Different CAD/CAM materials showed different surface morphology with fillers in different size, shape and density. Micro hardness and nano hardness of the studied materials increased systematically with an increase in filler loading. Mechanical properties of PICN ceramic were significantly influenced by the sintering temperatures of their ceramic matrices.

Key words Polymer-infiltrated Ceramic, Alumina, Resin Composite, Hardness, Elastic Modulus.

5.2 Introduction

With the incorporation of CAD/CAM technology in dentistry, novel microstructures for ceramic, resin composite and PEEK materials have been developed causing an important change in the clinical workflow for dental practitioners and technicians.

Ceramics in general have good mechanical and optical properties, as well as excellent biocompatibility (138, 241, 242). However, it is hard and brittle which is a major drawbacks as this affects its laboratory and clinical performance. Glass-matrix ceramics have mechanical problems such as brittleness and high abrasiveness to opposing enamel which could be related to their strong surface hardness (243, 244): this might also affect its CAD/CAM machinability(245).

Resin composites with various matrix compositions and different percentages of ceramic fillers are currently available as monolithic blocks fabricated by CAD/CAM systems. CAD/CAM resin composite restorations show superior mechanical properties compared to conventionally polymerised resins (246). This is due to the fact that the resin composite blocks for use with CAD/CAM are produced under controlled conditions with high levels of pressure and temperature that are impossible to meet with 'conventional' chairside polymerisation [2-4]. CAD/CAM composite restorations exhibit more colour stability and withstand more fracture load compared to conventional composite restorations [5, 6]. However, compared to ceramic, resin composites in general have less desirable wear, biocompatibility and mechanical properties (193).

PEEK shows promising mechanical properties that could make it a good alternative material. The tensile strength of PEEK polymer is comparable to that of enamel and dentine. A 3-unit fixed partial denture made of PEEK-based CAD/CAM material demonstrated a higher fracture resistance compared to lithium disilicate glass ceramic, alumina and zirconia (247, 248). Moreover, the abrasive property is good and comparable to metallic alloy (249).

Polymer infiltrated ceramic network (PICN) has been suggested as an alternative material, combining the elastic modulus of resin composite with the long-term aesthetic stability of ceramics (198). This material is composed of 75 vol% porous feldspathic porcelain infiltrated with 25% resin polymers namely, UDMA and TEGDMA, based on a similar

concept of manufacturing glass-infiltrated ceramic (In-Ceram) (103). Glass-ceramic based PICN shows promising results for single crowns (250), and developing methods to improve this material to be used for short/long span bridges through microstructure refinement has become a primary focus for many researchers. Monolithic alumina that has smaller grain size and better mechanical behaviour and higher fracture toughness (77) could be a good substitute for feldspathic porcelain in PICN materials.

In general, further investigation of CAD/CAM composites in many aspects such as mechanical properties, bonding, and biocompatibility is highly needed. Most importantly, their mechanical properties such as flexural strength, flexural modulus, modulus of elasticity, and hardness that can predict the material clinical success and performance are important to be evaluated. Hardness is a good indicator of the ability of a material to resist local permanent deformation under occlusal load (251).

Several indentation techniques have been developed to measure the mechanical properties of materials from a contact of known geometry. Recently, the use of new sensors and actuators allow indentation testing to be performed at submicron scales. This relatively new technique is called nano-indentation and has been popular in investigating the mechanical properties of many materials such as, polymers, metals, glasses and ceramics, with progress in mechanical testing particularly in terms of control, sensitivity and data collections. The most commonly properties tested via nano-indentation are hardness and modulus of elasticity.

The aim of this study was to investigate different sets of polymer-infiltrated ceramics, focusing on their mechanical coherence and to compare them to different sets of CAD/CAM blocks and conventional resin composites. The mechanical coherence in this study was evaluated by indentation tests. Two null hypotheses were tested in the current study: the first null hypothesis was that there would be no difference between PICN ceramics and other CAD/CAM and conventional resin composite materials in terms of nano-hardness, micro-hardness and elastic modulus. The second null hypothesis was that there would be no correlation between hardness values at micro and nano scales, and between the ceramic filler loading measured in wt% and the hardness values measured at the two scales.

5.3 Materials and Methods:

A total of 12 restorative materials with different compositions were investigated in the study. Six were commercial CAD/CAM blocks; two were conventional composite and four were model CAD/CAM PICN materials. Material and manufacturer details are listed in Table 5.1.

Table 5.1 CAD/CAM materials used in the current study.

Category	Material's Name	Code	Company	Lot Number	Compositions
Resin composite CAD/CAM blocks	Cerasmart	CS	GC Dental Products Europe, Leuven, Belgium	1502091	Nanoceramic composite (BisMEPP, UDMA, DMA) with 71 wt% silica (20nm) and barium glass (200 nm) nanoparticles.
	Lava Utimate	LU	3M ESPE, Seefeld, Germany	N750333	Composite resin material (BisGMA, UDMA, BisEMA, TEGDMA) with 80 wt% silica and zirconia nanoparticles (4-11nm)
	Grandio® blocs	GB	VOCO GmbH, Cuxhaven, Germany	1723181	TEGDMA, Urethane- adduct Barium-alumino-borosilicate (0.5-2µm); fumed silica (20-60nm) 86 wt%
PICN Ceramics	VITA Enamic	VE	VITA Zahnfabrik, Bad Säckingen, Germany	46680	Polymer-infiltrated-feldspatic ceramic-network material (UDMA, TEGDMA) with 86 wt% ceramic
	Model polymer infiltrated alumina	Exp125 Exp130 Exp135 Exp155	Boston University	---	UDMA,TEGDMA,BP,MPS,Ethanol, Distilled water, Glacial acetic acid , (0.4 µm) alumina ceramic.
Ceramic CAD/CAM blocks	Vita Mark II	VM	VITA Zahnfabrik, Bad Säckingen, Germany	40870	Feldspathic ceramic
PEEK CAD/CAM Blocks	DentoKeep	DK	Nt-trading , Germany	G15DK1401	PEEK polymer based ceramic,20% Titanium Oxide
Indirect resin Composite	Sinfony	Si	3M ESPE, St Paul, MN	3788554	HEMA and 10% to 30% (octahydro-4,7-methano1H-indenediyl) bis(methylene)diacrylate), strontium-aluminium borosilicate glass, silicon oxide, silane and photoinitiators. Filler compositions= 50 wt%
Direct resin Composite	Spectrum TPH3	Sp	Dentsply Detrey GmbH, Konstanz, Germany	1708001024	Bis-GMA, bis-EMA, TEGDMA. Barium aluminio-borosilicate (<1m). Barium fluoro- aluminio borosilicate (<1µm) Highly dispersed silicon dioxide (10–20nm) Filler compositions=57 wt%

5.3.1 Manufacturing of PICN

Porous alumina matrices with nano-sized alumina particles were fabricated initially by slip casting into disc shaped specimens (15x2 mm) before being partially sintered at different temperatures (1250 °C, 1300 °C, 1350 °C and 1550 °C). The ceramic matrices were then conditioned with a silane coupling agent- methacryloxypropyltrimethoxysilane (MPS) prior to resin infiltration to ensure that the polymer network was chemically cross-linked to the ceramic network to form an interpenetrating network system. The chemically conditioned porous inorganic network was infiltrated with a cross-linking polymer mixture and initiator by capillary action. The polymerisation process was induced by heat (100 °C) and pressure (138 MPa), leading to a polymer-infiltrated-ceramic-network material.

5.3.2 Sample Preparation and Hardness Assessment:

A pilot study was conducted on specimens from each group to identify the sample size, applied load and the dwell time (s) for the nano- and micro-hardness experiments. Five samples from each group were found to be sufficient to indicate the statistical significant difference among the groups. For conventional direct resin composite, samples were prepared using a PFTE mould with an internal diameter of 15.0 mm and 2 mm thickness according to the dimensions specified by ISO FDIS 4049:2009 (170). Samples were fabricated by applying each material into the mould placed against a clear matrix strip and a glass slab. The mould was slightly overfilled with the material and the excess was then extruded by applying another polyester matrix strip and a glass slab and pressed firmly. Care was taken to minimize entrapped air while uncured materials were applied into the mould. Each sample was then cured for 20 s at five overlapping sections of the top and bottom surfaces using an LED light curing unit (EliparTM, 3M ESPE, USA), with an 10 mm diameter light exit, under standard curing mode. The light curing unit had an output irradiance of circa 1200 mW/cm^2 and wavelength range 430-480 nm as stated by the manufacturer. After curing, each sample was gently pushed out from the mould and excess flash at the periphery was removed using a sharp blade.

For conventional indirect resin composite, samples were initially prepared following the same procedure as for the direct, then polymerisation was carried out in two cycles,

according to the manufacturer instructions. The first cycle was performed using a light curing unit (Visio Alpha, 3M ESPE, USA) with output irradiance of circa 400 mW/cm^2 for 15 s; the second cycle was photo-polymerization (Visio Beta, 3M ESPE, USA) under vacuum at 40°C for 15 min.

For CAD/CAM materials, 30 bar-shaped specimens (12x4x2 mm) were sectioned from CAD/CAM blocks to perform hardness assessments at nano and micro levels. The specimens were sectioned using a precision cutting machine (Isomet 1000, Buehler, LakeBluff, USA).

All the samples were mounted in phenolic ring moulds (25x15 mm) (Buehler, Coventry, UK) and embedded in epoxy resin (Buehler, Coventry, UK) and sequentially polished with silicon carbide grinding papers (P320, P600, P800, P1200, P2500 and P4000) and finished with 1 and 0.25 micron diamond paste using an OmegaPol metallurgical polisher machine (Spectrographic, United Kingdom). Light finger pressure was applied on the specimen against the felt cloths of the polishing machine, with each polishing step carried out for 2 min. Polished specimens were then checked using a light microscope at 10x,20x and 100x magnifications to ensure absence of scratches. An ultrasonic bath (Nusonic, Transsonic T310, Germany) was used to clean specimens in distilled water for 10 min. Each specimen was stored dry in a clean container at room temperature for 24 h before investigation.

5.3.3 Determination of Ceramic Content

Ceramic weight contents of the test materials were determined by the standard ash method described in ISO 1172:1999 (184). The concept of this method is based on removing the organic matrix in a resin composite material by burning. All the specimens (n=3) were stored in a desiccator at 37 °C for 24h. A pre-heated silica crucible was used to contain the specimen throughout the experiment. The weight of each specimen was measured to an accuracy of 0.01 mg using a calibrated electronic analytical balance (A&D, A&D Instrument LTD, Oxford,UK). Specimens were heated in an electric furnace (Programat EP 5000, Ivoclar Vivadent, Liechtenstein, Austria) at 600°C (1200 °C for DK group-Figure 5.5) for 30 minutes to burn out the organic matrix and then placed back in the desiccator to cool down before re-weighing. The latter weight consisted only of the inorganic component.

Ceramic weight fraction (wt%) was determined with the following formula:

$$Ceramic\ wt\% = \frac{(w_3 - w_1)}{(w_2 - w_1)} x100 \quad \textbf{(30)}$$

Where:

w_1 is the initial mass of the dry silica crucible.

w_2 is the initial mass of dry silica crucible plus dried sample.

w_3 is the final mass of the silica crucible and the residue of the burned sample.

5.3.4 Nanoindentation Assessment

Nano-hardness measurements were performed at room temperature using a nanoindentor device (Nanovea M3, USA). The device is fully automated with touch screen, automated controlled load and depth allowing work on different types of samples for quick nanoindentation results under ASTM standard including hardness, elastic modulus and creep depth.

A Berkovich indenter with cone angle of 130.54° was used. The Poisson's Ratios of the indenter was 0.07, and the elastic modulus was 1140 GPa. Nanoindentation was performed at a 50 g load with 10 s pause/dwell. The sample was attached with cyanoacrylate adhesive to the provided metallic sample mounting block (38x15mm) which was magnetically attached to the sample holder of the nanoindenter device. Calibration indents were made on a fused silica sample with an elastic modulus of 71.3 GPa and hardness of 8.9 GPa.

Five continuous indents with a spacing of 250 µm were performed in a line. Five sets of 5 tests were performed on each test material. Nano hardness was calculated based on the following formula:

$$H = \frac{P}{A_p} \quad \textbf{(31)}$$

Where P is the applied load in mN and Ap is the projected area of the indentation. Elastic modulus was determined by the machine from the slope of the unloading curve of the load displacement data at the maximum load based on the Oliver and Pharr method (152) as below:

$$E = \frac{1}{2} \times \frac{\sqrt{\pi}}{\sqrt{A}p} \times \frac{dh}{dp} \quad \textbf{(32)}$$

Where *dh* is the change in depth; *dp* is the difference in load.

5.3.5 Microhardness Assessment

A specialised micro-hardness instrument (FM-700, Future Tech Corp., Japan) with a Vickers diamond indenter was used. Five sequential measurements with a spacing equal to 4 times the diameter of the indentation were taken for each surface with fixed 100 g load applied for 10 s (dwell time). The hardness was automatically calculated by the machine via the following formula:

$$VHN = 0\ 1891 \times \frac{P}{d^2} \quad \textbf{(33)}$$

Where:

P is the applied load in Kgf.

d^2 is the Surface area of indentation in mm.

5.3.6 SEM Analysis:

Scanning Electron Microscopy (FEI Quanta 650 FEG, Oxford Instruments, UK) was used to characterise the cross-sectional microstructure of the CAD/CAM materials used in the present study. Specimens were ultrasonically cleaned and dried with hot air. After gold/palladium coating using a sputter coater (Quorum Q150T-S, Quorum Technologies Ltd, UK), specimens were viewed under a field emission mode with an accelerating voltage of 10KV and a working distance of 10 mm. Images at different magnifications were taken.

5.3.7 Statistical Analysis:

The data for all groups were collected and analysed statistically using SPSS 23.0 (IBM SPSS Statistics, SPSS Inc., Chicago, IL, USA) and checked for normality using Shapiro-Wilk tests. A one-way ANOVA was used to analyse all data. Tukey *post-hoc* testing was used to assess the difference in terms of elastic moduli, micro- and nano-hardness between the groups. A Pearson product moment correlation analysis was used to assess the relationship between different variables. Significance level for all tests was set at $\alpha=0.05$.

5.4 Results

Mean and standard deviations for nano-hardness, micro-hardness, elastic modulus, ceramic density and ceramic contents are presented in Table 5.2 and Figure 5.1. The mean values for nano-hardness ranged from 0.29 to 7.13 GPa. For the micro-hardness, the mean values ranged from 25.82 to 619.41 HV. Elastic modulus mean values ranged from 03.49 to 102.9 GPa. Ceramic density for the model groups ranged from 71.72% to 91.5%. Measured ceramic contents ranged from 25.73% to 91.71%.

Statistically significant differences were found between the tested materials for all the studied mechanical properties (p=0.001). Material Exp 155 demonstrated the highest mean values in terms of nano-hardness (7.13 GPa), micro-hardness (619.41 HV), and elastic modulus (102.9 GPa). While Si and Sp showed the lowest values for nano-hardness (0.29 GPa), and elastic modulus (03.49 and 03.76 GPa, respectively). For the micro-hardness, DK showed the lowest value of (25.82 HV). A positive correlation was found between the amount of ceramic (in wt%) and both micro-hardness and nano-hardness of the studied CAD/CAM materials (Pearson correlation coefficient= 0.82 and 0.79, p=0.001, respectively) (Figure 5.3-b and c). A positive correlation was also found between ceramic density% and sintering temperatures of the model PICN materials and hardness values at micro and nano levels (Pearson correlation coefficient= 0.72 and 0.76, p=0.001, respectively). In addition, a positive correlation was found between nano-hardness and micro-hardness values for all the tested materials (Pearson correlation coefficient=0.94, p<0.001) (Figure 5.3).

Typical force–displacement curves for the materials tested are shown in Figure 5.2. As the hardness or the stiffness of the materials increase the indenter displacement at maximum load is reduced, so it is not surprising that the VM samples showed the lowest penetration. In addition, the increase in displacement at peak load, which is an indication of the visco-elastic deformation occurring, increases as the indenter displacement at the start of the peak force hold increases. There is little evidence for visco-elastic deformation of the VM group. On unloading there is elastic recovery of the region around the impression and the final indent depth is reduced compared to the maximum indenter displacement. For the VM material the elastic recovery is dominated by the removal of the elastic deflection of the surface under load. Considerable elastic recovery

as well as visco-elastic deformations was noticed for Si,Sp and DK. For the PICN materials there was relatively little recovery which occured at the lower end of the unloading curve with minimal visco-elastic deformation.

Variation in shape, size, and density of crystal particles in polymer matrices were demonstrated in the SEM images (Figure 5.4). In CS (Figure 5.4-a), it is readily visible that there were ceramic nanoclusters surrounded by resin polymer matrix. Also evident were what seem to be some voids scattered all around. LU (Figure 5.4-b), on the other hand, showed larger sized ceramic particles embedded in a polymer matrix with fewer voids compared to the CS specimen. DK (Figure 5.4-c) showed a much smoother surface with fewer ceramic particles but regularly distributed on the matrix of PEEK polymer. VE (Figure 5.4-d) showed the double phases, with a porous ceramic network (light grey areas) infiltrated by polymer matrix (grey areas).

The model PICN showed a porous microstructure that consists of a network of smaller alumina grains, surrounded by interpenetrating polymer phase and some open pores (Figure 5.4;e-h). The grains continue to grow in size and the microstructure become relatively denser as the temperature increased to 1350 °C (Figure 5.4-g). At higher temperature (1550°C), the crystal structure became more compact and much denser, composed of faceted grains with larger size microstructure and distinct grain boundaries with sharp edges (Figure 5.4-h). Disappearing pores were noticed between the grains in Exp155.

Table 5.2 Mechanical properties and measured ceramic compositions data for PICN (dark grey), Feldspathic ceramic (dark blue), PEEK (light blue), bulk filled composite (light grey) and CAD/CAM composite blocks. Values represent the mean and standard deviation (SD). The ceramic density% was determined previously in Chapter 4.

Material	Nano hardness (GPa)	Micro hardness (HVN)	Elastic Modulus (GPa)	Ceramic density %	Manufacturer reported filler (wt%)	Measured Ceramic (wt%)
CS	0.78 (0.05)[a]	069.79 (01.71)[a]	10.25 (0.45)[a]	--	71	67.08 (0.28)
LU	1.17 (0.04)[b]	105.96 (01.64)[b]	15.05 (0.97)[b]	--	80	76.87 (0.43)
VE	2.81 (0.28)[c]	276.62 (12.60)[c]	33.74 (3.58)[c]	--	86	86.37 (1.30)
VM II	7.05 (0.38)[d]	499.92 (27.28)[d]	76.40 (3.77)[d]	--	100	100.0 (0.00)
DK	0.32 (0.02)[e]	025.82 (00.62)[e]	04.66 (0.62)[e]	--	20	25.73 (0.20)
GB	1.21 (0.17)[b]	123.06 (06.58)[b]	09.21 (1.92)[a]	--	86	84.55 (0.23)
Si	0.29 (0.08)[e]	043.23 (07.93)[a,e]	03.54 (1.02)[e]	--	50	50.26 (0.31)
Sp	0.29 (0.04)[e]	031.20 (01.22)[e]	03.49 (0.39)[e]	--	57	53.94 (1.25)
Exp125	1.33 (0.31)[b]	200.31 (37.74)[f]	17.89 (3.43)[f]	71.72 (3.54)	--	86.64 (2.85)
Exp130	1.78 (0.37)[f]	251.58 (25.51)[c]	30.18 (3.79)[g]	77.58 (5.38)	--	88.14 (2.21)
Exp135	4.38 (0.59)[g]	476.85 (30.82)[d]	45.46 (3.31)[h]	82.69 (5.46)	--	89.80 (2.99)
Exp155	7.13 (0.89)[d]	619.41 (81.93)[g]	102.9 (4.67)[i]	91.50 (6.48)	--	91.71 (1.45)

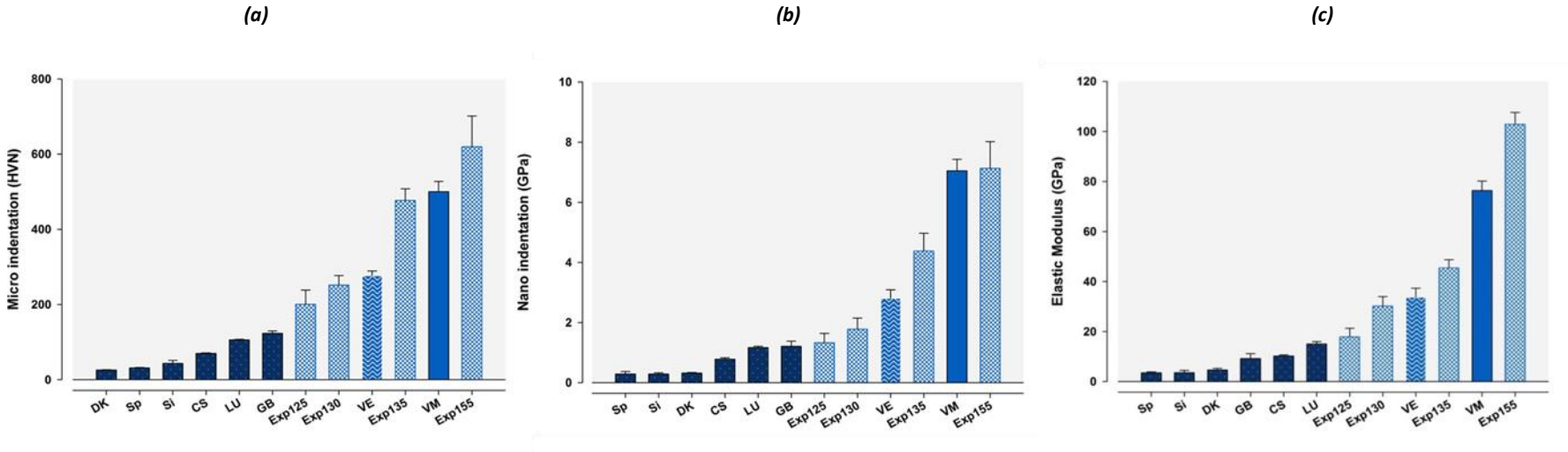

Figure 5.1 The average effect of the microstructural compositions on a) Micro hardness b) Nano hardness and c) Elastic modulus of CAD/CAM ceramic materials. The error bars represent the SD (n=5).

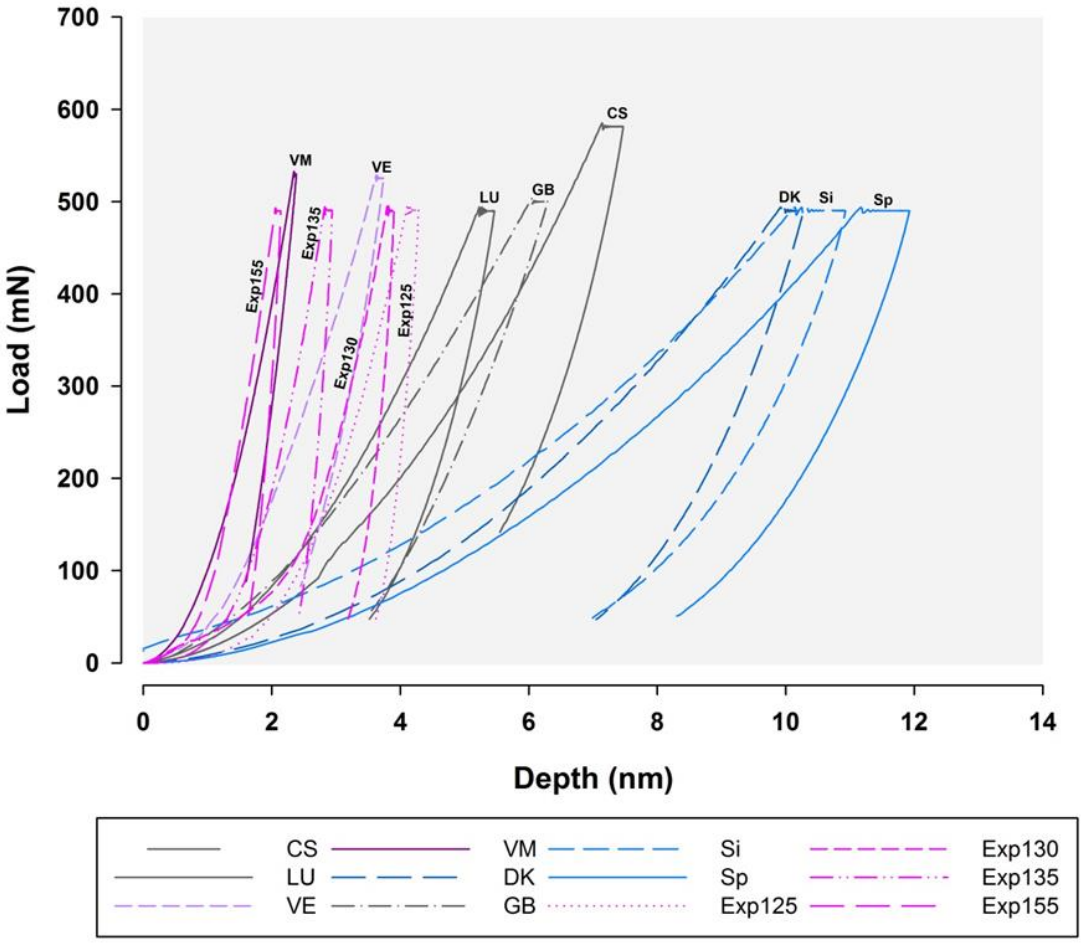

Figure 5.2 Comparison of the load displacement curves behaviour of the nano indentaion tests in the different groups. The differences in elastic and visco-elastic behaviours of the test materials under test load can be clearly appreciated. VM hardly demonstrated any indentation creep as compared to PICN and resin composites.

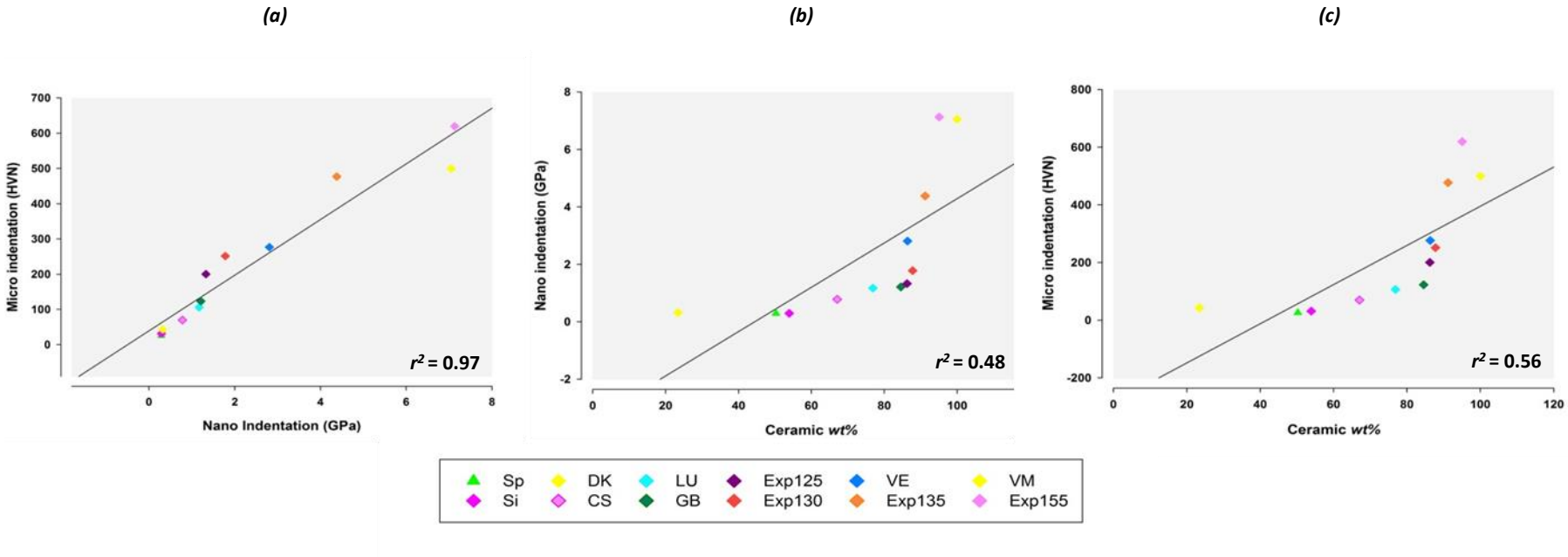

Figure 5.3 Linear regression analysis plot showing a positive correlation between the two measuring scales of hardness property in the tested materials (a),ceramic wt% and hardness values measured at nano (b) and micro (c) scales.

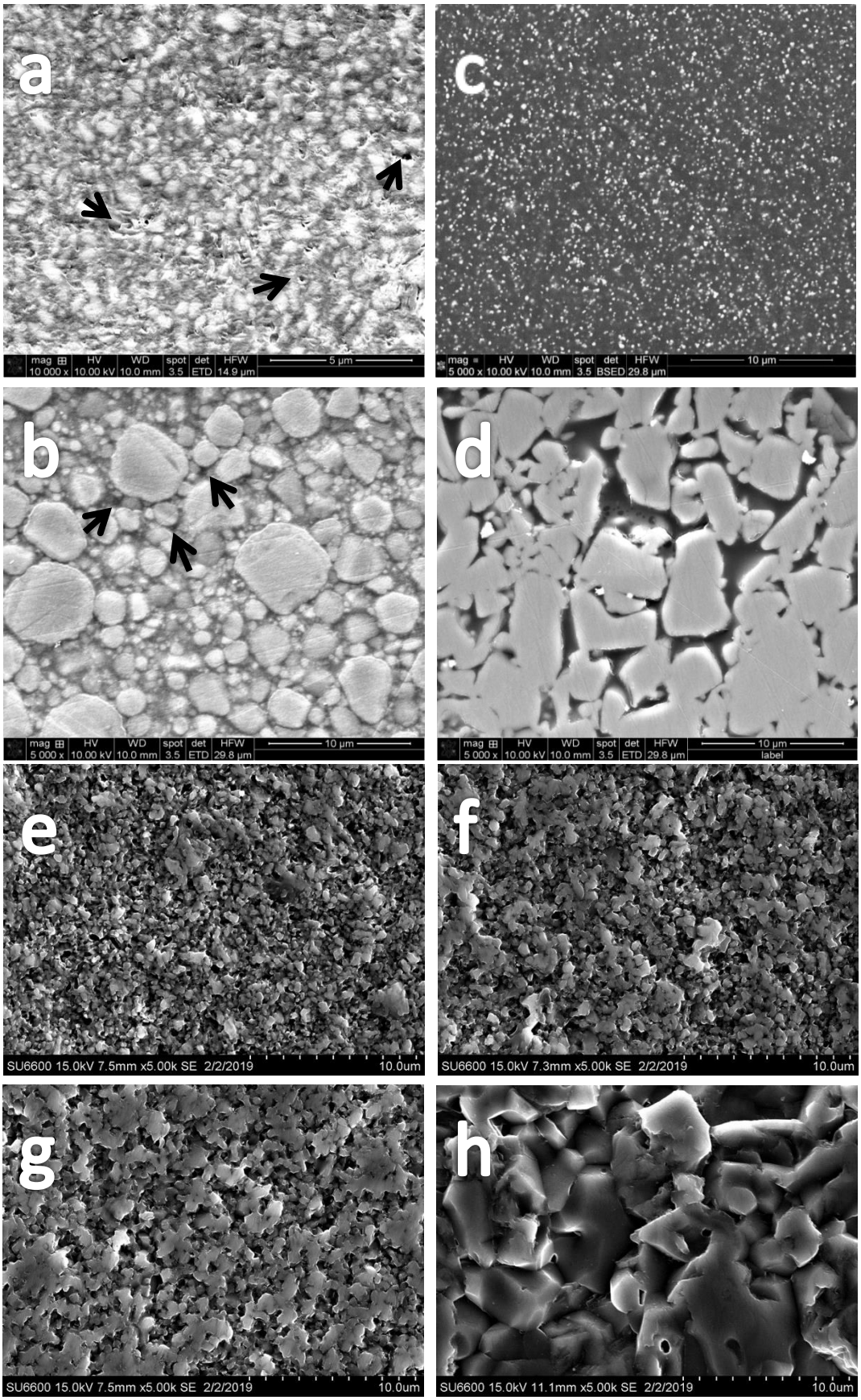

Figure 5.4 SEM images (x5K) shows different surface topographies of a) CS, b) LU c)DK, d) VE ,e)Exp125, f)Exp130, g)Exp135 and h)Exp155. Arrows are pointing to examples of voids in a tested specimen.

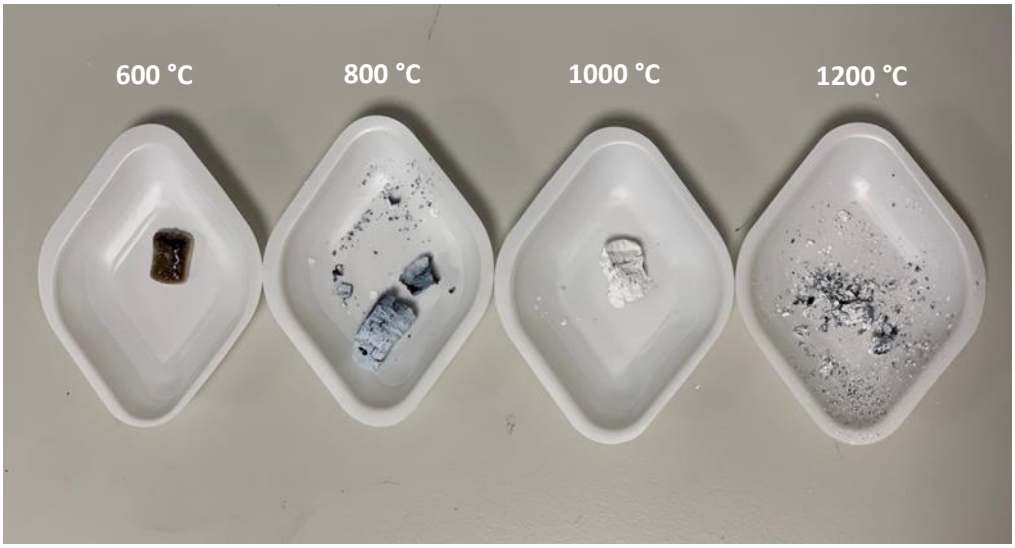

Figure 5.5 Eliminating the PEEK polymer in DK requires higher temperature and in this case 1200 °C was found to be sufficient.

5.5 Discussion:

Measurement of mechanical properties such as strength and elasticity of a material would help predict the performance of the material intraorally. For a material to be successful in the oral environment, it must withstand challenging conditions such as: continuous masticatory loading, thermal alteration and abrasive factors, e.g., brushing. During mastication, the bite force comprises a vertical compression loading on the occlusal surface of the tooth and/or the restoration (252). Previous studies have investigated the effect of compressive loads on elastic and mechanical properties such as the stress strain curves and hardness of dental restorative materials (22, 34, 44, 253).

Various techniques have been used to investigate the mechanical properties at macro or micro levels; with the introduction of nano technology, these properties can be also measured at nano scales. Nano indentation is now widely accepted to investigate the surface mechanical properties of dental materials. Three reasons have been proposed for the importance of nano indentation to study the surface mechanical properties of dental materials (254). First, the applied load and the displacement of the indenter are continuously monitored and recorded. Second, relatively smaller specimen preparations are required compared to macro or micro indentations. Third, different experimental parameter options are generally available, e.g., type of the tested material, indenter type, load and dwell time. However, the correlation between the surface mechanical properties at different measurement scales has not been studied. This study aimed to investigate, compare and correlate mechanical properties of PICN and other CAD/CAM materials at micro and nano measurement scales.

For hardness assessment, ceramic specimens were prepared with 2 mm thickness for ease of handling. Such thickness was also exceeded minimum thickness as required by instrument manufacturer. Specimens were mounted in acrylic to ensure optimum seating of the specimen while the examination was taking place.

Sample polishing has no direct effect on micro hardness but it provides a clear picture of the indentation which helps in obtaining accurate results (255). In contrast, with nano-indentation specimens with a smooth surface is required to avoid higher and inconsistent

indentation values (256-258). The applied load was selected to be 100 g for the micro indentation and 50 g for the nano indentation as confirmed by the pilot study.

The findings of this study support the rejection of the first null hypothesis as all the tested materials were significantly different in terms of the tested mechanical properties (micro-hardness, nano-hardness, and elastic modulus). In general, ceramics were statistically different from CAD/CAM and conventional resin composite materials. The findings are in agreement with prior literature in that ceramic materials show substantially higher hardness values than CAD/CAM resin composite (109). All PICNs (except Exp155) tested in the current study have hardness values in the range 2.81 to 4.38 GPa which is lower than the hardness of human enamel (3.5- 5.5 GPa)(259). This might be an advantage especially when it comes to protecting the opposing natural teeth from wear. These finding were consistent with previous studies (109, 198). The hardness levels of the PICN sintered at 1550°C (7.13GPa and 619.41 VHN) were greater than that of enamel. A dental material that is harder than natural enamel may cause more severe wear to the opposing dentition (101), although hardness of ceramic alone is not a reliable predictor of the wear of the opposing teeth(260). Other factors such as surface roughness of the restoration and other oral and environmental factors need to be considered before giving a conclusive answer (261).

In dental composite materials, filler particle size, shape, and compositions have been proven to have a great influence on their mechanical properties (262, 263). This study has confirmed that these parameters have similar correlations with mechanical properties of CAD/CAM resin composite materials. In terms of ceramic contents, linear regression analysis showed a positive correlation between the amount of ceramic (in wt%) and hardness at both micro and nano levels (r^2=0.56 and 0.48,respectively). Exp155 with 92% ceramic had the highest values which were significantly different from the other CAD/CAM materials (p=0.001).

Filler morphology is also important in determining the overall mechanical properties. Composites with round filler particles have higher filler packing compared to composites with irregular shaped composite (264) and it has also been reported that this influences the mechanical properties in resin composite as the spherical shaped fillers tend to distribute stresses better than fillers with sharp edges (24, 265, 266). This is confirmed in

this study, as LU with spherical shaped particles had relatively higher modulus of elasticity compared to GB with irregular shaped fillers (15.05 and 9.21 GPa, respectively).

The composition of the ceramic particles also plays a role in the overall mechanical properties of the tested materials. DK specimens which contain only 20% ceramic particles showed similar mechanical properties to Si and Sp conventional resin composites with 50 % and 57% fillers respectively. This could be explained by the different mechanical properties of the ceramic composition: titanium oxide fillers in DK are much harder than the glass fillers in the resin composite. The reported hardness of TiO_2 is up to 38 GPa while glass filler hardness ranges from 5 to 10 GPa (267).

The results of the current study showed that the micro-hardness value of the conventional indirect resin composite (Si) was not significantly different than one of the CAD/CAM resin composite (CS). This might highlight the influence of the polymerisation method on the mechanical properties of resin composite. The indirect composite was polymerized using proprietary curing units which combine heat, vacuum, and high intensity light to enhance the degree of conversion of the resin matrix. Therefore, the expectation is that the conversion of the methacrylate group would be enhanced, increasing the cross-link density of the set material (268). Previous studies have revealed significant improvement in mechanical properties following post-curing (269, 270).

The sintering process is an important step in achieving good microstructural integrity and optimising the mechanical properties of dental ceramics (124, 271). In this study, sintering temperature was found to have a significant effect on the mechanical properties of polymer-infiltrated polycrystalline ceramics. With increased sintering temperature, the increased grain growth, or inter-particle contact, results in increased density and strength. At 1250°C, hardness was significantly the lowest at both measurement scales; sintering Al_2O_3 ceramics at this temperature results in particles not adequately expanding to achieve full density. The gaps, however, that appear between grains as a result of porosity may facilitate polymer infiltration leading to interlocking phases of ceramic and polymer. Increasing the amount of polymer infiltration may lead to an increase in deformation during hardness indentation test, resulting in a low hardness value. At 1550°C, PICN showed a similar hardness value to feldspathic porcelain at the nano scale but significantly higher at the micro scale. In general, alumina which is the main ceramic

constitute in the model PICN is much harder than feldspathic porcelain (77). The similarity at nano scale could be attributed to the polymer interlocking phase in this material which was reported to have a hardness range of 14-15 VHN (272).

A similar trend was also found with elastic moduli in this study. The elastic modulus of the resin composite materials ranged from 3.49 to 15.05 GPa and are significantly lower than the elastic modulus of the commercial PICN (VE;33.05 GPa) and feldspathic ceramic (VM; 76.40 GPa). Similar findings were reported in previous studies where VE demonstrated an elastic modulus value between that of resin composite and glass-ceramic (103, 109, 273). The elasticity values of 18–103 GPa (in model PICN) are comparable to those reported for human enamel (between 48–105.5 GPa)(274). To the author's knowledge, no commercial PICN material has exhibited values in this elastic modulus range. A low elastic modulus material (less than enamel and dentin) will concentrate and transmit the stress to the tooth (275). A higher concentration of stress was found to be transferred to the tooth structure with materials exhibiting low elastic modulus (276). Because of this, there would be a greater deflection of the cusps and consequently a higher probability of fracture in the tooth compared to the restoration itself. It has been suggested that the modulus of elasticity of the supporting structure would have a significant effect on the longevity of all ceramic crowns (277), and the fracture resistance of an all-ceramic crown increases as the modulus of elasticity of the supporting material increases. Owing to their high modulus of elasticity and their match with enamel, the PICN materials may offer a more uniform stress distribution, especially during loading, and the tooth as well as the restorative crown would be protected from cracking.

Analysis of the load-displacement curves for the nano-indentation experiment (Figure 5.2) revealed typical indentation force versus indentation depth curves for the tested CAD/CAM ceramics. The large variations of the residual indentation depths highlights the variation in ability to resist deformation and in the hardness. Using an Oliver and Pharr method of analysis (278), the stress-induced reversible phase transition leads to the large recovery depth of PEEK based ceramic (DK) and conventional resin composites (Si and Sp) compared to other materials. On the load–displacement curves of feldspathic ceramic (VM), the high initial unloading slope and small recovery depth highlights its high stiffness and modulus of elasticity.

Hardness testing by nano-indentation has some advantages in that it is simple, reproducible and relatively non-destructive. However, it is technique sensitive and highly dependent on the flatness and smoothness of a specimen. Measured properties of a material under nano-indentation may vary according to its behaviour under load; this behaviour can be in the form of 'sink-in ' or 'pile-up' which occurs in the region around the indentation. When it occurs, the measured projected contact area might lead to either an over or underestimated elastic modulus. Using the Oliver and Pharr (152) method in calculating the modulus can reduce the error that might result from such behaviour.

While the elastic recovery is monitored in nano-indentation, in micro-indentation methods it is assumed that elastic recovery does not occur once the load is removed. Moreover, the hardness number is calculated based on the surface impression, which might be distorted, rather than the projected area (279). Therefore, in order to validate the readings, data of micro-and nano-hardness in all the tested materials were statistically analysed for any correlation. Statistical analysis confirmed significant positive correlation between micro and nano hardness values in all tested materials (p=0.001), therefore, the second null hypothesis was rejected.

Although both tests have been used to provide information on the hardness property, their values cannot be directly or simply compared due to different testing mechanisms and these include: indenter type, test settings, and loading force. In nano-indentation, the hardness depends on the applied load and continuously monitored indentation depth and expressed as a function of the applied load (P) and the size of the contact area (A) of indentation (280). However, in Vickers micro-indentation, the hardness relies on the surface area of a square-shaped indentation. The indentation surface area is determined according to the average length of both diagonals (d) of the square-shaped indentation (279).

5.6 Conclusions:

1. Different CAD/CAM resin composite showed different surface morphology of their filler contents with variations in size, shape and density.

2. Micro-hardness and nano-hardness of the studied PICN and other CAD/CAM composite materials increased systematically with an increase in ceramic contents (wt %).

3. A correlation between the nano-hardness and the micro-hardness against ceramic contents was noticed.

4. Sintering temperature appeared to have an effect on the ceramic density and consequently influenced the mechanical properties of PICN materials.

Chapter 6

The Use of The Peak-Force™ Quantitative Nano-mechanical Mapping AFM-based Method for Elastic Modulus and Surface Roughness Measurements of Polymer Infiltrated Ceramics

6.1 Abstract

Objectives

The aim of this *in vitro* investigation was to assess and compare surface characteristics and nanomechanics of several types of CAD/CAM resin composite blocks and polymer infiltrated ceramic network (PICN) materials.

Material and Methods

Three CAD/CAM resin composites; Lava Ultimate (LU), Cerasmart (CS) and Grandio Bloc (GB), one commercial PICN block ;Vita Enamic (VE) and four model PICN materials sintered at different temperatures (Exp.125, Exp.130, Exp 135 and Exp 155) were tested. Forty samples were prepared with the dimensions of 14×12×2 mm for resin ceramic and VE blocks and 15x2 mm for model PICN materials. All samples were scanned using atomic force microscopy (AFM) at multiple locations and two different scan sizes (20x20µm and 3x3µm). Surface optical gloss at 60° was also determined for all the groups. Data were analysed using one-way ANOVA, and Tukey's *post hoc* test (α=0.05).

Results

Resin composite blocks showed smoother surfaces compared to the PICN materials. The average surface roughness values (Ra) ranged between 7.75 nm to 31.21 nm and the gloss value ranged between 56.43 GU and 91.81 GU. The highest surface roughness value was found for Exp.125 (31.21 nm) while LU showed the lowest roughness value (7.75 nm) (the difference being statistically significant: p=0.001). Variation was noticed in terms of nanomechanical mapping within and between the groups. Images generated from the elastic modulus map values clearly indicated that all PICN materials had more than one phase and very different components.

Conclusions

CAD/CAM resin composite blocks exhibited higher gloss and lower roughness values compared to PICN materials. However, both the commercial and model PICN materials showed more stiffness than resin composite with the presence of at least two different phases. Sintering temperature appears to have a significant effect on material topography and nanomechanical properties. Model PICN sintered at 1550 °C showed comparable range of E modulus values to those of enamel.

Key words Hybrid-ceramic, CAD/CAM; Ceramic resin composites; elastic modulus; Atomic force microscopy.

6.2 Introduction:

In contemporary restorative dentistry, dental materials with comparable mechanical and aesthetic properties to natural teeth are always in demand. With the advances in CAD/CAM technology novel materials with enhanced properties have been developed. Polymer infiltrated ceramic network (PICN) has been introduced as an alternative restorative material with an elastic modulus similar to resin composite and with the long-term aesthetic stability of ceramics (103). The bulk mechanical properties of PICN and other resin-ceramic composite materials have been explored previously (103, 106, 198, 281, 282). CAD/CAM resin-ceramic composites exhibit higher flexural strength and modulus of elasticity compared to conventional direct resin composite whereas PICN has comparable values to advanced glass ceramics (282).

A glass ceramic based PICN material (Enamic) has shown promising results for use as a single crown (201). However, due to its relatively low flexural strength (below 300MPa) and fracture toughness (112), this material it is not recommended to be used for more than one unit prosthesis (206). Modifying the ceramic part in PICN might develop an alternative material that can be used for short/long span bridges. Monolithic alumina that has small grain size and better mechanical behaviour and higher fracture toughness could be a good substitute for the feldspathic porcelain in glass based PICN material.

Clinical and laboratory studies have shown that the elastic modulus of supporting resin composite adhesives has direct influence on the flexural failure of all-ceramic dental crowns (283-287). The elastic modulus correlates to the stiffness of a material and is defined mathematically as the slope of the stress–strain curve within the proportional limit(288). It is directly related to the amount of deformation when a material is subjected to an external load. Any material used in posterior restorations must have an elastic modulus value high enough to withstand the high masticatory forces in this area (289).

Indentation tests provide important information about material deformation and elastic behaviour (290). In dentistry, such tests can be performed at two different levels, namely micro- and nano-indentation. Micro- indentation is considered as the traditional approach for measuring the elastic properties of dental materials and is usually performed through standardised procedures like Vicker's or Knoop hardness tests wherein a stylus of standardized geometry is driven into a sample material to calculate

the hardness from a residual imprint. For hybrid materials where more than a single phase is present, micro-hardness tests are not the instrument of choice as the measured hardness values are representing the bulk structures rather than the individual phases.

Nano-indentation techniques are well-established to quantitatively determine the mechanical properties of materials on the nanoscale (152). Unlike the micro tips, a nanoindenter tip normally has a radius range between a hundred nanometres to several tens of microns, which when it is forced into the material, enables the instrument to measure the load versus penetration relationship. The main advantage in comparison with conventional micro-indentation is that material parameters are obtained from a very small volume, typically from tens of nanometres to micrometres. However, the standard nano-indentation technique requires a locally homogenised volume at the micro-scale (291) and for heterogeneous or porous materials such as hybrid ceramics, which can reveal the micromechanical properties of individual phases, the technique is still limited.

Unlike the instrumented nano indenter, Atomic force microscopy (AFM) has a significantly smaller indentation load (force sensitivity <0.05 nN), shallower indentation depth (displacement sensitivity $\lesssim$ 0.05 nm)(292), and effective contact volume, which allows for investigation of local mechanical properties at a smaller scale, previously inaccessible via the 'standard' instrumented nanoindentation approach (293). The determination of the elastic properties of CAD/CAM restorative materials using an AFM approach is relatively novel and few studies that have undertaken such investigations.

The use of atomic force microscope (AFM) has been used widely in medical research since its invention in 1986 (294, 295). Currently, it is widely considered to be the instrument of choice for analysing surfaces at the nano-scale or, in some cases, atomic scale. This is mainly due to the fact that this instrument is able to measure forces and distances at a very high resolution, and to non-destructively explore the topography of a sample within different ambient conditions with minimal or no sample preparation (296). In addition to this, AFM has a major ability to measure the mechanical properties of a material based on measuring the forces between the probe and the sample as a function of their mutual separation (297, 298).

For studying nanomechanical properties, peak-force quantitative nanomechanical mapping (PF-QNMTM) allows quantitative characterisation of a material at a nano-scale

level (299-301). Such a technique continuously measures sinusoidal force distance curves at high speed while raster scanning (a rectangular pattern of image capture). Tip-sample force is directly controlled using a continuous feedback loop. Curves are analysed in real-time to generate modulus and adhesion maps. The captured force curves can be fully accessed offline for additional nanomechanical analysis. The major advantage of this new technique is the feedback-controlled sinusoidal drive that uniquely enables the highest speed and highest lateral resolution property mapping with precise force control (302).

AFM can also be used to obtain important quantitative information on the surface topography of a dental material (296). A glossy and perfectly smooth surface is a fundamental requirement for a desirable aesthetic appearance. A smooth surface also plays an important role in preventing the formation of discolouring films and plaque accumulation. Moreover, a surface smoothness decreases the coefficient of friction and subsequently this may reduce the wear rate (303), which in turn can improve the clinical performance of the restorations. Surface quality also affects the fracture resistance in brittle materials such as resin composites (304).

Polymer infiltrated ceramics and nano-ceramic resins are reported to have several advantages compared to conventional restorative materials. However, no sufficient information on the possible connections between the structure and functionality of these materials, which comprise both micro-sized and nano-sized fillers, on a sub-micrometric scale is available. Knowing the relationship between material structure and mechanical properties is a critical issue for the proper selection of any restorative material. Therefore, the purpose of this study was to investigate and evaluate the physico-mechanical properties of different types of PICN ceramics in comparison with resin composite materials on a sub-micrometric scale, especially focusing on the elastic mechanical properties using a PF-QNMTM technique.

The specific objectives were:

a) To evaluate and compare the surface characteristics including roughness and gloss parameters of different types of PICN materials and resin composites.

b) To evaluate elastic modulus values of different types of PICN materials obtained via PF-QNMTM technique and compare them with those of resin composites.

c) To evaluate the effect of sintering temperature on the surface roughness and elastic modulus of fabricated model PICN materials.

d) To use a PF-QNMTM technique to conduct nano-mechanical mapping of each of the tested materials.

The null hypotheses were:

a) There is no difference in terms of gloss and surface roughness parameters between PICN and resin composite materials.

b) There is no difference in terms of surface roughness parameters between model PICN groups with different sintering temperatures.

c) There is no difference in terms of elastic modulus values obtained via PF-QNMTM between PICN and resin composites materials.

d) There is no difference in terms of elastic modulus values obtained via PF-QNMTM between model PICN groups with different sintering temperatures.

6.3 Materials and methods:

6.3.1 Manufacturing of Polymer Infiltrated Alumina:

Porous alumina matrices with nano-sized alumina particles were fabricated initially by slip casting into disc shaped specimens (15x2 mm) before being partially sintered at different temperatures (1250 °C, 1300 °C, 1350 °C and 1550 °C). The ceramic matrices were then conditioned with a methacryloxypropyltrimethoxysilane (MPS) silane coupling agent prior to resin infiltration to ensure that the polymer network was chemically cross-linked to the ceramic network to form an interpenetrating network system. The chemically conditioned porous inorganic network was infiltrated with a cross-linking polymer mixture and

initiator by capillary action. The polymerisation process was induced by heat and pressure, leading to a polymer-infiltrated-ceramic-network material.

6.3.2 Materials and Samples Preparation:

A total of eight polymer-based ceramics (intended for use with CAD/CAM) were investigated in this study, namely Enamic (Vita Zahnfabrik), Cerasmart (GC Dental Products) and Lava Ultimate (3M) and four model polymer-infiltrated ceramic materials (Table 6.1). Five samples (12x14x2 mm) were sectioned from standard sized milling blocks of each material (VE, CS, LU) using a water-cooled precision cutting machine (Isomet 1000, Buehler, LakeBluff, USA). PICN model groups were fabricated from a disc-shaped mould (15x2 mm). All the samples were sequentially polished with silicon carbide grinding papers (P320, P600, P800, P1200, P2500 and P4000) and finished with 1 micron and 0.25 micron diamond paste using an OmegaPol metallurgical polisher machine (Spectrographic, United Kingdom). An ultrasonic bath (Nusonic, Transsonic T310, Germany) was used to clean specimens in distilled water for 10 min. Each specimen was stored dry in a clean container at room temperature for 24 h before investigation.

Table 6.1 A list of the CAD/CAM materials investigated in the current study.

Category	Material's Name	Code	Sintering Temperature (°C)	Company	Lot Number	Compositions
CAD/CAM Resin Composite blocks	Cerasmart	CS	N/A	GC Dental Products Europe, Leuven, Belgium	1502091	Nanoceramic composite (BisMEPP, UDMA, DMA) with 71 wt% silica (20nm) and barium glass (200nm) nanoparticles.
	Lava Utimate	LU	N/A	3M ESPE, Seefeld, Germany	N750333	Composite resin material (BisGMA, UDMA, BisEMA, TEGDMA) with 80 wt% silica (20nm) and zirconia (4-11nm) nanoparticles
	Grandio® blocs	GB	N/A	VOCO GmbH, Cuxhaven, Germany	1723181	BisGMA, TEGDMA, Urethane-BisGMA adduct Barium-alumino-borosilicate (0.5-2µm); fumed silica (20-60nm) 86 wt%.
PICN Ceramics	VITA Enamic	VE	N/A	VITA Zahnfabrik, Bad Säckingen, Germany	46680	Polymer-infiltrated-feldspathic ceramic-network material (UDMA, TEGDMA) with 86 wt% glass ceramic.
	Polymer infiltrated alumina	Exp125 Exp130 Exp135 Exp155	1250 1300 1350 1550	Boston University	_____	UDMA,TEGDMA,BP,MPS,Ethanol, Distilled water, Glacial acetic acid , alumina (80wt%-95wt% crystalline ceramic).

6.3.3 Atomic Force Microscope (AFM)

Atomic force microscopy was conducted using a Bruker Catalyst™ BioAFM (Bruker UK Ltd., Coventry, U.K with a Nanoscope V controller, and operated under the Nanoscope controller software (v9.1). Images were captured in air at a humidity of <45% using pre-calibrated NM-RC-C diamond tipped probes (Bruker SAS, France) using Peakforce Quantitative Nanomechanical (PFQNM) tapping mode. Data capture was performed at 5 locations on each sample with a 20x20 µm and a 3x3 µm images being collected at each site. Imaging was performed at approximately 1Hz and at a resolution of 256 samples/line. Topography, and DMT modulus channel data were post-processed using Nanoscope Analysis (v1.50); the calibration data supplied with the probes was inputted to the controller software at the capture stage. Average roughness (R_a), the root mean square roughness (Rq), and maximum roughness depth (R_{max}) values were extracted for all samples.

The elastic modulus of the sample was derived from AFM force curves and was based on the Derjaguin-Muller-Toporov (DMT) model (185), which was implemented into the Bruker NanoScope Analysis software. By definition, the DMT model fits the following equation.

$$F - F_{adh} = \frac{3}{4} E^* \sqrt{R(d - d_h)}^3 \quad \textbf{(34)}$$

Where

F is the applied force,

F_{adh} the adhesion force between probe and the surface,

R is the tip radius,

$d - d_h$ the sample deformation,

*E** is the elastic modulus.

6.3.4 Gloss Measuremnt

The gloss of each specimen was measured using a glossometer instrument (Electomer 400, Novo-Curve, Electomer inc., Rochester Hills, Michigan). The instrument was calibrated after every 3 readings according to the manufacturer instructions. To record the gloss value, each specimen was centrally positioned -at an operating angle of 60°- over the hidden aperture which is pinpointed by intersection of white lines marked on the top of the sample plate. Before pressing the read button, the specimen was covered with a black cover to prevent light interference.

6.3.5 Statistical Analysis:

The data for all groups were collected and analysed statistically using SPSS 23.0 (IBM SPSS Statistics, SPSS Inc., Chicago, IL, USA) and checked for normality using Shapiro-Wilk tests. A one-way ANOVA was used to analyse all data. Tukey *post-hoc* testing was used to assess the difference in terms of surface roughness parameters and elastic moduli between PICN and resin composite materials. A Pearson Product Moment correlation analysis was used to assess the relationship between different variables. The significance level for all tests was set at α=0.05. Data were plotted using Sigma Plot and Excel programmes.

6.4 Results:

Surface roughness parameters (Ra, Rq and Rmax) and gloss values are presented in Table 6.2 and Figure 6.1. Mean and standard deviations of elastic moduli obtained via PF-QNMTM for the test materials are listed in Table 6.3. The average surface roughness values (Ra) ranged from 7.75 nm to 13.16 nm for the resin composite CAD/CAM groups whereas it ranged from 20.85 nm to 31.21 nm for the PICN ceramic groups. Overall, the highest surface roughness value was found for Exp.125 (31.21 nm) while LU showed the lowest roughness value (7.75 nm) (p=0.001).

Gloss values for the resin composite CAD/CAM groups ranged from 75.03 GU to 91.81 GU while it ranged from 56.43 GU to 65.97 for the PICN ceramic groups. LU exhibited the glossiest surface (91.81 GU) while Exp.125 showed the lowest gloss value (56.43 GU). A significant negative correlation was found between Ra and GU for all test materials (Figure 6.2). A similar significant correlation was found between the sintering temperature and the Ra values of the model PICN materials (Pearson correlation coefficient= -0.85, p= 0.001). Gloss demonstrated positive correlation with the sintering temperature of PICN model groups (Pearson correlation coefficient= 0.5, p= 0.001).

Statistically significant differences were found between the tested materials for the average elastic modulus (p=0.001). The elastic modulus values of all the test materials ranged from 08.44 GPa to 84.28 GPa (Table 6.3). CS demonstrated the lowest value (08.44 GPa) while Exp.155 showed the highest value (84.28 GPa). A significant positive correlation was found between the sintering temperature and the elastic modulus values of the PICN model materials (Pearson correlation coefficient= 0.85, p= 0.001).

Maps of surface roughness of 20x 20 μm and the elastic modulus of the 3x3 μm scans for the different materials are shown in (Figure 6.3- Figure 6.10) and Figure 6.11, respectively. Variation was noticed in terms of nanomechanical mapping within and between the groups. All the images generated from the elastic modulus map values clearly indicated that all the studied materials had more than one phase and very different components.

Table 6.2 Mean and (SD) of the surface roughness parameters investigated in this study. Values with the same superscript letters represent non-significantly different groups (Tukey post hoc test at significance level (α) of 0.05).

Materials	Ra (nm)	Rq (nm)	Rmax (nm)	Gloss
CS	11.67 (0.2)[a]	26.92 (0.3)[a]	120.3 (02.1)[a]	82.01 (3.9)[a]
LU	07.75 (0.1)[b]	10.50 (0.6)[b]	215.0 (21.6)[b]	91.81 (1.37)[b]
GB	13.16 (0.5)[a]	28.91 (1.9)[a]	123.5 (10.4.)[a]	75.03 (0.69)[c]
VE	22.69 (1.4)[c]	41.18 (2.9)[c]	525.4 (18.9)[c]	58.61 (2.02)[d]
Exp 125	31.21 (3.6)[d]	54.01 (5.4)[d]	624.1 (32.7)[d]	56.43 (4.34)[d]
Exp 130	24.59 (1.8)[c]	40.27 (3.8)[c]	524.8 (27.5)[c]	59.91 (5.19)[d]
Exp 135	20.85 (3.5)[c,e]	36.64 (2.5)[e]	459.1 (10.6)[e]	60.99 (5.74)[d,e]
Exp155	18.94 (1.1)[e]	32.61 (2.5)[b]	445.9 (10.8)[e]	65.97 (4.35)[e]

Table 6.3 Mean and (SD) of the elastic modulus as obtained via PF-QNMTM technique. Values with the same superscript letters represent non-significantly different groups (Tukey post hoc test at significance level (α) of 0.05).

Material	Elastic Modulus (GPa)
CS	08.44 (0.18)[a]
LU	16.82 (2.08)[b]
GB	09.64 (0.97)[a]
VE	23.06 (1.47)[c]
Exp 125	23.45 (4.77)[c]
Exp 130	23.56 (7.60)[c]
Exp 135	34.19 (2.97)[d]
Exp 155	84.28 (6.47)[e]

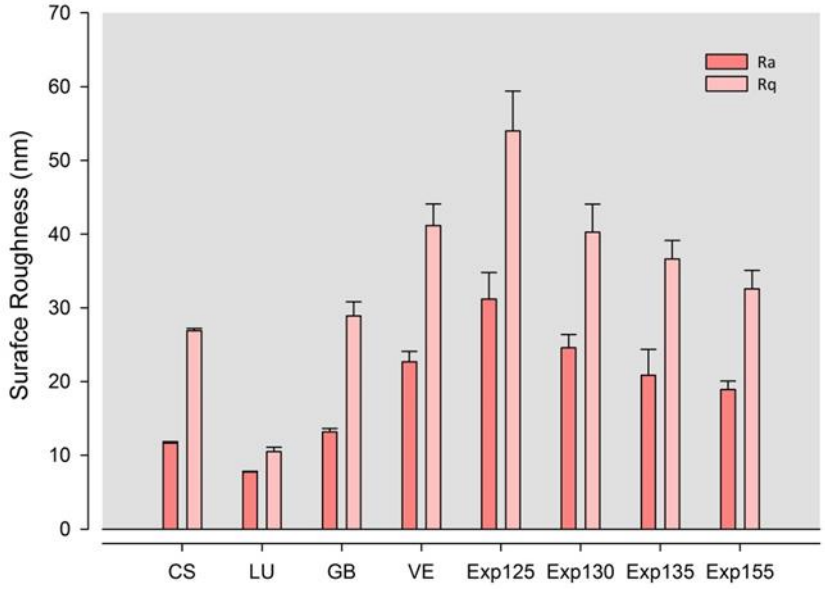

Figure 6.1 Surface roughness analysis shows variations in Ra and Rq mean values between the groups. Exp 1250 model PICN material had the roughest surface and lava ultimate had the smoothest one among all the other. Error bars represent standard deviations (SD).

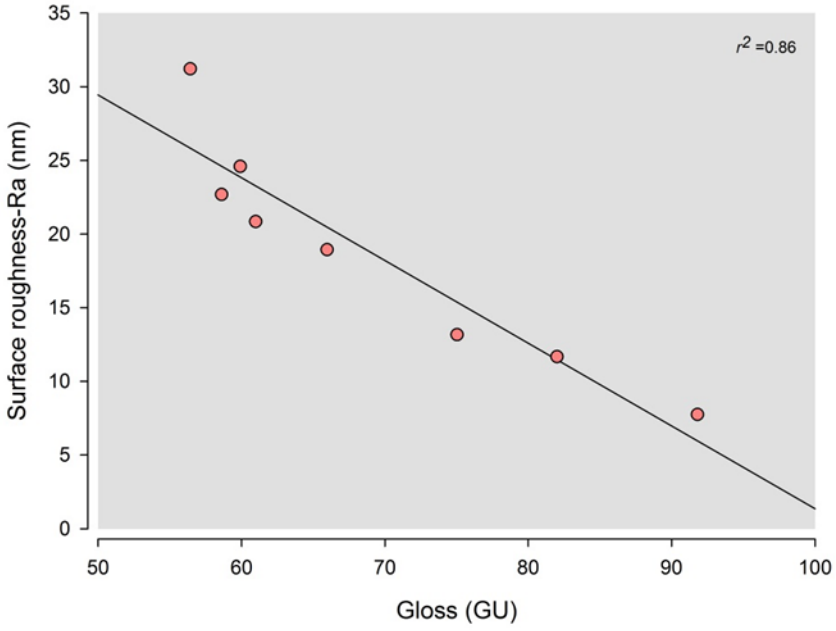

Figure 6.2 Linear regression analysis to show the negative correlation (r^2= 0.86) between the average surface roughness (Ra) and surface gloss of test materials.

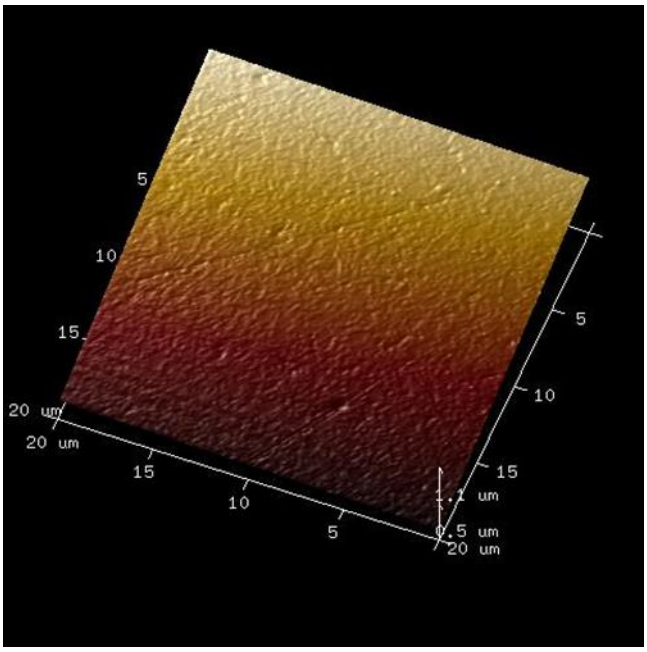

Figure 6.3 A 3D AFM image of Cerasmart nanoceramic. Surface depressions on the surface suggested fillers dislodgments.

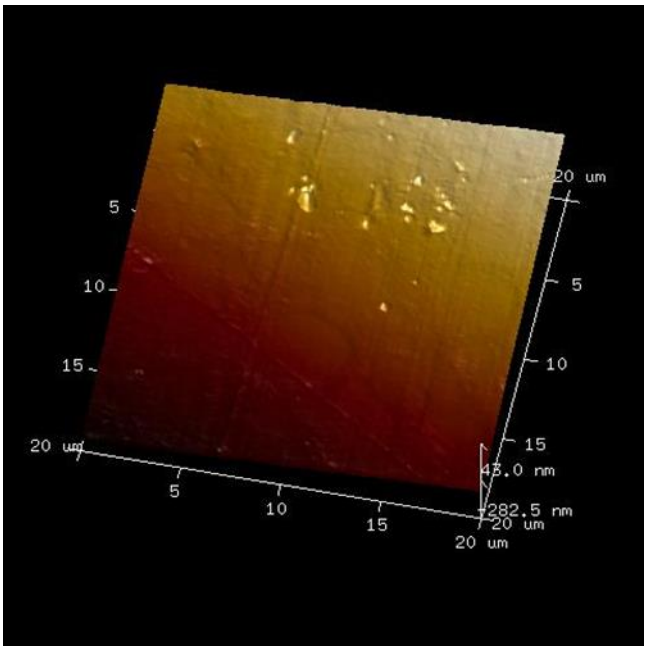

Figure 6.4 A 3D AFM image of Lava Ultimate. Low surface profile is interrupted by rounded shinny projections on surface.

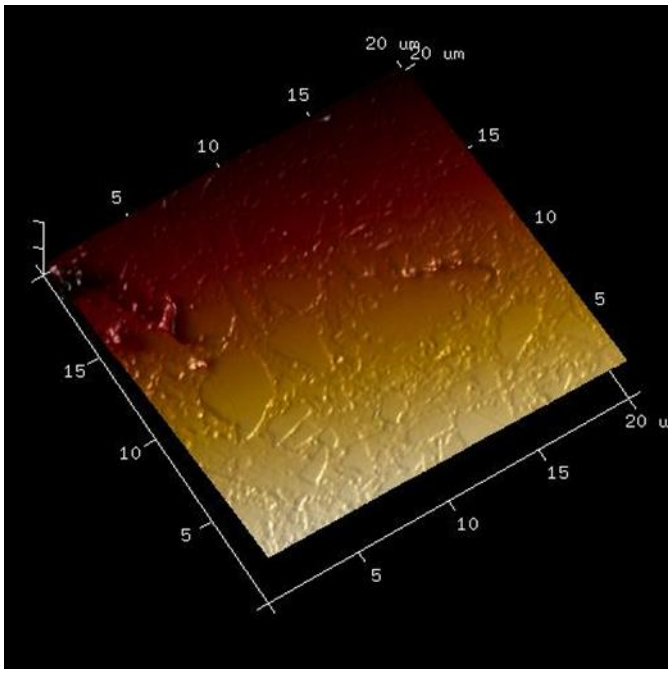

Figure 6.5 A 3D image of Grandio Bloc. Glass filler dislodgments clearly appear on the top left of the image.

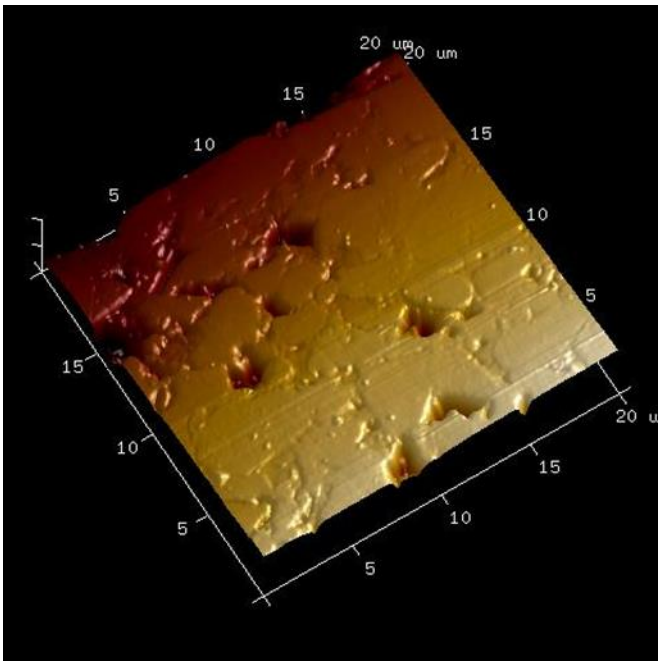

Figure 6.6 A 3D image of Vita Enamic. Surface depressions represent the polymer interlocking phase.

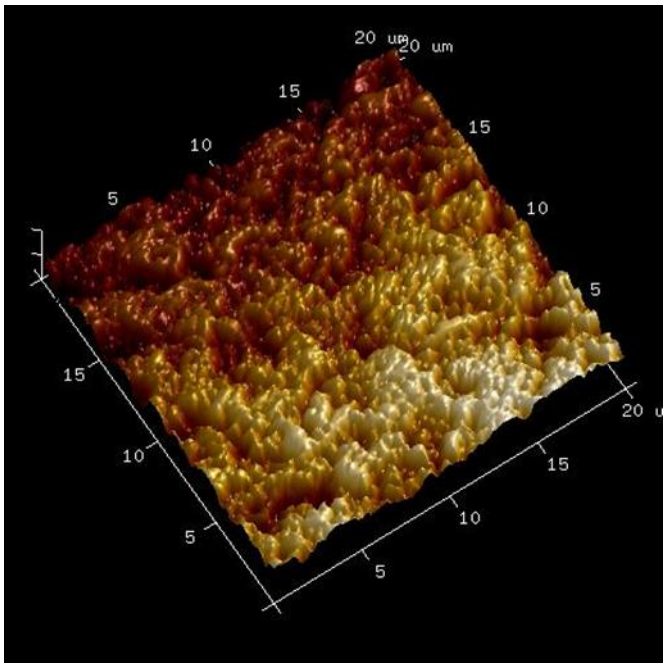

Figure 6.7 A 3D image of PICN model material sintered at 1250 °C.

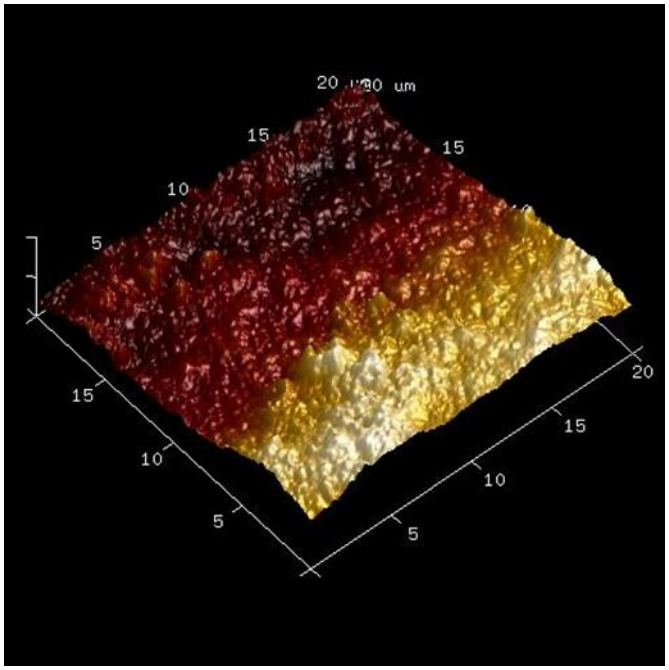

Figure 6.8 A 3D image of PICN model material sintered at 1300 °C.

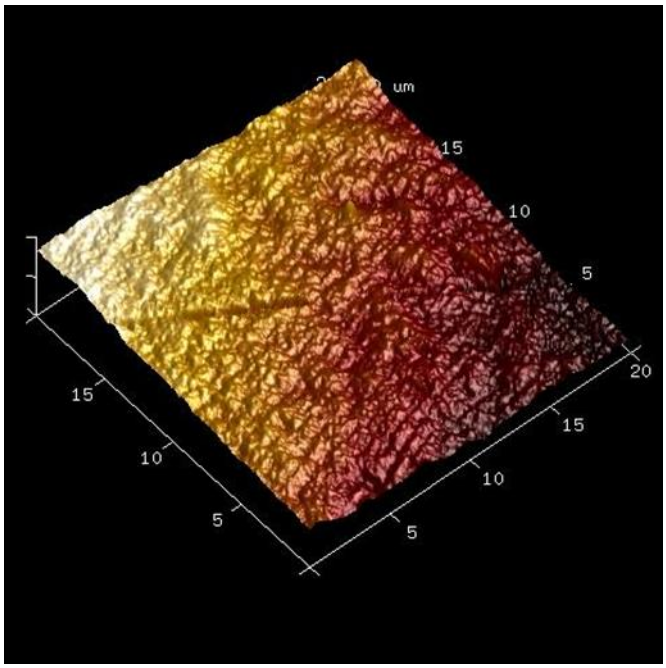

Figure 6.9 A 3D image of PICN model material sintered at 1350 °C.

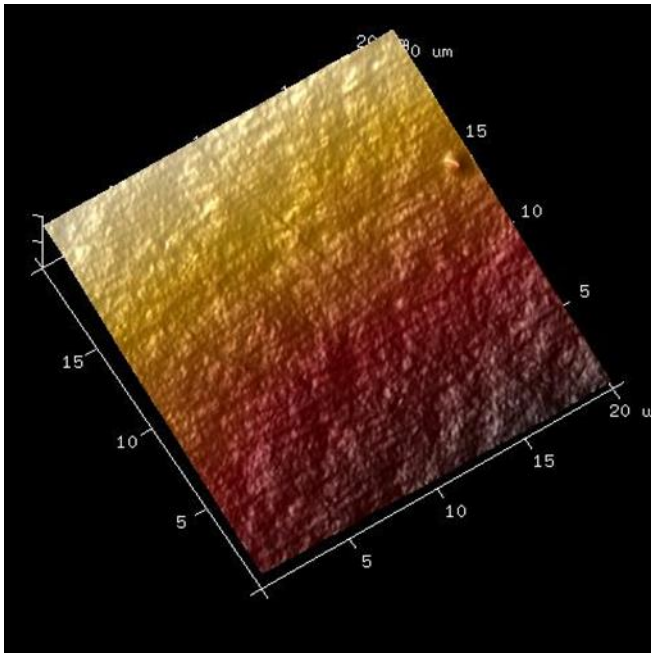

Figure 6.10 A 3D image of PICN model material sintered at 1550 °C.

1. Elastic Modulus Analysis

a) Cerasmart

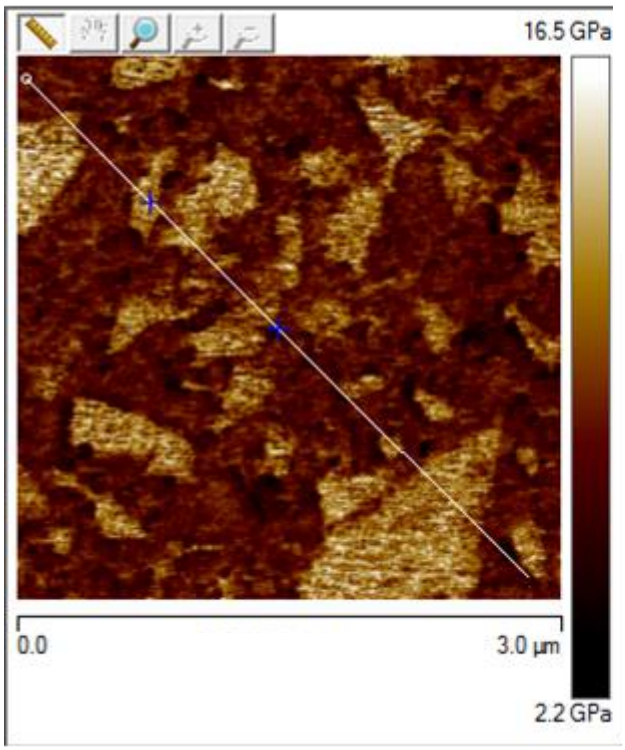

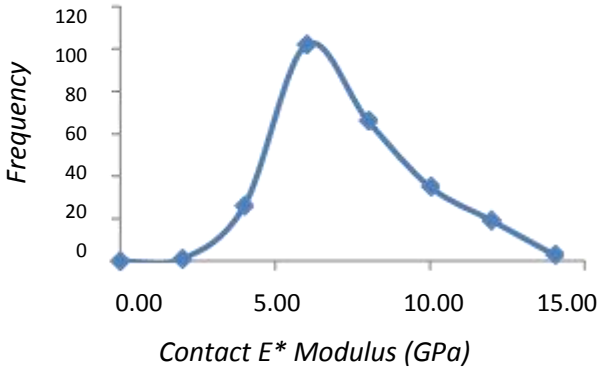

b) Lava Ultimate

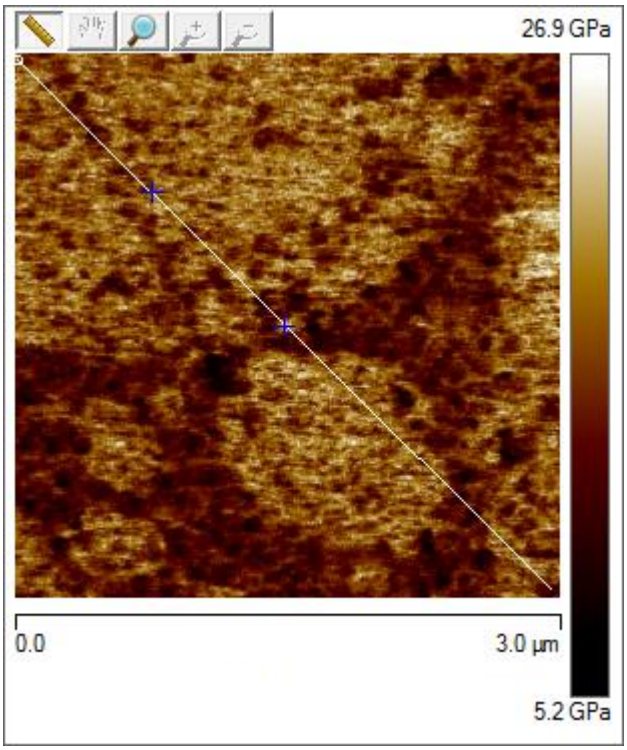

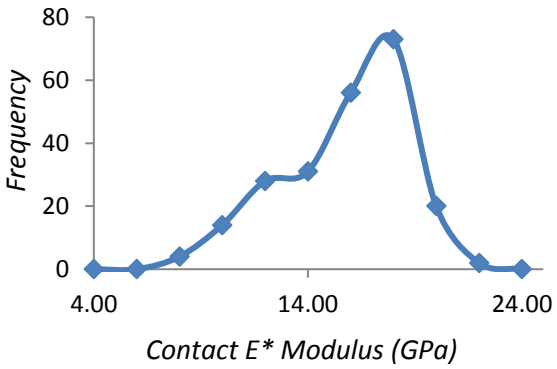

c) *Grandio Bloc*

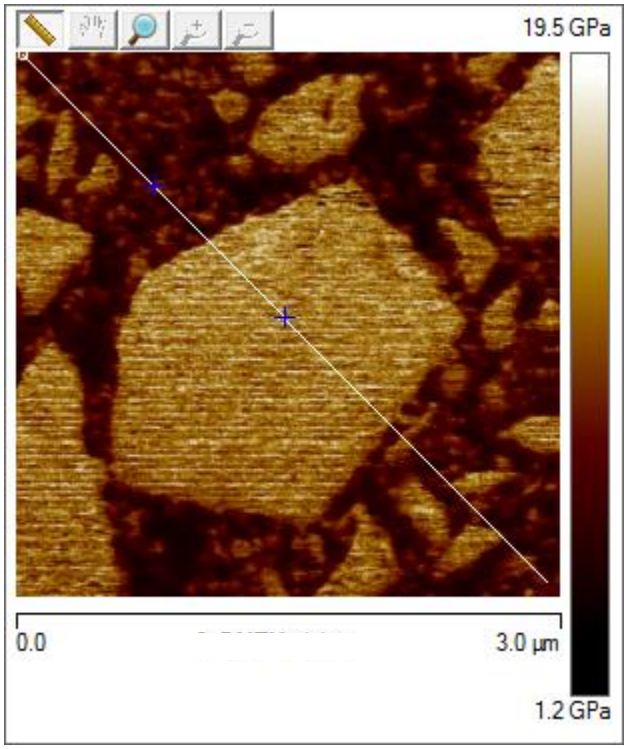

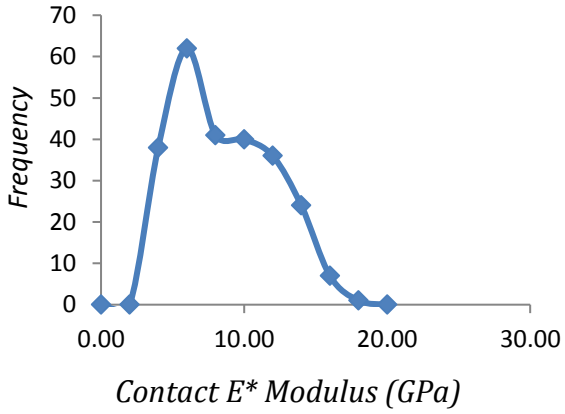

d) *Vita Enamic*

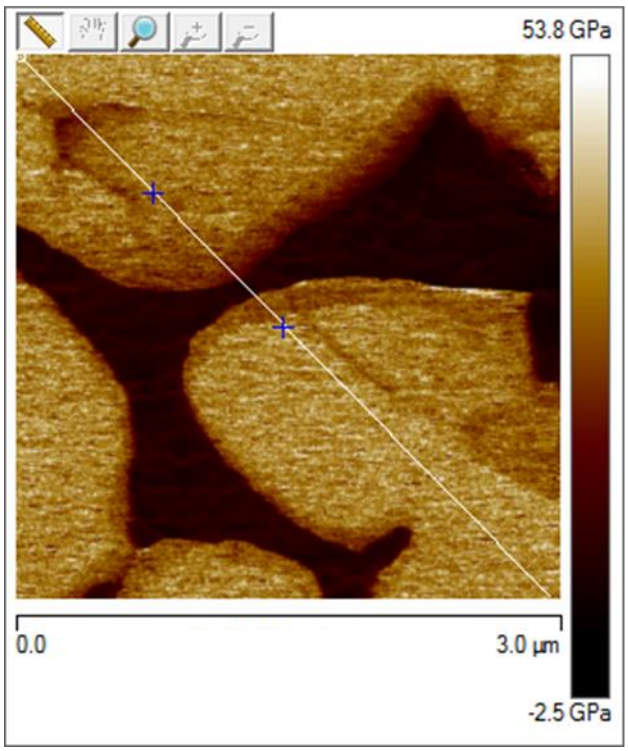

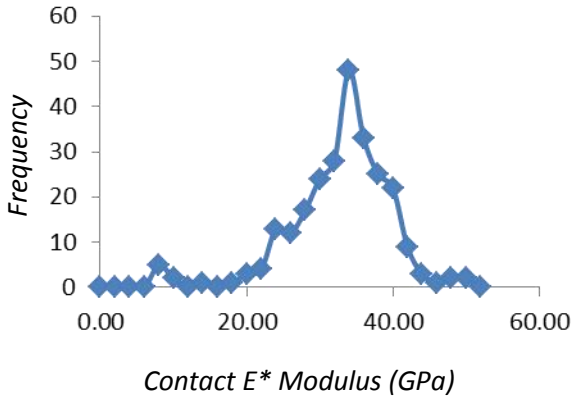

e) Exp125

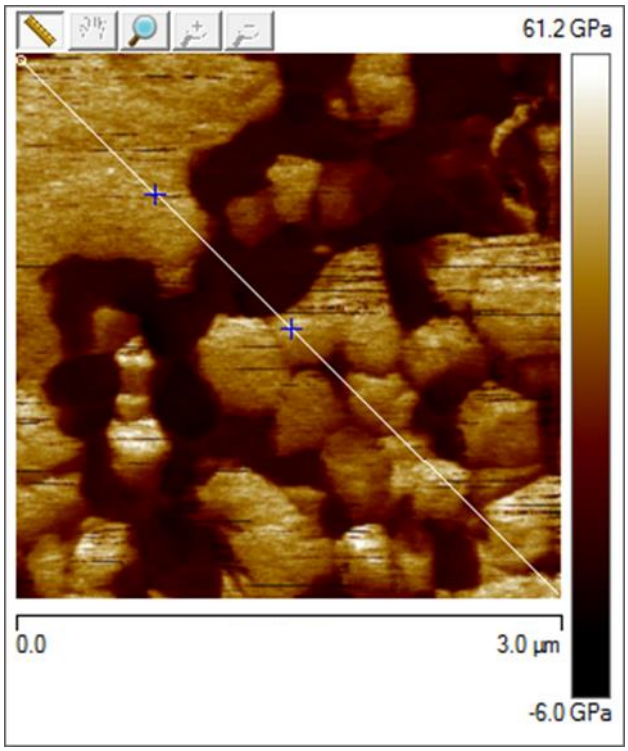

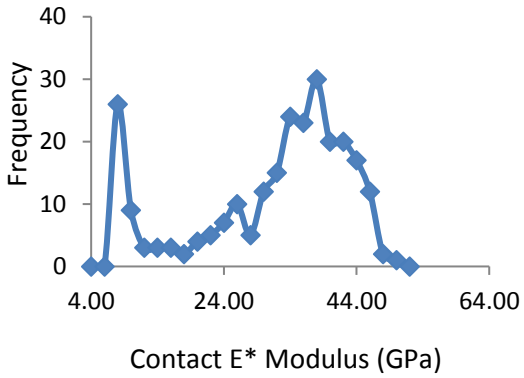

f) Exp130

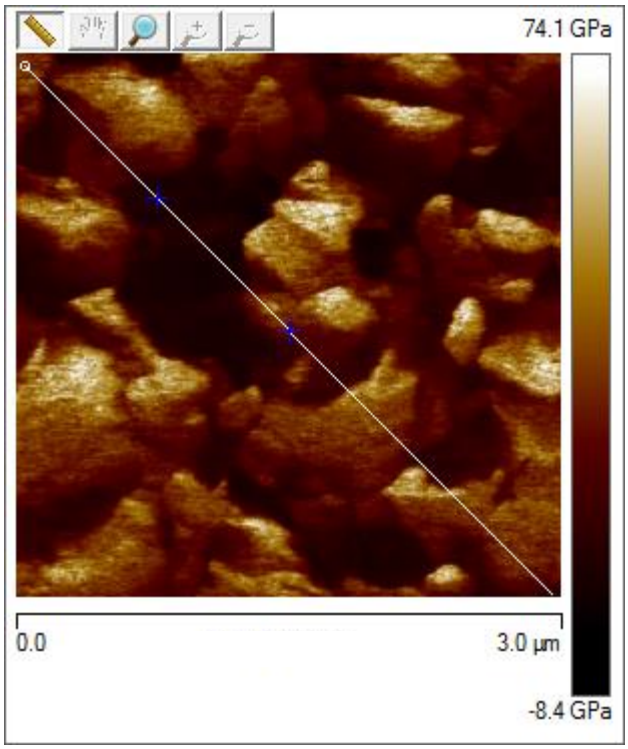

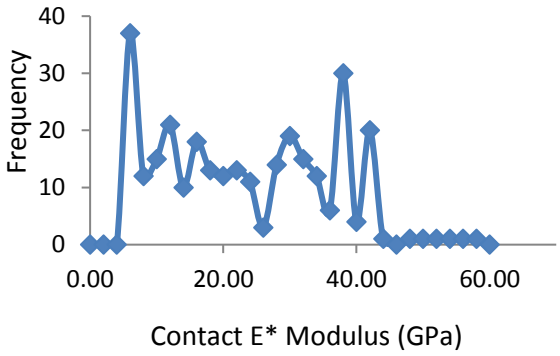

g) Exp135

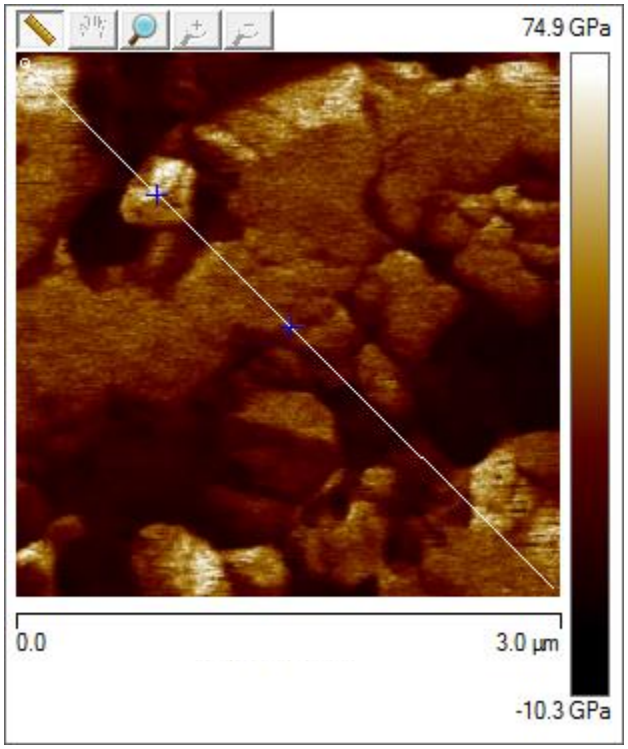

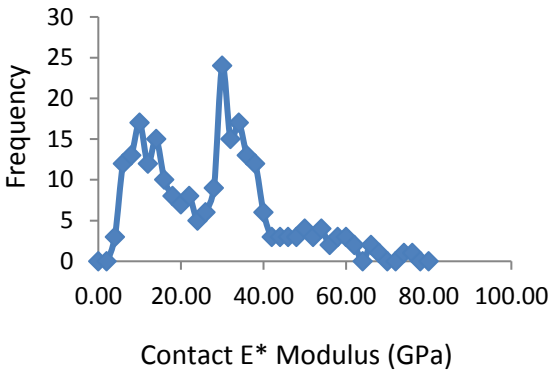

h) Exp155

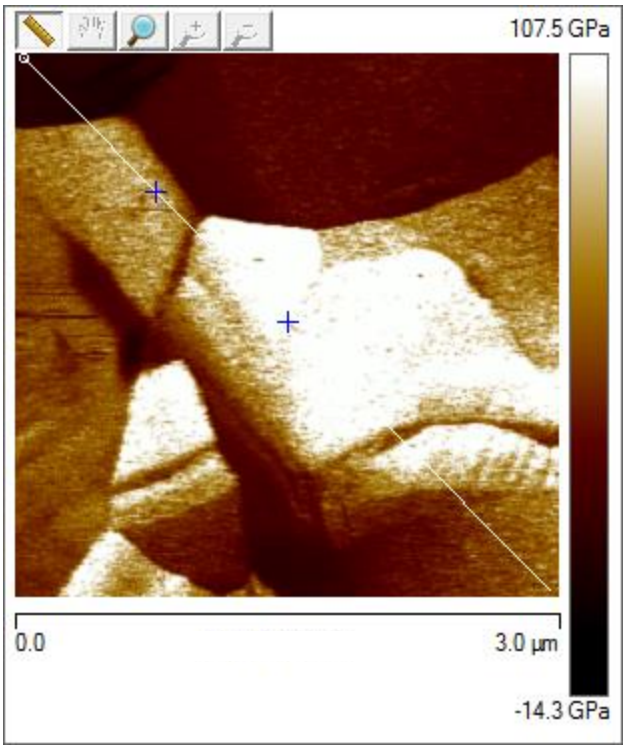

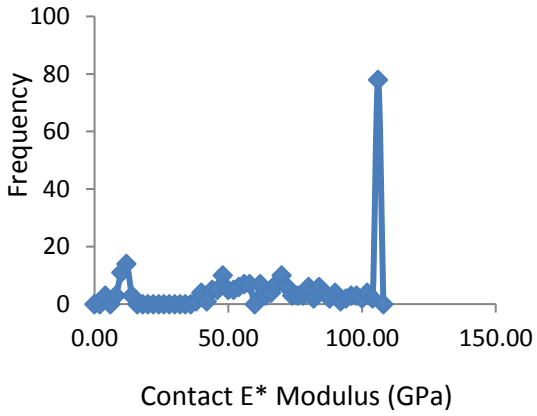

Figure 6.11 Atomic force microscopy images of the E modulus of the three materials generated with 3x3µm scans for; a) Cerasmart, b) Lava Ultimate and c) Grandio bloc d) Vita Enamic e) Exp 125 f) Exp 130 g) Exp135 and h) Exp 155. Adjacent to the image scans are plots of the E modulus generated from the frequency distributions from all the contact points associated with the AFM scan.

6.5 Discussion:

The determination of elastic modulus using AFM nanomechanics for CAD/CAM materials is relatively novel as very few studies have undertaken this investigation for different materials (305-307). However, it should be mentioned that the quantitative interpretation of the AFM nanomechanics data is not straightforward. This is due to the fact that there are some critical conditions that should be considered when running such an investigation. These conditions, which could impact the precision of the force-displacement measurements to some extents, are related to both the instrument itself and/or the tested sample (293). Among these challenging conditions are (i) a blunt and or damaged tip combined with the intrinsic compliance of the AFM cantilever probe might result in distorted force−displacement curve and erroneous contact area ; (ii) as with other nanoindentation instruments, a smooth and flat sample surface is highly important for accurate contact area determination ; (iii) an AFM probe with a larger tip angle (e.g., a cube-corner) is generally used for nanomechanical measurements; however, this might reduce the resolution particularly in 3D imaging; (iv) indentation-triggered effects, such as 'pile-up' and 'sink-in' at the periphery of the indenter (also encountered in standard nanoindentation) (308), creep/viscoelasticity and adhesion interactions during indenter unloading could affect the quality and reproducibility of the data (309).

In this study, the above issues were addressed from the beginning and minimized where possible. Each specimen was sequentially polished up to 0.25 µm and then cleaned in an ultrasonic bath with distilled water to remove any surface debris and impurities. Diamond tips with less than 15 nm radii were used to overcome the instrument and or sample compliance. The use of diamond tips, which were recently introduced to the market, provides several advantages: these include wear-resistance and stable shape during imaging, as well as improved and more reliable electrical measurements with a conductive diamond material (310). Using a diamond tip also decreases the chance of contamination and thus image artefacts. This is due to the chemical inertness of the material which makes it less prone to particle adsorptions. In addition, they rapidly achieve thermal equilibrium when in contact with the sample surface due to the high thermal conductivity of diamond (311).

Surface roughness in general is a measure of surface texture and is often quantified by the deviations of a surface from its ideal form. If the deviations are large, then the surface is considered to be rough; if they are small, then the surface is considered smooth. The conventional measurement of a sample surface is obtained by a contact stylus profiler (312) and limitations include a large stylus radius, a large force and low magnification in the plane, and possible misrepresentation of the real surface topography owing to the finite dimension of the stylus tip (313). On the ultramicroscopic or nano-scale of a surface, AFM has been developed to obtain a three-dimensional image of a material surface on a molecular scale. AFM has been shown to be the most suitable method to measure surface roughness in glass-ceramic materials when compared with stylus and optical profilometers (314). This is because AFM has better spatial resolution and is able to detect submicron wavelength which therefore results in accurate measurements of surface roughness (314).

In this study, vertical roughness parameters (Ra,Rq and Rmax) were selected to measure surface roughness. Ra is commonly used to estimate the average surface quality of resin composite and other restorative materials. Rq, on the other hand is more sensitive to occasional highs and lows, making it a valuable complement to Ra (315). Rmax was chosen to determine if any major surface defect on the surface was encountered (315).

From the results presented in Table 6.2, it can be concluded that the first null hypothesis was rejected as there was a statistically significant difference in terms of surface roughness and gloss between the resin composite groups and PICN ceramic groups (p=0.001). The differences in the surface roughness parameters of the resin composite materials might be ascribed to variations in their filler size, geometry and composition. The lowest values of roughness parameters were for LU composite. This is probably because of the monomodal spherical-shape series with a small filler particle size of less than 25 nm in this material (316). CS and GB are considered as resin composite materials with multimodal irregular-shape filler with different particles sizes which may explain the significantly higher roughness values compared to LU. This is in agreement with previous studies concluding that a higher surface roughness is associated with larger and irregular filler particles (317-319). PICN ceramic groups on the other hand showed higher roughness values compared to the resin-ceramic composite groups: similar findings have been reported previously (320, 321). This could be explained by the difference in

microstructural compositions between PICN ceramic and resin composite materials. Unlike resin composites, PICN ceramics are an interpenetrating phase composite with a combination of ceramic and base resin polymer. Ceramic, which is considered the main component in such a material, demonstrates superior surface contour and texture when glazed compared to with finishing and polishing systems (322-325). However, due to the presence of the polymer phase in PICN ceramics, a glazing step is almost impossible without compromising the polymer component as this would be 'melted' away in the oven during the firing process. It should be noted though that although the PICN ceramic groups in the current study produced a rougher surface when compared to resin composite, the difference in value was not of clinical importance; the threshold Ra value for plaque retention is 0.2 µm (326, 327), whereas in our study, the roughness of all tested materials was below that threshold.

The surface roughness values of our model PICN ceramics in this study showed a strong negative correlation with their sintering temperature; hence the second null hypothesis was rejected. As the sintering temperature increases, the grains become matured, develop, and combine to complete grain boundaries and the ceramic matrix will then be gradually densified. Such densification results in a well-developed microstructure with fewer residual pores which may eventually decrease the roughness and enhance the appearance of ceramic material (211, 328).

A significant difference was also found in elastic modulus values between resin-ceramic composite and PICN ceramic groups, thus the third null hypothesis was rejected. This confirms that mechanical properties are highly influenced by the microstructural compositions of CAD/CAM materials. GB with 86 wt% filler demonstrated a significantly lower elastic modulus value compared to LU with a relatively lower filler load (80 wt%). Such a difference can be explained on the basis of their filler type with different mechanical properties. LU contains a proprietary blend of two fillers: zirconia and silica nano particles agglomerated into clusters whereas GB contains glass and silica fillers. The elastic modulus of zirconia is significantly higher than glass ceramic (329). Regarding our model PICN material; there were variations in the elastic modulus values for all the groups. Except for Exp.155, the other three groups show two ranges of elastic modulus values (Figure 6.11). On close inspection, these two ranges clearly indicate the presence of interpenetrating phases of polymer and ceramic in these materials. This is mostly seen

in Exp.125 and this may be due the fact that the alumina matrix in this group is the more porous compared to the other groups. This in turn would have increased the polymer/ceramic ratio with greater infiltration of the polymer phase. As the temperature increases, the size of pores decreases (330) which may affect the polymer infiltration process, leaving the polymer to coat the ceramic particles instead of interpenetrating them. This coating may have created a third phase, a 'polymer-coated ceramic' phase, which could explain the relatively high intermediate values between the lowest and the highest elastic modulus readings. In Exp.155, the pore size is the least, which decreases the polymer/ceramic ratio, this probably explains the presence of one dominant range of elastic modulus values in this group. Overall, the findings of this study confirm that increasing the sintering temperature results in a significant increase in the elastic modulus of PICN materials, in-line with previous studies (218, 330, 331).

Numerous indentation studies exist characterizing PICN ceramics at micro-scale indents and correspondingly induced contact stress-fields commonly having dimensions of up to some tens of micrometres, covering the interlocking phases of such materials (109, 332-334). In this study, the elastic modulus of the CAD/CAM polymer-infiltrated ceramic materials has been investigated on smaller levels of hierarchy to gain an understanding of the structure/behaviour relationship as well as their potential clinical performance. These materials were developed with the purpose of simulating the properties of enamel and dentin (282). Previous work has correlated the elastic modulus of polymer-infiltrated ceramic to that of human enamel (103), however that was based on the bulk of the material, neglecting the fact that these materials have a dual phase microstructure. Also of note is that the microstructure of enamel has a hierarchical order with multiple levels that involves crystalline, prisms, schmelzmuster and dentition levels (335). Each level is structurally unique but interdependent in terms of mechanical characteristics (336). Comparison on a smaller level is important due to the fact that the structural organization of enamel increases its tolerance to damage by toughening mechanisms associated with the hierarchy, which can be critical to achieve in a restorative material to convey equal durability to that of enamel(336). At the smallest scale, enamel consists of hydroxyapatite crystallites and proteins which have very high (120 GPa) and very low (~1 GPa) values of elastic modulus (274). In the current study, VE had a range between 8- 34 GPa which may indicate that the material does not necessarily have a similar structure/behaviour to

enamel. Interestingly, however, Exp.155 did show a comparable elastic modulus range (4-106 GPa) to enamel. In Exp.155 the total inorganic part constitutes ~92%. Given that enamel is composed of roughly 95% to 98% inorganic material (337, 338), this may highlight the potential similarity in structure/behaviour relationships between Exp.155 and enamel.

6.6 Conclusions:

- AFM is a good tool to map the elastic modulus of PICN materials at the nano-scale. However, consideration should be taken during tip selection and sample preparation.
- The surface roughness profiles of resin composite CAD/CAM materials were significantly lower than both commercial and novel PICN materials.
- The sintering temperature of PICN had a strong influence on surface profile and nano-mechanical properties.
- Different PICN materials showed different phase distributions as well as different elastic properties.

Chapter 7

Hydrolytic Stability of a Novel PICN Ceramics and Various Conventional Resin Composite and CAD/CAM Blocks

7.1 Abstract

Objectives

The aim of this study was to assess sorption and solubility of polymer-infiltrated ceramic network (PICN) and other CAD/CAM and conventional resin composites after seven-month storage in water.

Material and methods

Three CAD/CAM resin composites: Lava Ultimate (LU), Cerasmart (CS) and Grandio Bloc (GB); one commercial PICN (Vita Enamic,VE) and four model PICN materials sintered at different temperatures (Exp.125, Exp.130, Exp 135 and Exp 155); one ceramic filled poly-ether-ether-ketone (PEEK) (Dentokeep, DP); one feldspathic ceramic block (Vitabloc Mark II, VM) and two conventional resin composite (Sinfony,Si and TPH Spectrum, TPH) were tested. 60 samples were prepared with the dimensions of 14×12×1 mm for CAD/CAM and DP materials, and 15x1 mm for model PICN and conventional resin materials. All samples were immersed into distilled water for a seven month period and weighed at different time intervals. Data were analysed using one-way ANOVA, and Tukey's *post hoc* test (α=0.05).

Results

Resin composite groups showed significantly higher water sorption values compared to DP, VM and PICN ceramic groups ($p \leq 0.02$). For resin composite, water sorption values ranged from 19.13 μg/mm^3 to 38.1 μg/mm^3 and for PICN ceramics from 02.51 μg/mm^3 to 7.84 μg/mm^3. TPH had the highest sorption and solubility values (38.10 μg/mm3 and 05.04 μg/mm3, respectively) while VM had the lowest sorption value 0.67 μg/mm3 and VE had the lowest solubility value -0.55 μg/mm3.

Conclusions

Water sorption of CAD/CAM composite blocks are material-dependent and are affected by the filler weight percentage. Commercial and model PICN ceramics showed hydrolytic stability between resin composite and conventional ceramic, reflecting its microstructural components. Sintering temperature appears to have a significant effect on the hydrolytic stability of PICN ceramics.

Key words: Polymer infiltrated ceramic, resin composite, sorption, solubility, CAD/CAM.

7.2 Introduction:

Adhesively bonded resin composites and dental ceramics are the two main classes of aesthetic restorative materials. Resin-based composites are composed of an organic polymer matrix and reinforcing inorganic filler particles (18, 339). Dental ceramics, on the other hand, are essentially inorganic materials commonly composed of a crystalline phase and/or glass matrix (74). Advances in both materials make it possible to expand their uses in restorative dentistry. However, there are still some clinical challenges that may affect the performance and the longevity of resin composites and dental ceramics as restorative materials.

Materials with different polymer composition and variable percentages of ceramic and resin fillers are available as monolithic materials fabricated for computer-aided design and computer-aided manufacturing (CAD/CAM) techniques. The polymers most frequently used are poly(methyl methacrylate) (PMMA), composite resin, or polyetheretherketone (PEEK)-based materials. PEEK has good mechanical properties and has been evaluated for use for fixed dental prostheses in load-bearing areas (247, 248). PMMA has been used frequently with CAD/CAM technology to get the benefit of a controlled manufacturing process including temperature and pressure to produce new materials with improved properties (340-343). A polymer-infiltrated-ceramic-network (PICN) is one of the recently introduced materials that offer a new classification in aesthetic dental restorative materials. Its fabrication concept is based on the infiltration by capillary action- of resin polymer into a porous pre-sintered ceramic to produce a PICN material that aims to combine the properties of resin composite and dental ceramic.

In general, variation in the composition of CAD/CAM materials may affect long term behaviour in oral environment (340, 344). Oral cavity is very hostile environment with conditions that can be challenges for restorative materials to survive for a long term period. These challenging factors include; pH and temperature changes, intermittent loading due to chewing and endogenous or exogenous chemical by-products (345, 346). The durability of any restorative material can therefore be affected by their ability to withstand these conditions with minimal or no deterioration of their mechanical properties.

In the wet oral environment, the main component is water which comprises about 99 % of natural saliva (347). It dissolves glass by hydration, hydrolysis, and ion exchange reactions. The dissolution gives rise to selective leaching of alkali ions in ceramic materials and changes in the surface characteristics and mechanical properties (346, 348). The chemical durability of resin-based and ceramic materials is influenced by a variety of factors such as the composition and microstructure of these materials, the chemical character of the medium, exposure time, and temperature (348-350) .

Measuring water uptake by a material that has to function in an aqueous environment (i.e. the oral cavity) is crucially important. Water uptake or water sorption, is the process by which water molecules are taken up by a hydrophilic material until an equilibrium is reached (351). The water sorption, or more specifically the water absorption, characteristics of dental resin composite are well documented in the literature. From a biological point of view, absorption can contribute to free-monomer elution which may eventually lead to the ingress of microorganisms and or an allergic reaction to the patient (161, 352, 353). Furthermore, water absorption has deleterious effect on the mechanical properties of dental materials (353-355). In dental polymers, water sorption is a diffusion controlled phenomenon that can be explained by two theories: the free volume theory, and the interaction theory (353). The free volume theory is based on the invasion of water molecules into the polymer mass and occupying the small voids between polymer chains, whereas in interaction theory; water molecules bind to specific ionic groups of the polymer chain depending on the water affinity of these groups(356). In general, water sorption not only acting as a plasticiser by preventing chain enlargement but also forcing them apart (357). Moreover, especially in dental resin composite, absorbed water can promote resin-filler bond breakage. This can cause internal strains and may facilitate the release of unreacted free monomer (358).

The quantity of the absorbed water depends on the chemical affinity of the polymer to water, the availability of micro-voids inside the polymer and the resistance of a polymer to a swelling deformation stress. From this perspective, different resin polymers behave differently in terms of water absorption and solubility (161, 352). Dental polymer networks based on dimethacrylate monomers can absorb moisture to the extent of several percent of their total weight (18, 359) .

Since the composition and the microstructure of PICN materials are different from conventional ceramics, this may affect the chemical and mechanical durability when exposed to oral simulated conditions. However, the literature is still lacking data regarding their long-term stability in aqueous media compared to resin composite materials.

The aim of this study is to assess the water sorption and solubility of a model PICN ceramics and established commercial CAD/CAM and conventional resin composite materials after 7 months of distilled water storage. The null hypotheses to be assessed are: i) there is no significant effect of material type on sorption and solubility; and ii) there is no significant long-term mass change during 7 months of water storage for all the tested materials.

7.3 Materials and Methods:

7.3.1 Preparation of The Samples

Twelve materials including conventional and CAD/CAM resin composites, PEEK based ceramic, CAD/CAM ceramic and PICN ceramic, were investigated. Details of these materials are listed in Table 7.1. Samples were prepared (n=5) and polished according to each material type.

For conventional resin composite and model PICN materials, samples were prepared the diameter of 15.0 ± 0.1 mm and 1 ± 0.1 mm thickness according to the dimensions specified by ISO FDIS 4049:2009 (170). Samples from CAD/CAM resin blocks and commercial PICN materials were sectioned and prepared (14×12×1 mm) using a precision cutting machine (Isomet 1000, Buehler, LakeBluff, USA) under running water. Details on the samples prerpataion including finishing and polishing were mentioned previously in Chapter 5.

All specimens from all the groups were soaked into an ultrasonic bath (Nusonic, Transsonic T310, and Germany) in distilled water for 5 min to clean them from debris and contaminations.

Table 7.1 Test materials and manufacturer information.

Category	Material's Name	Code	Company	Lot Number	Compositions
Resin composite CAD/CAM blocks	Cerasmart	CS	GC Dental Products Europe, Leuven, Belgium	1502091	Nanoceramic composite (BisMEPP, UDMA, DMA) with 71 wt% silica (20nm) and barium glass (200 nm) nanoparticles.
	Lava Utimate	LU	3M ESPE, Seefeld, Germany	N750333	Composite resin material (BisGMA, UDMA, BisEMA, TEGDMA) with 80 wt% silica and zirconia nanoparticles (4-11nm)
	Grandio® blocs	GB	VOCO GmbH, Cuxhaven, Germany	1723181	TEGDMA, Urethane- adduct Barium-alumino-borosilicate (0.5-2µm); fumed silica (20-60nm) 86 wt%
PICN Ceramics	VITA Enamic	VE	VITA Zahnfabrik, Bad Säckingen, Germany	46680	Polymer-infiltrated-feldspatic ceramic-network material (UDMA, TEGDMA) with 86 wt% ceramic
	Model polymer infiltrated alumina	Exp125 Exp130 Exp135 Exp155	Boston University	---	UDMA,TEGDMA,BP,MPS,Ethanol, Distilled water, Glacial acetic acid , (0.4 µm) alumina ceramic.
Ceramic CAD/CAM blocks	Vita Mark II	VM	VITA Zahnfabrik, Bad Säckingen, Germany	40870	Feldspathic ceramic
PEEK CAD/CAM Blocks	DentoKeep	DP	Nt-trading , Germany	G15DK1401	PEEK polymer based ceramic,20% Titanium Oxide
Indirect resin Composite	Sinfony	Si	3M ESPE, St Paul, MN	3788554	HEMA and 10% to 30% (octahydro-4,7-methano1H-indenediyl) bis(methylene)diacrylate), strontium-aluminium borosilicate glass, silicon oxide, silane and photoinitiators. Filler compositions= 50 wt%
Direct resinComposite	Spectrum TPH3	Sp	Dentsply Detrey GmbH, Konstanz, Germany	1708001024	Bis-GMA, bis-EMA, TEGDMA. Barium aluminio-borosilicate (<1m). Barium fluoro- aluminio borosilicate (<1µm) Highly dispersed silicon dioxide (10–20nm) Filler compositions=57 wt%

Samples were then transferred into separate labelled glass vials and stored in a lightproof desiccator with anhydrous self-indicating silica gel at (37 ± 1) °C. After 22 h, all the samples were moved into another desiccator maintained at room temperature (23 ± 1) °C for 2 h and then weighed to an accuracy of 0.01 mg using a calibrated electronic analytical balance (Ohaus Analytical Plus, Ohaus Corporation, USA). The measuring process was repeated on a daily basis until the mass change was not more than 0.1 mg at any 24 h time period according to ISO FDIS 4049:2009 specifications. The constant mass was then recorded as m1. Sample dimensions were measured using an electronic digital calliper (Powerfix, OWIM GmbH & Co., KG, Germany) with an accuracy of 0.01 mm. Three measurements were recorded for each dimension and the average was then used to calculate the volume (V) of each sample in mm^3.

7.3.2 Sorption and Solubility

Five samples from each material were stored in 10 ml of distilled water in individual glass vials at 37 ± 1 °C. The samples were weighed at different time intervals (1, 7, 14, 30, 60, 90, 180 , 210 days). The mass recorded at each time was denoted as m2 (t). For every weighing cycle, samples were dried on a filter paper and air-blown before measurements and after weighing were returned into their vials with renewed storage water to avoid variations in the pH with storage. At the end of the storage period, samples were reconditioned to a constant mass in a desiccator following the same conditioning protocol described above. The recorded mass was then denoted as m3.

The percentage mass change was calculated by the following equation:

$$Mg(\%) = \frac{m2\ (t) - m1}{m1} \times 100 \quad \textbf{(35)}$$

This represents the apparent percentage amount of water absorbed by the tested material.

The percentage solubility which represents the total weight of components (including unreacted monomers, additives, or fillers) extracted by water was calculated by:

$$SL(\%) = \frac{m1-m3}{m1} \times 100 \quad \textbf{(36)}$$

To calculate the actual percentage amount of water absorbed by the tested material at the end of the storage period, the following formula was used:

$$SP\ (\%) = \frac{m2\ (7months)-m3}{m1} \times 100 \quad \textbf{(37)}$$

Water sorption (μg/mm^3) of each tested sample was calculated according to the following:

$$SP = \frac{m2-m3}{V} \quad \textbf{(38)}$$

Solubility measured in micrograms per cubic millimetre (μg/mm3) for each tested sample was calculated by:

$$SL = \frac{m1-m3}{V} \quad \textbf{(39)}$$

7.3.3 Statistical Analysis

The data were entered into a statistical software package (SPSS, V23, Chicago, USA) and checked for normality using a Shapiro-Wilk's test. Mean mass change, sorption and solubility values of different materials were compared using one-way analysis of variance (ANOVA) followed by Tukey *post hoc* analysis for multiple comparisons. Pearson product moment correlation analyses were used to assess the relationship between different variables. Significance level for all tests was set at α=0.05.

7.4 Results:

The results of mass change, sorption and solubility are shown in Table 7.2 and Figure 7.2. Generally, resin composite groups showed significantly higher values compared to DP, VM and PICN ceramic groups (VE,Exp125,Exp130,Exp135 and Exp155). The rank of water sorption was as follows: TPH > LU > Si > CS > GB > Exp125 > VE > Exp130 > Exp135 > DP > Exp155 > VM, whereas the rank of water solubility was: TPH > LU > CS > GB > Si > VM > Dp > Exp155 > Exp125 > Exp135 > Exp130 > VE. TPH had the highest sorption and solubility values (38.10 μg/mm^3 and 05.04 μg/mm^3, respectively) while VM had the lowest sorption value (0.67 μg/mm^3) and VE had the lowest solubility value (-0.55 μg/mm^3).

All the tested materials showed statistically significant mass change with time upon storage in water (p<0.001) (Figure 7.1). The highest rate of mass change in all the materials was in the first 30 days of storage followed by slower mass change until equilibrium was reached two to three months later. PICN ceramics, VM and DP showed a slower rate of increase of mass until equilibrium was reached after two to three weeks. TPH on the other hand, demonstrated a high rate of mass change in the period between two weeks and two months.

VE showed no significant difference compared to Exp 125 in terms of mass change, sorption and solubility (p≥0.2). The rest of the model groups (Exp 130, Exp135 and Exp 155) showed no significant differences with VE in terms of solubility (p≥0.8). Exp135 and Exp 155 showed significant lower mass change % (0.13% and 0.08%, respectively) and water sorption (03.83 μg/mm^3, 02.51 μg/mm^3, respectively) than VE (0.42% and 07.84 μg/mm^3) (p≤0.001).

In terms of model PICN ceramic, a negative correlation was found between the sintering temperature and water sorption (Pearson correlation coefficient= -0.98, p=0.001). A similar negative correlation was also found with mass change (Pearson correlation coefficient= -0.94, p= 0.001). On the other hand, no correlation was found between sintering temperature and water solubility (Pearson correlation coefficient= 0.31, p= 0.1) (Figure 7.3).

Table 7.2 Mass change (%), Sorption, and solubility after seven months of storage in distilled water. Values represent the mean and standard deviation. SP is sorption of the material, and SL is solubility. Values with similar superscript letters per column represent homogenous groups (Tukey *post hoc* test, α= 0.05).

Category	Material	Mass Change (%)	SP (µg/mm³)	SP (%)	SL (µg/mm³)	SL (%)
Resin composite CAD/CAM blocks	GB	01.10 (0.14)^{a}	19.13 (02.4)^{a}	1.16 (0.10)^{a}	00.91 (0.23)^{a}	0.05 (0.01)^{a,d}
	LU	01.65 (0.09)^{b}	33.78 (1.18)^{b}	1.89 (0.08)^{b}	04.30 (0.24)^{b}	0.24 (0.02)^{b}
	CS	01.21 (0.11)^{a}	22.87 (2.24)^{c}	1.27 (0.10)^{a}	01.14 (0.16)^{a}	0.06 (0.01)^{a,d}
PICN Ceramics	VE	00.42 (0.11)^{c}	07.84 (1.69)^{d}	0.39 (0.10)^{c}	-00.55 (0.12)^{c}	-0.03 (0.01)^{c}
	Exp125	00.30 (0.05)^{c,e}	09.12 (0.94)^{d}	0.29 (0.08)^{c,d}	-00.33 (0.12)^{c}	-0.01 (0.001)^{c,d}
	Exp130	00.23 (0.01)^{e,f}	06.87 (0.29)^{d}	0.21 (.001)^{d,e}	-00.39 (0.07)^{c}	-0.01 (0.002)^{c,d}
	Exp135	00.13 (0.01)^{d,f}	03.83 (0.53)^{f}	0.11 (0.01)^{e}	-00.36 (0.05)^{c}	-0.01 (0.001)^{c,d}
	Exp155	00.08 (0.04)^{d,f}	02.51 (0.87)^{e,f}	0.07 (0.03)^{e,f}	-00.28 (0.09)^{a,c}	-0.01 (0.002)^{c,d}
Ceramic CAD/CAM blocks	VM	00.04 (0.02)^{d}	00.67 (0.23)^{e}	0.04 (0.01)^{f}	00.05 (0.02)^{a,c}	0.003(0.001)^{a,c,d}
PEEK CAD/CAM Blocks	DP	00.20 (0.03)^{d,e}	02.85 (0.37)^{e,f}	0.19 (0.02)^{d,e}	-00.14 (0.04)^{a,c}	-0.01 (0.002)^{a,c,d}
Indirect resin Composite	Si	01.66 (0.09)^{b}	25.05 (0.92)^{c}	1.69 (0.08)^{g}	00.55 (0.12)^{a,c}	0.03 (0.008)^{d}
Direct resin Composite	TPH	01.63 (0.11)^{b}	38.10 (0.69)^{h}	1.74 (0.07)^{b}	05.04 (1.90)^{b}	0.2 (0.09)^{b}

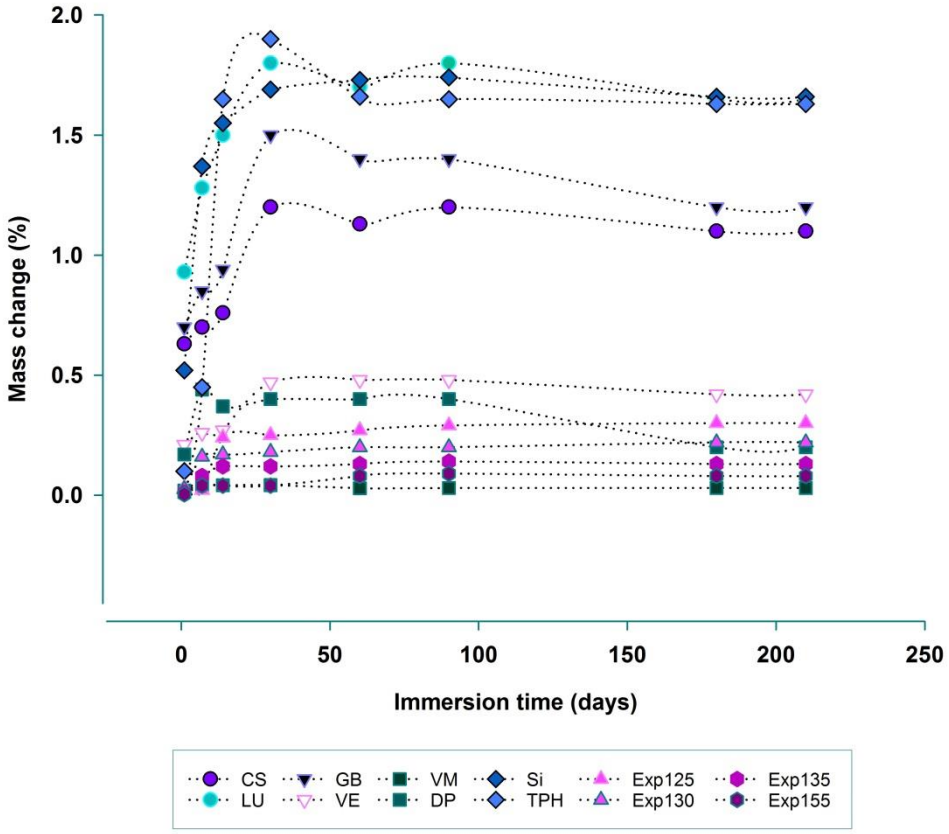

Figure 7.1 Mean percentage mass change (Mg %) of all the tested materials immersed in distilled water over seven month period.

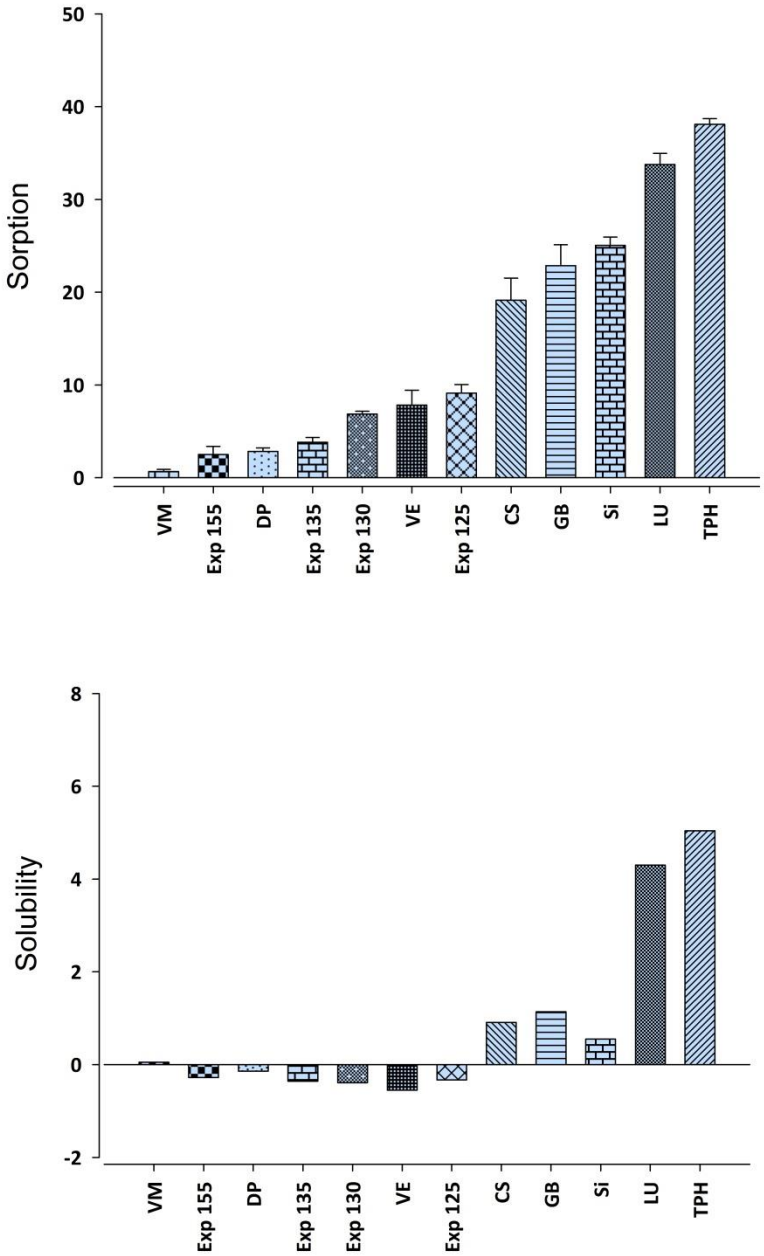

Figure 7.2 A bar chart illustrating the mean sorption (top) and solubility (bottom) of test materials after seven months immersion in distilled water. Error bars represent the standard deviation.

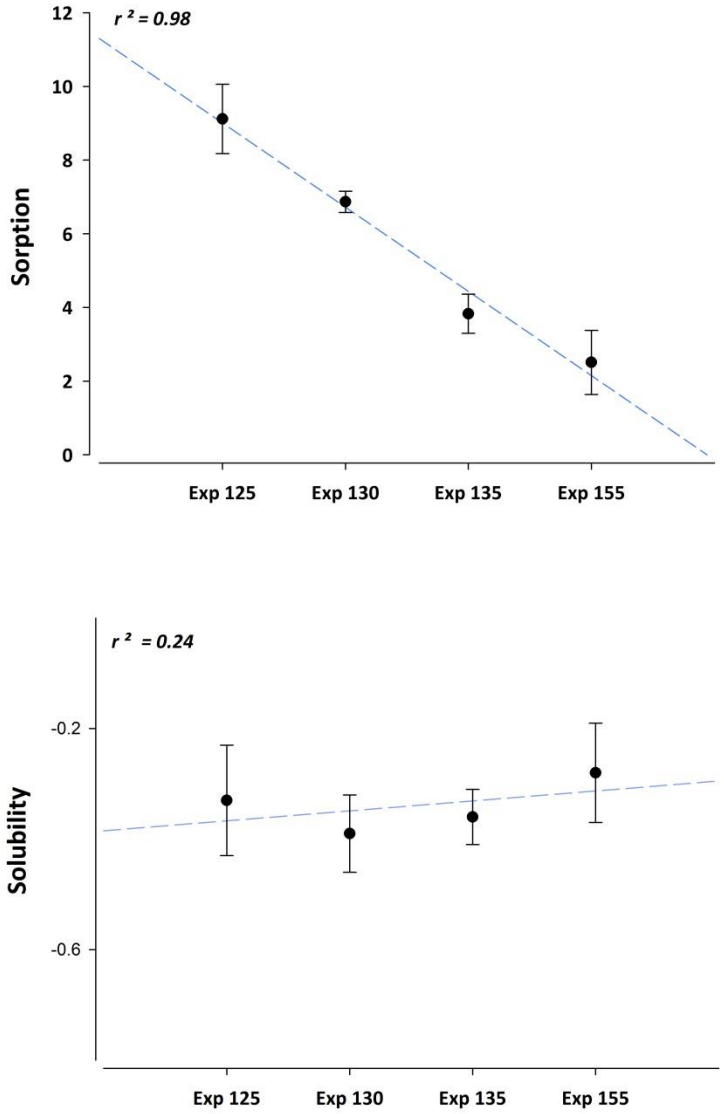

Figure 7.3 Linear regression graphs to show the correlation between the sintering temperature of the model PICN materials and the mean together with the SD values of the sorption (r^2=0.98) and the solubility (r^2=0.24).

7.5 Discussion:

In this study, water sorption and solubility of several CAD/CAM ceramic and PCIN materials were assessed over a seven-month period in distilled water. Significant differences in water sorption and solubility values were found between different materials, thus the first null hypothesis was rejected. All the tested materials reached a plateau after a period of two to three months, so the second null hypothesis was accepted.

Water was chosen as a storage medium as it is commonly found in the oral environment. Previous studies have shown that water plays an important role in the chemical degradation of resin composite materials resulting in both hydrolytic reactions and expansion of the material (360-362). In that respect, water sorption and solubility of composite materials is of a great interest.

In this study, VM, DP and Exp.155 demonstrated significantly lower sorption in water compared to other materials (0.67, 2.85 and 2.51 $\mu g/mm^3$, respectively) while TPH showed significantly the highest value (38.1 $\mu g/mm^3$). Sorption of VM was higher than that reported previously (0.1 $\mu g/mm^3$) and this could be attributed to the relative long storage period in our study (7 months) compared to one week in a previous study (363). Low sorption values of DP were also reported in previous studies with different storage periods (364-366). Sorption of DP was comparable to a previous reported sorption value for a PEEK material (0.2% and 0.44%, respectively)(365). As expected, DP demonstrated relatively lower sorption value owing to the hydrophobic nature of its PEEK polymer matrix (367). Sorption of TPH was comparable to previously reported values for conventional resin composite materials (352, 368). According to the ISO standard for dental restorative resins, the maximum recommended value for water sorption is 40 $\mu g/mm^3$ and in this study none of the tested materials exceeded this limit after 7 months of storage.

With the exception of LU and TPH, the sorption values in this study were negatively correlated to the amount of filler loading of resin composite which is in line with previous studies (368-370). As filler weight increases, the polymer matrix decreases and consequently water uptake is reduced as it is a phenomenon mostly associated with the

polymeric phase. High sorption values were found for LU and TPH despite their relatively high filler content (86wt% and 75wt%, respectively), which might be attributed to the particular resin-matrix monomer content as both LU and TPH share the same monomer (Bis-GMA). The water absorption potential of Bis-GMA has been shown to be higher than other monomers such as UDMA, TEGDMA, and Bis-EMA (342, 371, 372). For LU, this might also be attributed to the zirconium oxide content of the filler, which has been shown to result in reduced stability of the silane coupling agent (373) . This can weaken the filler-matrix interface and eventually provides paths for water diffusion and progressive material degradation (359, 374). A comparable sorption value for LU has been previously reported (30.7 $\mu g/mm^3$) after one week of water storage (363). For TPH, the high sorption value can be also explained on the basis of the filler composition. The mechanism of hydrolytic degradation may be enhanced in dental composite if the filler particles have metallic ions in their compositions (375). Barium (in TPH) is an electropositive element which tends to react with water molecules. With the loss of this element into water, the charge balance of the silica network is changed and re-established with the penetration of hydrogen ions of the water into the spaces previously occupied by barium. As the concentration of hydroxyl ions increase, the siloxane (Si-O-Si) bonds of the silica network start to break forming surface degradation (376, 377).

Unsurprisingly, both commercial and model PICN groups demonstrated sorption mean values ranged between the values of ceramic and resin composite materials. Sorption of VE was comparable to that reported previously (7$\mu g/mm^3$) after a shorter immersion time (one week)(363); however, it was slightly higher than the value reported by the manufacture (5.7 $\mu g/mm^3$)(378). The variation of the sorption values of model PICN ceramic highlighted the significant negative correlation with their sintering temperatures (r^2=0.98). Unlike the solubility, sorption appears to be more related to the sintering temperature of PICN ceramics. As the sintering temperature increases, the ceramic to polymer ratio increases and consequently the water uptake is reduced and this is in agreement with previous studies (369, 370).

Sorption and solubility were strongly correlated (r^2=0.96), and this is consistent with previous studies and reflects a two-way diffusion process in resin composites (379, 380). However, that does not necessarily mean that materials with high water sorption demonstrate high solubility and vice-versa (356). Solubility of resin composite in water is

strongly related to its chemical composition and is mainly attributed to the leaching of unreacted free residual monomers, additives, fillers, and filler components (381, 382). The susceptibility of a monomer to be leached out relies mainly on its hydrophilicity and its degree of conversion, and the higher the degree of conversion, the lower the amount of unreacted monomers and the lower the solubility (164, 380, 383).

All conventional and CAD/CAM composite materials showed positive solubility values, whereas all PICN ceramic materials showed negative values. Negative sorption values do not necessarily mean that no solubility occurred in these materials but it may suggests low solubility. Also, it might indicate a possible penetration of the water into the surface of the material due to hydrophilicity of the resin matrix and/or hydrolytic instability of the interfacial coupling between ceramic and resin matrix. Negative solubility results have been previously reported for various restorative materials including CAD/CAM materials (353, 363, 379, 384, 385).

7.6 Conclusions:

1. Water sorption and solubility of resin composites are material-dependent and are highly affected by the filler loading and properties of the polymeric matrix.
2. PICN ceramic showed hydrolytic stability between resin composite and conventional ceramic, reflecting its microstructural components.
3. Sintering temperature appears to have a significant effect on the PICN ceramic susceptibility to water sorption but not solubility.

Chapter 8

General Discussion, Conclusions and Future Work Recommendations

8.1 General Discussion

The aim of this research was to fabricate and characterise polymer infiltrated polycrystalline ceramics in terms of physico-mechanical properties and compare them with selected conventional and CAD/CAM resin composite and ceramic materials. The two conventional resin composites examined were indirect and direct resin composite materials (Sinfony,Si and TPH Spectrum,TPH, respectively). The CAD/CAM resin composite materials were Lava Ultimate (LU), Cerasmart (CS) and Grandio Bloc (GB) whereas the commercially available PICN tested was Vita Enamic (VE). Dentokeep (DP) and Vitabloc Mark II (VM) were also examined as the former represents PEEK based materials and the later represents CAD/CAM ceramic materials.

Resin composites in general are among the most widely employed direct restorative materials in dentistry. Several advantages of dental composite make it a more favourable restorative material than any other. It has the ability to replace dental tissues in both appearance and function, and also to be bonded to the tooth structure. The indications for resin composites have been extended to include restoration of posterior teeth, and more than half of posterior direct restorations currently rely on composite materials (386). However, there are some major deficiencies in this material which can affect its longevity. Examples of these deficiencies are the susceptibility of dental composites to absorb moisture and to undergo hydrolytic degradation which eventually affects their mechanical performance and biocompatibility.

With the introduction of computerised technology, CAD/CAM resin composite materials have become available in the dental market. Because CAD/CAM resin composite materials are manufactured by compressing (polymerization under pressure up to several thousand bars) and heat-curing and in a standardized and tightly controlled environment, the mechanical properties show relatively improvement compared to conventionally produced resin composite materials (282, 387, 388). This is due to higher conversion rate (90%-95%) in CAD/CAM composites compared to conventional composites (50%-60% for direct composites and 70%-80% indirect composites) (389-392).

PICN is another form of recently introduced CAD/CAM materials where resin composites and ceramics are combined in a single material (105). The three-dimensional

interconnectivity of PICN differs from resin composites with discrete fibres or particles dispersed in a polymer matrix. The purpose of developing PICN is to enhance or tailor the physical and mechanical properties of the constituent phases. Each constituent phase within PICN contributes its own properties resulting in effective properties of the topologically interconnected microstructure. Therefore, considerable attention has been directed towards PICN materials.

Fabrication of a new interpenetrating phase polycrystalline ceramics with optimal mechanical properties and aesthetics is an area of ongoing research in restorative dentistry. A few published studies have shown initial promising results regarding the mechanical properties (141, 393). When evaluating the indications for these materials, it is important to consider properties such as mechanical properties and long-term durability under intraoral conditions and it is also important to investigate these properties of new materials *in vitro*.

In Chapter four, the effect of sintering temperature on the densities and optical and mechanical properties of fabricated PICN models was investigated. At a microstructure level, polymer infiltrated ceramics consist of two phases, ceramic phase with grains and grains boundaries and polymer phase. The grains form as a result of ceramic consolidation (sintering) process at high sintering temperature. Consolidation of ceramic is a thermally activated process which begins when the ceramic particles adhere together and necks start to form (137, 394). The complete consolidation occurs when grains boundaries and grains corners are established and pores are closed leading to an almost completely dense material. Full densification of polycrystalline ceramics may be associated with shrinkage and abnormal grain growth (137). Therefore, it could be a preferred way to produce dense materials by infiltrating polymer into a ceramic matrix that is sintered at a relatively low temperature to control grain growth and its influence on properties. As confirmed in this study, polymer infiltration did improve the density of alumina matrices that were pre-sintered at lower temperatures. Not only that, but it was also found that as the sintering temperature decreases (and hence porosity increases), the infused density increases.

Another finding in this study is that optical properties are also affected by the sintering temperature. In the evaluation of optical properties, contrast ratio, translucent

parameter and light transmission are generally used in literature. These parameters are also used to measure translucency in dental ceramics. Translucency, which is considered a primary factor in achieving aesthetic dental ceramics (395, 396), is generally influenced by factors such as crystalline structure, grain size and pigments, as well as number, size and distribution of defects and porosity (397). Sintering temperature can improve the crystalline structure and eliminate the inter-particle pores consistent with the light transmittance (398). In that perspective, samples that were sintered at 1550 °C were the most translucent among the groups whereas those sintered at 1250 °C showed the least translucency. This confirms the findings of previous studies (225, 226); as the sintering temperature increases, the translucency increases by increasing grain size, sintered density, and reducing porosity, ultimately providing a more compact crystalline structure of ceramic. Larger grains increase the translucency of ceramics by producing fewer grain boundaries but this, however, may reduce its mechanical properties (226, 399).

Flexural strength of PICN was also investigated in this research as it is one of the most important parameters for evaluating the mechanical properties of ceramic materials in dentistry (227). Biaxial flexural strength test using a piston on three balls was chosen as it can eliminate the tensile stress at a central loading area and at the edges of ceramic specimens(232). Previous studies have reported that in porous ceramics, increasing their sintering temperature results in an increase of their flexural strength (233, 234). In our study, there was a positive correlation between the sintering temperature and the density of porous ceramic but this was not the case after polymer infiltration. Increasing the sintering temperature did not significantly influence the strength of the polymer infiltrated ceramics. This may be due to the significance of the polymer infiltration step in strengthening porous ceramic materials. The flexural strength of partially sintered alumina (1250°C -1350°C) has been reported to be less than 200 MPa (236): in our study, all the values obtained from different sintering temperatures were above 300 MPa. The likely explanation for such an increase in the flexural strength is that residual stress from the polymerization shrinkage of heat cured resin probably constrains the system mechanically, creating tension stresses (141). These tension stresses have to be overcome in the process of rupture and crack propagation and this enhances the strength.

In Chapter five, the mechanical properties of our model PICN were compared with comparable commercial materials commonly used in restorative dentistry. Hardness at

two different levels of measurements (micro and nano) as well as elastic modulus were investigated. All PICNs (except Exp155) tested in the current study have hardness values ranged from 1.33 to 4.38 GPa which are substantially lower than the hardness of human enamel (3.5- 5.5 GPa) (256). This might be an advantage especially when it comes to protecting the opposing natural teeth from advanced wear. These finding were consistent with previous studies (109, 252). The hardness levels of the PICN sintered at 1550°C (7.13GPa and 619.41 VHN) were significantly greater than that of enamel. A dental material that is harder than natural enamel may cause more severe wear to the opposing dentition (101). However, although it is usually associated with enamel wear, hardness of ceramic alone is not a reliable predictor of the wear of the opposing teeth (260). Other factors such as surface roughness of the restoration and other oral and environmental factors are needed to be considered before giving a conclusive answer (261).

In terms of elastic modulus, the values of 18–103 GPa (in model PICN materials) are comparable to those reported for human enamel (between 48–105.5 GPa) (274). To the author's knowledge, no commercial PICN material has exhibited values in this elastic modulus range. A low elastic modulus material (less than enamel and dentin) will concentrate and transmit the stress to the tooth a tensile stress (275). Such stress can cause tooth damage during mastication loading. Owing to their high modulus of elasticity and their match with enamel, PICN materials may offer a more uniform stress distribution, especially during loading, and the tooth as well as the restorative crown would be protected from cracking.

Appreciating the hierarchical-dependant properties of human enamel, and as elastic moduli are key parameters in describing the deformation behaviour of materials, in this research an emphasis was placed on quantifying the elastic properties of PICN materials at different levels. By integrating AFM and nano-indentation investigations the micro- and nano-mechanical properties can be obtained. In Chapter 6, AFM was employed where sample surface topography was scanned to provide high-resolution images with three-dimensional representation of the sample. The major advantage of this technique over instrumented nano-indentation is the ability to map the surface height topography and provide in-situ quantification of elastic properties by selecting the location of the indentations within a few tenths of nanometres.

Variations in the elastic modulus values obtained via AFM were noticed in all the PICN groups. Except Exp155, all the other three groups show two ranges of the elastic modulus values. On close inspection, these two ranges clearly indicate that presence of interpenetrating phases of polymer and ceramic in this material. This feature is mostly represented in Exp125 and this may be due the fact that the alumina matrix this group is the most porous compared to the other groups. This in turn may have maximised the polymer/ceramic ratio with proper infiltration of polymer phase. As the temperature increases, the size of pores decreases (330), which may have affected the polymer infiltration process leaving the polymer to coat the ceramic phase instead of interpenetrating them. This coating may have created a third phase- we may call it a 'polymer coated ceramic' phase, which could explain the relatively higher intermediate values between the lowest and the highest elastic modulus readings. In Exp155, the pore size is the least among the groups which decreases the polymer/ceramic phase ratio. This probably explains the presence of one dominant range of elastic modulus values in this group. Overall, the findings of this study confirm that increasing the sintering temperature results in a significant increase in the elastic moduli of PICN materials, in line with previous studies (218, 330, 331).

Comparing the elastic moduli generated from nano-indentation with those obtained from AFM analysis reveals generally good agreement in resin composite materials (CS, LU and GB). However, agreement is slightly lower for Cerasmart, this could be explained by the presence of stiffer particles 100 to 250 nm in diameter which upon close inspection seem to be broken pre-reacted ceramic-composite particles containing nano fillers. In PICN, the values obtained from the instrumented nano-indentation are higher than AFM. This may be related to the relatively larger indenter size in nano-indentation compared to the AFM (r= 35-250 µm and 6-15 nm, respectively), which may have resulted in the nano-indenter force-displacement response to be influenced by the limited size polymer phase and its surrounding stiffer ceramic phase.

In Chapter 7, water sorption and solubility of PICN materials as well as conventional and CAD/CAM resin composite materials were assessed after 7 months of distilled water storage using the ISO method (170). Mass changes of the materials were regularly measured during the storage period in order to assess the long-term sorption kinetics and hydrolytic stability of the materials.

The results of this study showed that significant differences in water sorption and solubility exist between different materials. All the tested materials showed stable mass after a period of two to three months. Sorption and solubility in this study were positively correlated (r^2=0.96), which indicates a two-way diffusion process in the test materials. In line with previous studies (379, 380), water sorption of PICN and composite materials also appeared to be influenced by the degree of ceramic contents (as measured in Chapter 5) since a negative correlation between ceramic contents and sorption of composite materials was found (Pearson correlation coefficient = -0.4, p= 0.01).

A similar trend was also found between the sintering temperature and the water sorption in PICN model materials. The strong negative correlation with their sintering temperatures (r^2=0.98) highlights the important role of sintering temperature in the hydrolytic stability of PICN materials. Previous studies have shown that water sorption by ceramic materials is influenced by their microstructures (400). Water sorption indicates the level of porosity of a ceramic part. The smaller the porosity of a piece, the smaller the amount of water it absorbs. In PICN, the porosities ideally are closed after polymer infiltration, however, due to the nature of resin polymer used (UDMA,TEGDMA) with their relative hydrophilicities, and the tri-dimensional structures and free volume (383), water sorption in PICN materials cannot be avoided.

Surface texture parameters roughness and gloss were also addressed in this research due to their major influence on plaque accumulation, discoloration, wear and the aesthetics of dental restorations (303, 304). There was statistical significant difference in terms of surface roughness and gloss between resin ceramic composite groups and PICN ceramic groups (p=0.001). The differences in the surface roughness parameters of the resin composite materials might be ascribed to variation in their filler size, geometry and composition. The lowest values of roughness parameters were seen with resin composite materials. This could be due to the difference in microstructural compositions between PICN ceramic and resin composite materials. Unlike resin composites, PICN ceramics are composed of interpenetrating phase composite with combination of ceramic and resin polymer. Ceramic which is considered the main component in such materials demonstrates superior surface contour and texture when glazed compared to different finishing and polishing systems (322-325), however, due to the presence of a polymer phase in PICN, a ceramic glazing step is almost impossible without compromising the

polymer component as this would be simply melted away in the oven during the firing process. The manufacturer suggests a semi-glazing approach using monomer-based glaze material which can be applied to the specimens directly, and then cured via light curing device. However, its efficiency is still questionable and to the author's knowledge no clinical study has yet investigated its long term durability.

The sintering temperature appeared to have a significant effect on the surface roughness values of PICN materials. As the temperature increases, the grains become matured, developed, and combined to complete grain boundaries and the ceramic matrix will then be gradually densified. Such densification will result in a well-developed microstructure with fewer residual pores which may eventually decrease the roughness and enhance the appearance. In this study, although the surface roughness of PICN was below the Ra threshold value for plaque retention (0.2 μm) (326, 327), it was still higher than resin composite materials. Such findings may highlight the need for future studies to further investigate the surface polishability of PICN materials.

Properties of PICN ceramic materials can be tailored to suit a wider range of uses by modifying several fabrication factors, such as the type of ceramic used, type of monomers, quality of coupling agent, and conditions related to the sintering process of the ceramic part. The main focus of this research was the sintering temperature and its effect on the physical and mechanical properties of PICN materials. Overall, the findings confirmed that increasing the sintering temperature resulted in improving the mechanical and the optical properties of PICN. However, increasing the temperature up to 1550 °C resulted in less polymer infiltration as well as a significantly harder material than enamel. Such difference in hardness properties may cause more severe wear to the opposing dentition. Therefore, it might be useful for future research is to maintain the sintering temperature of alumina based ceramic matrices below 1550 °C.

In general, the outcomes of this research demonstrate the potential suitability of polymer-infiltrated polycrystalline ceramic-networks (PICN) for CAD/CAM based dental restorative materials. This conclusion is based on the findings of the *in vitro* studies where the model PICN materials were compared to available dental restorative materials. It is very clear that PICN has greater mechanical strength and hydrolytic stability than

conventional and CAD/CAM resin composite materials, although further studies are still necessary to prove the usefulness of PICN model as a dental restorative material.

8.2 Conclusions

1. Sintering temperature has a significant effect on microstructure, porosity and ceramic density and consequently influences the mechanical properties of PICN materials.
2. The density of ceramic matrices increases significantly after polymer infiltration.
3. The increase in sintering temperature results in a significant improvement in the optical properties but not the biaxial flexural strength.
4. Ceramic matrix density has a significant influence on the flexural strength of polymer infiltrated ceramics. Groups that initially had higher matrix density showed higher strength.
5. Different CAD/CAM resin composite materials showed different surface morphology of fillers in different size, shape and density.
6. Micro hardness and nano hardness of the studied PICN and other CAD/CAM composites materials increased systematically with an increase in ceramic contents.
7. A correlation between the nano-hardness and the micro-hardness against ceramic contents was noticed.
8. AFM is a good tool to map the elastic modulus of PICN materials at the nano-scale. However, consideration should be taken during tip selection and sample preparation.
9. The surface roughness profiles of resin nano-ceramic CAD/CAM materials were significantly lower than both commercial and model PICN ceramic materials.
10. The sintering temperatures of PICN materials showed strong influence on their surface profiles and nano-mechanical properties.
11. Dental PICN materials show hierarchical structures with different phase distributions as well as different elastic properties.
12. At a small hierarchy level, commercial PICN exhibits a lower range of elastic modulus values than previously reported values of enamel.

13. Water sorption and solubility of resin composites are material-dependent and are highly affected by the filler loading and properties of the polymeric matrix.
14. PICN ceramic showed hydrolytic stability between resin composite and conventional ceramic, reflecting its microstructural components.
15. Sintering temperature appears to have a significant effect on the PICN ceramic susceptibility to water sorption but not solubility.

8.3 Limitations

The main limitation of the current research is that it is based on *in vitro* studies which necessitate further *in vivo* assessment of materials. However, *in vitro* assessment is considered the first line for assessing materials and it provides better control of variables and standardization of experimental procedures than clinical-based studies.

The present study revealed novel and significant results relating to manufacturing and properties of polymer infiltrated polycrystalline ceramics. Optical properties of these recently developed materials were not studied by any previously published studies. Also, this study focused on manufacturing ceramic matrix by slip casting and partially sintering of a selected type of ceramic powder (alumina A16SG). Other brands with different particle sizes may require different processing and result in other forms of microstructures that may significantly influence the properties.

In terms of the methodological approaches used in the present research, there are limitations involved with some techniques as discussed in previous chapters. For example, nanoindentation might be a precise method to investigate materials with microstructural constituents, such as microfilled or nanofilled composites (401), however, its accuracy can be impaired for various reasons, mainly due to thermal changes and mechanical vibration and acoustic noise (280). Other factors, such as the indenter tip size effect and its relation to the filler particle size (402) and the maximum load used are also relevant; i.e., if the indenter tip size or load were too small it would not provide sufficient information about the bulk material properties (401). However, the appropriate indenter size along with appropriate load will provide sufficient information about the material properties. Also, there is no microscope linked to the Nanovea machine, so the location of the tested point can only be determined by naked eyes.

Another limitation may be associated with the sorption analysis using the gravimetric analysis technique. It may be argued that water diffusion through the samples might not be uniform and may not involve the entire volume of the sample which may result in discrepancies in some of the sorption calculations. However, as long as the methodological approach is following the recommended standards, data are considered comparable and valid for assessing the stability of materials in the specified storage media.

8.4 Recommendations

To complement the findings of the current research, the following future areas are suggested:

- Using a polymer with a refractive index close to that of the ceramic matrix for improving optical properties and investigating the influence of various microstructures of different types of polycrystalline ceramics on both optical and mechanical properties.

- Qualitative and quantitative assessments of eluted monomer composition of the resin matrix by high performance liquid chromatography/mass spectroscopy.

- Study of the cytotoxicity and biofilm formation associated with different types of PICN materials and how these may be affected by the type and quantity of monomer in the resin matrix network.

- Assessment of the mechanical performance and fatigue limit of PICN materials after thermo-cycling and accelerated mechanical loading.

References:

1. Fejerskov O, Kidd E. Dental caries: the disease and its clinical management: John Wiley & Sons; 2009.

2. Selwitz RH, Ismail AI, Pitts NB. Dental caries. Lancet. 2007;369(9555):51-9.

3. Fejerskov O. Concepts of dental caries and their consequences for understanding the disease. Community Dent Oral Epidemiol. 1997;25(1):5-12.

4. Phillips RW. Phillips' science of dental materials. London: Elsevier/Saunders; 2013.

5. Anusavice KJ. Quality evaluation of dental restorations: criteria for placement and replacement: proceedings of the International Symposium on Criteria for Placement and Replacement of Dental Restorations, Lake Buena Vista, Florida, October 19-21, 1987: Quintessence Pub Co; 1989.

6. Birgitha N. Natural fiber composites optimization of microstructure and processing parameters: Thesis; 2007.

7. Peutzfeldt A. Resin composites in dentistry: the monomer systems. Eur J Oral Sci. 1997;105(2):97-116.

8. Peyton FA. History of resins in dentistry. Dent Clin North Am. 1975;19(2):211-22.

9. Millich F, Jeang L, Eick JD, Chappelow CC, Pinzino CS. Elements of light-cured epoxy-based dental polymer systems. J Dent Res. 1998;77(4):603-8.

10. Craig R, Welker D, Rothaut f, Krumbholz K, Stefan K, Dermann K, et al. Dental Materials. Ullmann's Encyclopedia of Industrial Chemistry. Weinheim: VCH; 2006.

11. Khatri CA, Stansbury JW, Schultheisz CR, Antonucci JM. Synthesis, characterization and evaluation of urethane derivatives of Bis-GMA. Dent Mater. 2003;19(7):584-8.

12. Moszner N, Fischer UK, Angermann J, Rheinberger V. A partially aromatic urethane dimethacrylate as a new substitute for Bis-GMA in restorative composites. Dent Mater. 2008;24(5):694-9.

13. Kalipcilar B, Karaagaclioglu L, Hasanreisoglu U. Evaluation of the Level of Residual Monomer in Acrylic Denture Base Materials Having Different Polymerization Properties. J Oral Rehabil. 1991;18(5):399-401.

14. Foster J, Walker R. Dental filling materials. US Patent No. 3,825; 1974.

15. Kerby RE, Knobloch LA, Schricker S, Gregg B. Synthesis and evaluation of modified urethane dimethacrylate resins with reduced water sorption and solubility. Dent Mater. 2009;25(3):302-13.

16. Pitel M. Low-shrink composite resins: a review of their history, strategies for managing shrinkage, and clinical significance. Compend Contin Educ Dent. 2013;34(8):578-90.

17. Geurtsen W, Leyhausen G. Concise review biomaterials & bioengineering: chemical-biological interactions of the resin monomer triethyleneglycol-dimethacrylate (TEGDMA). J Dent Res. 2001;80(12):2046-50.

18. Ferracane JL. Current trends in dental composites. Crit Rev Oral Biol Med. 1995;6(4):302-18.

19. Habib E, Wang R, Wang Y, Zhu M, Zhu X. Inorganic fillers for dental resin composites: present and future. ACS BIOMATER SCI ENG. 2015;2(1):1-11.

20. Lutz F, Phillips RW. A classification and evaluation of composite resin systems. J Prosthet Dent. 1983;50(4):480-8.

21. Ferracane JL. Resin composite—state of the art. Dental materials. 2011;27(1):29-38.

22. Willems G, Lambrechts P, Braem M, Celis JP, Vanherle G. A Classification of Dental Composites According to Their Morphological and Mechanical Characteristics. Dent Mater. 1992;8(5-6):310-9.

23. Cramer NB, Stansbury JW, Bowman CN. Recent advances and developments in composite dental restorative materials. J Dent Res. 2011;90(4):402-16.

24. Beun S, Glorieux T, Devaux J, Vreven J, Leloup G. Characterization of nanofilled compared to universal and microfilled composites. Dental Materials. 2007;23(1):51-9.

25. Mitra S, Wu D, Holmes B. An application of nanotechnology in advanced dental materials. J Am Dent Assoc. 2003;134(10):1382-90.

26. Plueddemann E. Performance of Silane Coupling Agents. Silane Coupling Agents: Springer; 1991. p. 153-81.

27. Moszner N, Salz U. Recent developments of new components for dental adhesives and composites. Macromol Mater Eng. 2007;292(3):245-71.

28. Craig R, Peyton F, Asgar K. Restorative dental materials. St.Louis: Mosby; 1975.

29. AlQahtani MQ, AlShaafi MM, Price RB. Effects of single-peak vs polywave light-emitting diode curing lights on the polymerization of resin cement. J Adhes Dent. 2013;15(6):547-51.

30. AlQahtani MQ, Michaud PL, Sullivan B, Labrie D, AlShaafi MM, Price RB. Effect of High Irradiance on Depth of Cure of a Conventional and a Bulk Fill Resin-based Composite. Oper Dent. 2015;40(6):662-72.

31. Chang HS, Kim JW. Early hardness and shear bond strength of dual-cure resin cement light cured through resin overlays with different dentin-layer thicknesses. Oper Dent. 2014;39(4):398-406.

32. Reges RV, Moraes RR, Correr AB, Sinhoreti MA, Correr-Sobrinho L, Piva E, et al. In-depth polymerization of dual-cured resin cement assessed by hardness. J Biomater Appl. 2008;23(1):85-96.

33. Rueggeberg F, Caughman W, Curtis J, Davis H. Factors affecting cure at depths within light-activated resin composites. Am J Dent. 1993;6(2):91-5.

34. Tanimoto Y, Hirayama S, Yamaguchi M, Nishiwaki T. Static and dynamic moduli of posterior dental resin composites under compressive loading. J Mech Behav Biomed Mater. 2011;4(7):1531-9.

35. Della Bona A, Benetti P, Borba M, Cecchetti D. Flexural and diametral tensile strength of composite resins. Braz Oral Res. 2008;22(1):84-9.

36. Tanimoto Y, Nishiwaki T, Nemoto K, Ben G. Effect of filler content on bending properties of dental composites: Numerical simulation with the use of the finite-element method. J Polym Sci Pol Phys. 2004;71(1):188-95.

37. Lu H, Lee YK, Oguri M, Powers JM. Properties of a dental resin composite with a spherical inorganic filler. Oper Dent. 2006;31(6):734-40.

38. Banava S, Salehyar S. In vitro comparative study of compressive strength of different types of composite resins in different periods of time. Iranian Journal of Pharmaceutical Sciences. 2008;4(1):69-74.

39. Poggio C, Lombardini M, Gaviati S, Chiesa M. Evaluation of Vickers hardness and depth of cure of six composite resins photo-activated with different polymerization modes. J Conserv Dent. 2012;15(3):237-41.

40. Price RB, Felix CA, Andreou P. Evaluation of a dual peak third generation LED curing light. Compend Contin Educ Dent. 2005;26(5):331-2, 4, 6-8 passim; quiz 48.

41. Mobarak E, Elsayad I, Ibrahim M, El-Badrawy W. Effect of LED light-curing on the relative hardness of tooth-colored restorative materials. Oper Dent. 2009;34(1):65-71.

42. Willems G, Celis JP, Lambrechts P, Braem M, Vanherle G. Hardness and Young's modulus determined by nanoindentation technique of filler particles of dental restorative materials compared with human enamel. J Biomed Mater Res. 1993;27(6):747-55.

43. Indrani DJ, Cook WD, Televantos F, Tyas MJ, Harcourt JK. Fracture toughness of water-aged resin composite restorative materials. Dent Mater. 1995;11(3):201-7.

44. Braem M, Finger W, Vandoren VE, Lambrechts P, Vanherle G. Mechanical-Properties and Filler Fraction of Dental Composites. Dental Materials. 1989;5(5):346-9.

45. Mjor IA, Jokstad A, Qvist V. Longevity of posterior restorations. Int Dent J. 1990;40(1):11-7.

46. Norman RD, Wright JS, Rydberg RJ, Felkner LL. A 5-year study comparing a posterior composite resin and an amalgam. J Prosthet Dent. 1990;64(5):523-9.

47. Abell AK, Leinfelder KF, Turner DT. Microscopic observations of the wear of a tooth restorative composite in vivo. J Biomed Mater Res. 1983;17(3):501-7.

48. Kusy RP, Leinfelder KF. Pattern of wear in posterior composite restorations. J Dent Res. 1977;56(5):544.

49. Sarrett DC, Soderholm KJ, Batich CD. Water and abrasive effects on three-body wear of composites. J Dent Res. 1991;70(7):1074-81.

50. Soderholm KJ, Lambrechts P, Sarrett D, Abe Y, Yang MC, Labella R, et al. Clinical wear performance of eight experimental dental composites over three years determined by two measuring methods. Eur J Oral Sci. 2001;109(4):273-81.

51. Vrochari A, Petropoulou A, Chronopoulos V, Polydorou O, Massey W, Hellwig E. Evaluation of surface roughness of ceramic and resin composite material used for conservative indirect restorations, after repolishing by intraoral means. J Prosthodont 2017;26(4):296-301.

52. Dogheim A, El Kady A, Ghoneim M, Abdelmotie M. In Vitro Comparative Study Of Lava Ultimate Cad/Cam Restorative System In Comparison To Ips E-Max Press. Alex Dent J. 2016;41(2):156-62.

53. Bernardo M, Luis H, Martin M, Leroux B, Rue T, Leitão J, et al. Survival and reasons for failure of amalgam versus composite posterior restorations placed in a randomized clinical trial. J Am Dent Assoc. 2007;138(6):775-83.

54. Hamama H. 19 - Recent advances in posterior resin composite restorations. In: Asiri AM, Inamuddin, Mohammad A, editors. Applications of Nanocomposite Materials in Dentistry: Woodhead Publishing; 2019. p. 319-36.

55. Bentley C, Drake C. Longevity of restorations in a dental school clinic. Journal of Dental Education. 1986;50(10):594-600.

56. Larsen IB, Freund M, Munksgaard EC. Change in surface hardness of BisGMA/TEGDMA polymer due to enzymatic action. J Dent Res. 1992;71(11):1851-3.

57. De Gee AJ, Wendt SL, Werner A, Davidson CL. Influence of enzymes and plaque acids on in vitro wear of dental composites. Biomaterials. 1996;17(13):1327-32.

58. Sarrett DC, Coletti DP, Peluso AR. The effects of alcoholic beverages on composite wear. Dent Mater. 2000;16(1):62-7.

59. Taylor J. History of dentistry: A practical treatise for the use of dental students and practitioners: Lea & Febiger; 1922.

60. Carter CB, Norton MG. Ceramic materials: science and engineering. New York: Springer; 2007.

61. Shenoy A, Shenoy N. Dental ceramics: An update. J Conserv Dent. 2010;13(4):195-203.

62. McLaren E, Giordano R. Ceramics Overview: Classification by microestructure and processing methods. Compend Contin Educ Dent 2010;31(9).

63. Kelly JR. Dental ceramics: current thinking and trends. Dental clinics of North America. 2004;48(2):513-30.

64. Griggs JA. Recent advances in materials for all-ceramic restorations. Dent Clin North Am. 2007;51(3):713-27, viii.

65. Duret F, Preston JD. CAD/CAM imaging in dentistry. Curr Opin Dent. 1991;1(2):150-4.

66. Bindl A, Mormann WH. An up to 5-year clinical evaluation of posterior in-ceram CAD/CAM core crowns. International Journal of Prosthodontics. 2002;15(5):451-6.

67. Otto T, De Nisco S. Computer-aided direct ceramic restorations: a 10-year prospective clinical study of Cerec CAD/CAM inlays and onlays. Int J Prosthodont. 2002;15(2):122-8.

68. Christensen RP, Galan AD, Mosher TA. Clinical status of eleven CAD/CAM materials after one to twelve years of service. J Prosthet Dent. 2006;20:9-+.

69. Bindl A, Luthy H, Mormann WH. Fracture load of CAD/CAM-generated slot-inlay FPDs. International Journal of Prosthodontics. 2003;16(6):653-60.

70. Giordano R. Materials for chairside CAD/CAM–produced restorations. J Am Dent Assoc. 2006;137:14S-21S.

71. Pallesen U, van Dijken JW. An 8-year evaluation of sintered ceramic and glass ceramic inlays processed by the Cerec CAD/CAM system. Eur J Oral Sci. 2000;108(3):239-46.

72. Zimmer S, Gohlich O, Ruttermann S, Lang H, Raab WH, Barthel CR. Long-term survival of Cerec restorations: a 10-year study. Oper Dent. 2008;33(5):484-7.

73. Lampe K, Luthy H, Mormann WH. Fracture load of all-ceramic computer crowns. In: Mormann W, editor. CAD/CAM in Aesthetic Dentistry,CEREC 10 year anniversary symposium; Chicago, IL: Quintessence; 1996. p. 463-82.

74. Della Bona A. Bonding to ceramics: scientific evidences for clinical dentistry. Sao Paulo: Artes Médicas; 2009.

75. Beall GH. Mica glass-ceramics. Google Patents; 1972.

76. Matinlinna J. Processing and bonding of dental ceramics. Non-metallic biomaterials for tooth repair and replacement. Cambridge: Elsevier; 2013. p. 129-60.

77. Seghi RR, Denry IL, Rosenstiel SF. Relative fracture toughness and hardness of new dental ceramics. J Prosthet Dent. 1995;74(2):145-50.

78. Gladys S, Van Meerbeek B, Inokoshi S, Willems G, Braem M, Lambrechts P, et al. Clinical and semiquantitative marginal analysis of four tooth-coloured inlay systems at 3 years. J Dent. 1995;23(6):329-38.

79. Li RW, Chow TW, Matinlinna JP. Ceramic dental biomaterials and CAD/CAM technology: state of the art. J Prosthodont Res. 2014;58(4):208-16.

80. Reich S, Fischer S, Sobotta B, Klapper HU, Gozdowski S. A preliminary study on the short-term efficacy of chairside computer-aided design/computer-assisted manufacturing- generated posterior lithium disilicate crowns. Int J Prosthodont. 2010;23(3):214-6.

81. Fasbinder DJ, Dennison JB, Heys D, Neiva G. A clinical evaluation of chairside lithium disilicate CAD/CAM crowns: a two-year report. J Am Dent Assoc. 2010;141 Suppl 2:10S-4S.

82. Kern M, Sasse M, Wolfart S. Ten-year outcome of three-unit fixed dental prostheses made from monolithic lithium disilicate ceramic. J Am Dent Assoc. 2012;143(3):234-40.

83. Sola-Ruiz MF, Lagos-Flores E, Roman-Rodriguez JL, Highsmith Jdel R, Fons-Font A, Granell-Ruiz M. Survival rates of a lithium disilicate-based core ceramic for three-unit esthetic fixed partial dentures: a 10-year prospective study. Int J Prosthodont. 2013;26(2):175-80.

84. Heffernan MJ, Aquilino SA, Diaz-Arnold AM, Haselton DR, Stanford CM, Vargas MA. Relative translucency of six all-ceramic systems. Part II: core and veneer materials. J Prosthet Dent. 2002;88(1):10-5.

85. Conrad HJ, Seong WJ, Pesun IJ. Current ceramic materials and systems with clinical recommendations: a systematic review. J Prosthet Dent. 2007;98(5):389-404.

86. Roediger M, Gersdorff N, Huels A, Rinke S. Prospective evaluation of zirconia posterior fixed partial dentures: four-year clinical results. Int J Prosthodont. 2010;23(2):141-8.

87. Sailer I, Pjetursson B, Zwahlen M, Hämmerle C. A systematic review of the survival and complication rates of all-ceramic and metal–ceramic reconstructions after an observation period of at least 3 years. Part II: fixed dental prostheses. Clin Oral Implants Res. 2007;18(s3):86-96.

88. Raigrodski A, Chiche G, Potiket N, Hochstedler J, Mohamed S, Billiot S, et al. The efficacy of posterior three-unit zirconium-oxide–based ceramic fixed partial dental prostheses: A prospective clinical pilot study. J Prosthet Dent. 2006;96(4):237-44.

89. Vult V. All-ceramic fixed partial dentures. Studies on aluminum oxide-and zirconium dioxide-based ceramic systems. Swed Dent J Suppl. 2004(173):1-69.

90. Fradeani M, D'Amelio M, Redemagni M, Corrado M. Five-year follow-up with Procera all-ceramic crowns. Quintessence Int. 2005;36(2):105-13.

91. Wolfart S, Bohlsen F, Wegner SM, Kern M. A preliminary prospective evaluation of all-ceramic crown-retained and inlay-retained fixed partial dentures. Int J Prosthodont. 2005;18(6):497-505.

92. Esquivel-Upshaw JF, Anusavice KJ, Young H, Jones J, Gibbs C. Clinical performance of a lithia disilicate-based core ceramic for three-unit posterior FPDs. Int J Prosthodont. 2004;17(4):469-75.

93. Mörmann W, Bindl A. All-ceramic, chair-side computer-aided design/computer-aided machining restorations. Dent Clin N Am. 2002;46(2):405-26, viii.

94. Pröbster L. Four year clinical study of glass-infiltrated, sintered alumina crowns. J Oral Rehabil. 1996;23(3):147-51.

95. Al-Amleh B, Lyons K, Swain M. Clinical trials in zirconia: a systematic review. J Oral Rehabil. 2010;37(8):641-52.

96. Aboushelib MN, de Jager N, Kleverlaan CJ, Feilzer AJ. Microtensile bond strength of different components of core veneered all-ceramic restorations. Dent Mater. 2005;21(10):984-91.

97. Jalalian E, Heidari M, Aminimanesh M, Rezaei C. Effect of Veneering Ceramic Thickness on Fracture Strength of All-Ceramic Lithium Disilicate Restorations. J Res Med Dent Sci. 2018;6(2):514-9.

98. Ge C, Green CC, Sederstrom D, McLaren EA, White SN. Effect of porcelain and enamel thickness on porcelain veneer failure loads in vitro. J Prosthet Dent. 2014;111(5):380-7.

99. Proos KA, Swain MV, Ironside J, Steven GP. Influence of core thickness on a restored crown of a first premolar using finite element analysis. Int J Prosthodont

2003;16(5):474-80.

100. Della Bona A, Donassollo TA, Demarco FF, Barrett AA, Mecholsky JJ, Jr. Characterization and surface treatment effects on topography of a glass-infiltrated alumina/zirconia-reinforced ceramic. Dent Mater. 2007;23(6):769-75.

101. He LH, Swain M. A novel polymer infiltrated ceramic dental material. Dent Mater. 2011;27(6):527-34.

102. Holand W, Schweiger M, Rheinberger VM, Kappert H. Bioceramics and their application for dental restoration. Adv Appl Ceram. 2009;108(6):373-80.

103. Della Bona A, Corazza PH, Zhang Y. Characterization of a polymer-infiltrated ceramic-network material. Dent Mater. 2014;30(5):564-9.

104. Stawarczyk B, Liebermann A, Eichberger M, Guth JF. Evaluation of mechanical and optical behavior of current esthetic dental restorative CAD/CAM composites. J Mech Behav Biomed Mater. 2015;55:1-11.

105. Swain MV, Coldea A, Bilkhair A, Guess PC. Interpenetrating network ceramic-resin composite dental restorative materials. Dent Mater. 2016;32(1):34-42.

106. Coldea A, Swain MV, Thiel N. In-vitro strength degradation of dental ceramics and novel PICN material by sharp indentation. J Mech Behav Biomed Mater. 2013;26:34-42.

107. Petrini M, Ferrante M, Su B. Fabrication and characterization of biomimetic ceramic/polymer composite materials for dental restoration. Dent Mater. 2013;29(4):375-81.

108. Facenda J, Borba M, Corazza P. A literature review on the new polymer-infiltrated ceramic-network material (PICN). J Esthet Restor Dent. 2018;30.

109. Albero A, Pascual A, Camps I, Grau-Benitez M. Comparative characterization of a novel cad-cam polymer-infiltrated-ceramic-network. J Clin Exp Dent. 2015;7(4):e495-500.

110. Argyrou R, Thompson GA, Cho SH, Berzins DW. Edge chipping resistance and flexural strength of polymer infiltrated ceramic network and resin nanoceramic restorative materials. J Prosthet Dent. 2016;116(3):397-403.

111. Choi B, Kim S, Im Y, Lee J, Lee H. Uniaxial and biaxial flexural strengths of resin-composite CAD-CAM blocks. Dent Mater. 2015(31):e31-e2.

112. Homaei E, Farhangdoost K, Pow EHN, Matinlinna JP, Akbari M, Tsoi JKH. Fatigue resistance of monolithic CAD/CAM ceramic crowns on human premolars. Ceram Int. 2016;42(14):15709-17.

113. Coldea A, Fischer J, Swain MV, Thiel N. Damage tolerance of indirect restorative materials (including PICN) after simulated bur adjustments. Dent Mater. 2015;31(6):684-94.

114. de Kok P, Kleverlaan CJ, de Jager N, Kuijs R, Feilzer AJ. Mechanical performance of implant-supported posterior crowns. J Prosthet Dent. 2015;114(1):59-66.

115. Della Bona A, Corazza PH, Zhang Y. Characterization of a polymer-infiltrated ceramic-network material. Dent Mater. 2014;30(5):564-9.

116. Quek SHQ, Yap AUJ, Rosa V, Tan KBC, Teoh KH. Effect of staining beverages on color and translucency of CAD/CAM composites. J Esthet Restor Dent

2018;30(2):E9-E17.

117. Alharbi A, Ardu S, Bortolotto T, Krejci I. Stain susceptibility of composite and ceramic CAD/CAM blocks versus direct resin composites with different resinous matrices. Odontology. 2017;105(2):162-9.

118. Schurmann M, Olms C. Shade Stability of Polymer Infiltrated and Resin Nano Ceramic Crowns after Dynamic Chewing Simulation. Eur J Prosthodont Restor Dent. 2018;26(4):174-83.

119. Flury S, Schmidt SZ, Peutzfeldt A, Lussi A. Dentin bond strength of two resin-ceramic computer-aided design/computer-aided manufacturing (CAD/CAM) materials and five cements after six months storage. Dent Mater J. 2016;35(5):728-35.

120. Elhomiamy E. Wear Behaviour and Surface Roughness of Polymer Infiltrated Ceramic Material Compared to Pressable Glass Ceramic. Alex Dent J. 2015;40(1).

121. Mormann WH, Stawarczyk B, Ender A, Sener B, Attin T, Mehl A. Wear characteristics of current aesthetic dental restorative CAD/CAM materials: two-body wear, gloss retention, roughness and Martens hardness. J Mech Behav Biomed Mater. 2013;20:113-25.

122. Ozarslan MM, Buyukkaplan US, Barutcigil C, Arslan M, Turker N, Barutcigil K. Effects of different surface finishing procedures on the change in surface roughness and color of a polymer infiltrated ceramic network material. J Adv Prosthodont. 2016;8(1):16-20.

123. Campos F, Almeida CS, Rippe MP, de Melo RM, Valandro LF, Bottino MA. Resin Bonding to a Hybrid Ceramic: Effects of Surface Treatments and Aging. Oper Dent. 2016;41(2):171-8.

124. Kelly JR, Nishimura I, Campbell SD. Ceramics in dentistry: historical roots and current perspectives. J Prosthet Dent. 1996;75(1):18-32.

125. Piconi C, Condo SG, Kosmač T. Alumina-and zirconia-based ceramics for load-bearing applications. Advanced ceramics for dentistry. New York: Elsevier; 2014. p. 219-53.

126. Al-Sanabani F, Madfa A, Al-Qudaimi N. Alumina ceramic for dental applications: a review article. Am J Mater Sci. 2014;1(1):26-34.

127. Kuntz M, Masson B, Pandorf T, Mendes G, Lago, B., Eds. Current state of the art of the ceramic composite material BIOLOX® DELTA. Strength of Materials. 2009:133-55.

128. Sinharoy S, Levenson L, Day DE. Influence of Calcium Migration on the Strength Reduction of Dense Alumina Exposed to Steam. Am Ceram Soc Bull. 1979;58(4):464-6.

129. Osterholm HH, Day DE. Dense alumina aged in vivo. J Biomed Mater Res. 1981;15(2):279-88.

130. Krainess FE, Knapp WJ. Strength of a dense alumina ceramic after aging in vitro. J Biomed Mater Res. 1978;12(2):241-6.

131. Dorre E, Hubner H. Alumina: Processing, Properties and Applications. Springer-Verlag. 1984:1984.

132. McLean JW, Hughes TH. The reinforcement of dental porcelain with ceramic oxides. Br Dent J. 1965;119(6):251-67.

133. Andersson M, Oden A. A new all-ceramic crown. A dense-sintered, high-purity alumina coping with porcelain. Acta odontologica Scandinavica. 1993;51(1):59-64.

134. Sadoun M, editor All ceramic bridges with the slip casting technique. The 7th International Symposium on Ceramics; 1988; Paris.

135. Zhang Y, Kelly JR. Dental Ceramics for Restoration and Metal Veneering. Dent Clin North Am. 2017;61(4):797-819.

136. Raghavan R. Ceramics in dentistry, sintering of ceramics-new emerging techniques: India; 2012.

137. Wang H, Liao Y, Chao Y, Liang X. Shrinkage and strength characterization of an alumina–glass interpenetrating phase composite for dental use. Dent Mater. 2007;23(9):1108-13.

138. Denry I, Kelly JR. Emerging ceramic-based materials for dentistry. J Dent Res. 2014;93(12):1235-42.

139. Steier VF, Koplin C, Kailer A. Influence of pressure-assisted polymerization on the microstructure and strength of polymer-infiltrated ceramics. J Mater Sci. 2013;48(8):3239-47.

140. Yoshimura H, Chimanski A, Cesar P. Systematic approach to preparing ceramic–glass composites with high translucency for dental restorations. Dent Mater. 2015;31(10):1188-97.

141. Chaiyabutr Y, Giordano R, Pober R. The effect of different powder particle size on mechanical properties of sintered alumina, resin-and glass-infused alumina. J Biomed Mater Res A. 2009;88(2):502-8.

142. Craig BD, Francis LF. Alumina/epoxy interpenetrating phase composite coatings: I, Processing and microstructural development. J Am Ceram Soc. 1998;81(12):3109-16.

143. Kim EH, Jung YG, Jo CY. Microstructure and Mechanical Properties of Heterogeneous Ceramic-Polymer Composite Using Interpenetrating Network. J Nanomater. 2012;2012:23.

144. Ashby MF. Engineering Materials and Their Properties. In: Ashby MF, editor. Materials Selection in Mechanical Design. Oxford: Butterworth-Heinemann; 2011. p. 31-56.

145. Anusavice K, Shen C, Rawls H. Phillips' science of dental materials. London: Elsevier Health Sciences; 2013.

146. Hammant B. The use of 4-point loading tests to determine mechanical properties. Composites. 1971;2(4):246-9.

147. Kusy R, Dilley G. Materials science elastic modulus of a triple-stranded stainless steel arch wire via three-and four-point bending. J Dent Res. 1984;63(10):1232-40.

148. Wagner WC, Chu TM. Biaxial flexural strength and indentation fracture toughness of three new dental core ceramics. J Prosthet Dent. 1996;76(2):140-4.

149. Addison O, Marquis PM, Fleming GJ. The impact of hydrofluoric acid surface treatments on the performance of a porcelain laminate restorative material. Dent Mater. 2007;23(4):461-8.

150. Mott BW. Micro-indentation hardness testing. London: Butterworths Scientific Publications; 1956.

151. Schuh C. Nanoindentation studies of materials. Materials Today. 2006;9(5):32-40.

152. Oliver WC, Pharr GM. An Improved Technique for Determining Hardness and Elastic-Modulus Using Load and Displacement Sensing Indentation Experiments. J Dent Res. 1992;7(6):1564-83.

153. Gao S, Gao S, Xu B, Yu H. Effects of Different pH-Values on the Nanomechanical Surface Properties of PEEK and CFR-PEEK Compared to Dental Resin-Based Materials. Materials. 2015;8(8):4751-67.

154. Jefferies SR. Abrasive finishing and polishing in restorative dentistry: a state-of-the-art review. Dent Clin North Am. 2007;51(2):379-97, ix.

155. Cenci M, Venturini D, Pereira-Cenci T, Piva E, Demarco F. The effect of polishing techniques and time on the surface characteristics and sealing ability of resin composite restorations after one-year storage. Oper Dent. 2008;33(2):169-76.

156. Ereifej N, Oweis Y, Eliades G. The effect of polishing technique on 3-D surface roughness and gloss of dental restorative resin composites. Oper Dent. 2012;38(1):E9-E20.

157. Heintze SD, Forjanic M, Ohmiti K, Rousson V. Surface deterioration of dental materials after simulated toothbrushing in relation to brushing time and load. Dent Mater. 2010;26(4):306-19.

158. Kumar RK, Seetharamu S, Kamaraj M. Quantitative evaluation of 3D surface roughness parameters during cavitation exposure of 16Cr–5Ni hydro turbine steel. Wear. 2014;320:16-24.

159. Garcia-Fierro J, Aleman JV. Sorption of water by epoxide prepolymers. Macromolecules. 1982;15(4):1145-9.

160. Ferracane JL. Hygroscopic and hydrolytic effects in dental polymer networks. Dent Mater. 2006;22(3):211-22.

161. Ferracane JL. Elution of leachable components from composites. J Oral Rehabil. 1994;21(4):441-52.

162. Durner J, Spahl W, Zaspel J, Schweikl H, Hickel R, Reichl FX. Eluted substances from unpolymerized and polymerized dental restorative materials and their Nernst partition coefficient. Dent Mater. 2010;26(1):91-9.

163. Rüttermann S, Krüger S, Raab WH, Janda R. Polymerization shrinkage and hygroscopic expansion of contemporary posterior resin-based filling materials—a comparative study. J Dent. 2007;35(10):806-13.

164. Sideridou ID, Karabela MM, Vouvoudi E. Volumetric dimensional changes of dental light-cured dimethacrylate resins after sorption of water or ethanol. Dent Mater. 2008;24(8):1131-6.

165. Bastioli C, Romano G, Migliaresi C. Water Sorption and Mechanical-Properties of Dental Composites. Biomaterials. 1990;11(3):219-23.

166. Musanje L, Shu M, Darvell BW. Water sorption and mechanical behaviour of cosmetic direct restorative materials in artificial saliva. Dent Mater. 2001;17(5):394-401.

167. Palin WM, Fleming GJ, Burke FJ, Marquis PM, Randall RC. The influence of short and medium-term water immersion on the hydrolytic stability of novel low-shrink dental composites. Dent Mater. 2005;21(9):852-63.

168. Um CM, Ruyter IE. Staining of resin-based veneering materials with coffee and tea. Quintessence Int. 1991;22(5):377-86.

169. Takahashi Y, Chai J, Kawaguchi M. Effect of water sorption on the resistance to plastic deformation of a denture base material relined with four different denture reline materials. Int J Prosthodont. 1998;11(1):49-54.

170. Standard I. ISO 4049 polymer based filling, restorative and luting materials. International Organization for Standardization. 2000;1:27.

171. Freestone IC, Middleton AP. Mineralogical Applications of the Analytical Sem in Archaeology. Mineralogical Magazine. 1987;51(359):21-31.

172. Kingery W. Microstructure analysis as part of a holistic interpretation of ceramic art and archaeological artifacts. Archeomaterials. 1987;1(2):91-9.

173. De Freitas A, Espejo L, Botta S, De Sa Teixeira F, Luz M, Garone-Netto N, et al. AFM analysis of bleaching effects on dental enamel microtopography. Appl Surf Sci. 2010;256(9):2915-9.

174. Dilber E, Yavuz T, Kara HB, Ozturk AN. Comparison of the effects of surface treatments on roughness of two ceramic systems. Photomed Laser Surg. 2012;30(6):308-14.

175. Sanches RP, Otani C, Damiao AJ, Miyakawa W. AFM characterization of bovine enamel and dentine after acid-etching. Micron. 2009;40(4):502-6.

176. Eaton P, West P. Atomic force microscopy: Oxford university press; 2010.

177. Greg H. Atomic Force Microscopy: Understanding Basic Modes and Advanced Applications. Hoboken: John Wiley & Sons, Inc.; 2012.

178. Jandt KD. Atomic force microscopy of biomaterials surfaces and interfaces. Surf Sci. 2001;491(3):303-32.

179. Voigtländer B. Scanning probe microscopy. Germany: Springer; 2015.

180. Kruk T. Atomic force microscopy (AFM). The Laboratory. 2013;18(1):46-50.

181. Benoit M, Selhuber-Unkel C, Braga P, Ricci D. Atomic Force Microscopy in Biomedical Research. Methods in Molecular Biology. 2011;736:355-77.

182. Morris VJ, Kirby AR, Gunning AP. Atomic force microscopy for biologists: Imperial College Press; 2010.

183. Young T, Monclus M, Burnett T, Broughton W, Ogin S, Smith P. The use of the PeakForceTM quantitative nanomechanical mapping AFM-based method for high-resolution Young's modulus measurement of polymers. Meas Sci Technol 2011;22(12):125703.

184. ISO E. 1172. Textile-glass-reinforced plastics-Prepregs, moulding compounds laminates-Determination of the textile-glass mineral-filler content-Calcination methods.1996.

185. Butt H, Cappella B, Kappl M. Force measurements with the atomic force microscope: Technique, interpretation and applications. Surf Sci Rep. 2005;59(1):1-152.

186. Mormann WH, Brandestini M, Lutz F, Barbakow F. Chairside computer-aided direct ceramic inlays. Quintessence Int. 1989;20(5):329-39.

187. Miyazaki T, Hotta Y, Kunii J, Kuriyama S, Tamaki Y. A review of dental CAD/CAM: current status and future perspectives from 20 years of experience. Dent Mater. 2009;28(1):44-56.

188. Ho GW, Matinlinna JP. Insights on Ceramics as Dental Materials. Part I: Ceramic Material Types in Dentistry. Silicon. 2011;3(3):109-15.

189. Ironside J, Swain M. Ceramics in dental restorations—a review and critical issues. J Aust Ceram Soc. 1998;34(2):78-91.

190. Giordano R. Method for fabricating endodontic orthodontic and direct restorations having infused ceramic network. Google Patents; 2001.

191. Li J, Zhang XH, Cui BC, Lin YH, Deng XL, Li M, et al. Mechanical performance of polymer-infiltrated zirconia ceramics. J Dent. 2017;58:60-6.

192. Hondrum SO. A review of the strength properties of dental ceramics. J Prosthet Dent. 1992;67(6):859-65.

193. Nguyen JF, Ruse D, Phan AC, Sadoun MJ. High-temperature-pressure polymerized resin-infiltrated ceramic networks. J Dent Res. 2014;93(1):62-7.

194. Wegner L, Gibson L. The mechanical behaviour of interpenetrating phase composites–I: modelling. Int J Mech Sci. 2000;42(5):925-42.

195. Clarke DR. Interpenetrating Phase Composites. J Am Ceram Soc. 1992;75(4):739-59.

196. Suárez M, Fernández A, Torrecillas R, Menéndez J. Sintering to transparency of polycrystalline ceramic materials. Sintering of Ceramics-New Emerging Techniques. London: IntechOpen; 2012.

197. Hong C, Zhang X, Han J, Meng S, Du S. Synthesis, microstructure and properties of high-strength porous ceramics. Ceramic Materials-Progress in Modern Ceramics. London: IntechOpen; 2012.

198. Coldea A, Swain MV, Thiel N. Mechanical properties of polymer-infiltrated-ceramic-network materials. Dent Mater. 2013;29(4):419-26.

199. Anusavice K, Shen C, Rawls H. Phillips' science of dental materials. London: Elsevier Health Sciences; 2012.

200. El Zhawi H, Kaizer MR, Chughtai A, Moraes RR, Zhang Y. Polymer infiltrated ceramic network structures for resistance to fatigue fracture and wear. Dent Mater. 2016;32(11):1352-61.

201. Naumova EA, Schneider S, Arnold WH, Piwowarczyk A. Wear Behavior of Ceramic CAD/CAM Crowns and Natural Antagonists. Materials (Basel). 2017;10(3):244.

202. Lim K, Yap AU, Agarwalla SV, Tan KB, Rosa V. Reliability, failure probability, and strength of resin-based materials for CAD/CAM restorations. J Appl Oral Sci. 2016;24(5):447-52.

203. Ludovichetti FS, Trindade FZ, Werner A, Kleverlaan CJ, Fonseca RG. Wear resistance and abrasiveness of CAD-CAM monolithic materials. J Prosthet Dent. 2018;120(2):318 e1- e8.

204. Ongun S, Kurtulmus-Yilmaz S, Meric G, Ulusoy M. A Comparative Study on the Mechanical Properties of a Polymer-Infiltrated Ceramic-Network Material Used for the Fabrication of Hybrid Abutment. Materials (Basel). 2018;11(9):1681.

205. Al-Sanabani FA, Madfa AA, Al-Qudaimi NHJAJMR. Alumina ceramic for dental applications: a review article. 2014;1(1):26-34.

206. Normalizacion OId. International Standard ISO 6872: Dentistry-ceramic Materials: ISO; 2008.

207. Yu B, Ahn JS, Lee YK. Measurement of translucency of tooth enamel and dentin. Acta odontologica Scandinavica. 2009;67(1):57-64.

208. Zheng J, Reed J. Effects of particle packing characteristics on solid-state sintering. J Am Ceram Soc. 1989;72(5):810-7.

209. Lim LC, Wong PM, Ma J. Colloidal processing of sub-micron alumina powder compacts. J Mater Process Tech. 1997;67(1-3):137-42.

210. Guazzato M, Albakry M, Ringer SP, Swain MV. Strength, fracture toughness and microstructure of a selection of all-ceramic materials. Part I. Pressable and alumina glass-infiltrated ceramics. Dent Mater. 2004;20(5):441-8.

211. Cheung KC, Darvell BW. Sintering of dental porcelain: effect of time and temperature on appearance and porosity. Dent Mater. 2002;18(2):163-73.

212. Kim BN, Hiraga K, Morita K, Yoshida H, Miyazaki T, Kagawa Y. Microstructure and optical properties of transparent alumina. Acta Materialia. 2009;57(5):1319-26.

213. Chen IW, Wang XH. Sintering dense nanocrystalline ceramics without final-stage grain growth. Nature. 2000;404(6774):168-71.

214. Lee YK. Translucency of Dental Ceramic, Post and Bracket. Materials (Basel). 2015;8(11):7241-9.

215. Chung CM, Kim JG, Kim MS, Kim KM, Kim KN. Development of a new photocurable composite resin with reduced curing shrinkage. Dent Mater. 2002;18(2):174-8.

216. Raymond C, Ronca S. Relation of Structure to Electrical and Optical Properties. Brydson's Plastics Materials: Elsevier; 2017. p. 103-25.

217. Lawson NC, Burgess JO. Gloss and Stain Resistance of Ceramic-Polymer CAD/CAM Restorative Blocks. J Esthet Restor Dent. 2016;28 Suppl 1:S40-5.

218. Cheng X, Jian-Feng Z, Shibao L. Polymer Infiltrated Ceramic Hybrid Composites as Dental Materials. Oral Health Den St. 2018;1(1).

219. Fujita K, Nishiyama N, Nemoto K, Okada T, Ikemi T. Effect of base monomer's refractive index on curing depth and polymerization conversion of photo-cured resin composites. Dent Mater J. 2005;24(3):403-8.

220. Emami N, Sjodahl M, Soderholm KJ. How filler properties, filler fraction, sample thickness and light source affect light attenuation in particulate filled resin composites. Dent Mater. 2005;21(8):721-30.

221. Ruyter IE, Oysaed H. Conversion in different depths of ultraviolet and visible light activated composite materials. Acta odontologica Scandinavica. 1982;40(3):179-92.

222. Hubbezoğlu I, Akaoglu B, Doğan A, Keskin S, Bolayır G, Ozcelik S, et al. Effect of Bleaching on Color Change and Refractive Index of Dental Composite Resins. Dent Mater. 2008;27:105-16.

223. Brodbelt RHW, Obrien WJ, Fan PL. Translucency of Dental Porcelains. Journal of Dental Research. 1980;59(1):70-5.

224. Spink LS, Rungruanganut P, Megremis S, Kelly JR. Comparison of an absolute and surrogate measure of relative translucency in dental ceramics. Dent Mater. 2013;29(6):702-7.

225. Zhang HB, Kim BN, Morita K, Yoshida H, Lim JH, Hiraga K. Optimization of high-pressure sintering of transparent zirconia with nano-sized grains. J Alloy Compd. 2010;508(1):196-9.

226. Zhang H, Kim BN, Morita K, Keijiro Hiraga HY, Sakka Y. Effect of sintering temperature on optical properties and microstructure of translucent zirconia prepared by high-pressure spark plasma sintering. Sci Technol Adv Mater. 2011;12(5):055003.

227. Awada A, Nathanson D. Mechanical properties of resin-ceramic CAD/CAM restorative materials. J Prosthet Dent. 2015;114(4):587-93.

228. Cheng M, Chen WO, Sridhar KR. Biaxial flexural strength distribution of thin ceramic substrates with surface defects. Int J Solids Struct. 2003;40(9):2249-66.

229. Harding D, Oliver W, Pharr G. Cracking during nanoindentation and its use in the measurement of fracture toughness. MRS Online Proceedings Library Archive. 1994;356.

230. Cuadrado N, Casellas D, Anglada M, Jimenez-Pique E. Evaluation of fracture toughness of small volumes by means of cube-corner nanoindentation. Scripta Materialia. 2012;66(9):670-3.

231. Thompson GA. Determining the slow crack growth parameter and Weibull two-parameter estimates of bilaminate disks by constant displacement-rate flexural testing. Dent Mater. 2004;20(1):51-62.

232. Ban S, Anusavice KJ. Influence of Test Method on Failure Stress of Brittle Dental Materials. Journal of Dental Research. 1990;69(12):1791-9.

233. Ersoy NM, Aydogdu HM, Degirmenci BU, Cokuk N, Sevimay M. The effects of sintering temperature and duration on the flexural strength and grain size of zirconia. Acta Biomater Odontol Scand. 2015;1(2-4):43-50.

234. Li W, Sun J. Effects of Ceramic Density and Sintering Temperature on the Mechanical Properties of a Novel Polymer-Infiltrated Ceramic-Network Zirconia Dental Restorative (Filling) Material. Med Sci Mon

2018;24:3068-76.

235. Wang K, Wang H, Zhou Y, Wu Y, Li G, Tian Y, editors. Effect of Sintering Temperature on the Microstructure and Mechanical Properties of Low-Cost Light-Weight Proppant Ceramics. IOP Conference Series: Materials Science and Engineering; 2017: IOP Publishing.

236. Acchar W, Silveira G, de Mello-Castanho SRH, Segadães AM, editors. Improving the properties of low temperature sintered alumina bodies with granite reject additions. Advances in Science and Technology; 2006: Trans Tech Publ.

237. Sen N, Us YO. Mechanical and optical properties of monolithic CAD-CAM restorative materials. J Prosthet Dent. 2018;119(4):593-9.

238. Chen YM, Smales RJ, Yip KH, Sung WJ. Translucency and biaxial flexural strength of four ceramic core materials. Dent Mater. 2008;24(11):1506-11.

239. Ahn JS, Lee YK. Difference in the translucency of all-ceramics by the illuminant. Dent Mater. 2008;24(11):1539-44.

240. Hasegawa A, Ikeda I, Kawaguchi S. Color and translucency of in vivo natural central incisors. J Prosthet Dent. 2000;83(4):418-23.

241. Barizon KTL, Bergeron C, Vargas MA, Qian F, Cobb DS, Gratton DG, et al. Ceramic Materials for Porcelain Veneers: Part Ii. Effect of Material, Shade, and Thickness on Translucency. Journal of Prosthetic Dentistry. 2014;112(4):864-70.

242. Messer RL, Lockwood PE, Wataha JC, Lewis JB, Norris S, Bouillaguet S. In vitro cytotoxicity of traditional versus contemporary dental ceramics. J Prosthet Dent. 2003;90(5):452-8.

243. Lee A, Swain M, He L, Lyons K. Wear behavior of human enamel against lithium disilicate glass ceramic and type III gold. J Prosthet Dent. 2014;112(6):1399-405.

244. Hmaidouch R, Weigl P. Tooth wear against ceramic crowns in posterior region: a systematic literature review. Int J Oral Sci. 2013;5(4):183-90.

245. Tsitrou EA, Northeast SE, van Noort R. Brittleness index of machinable dental materials and its relation to the marginal chipping factor. J Dent. 2007;35(12):897-902.

246. Abdullah AO, Tsitrou EA, Pollington S. Comparative in vitro evaluation of CAD/CAM vs conventional provisional crowns. J Appl Oral Sci. 2016;24(3):258-63.

247. Stawarczyk B, Eichberger M, Uhrenbacher J, Wimmer T, Edelhoff D, Schmidlin PR. Three-unit reinforced polyetheretherketone composite FDPs: influence of fabrication method on load-bearing capacity and failure types. Dent Mater J. 2015;34(1):7-12.

248. Beuer F, Steff B, Naumann M, Sorensen JA. Load-bearing capacity of all-ceramic three-unit fixed partial dentures with different computer-aided design (CAD)/computer-aided manufacturing (CAM) fabricated framework materials. European Journal of Oral Sciences. 2008;116(4):381-6.

249. Zok FW, Miserez A. Property maps for abrasion resistance of materials. Acta Mater. 2007;55(18):6365-71.

250. Chirumamilla G, Goldstein CE, Lawson NC. A 2-year Retrospective Clinical study of Enamic Crowns Performed in a Private Practice Setting. J Esthet Restor Dent. 2016;28(4):231-7.

251. Sakaguchi R, Powers J. Craig's restorative dental materials-e-book. Philadelphia,PA: Elsevier Health Sciences; 2012.

252. Silva CM, Dias KR. Compressive strength of esthetic restorative materials polymerized with quartz-tungsten-halogen light and blue LED. Braz Dent J. 2009;20(1):54-7.

253. Arcís R, López-Macipe A, Toledano M, Osorio E, Rodríguez-Clemente R, Murtra J, et al. Mechanical properties of visible light-cured resins reinforced with hydroxyapatite for dental restoration. Dent Mater. 2002;18(1):49-57.

254. Oyen ML, Cook RF. A practical guide for analysis of nanoindentation data. J Mech Behav Biomed Mater. 2009;2(4):396-407.

255. Johnson WM, Rapoff AJ. Microindentation in bone: hardness variation with five independent variables. J Mater Sci Mater Med. 2007;18(4):591-7.

256. Fischer-Cripps AC. Factors Affecting Nanoindentation Test Data. New York: Springer; 2000.

257. Huang H, Zhao H, Zhang Z, Yang Z, Ma Z. Influences of Sample Preparation on Nanoindentation Behavior of a Zr-Based Bulk Metallic Glass. Materials (Basel). 2012;5(6):1033-9.

258. Pathak S, Stojakovic D, Doherty R, Kalidindi SR. Importance of surface preparation on the nano-indentation stress-strain curves measured in metals. J Mater Res. 2009;24(3):1142-55.

259. Halgaš R, Dusza J, Kaiferova J, Kovacsova L, Markovska N. Nanoindentation testing of human enamel and dentin. Ceramics–Silikáty. 2013;57(2):92-9.

260. Rosentritt M, Preis V, Behr M, Hahnel S, Handel G, Kolbeck C. Two-body wear of dental porcelain and substructure oxide ceramics. Clin Oral Investig. 2012;16(3):935-43.

261. Seghi RR, Rosenstiel SF, Bauer P. Abrasion of human enamel by different dental ceramics in vitro. J Dent Res. 1991;70(3):221-5.

262. Kawaguchi M, Fukushima T, Horibe T. Effect of monomer structure on the mechanical properties of light-cured composite resins. Dent Mater. 1989;8(1):40-5.

263. Manhart J, Kunzelmann KH, Chen HY, Hickel R. Mechanical properties and wear behavior of light-cured packable composite resins. Dent Mater. 2000;16(1):33-40.

264. Kim KH, Ong JL, Okuno O. The effect of filler loading and morphology on the mechanical properties of contemporary composites. J Prosthet Dent. 2002;87(6):642-9.

265. Bayne SC, Heymann HO, Swift EJ. Update on Dental Composite Restorations. Journal of the American Dental Association. 1994;125(6):687-701.

266. Suzuki S, Leinfelder KF, Kawai K, Tsuchitani Y. Effect of particle variation on wear rates of posterior composites. Am J Dent. 1995;8(4):173-8.

267. Welsch G, Boyer R, Collings E. Materials properties handbook: titanium alloys: ASM international; 1993.

268. Brown D. The status of indirect restorative dental materials. Dental Update. 1998;25(1):23-8, 30-2, 4.

269. Soares CJ, Pizi ECG, Fonseca RB, Martins LRM. Mechanical properties of light-cured composites polymerized with several additional post-curing methods. Operative Dentistry. 2005;30(3):389-94.

270. McCabe JF, Kagi S. Mechanical properties of a composite inlay material following post-curing. Br Dent J. 1991;171(8):246-8.

271. Matsui K, Yoshida H, Ikuhara Y. Isothermal Sintering Effects on Phase Separation and Grain Growth in Yttria-Stabilized Tetragonal Zirconia Polycrystal. J Am Ceram Soc. 2009;92(2):467-75.

272. Faltermeier A, Rosentritt M, Reicheneder C, Mussig D. Experimental composite brackets: influence of filler level on the mechanical properties. Am J Orthod Dentofacial Orthop. 2006;130(6):699 e9-14.

273. Sonmez N, Gultekin P, Turp V, Akgungor G, Sen D, Mijiritsky E. Evaluation of five CAD/CAM materials by microstructural characterization and mechanical tests: a comparative in vitro study. BMC Oral Health. 2018;18(1):5.

274. Ang SF, Bortel EL, Swain MV, Klocke A, Schneider GA. Size-dependent elastic/inelastic behavior of enamel over millimeter and nanometer length scales. Biomaterials. 2010;31(7):1955-63.

275. Costa A, Xavier T, Noritomi P, Saavedra G, Borges A. The influence of elastic modulus of inlay materials on stress distribution and fracture of premolars. Oper Dent. 2014;39(4):E160-E70.

276. Desai PD, Das UK. Comparison of fracture resistance of teeth restored with ceramic inlay and resin composite: an in vitro study. Indian J Dent Res. 2011;22(6):877.

277. Scherrer SS, de Rijk WG. The fracture resistance of all-ceramic crowns on supporting structures with different elastic moduli. Int J Prosthodont. 1993;6(5):462-7.

278. Oliver WC, Pharr GM. Measurement of hardness and elastic modulus by instrumented indentation: Advances in understanding and refinements to methodology. J Mater Res. 2004;19(1):3-20.

279. DIN E. 6507. Metallic Materials-Vickers Hardness Test-Part 1: Test Method. Beuth Verlag, Berlin; 2006.

280. Fischer-Cripps AC. Nanoindentation testing. Nanoindentation. New York: Springer; 2011. p. 21-37.

281. Lauvahutanon S, Takahashi H, Shiozawa M, Iwasaki N, Asakawa Y, Oki M, et al. Mechanical properties of composite resin blocks for CAD/CAM. Dent Mater. 2014;33(5):705-10.

282. Mainjot AK, Dupont NM, Oudkerk JC, Dewael TY, Sadoun MJ. From Artisanal to CAD-CAM Blocks: State of the Art of Indirect Composites. J Dent Res. 2016;95(5):487-95.

283. Malament KA, Socransky SS. Survival of Dicor glass-ceramic dental restorations over 14 years. Part II: effect of thickness of Dicor material and design of tooth preparation. J Prosthet Dent. 1999;81(6):662-7.

284. Thompson VP, Rekow DE. Dental ceramics and the molar crown testing ground. J Appl Oral Sci. 2004;12(spe):26-36.

285. Malament KA, Socransky SS. Survival of Dicor glass-ceramic dental restorations over 16 years. Part III: effect of luting agent and tooth or tooth-substitute core structure. J Prosthet Dent. 2001;86(5):511-9.

286. Lawn BR, Pajares A, Zhang Y, Deng Y, Polack MA, Lloyd IK, et al. Materials design in the performance of all-ceramic crowns. Biomaterials. 2004;25(14):2885-92.

287. Kim JH, Miranda P, Kim DK, Lawn BR. Effect of an adhesive interlayer on the fracture of a brittle coating on a supporting substrate. J Mater Res. 2003;18(1):222-7.

288. Phillips RW. Skinner's science of dental materials. W B Saunders Company, xii+ 682, 26 x 18 cm, illustrated, 1973. 1973.

289. Lambrechts P, Braem M, Vanherle G. Evaluation of Clinical-Performance for Posterior Composite Resins and Dentin Adhesives. Oper Dent. 1987;12(2):53-78.

290. Lawn B, Wilshaw TR. Fracture of brittle solids. Cambridge: Cambridge university press; 1993.

291. Kralik V, Nemecek J. Comparison of nanoindentation techniques for local mechanical quantification of aluminium alloy. Mat Sci Eng a-Struct. 2014;618:118-28.

292. Cohen SR, Kalfon-Cohen E. Dynamic nanoindentation by instrumented nanoindentation and force microscopy: a comparative review. Beilstein J Nanotechnol. 2013;4:815-33.

293. Zeng Z, Tan J. AFM Nanoindentation To Quantify Mechanical Properties of Nano- and Micron-Sized Crystals of a Metal–Organic Framework Material. ACS Appl Mater Interfaces. 2017;9(45):39839-54.

294. Binnig G, Quate CF, Gerber C. Atomic Force Microscope. Physical Review Letters. 1986;56(9):930-3.

295. Binnig G, Gerber C, Stoll E, Albrecht T, Quate C. Atomic resolution with atomic force microscope. Europhysics Letters. 1987;3(12):1281.

296. Silikas N, Lennie A, England K, Watts D. AFM as a tool in dental research. Micro Ana. 2001:19-22.

297. Maivald P, J Butt H, A C Gould S, Prater C, Drake B, A Gurley J, et al. Using Force Modulation to Image Surface Elasticities with the Atomic Force Microscope. Nanotechnology. 1999;2:103.

298. Magonov SN, Vb E, Whangbo M-H. Phase Imaging and Stiffness in Tapping-Mode Atomic Force Microscopy. J Microsc

1997;375.

299. Trtik P, Kaufmann J, Volz U. On the use of peak-force tapping atomic force microscopy for quantification of the local elastic modulus in hardened cement paste2012. 215–21 p.

300. Schon P, Bagdi K, Molnar K, Markus P, Pukanszky B, Vancso GJ. Quantitative mapping of elastic moduli at the nanoscale in phase separated polyurethanes by AFM. Eur Polym J

2011;47(4):692-8.

301. Ferencz R, Sanchez J, Blümich B, Herrmann W. AFM nanoindentation to determine Young's modulus for different EPDM elastomers2012. 425–32 p.

302. Foster B. New Atomic Force Microscopy (AFM) Approaches Life Sciences Gently, Quantitatively, and Correlatively. American Laboratory. 2012;44:24-8.

303. Tjan AH, Chan CA. The polishability of posterior composites. J Prosthet Dent. 1989;61(2):138-46.

304. de Jager N, Feilzer AJ, Davidson CL. The influence of surface roughness on porcelain strength. Dent Mater. 2000;16(6):381-8.

305. Haq S, Srivastava R. Measuring the influence of materials composition on nano scale roughness for wood plastic composites by AFM. Measurement. 2016;91:541-7.

306. Verbiest GJ, Rost MJ. Resonance frequencies of AFM cantilevers in contact with a surface. Ultramicroscopy. 2016;171:70-6.

307. Lucas PW, Philip SM, Al-Qeoud D, Al-Draihim N, Saji S, van Casteren A. Structure and scale of the mechanics of mammalian dental enamel viewed from an evolutionary perspective. Evol Dev. 2016;18(1):54-61.

308. Ramamurty U, Jang J. Nanoindentation for probing the mechanical behavior of molecular crystals–a review of the technique and how to use it. CrystEngComm. 2014;16(1):12-23.

309. Sirghi L, Rossi F. Adhesion and elasticity in nanoscale indentation. Appl Phys Lett

2006;89(24):243118.

310. Mesa B, Magonov S. Novel diamond/sapphire probes for scanning probe microscopy applications. J Phys Conf Ser. 2007;61:770-4.

311. Obraztsov AN, Kopylov PG, Loginov BA, Dolganov MA, Ismagilov RR, Savenko NV. Single crystal diamond tips for scanning probe microscopy. Rev Sci Instrum. 2010;81(1):013703.

312. Whitehouse D. Stylus techniques. Characterization of solid surfaces. New York: Springer; 1974. p. 49-74.

313. Vorburger T. Surface finish metrology tutorial: US Department of Commerce, National Institute of Standards and Technology; 1990.

314. Poon CY, Bhushan B. Comparison of surface roughness measurements by stylus profiler, AFM and non-contact optical profiler. Wear. 1995;190(1):76-88.

315. ISO E. 4287: 2009. Geometrical Product Specifications -Surface texture: Profile method–Terms, definitions

surface texture parameters2009.

316. Marghalani HY. Effect of filler particles on surface roughness of experimental composite series. J Appl Oral Sci. 2010;18(1):59-67.

317. Draughn RA, Harrison A. Relationship between Abrasive Wear and Microstructure of Composite Resins. J Prosthet Dent. 1978;40(2):220-4.

318. Ryba TM, Dunn WJ, Murchison DF. Surface roughness of various packable composites. Oper Dent. 2002;27(3):243-7.

319. Scheibe KG, Almeida KG, Medeiros IS, Costa JF, Alves CM. Effect of different polishing systems on the surface roughness of microhybrid composites. J Appl Oral Sci. 2009;17(1):21-6.

320. Fasbinder DJ, Neiva GF. Surface Evaluation of Polishing Techniques for New Resilient CAD/CAM Restorative Materials. J Esthet Restor Dent. 2016;28(1):56-66.

321. Koizumi H, Saiki O, Nogawa H, Hiraba H, Okazaki T, Matsumura H. Surface roughness and gloss of current CAD/CAM resin composites before and after toothbrush abrasion. Dent Mater J. 2015;34(6):881-7.

322. Singh A, Sengupta B, Kuckreja H, Kuckreja KB. An in vitro study to compare glazed and polished surfaces of feldspathic porcelain and comparing three different polishing systems. Indian J Dent Res. 2017;9(5):21.

323. Vieira AC, Oliveira MC, Lima EM, Rambob I, Leite M. Evaluation of the surface roughness in dental ceramics submitted to different finishing and polishing methods. J Indian Prosthodont Soc. 2013;13(3):290-5.

324. Haralur SB. Evaluation of efficiency of manual polishing over autoglazed and overglazed porcelain and its effect on plaque accumulation. J Adv Prosthodont. 2012;4(4):179-86.

325. Tuncdemir A, Dilber E, Kara H, Ozturk A. The effects of porcelain polishing techniques on the color and surface texture of different porcelain systems. Mater Sci App. 2012;3(05):294.

326. Quirynen M, Bollen L, Papaioannou W, Van Eldere J, van Steenberghe D. The influence of titanium abutment surface roughness on plaque accumulation and gingivitis: Short-term observations. Int J Oral Maxillofac Implants. 1996;11(2).

327. Bollen CM, Papaioanno W, Van Eldere J, Schepers E, Quirynen M, Van Steenberghe D. The influence of abutment surface roughness on plaque accumulation and peri-implant mucositis. Clinical oral implants research. 1996;7(3):201-11.

328. Klinke T, Biffar R, editors. The Dependence of Sintering Parameters on the Surface Quality and Roughness of Ceramic Veneered PFM-Restorations. Key Engineering Materials; 2003: Trans Tech Publ.

329. Chun KJ, Lee JY. Comparative study of mechanical properties of dental restorative materials and dental hard tissues in compressive loads. J Dent Biomech. 2014;5(0):1758736014555246.

330. Hardy D, Green DJ. Mechanical-Properties of a Partially Sintered Alumina. J Eur Ceram Soc. 1995;15(8):769-75.

331. Nanjangud S, Brezny R, Green D. Strength and Young's modulus behavior of a partially sintered porous alumina. J Am Ceram Soc. 1995;78(1):266-8.

332. Hussain B, Le Thieu M, Johnsen G, Reseland J, Haugen H. Can CAD/CAM resin blocks be considered as substitute for conventional resins? Dent Mater. 2017;33(12):1362-70.

333. Lawson NC, Bansal R, Burgess JO. Wear, strength, modulus and hardness of CAD/CAM restorative materials. Dent Mater. 2016;32(11):e275-e83.

334. Leung BT, Tsoi JK, Matinlinna JP, Pow EH. Comparison of mechanical properties of three machinable ceramics with an experimental fluorophlogopite glass ceramic. J Prosthet Dent. 2015;114(3):440-6.

335. Koenigswald W, Clemens W. Levels of complexity in the microstructure of mammalian enamel and their application in studies of systematics. Scanning Microsc. 1992;6(1):195-217; discussion -8.

336. Giannini M, Soares CJ, de Carvalho RM. Ultimate tensile strength of tooth structures. Dent Mater. 2004;20(4):322-9.

337. Jacobson A. Oral development and histology, 3rd edition. Am J Orthod Dentofacial Orthop 2002;121(4):431-2.

338. Fincham AG, Moradian-Oldak J, Simmer JP. The structural biology of the developing dental enamel matrix. J Struct Biol. 1999;126(3):270-99.

339. Junior S, Scherrer S, Ferracane J, Della Bona A. Microstructural characterization and fracture behavior of a microhybrid and a nanofill composite. Dent Mater. 2008;24(9):1281-8.

340. Stawarczyk B, Ender A, Trottmann A, Ozcan M, Fischer J, Hammerle CH. Load-bearing capacity of CAD/CAM milled polymeric three-unit fixed dental prostheses: effect of aging regimens. Clin Oral Investig. 2012;16(6):1669-77.

341. Stawarczyk B, Ozcan M, Trottmann A, Schmutz F, Roos M, Hammerle C. Two-Body Wear Rate of Cad/Cam Resin Blocks and Their Enamel Antagonists. J Prosthet Dent. 2013;109(5):325-32.

342. Stawarczyk B, Sener B, Trottmann A, Roos M, Ozcan M, Hammerle CH. Discoloration of manually fabricated resins and industrially fabricated CAD/CAM blocks versus glass-ceramic: effect of storage media, duration, and subsequent polishing. Dent Mater J. 2012;31(3):377-83.

343. Czasch P, Ilie N. In vitro comparison of mechanical properties and degree of cure of bulk fill composites. Clin Oral Investig. 2013;17(1):227-35.

344. Alix S, Colasse L, Morvan C, Lebrun L, Marais S. Pressure impact of autoclave treatment on water sorption and pectin composition of flax cellulosic-fibres. Carbohydr Polym. 2014;102:21-9.

345. Milleding P, Carlen A, Wennerberg A, Karlsson S. Protein characterisation of salivary and plasma biofilms formed in vitro on non-corroded and corroded dental ceramic materials. Biomaterials. 2001;22(18):2545-55.

346. Kukiattrakoon B, Hengtrakool C, Kedjarune-Leggat U. Degradability of fluorapatite-leucite ceramics in naturally acidic agents. Dent Mater 2010;29(5):502-11.

347. Iorgulescu G. Saliva between normal and pathological. Important factors in determining systemic and oral health. J Med Life. 2009;2(3):303-7.

348. Bunker BC. Molecular Mechanisms for Corrosion of Silica and Silicate-Glasses. Journal of Non-Crystalline Solids. 1994;179:300-8.

349. Lynch ME, Folz DC, Clark DE. Use of FTIR reflectance spectroscopy to monitor corrosion mechanisms on glass surfaces. Journal of Non-Crystalline Solids. 2007;353(27):2667-74.

350. Ozcan M, Ccahuana V, Mesquita A, Nishioka R, Kimpara E, Bottino M. Surface degradation of glass ceramics after exposure to acidulated phosphate fluoride. J Appl Oral Sci. 2011;18(2).

351. Unemori M, Matsuya Y, Matsuya S, Akashi A, Akamine A. Water absorption of poly(methyl methacrylate) containing 4-methacryloxyethyl trimellitic anhydride. Biomaterials. 2003;24(8):1381-7.

352. Ortengren U, Wellendorf H, Karlsson S, Ruyter IE. Water sorption and solubility of dental composites and identification of monomers released in an aqueous environment. J Oral Rehabil. 2001;28(12):1106-15.

353. Wei Y, Silikas N, Zhang Z, Watts D. Diffusion and concurrent solubility of self-adhering and new resin–matrix composites during water sorption/desorption cycles. Dent Mater. 2011;27(2):197-205.

354. Yiu CK, King NM, Pashley DH, Suh BI, Carvalho RM, Carrilho MR, et al. Effect of resin hydrophilicity and water storage on resin strength. Biomaterials. 2004;25(26):5789-96.

355. Ito S, Hashimoto M, Wadgaonkar B, Svizero N, Carvalho RM, Yiu C, et al. Effects of resin hydrophilicity on water sorption and changes in modulus of elasticity. Biomaterials. 2005;26(33):6449-59.

356. Chaves L, Graciano F, Júnior O, do Vale Pedreira A, Manso A, Wang L. Water interaction with dental luting cements by means of sorption and solubility. Braz Dent Sci. 2012;15(4):29-35.

357. Levine H, Slade L. Water as a plasticizer: physico-chemical aspects of low-moisture polymeric systems. Water Sci. 1988;3:79-185.

358. Sideridou I, Tserki V, Papanastasiou G. Study of water sorption, solubility and modulus of elasticity of light-cured dimethacrylate-based dental resins. Biomaterials. 2003;24(4):655-65.

359. Kalachandra S. Influence of fillers on the water sorption of composites. Dent Mater. 1989;5(4):283-8.

360. Yap AU, Tan SH, Wee SS, Lee CW, Lim EL, Zeng KY. Chemical degradation of composite restoratives. J Oral Rehabil. 2001;28(11):1015-21.

361. Chen C, Chen Y, Lu Z, Qian M, Xie H, Tay FR. The effects of water on degradation of the zirconia-resin bond. J Dent. 2017;64:23-9.

362. Martos J, Osinaga P, Oliveira E, Castro L. Hydrolytic degradation of composite resins: effects on the microhardness Mater Res. 2003;6:599-604.

363. Lauvahutanon S, Shiozawa M, Takahashi H, Iwasaki N, Oki M, Finger W, et al. Discoloration of various CAD/CAM blocks after immersion in coffee. Rest Dent. 2017;42(1):9-18.

364. Liebermann A, Wimmer T, Schmidlin PR, Scherer H, Loffler P, Roos M, et al. Physicomechanical characterization of polyetheretherketone and current esthetic dental CAD/CAM polymers after aging in different storage media. J Prosthet Dent. 2016;115(3):321-8 e2.

365. Mensitieri G, Apicella A, Kenny JM, Nicolais L. Water Sorption Kinetics in Poly(Aryl Ether Ether Ketone). J Appl Polym Sci. 1989;37(2):381-92.

366. Grayson MA, Wolf CJ. The Solubility and Diffusion of Water in Poly(Aryl-Ether-Ether-Ketone) (Peek). J Polym Sci Pol Phys. 1987;25(1):31-41.

367. Ajami S, Coathup MJ, Khoury J, Blunn GW. Augmenting the bioactivity of polyetheretherketone using a novel accelerated neutral atom beam technique. J Polym Sci Pol Phys. 2017;105(6):1438-46.

368. Alshali RZ, Salim NA, Satterthwaite JD, Silikas N. Long-term sorption and solubility of bulk-fill and conventional resin-composites in water and artificial saliva. J Dent. 2015;43(12):1511-8.

369. Øysæd H, Ruyter I. Water sorption and filler characteristics of composites for use in posterior teeth. J Dent Res. 1986;65(11):1315-8.

370. Mortier E, Gerdolle DA, Jacquot B, Panighi MM. Importance of water sorption and solubility studies for couple bonding agent--resin-based filling material. Oper Dent. 2004;29(6):669-76.

371. Gajewski V, Pfeifer CS, Fróes-Salgado N, Boaro L, Braga RR. Monomers used in resin composites: degree of conversion, mechanical properties and water sorption/solubility. Braz Dent J. 2012;23(5):508-14.

372. Khokhar ZA, Razzoog ME, Yaman P. Color stability of restorative resins. Quintessence Int. 1991;22(9):733-7.

373. Druck CC, Pozzobon JL, Callegari GL, Dorneles LS, Valandro LF. Adhesion to Y-TZP ceramic: study of silica nanofilm coating on the surface of Y-TZP. J Polym Sci Pol Phys. 2015;103(1):143-50.

374. Van Noort R, Barbour M. Introduction to Dental Materials. Sheffield: Elsevier Health Sciences; 2014.

375. Soderholm KJ, Zigan M, Ragan M, Fischlschweiger W, Bergman M. Hydrolytic degradation of dental composites. J Dent Res. 1984;63(10):1248-54.

376. Charles R. Static fatigue of glass. I. J Appl Phys. 1958;29(11):1549-53.

377. Lovell MR, Dalgliesh RM, Richardson RM, Barnes AC, Enderby JE, Evans B, et al. Depth of water incorporation into float glass surfaces studied by neutron reflection. Phys Chem Chem Phys. 1999;1(9):2379-81.

378. VITA Zahnfabrik. Vita Enamic VITA Zahnfabrik: Technical and scientific documentation. [Internet].2016 [cited 2018 Nov 19]. Available from: https://cdn.vivarep.com/contrib/vivarep/media/pdf/4_4642_ENAMICTechnicalandScientific_20170830205744578.pdf

379. Malacarne J, Carvalho RM, de Goes MF, Svizero N, Pashley DH, Tay FR, et al. Water sorption/solubility of dental adhesive resins. Dent Mater. 2006;22(10):973-80.

380. Silva E, Almeida G, Poskus L, Guimarães J. Relationship between the degree of conversion, solubility and salivary sorption of a hybrid and a nanofilled resin composite. J Appl Oral Sci. 2008;16(2):161-6.

381. Soderholm KJ, Yang MC, Garcea I. Filler particle leachability of experimental dental composites. Eur J Oral Sci. 2000;108(6):555-60.

382. Van Landuyt K, Nawrot T, Geebelen B, De Munck J, Snauwaert J, Yoshihara K, et al. How much do resin-based dental materials release? A meta-analytical approach. Dent Mater. 2011;27(8):723-47.

383. Goncalves L, Filho JD, Guimaraes JG, Poskus LT, Silva EM. Solubility, salivary sorption and degree of conversion of dimethacrylate-based polymeric matrixes. J Polym Sci Pol Phys. 2008;85(2):320-5.

384. Fabre HS, Fabre S, Cefaly DF, de Oliveira Carrilho MR, Garcia FC, Wang L. Water sorption and solubility of dentin bonding agents light-cured with different light sources. J Dent. 2007;35(3):253-8.

385. Lopes LG, Jardim Filho Ada V, de Souza JB, Rabelo D, Franco EB, de Freitas GC. Influence of pulse-delay curing on sorption and solubility of a composite resin. J Appl Oral Sci. 2009;17(1):27-31.

386. Sadowsky SJ. An overview of treatment considerations for esthetic restorations: a review of the literature. J Prosthet Dent. 2006;96(6):433-42.

387. Nguyen JF, Migonney V, Ruse ND, Sadoun M. Resin composite blocks via high-pressure high-temperature polymerization. Dent Mater. 2012;28(5):529-34.

388. Alt V, Hannig M, Wostmann B, Balkenhol M. Fracture strength of temporary fixed partial dentures: CAD/CAM versus directly fabricated restorations. Dent Mater. 2011;27(4):339-47.

389. Knobloch LA, Kerby RE, Seghi R, van Putten M. Two-body wear resistance and degree of conversion of laboratory-processed composite materials. Int J Prosthodont. 1999;12(5):432-8.

390. Lovelh L, Newman S, Bowman C. The effects of light intensity, temperature, and comonomer composition on the polymerization behavior of dimethacrylate dental resins. J Dent Res. 1999;78(8):1469-76.

391. Ferracane JL, Condon JR. Post-cure heat treatments for composites: properties and fractography. Dent Mater. 1992;8(5):290-5.

392. Bausch JR, Delange C, Davidson CL. The Influence of Temperature on Some Physical-Properties of Dental Composites. Journal of Oral Rehabilitation. 1981;8(4):309-17.

393. Li W, Sun J. Effects of Ceramic Density and Sintering Temperature on the Mechanical Properties of a Novel Polymer-Infiltrated Ceramic-Network Zirconia Dental Restorative (Filling) Material. Med Sci Monit. 2018;24:3068-76.

394. Galmarini S. Ceramics: Sintering and microstructure. Work Pract Cer Proc: TP. 2011:1-15.

395. Xiong F, Chao YL, Zhu ZM. Translucency of newly extracted maxillary central incisors at nine locations. Journal of Prosthetic Dentistry. 2008;100(1):11-7.

396. Xiao B, Walter B, Gkioulekas I, Zickler T, Adelson E, Bala K. Looking against the light: how perception of translucency depends on lighting direction. J Vis. 2014;14(3):17.

397. Ilie N, Hickel R. Correlation between ceramics translucency and polymerization efficiency through ceramics. Dent Mater. 2008;24(7):908-14.

398. Jiang L, Liao Y, Wan Q, Li W. Effects of sintering temperature and particle size on the translucency of zirconium dioxide dental ceramic. J Mater Sci Mater Med. 2011;22(11):2429-35.

399. Tsukuma K. Transparent Titania Yttria Zirconia Ceramics. J Mater Sci Lett. 1986;5(11):1143-4.

400. Kato T, Ohashi K, Fuji M, Takahashi M. Water absorption and retention of porous ceramics fabricated by waste resources. J Ceram Soc Jpn. 2008;116(1350):212-5.

401. Masouras K, Akhtar R, Watts DC, Silikas N. Effect of filler size and shape on local nanoindentation modulus of resin-composites. J Mater Sci Mater Med. 2008;19(12):3561-6.

402. Alcala J, Giannakopoulos AE, Suresh S. Continuous measurements of load-penetration curves with spherical microindenters and the estimation of mechanical properties. J Mater Res. 1998;13(5):1390-400.

Appendices

Appendix I: SEM images (x10K) shows different surface topographies of the studied CAD/CAM composite materials.

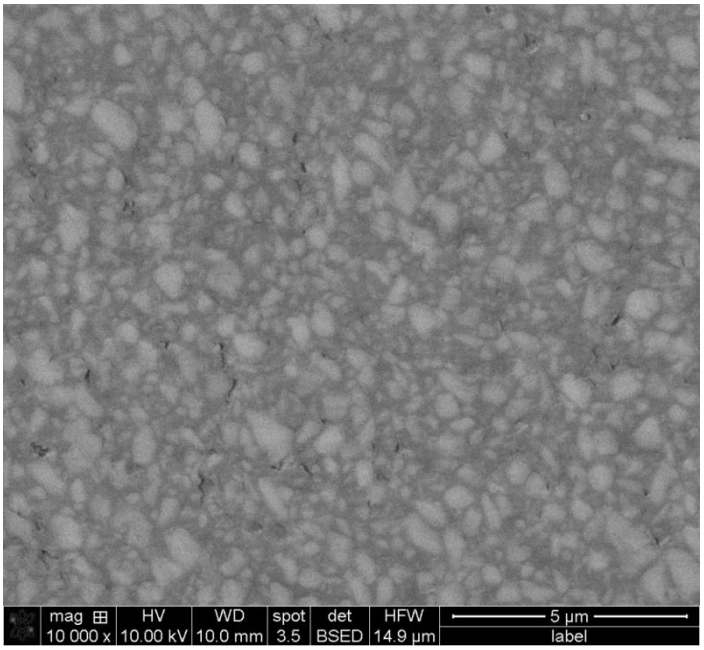

Figure 8.1 Cerasmart

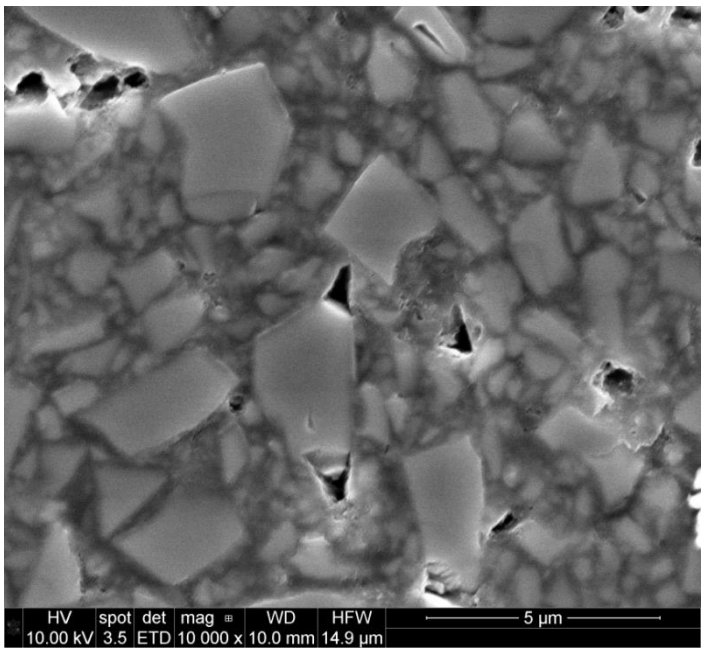

Figure 8.2 Gandio Bloc

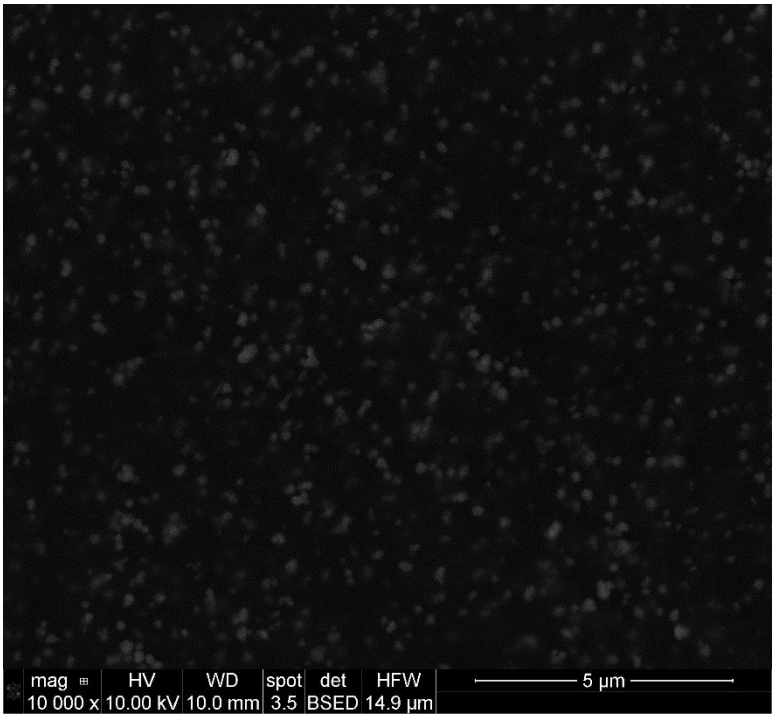

Figure 8.3 Dentokeep

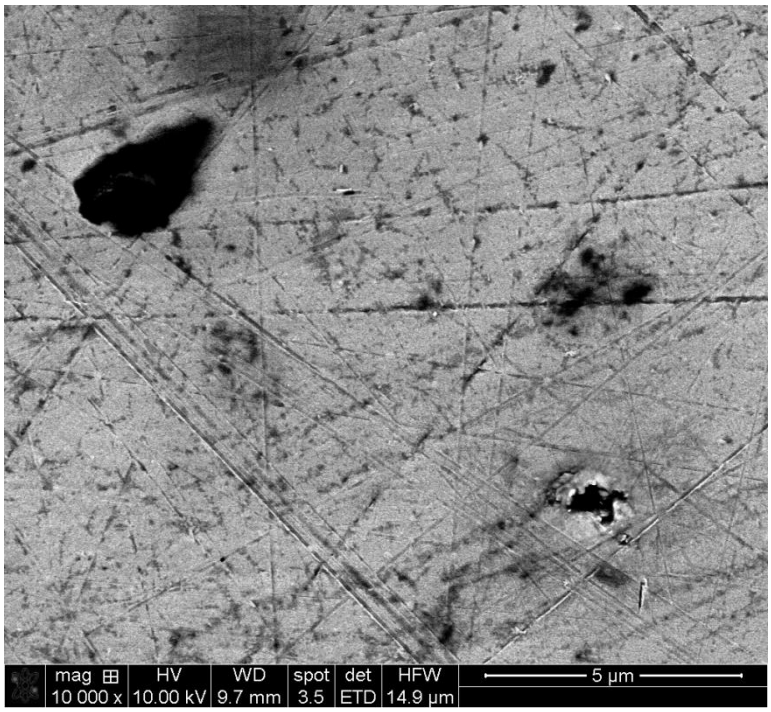

Figure 8.4 Vita MarkII

Appendix II:

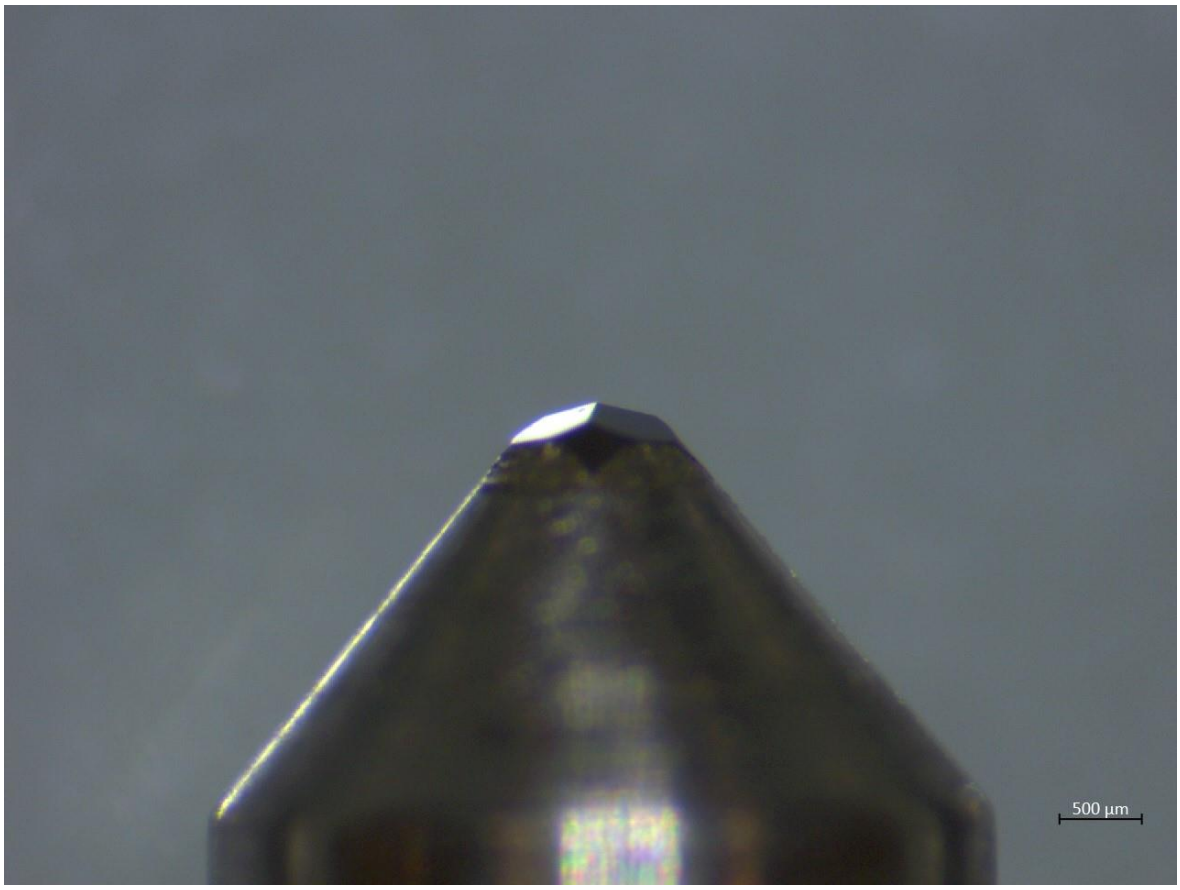

Figure 8.5 Berckovich nano-indentor

Appendix III:

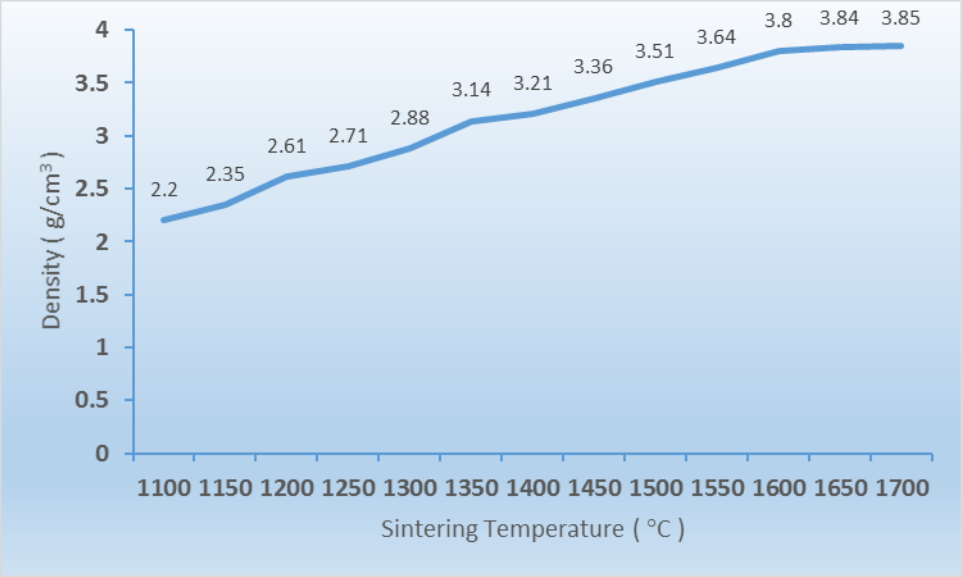

Figure 8.6 Density- temperature curve for alumina matrices.